Mars Deploy

Final Report of the Design Synthesis Exercise

by

Group 22

Student Name	Student Number
Aleksandrs Vinarskis	4880420
Dave van Winden	4668324
Floris van Kesteren	4844866
Luca Elbracht	4778138
Matthias Christiaens	4881826
Owen McLaughlin	4671031
Pepijn Deroo	4778332
Seppe Wille	4775805
Tijs Palings	4657098
Yosuke Hordijk	4780922

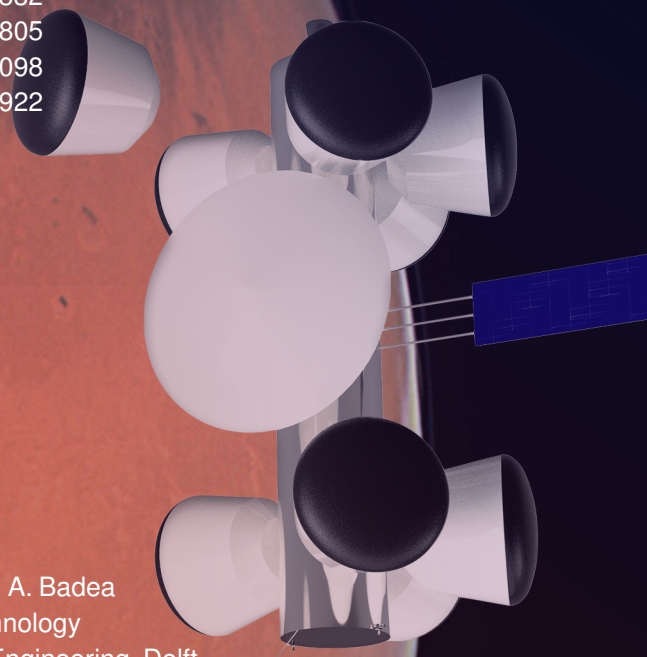

Tutor: Dr. ir. B. Root
Coaches: Ir. I. Uriol Balbin and Ir. A. Badea
Institution: Delft University of Technology
Place: Faculty of Aerospace Engineering, Delft

Project Duration: 19th April - 5th July, 2021

TU Delft
Faculty of Aerospace Engineering

This page is intentionally left empty.

Executive Overview

Mars is widely seen as the next logical step in human exploration of our solar system. Over the last decades in particular, the interest in Mars from the general public and industry has gradually become stronger, fueled by exciting missions such as NASA's Ingenuity helicopter and new space companies such as SpaceX. However, in order to build any kind of human settlement on Mars, a source of heat and water will be of utmost importance. Previous Mars missions, and NASA's InSight in particular, have proven that Mars is still geologically alive and does experience seismic activity. The aim of the Mars Deploy mission is to build upon InSight's legacy by following the mission need statement: ***"Investigate the tectonic and geologic behaviour of Mars to benefit the search for heat and water sources in preparation of human exploration of the planet."***

While InSight has shown that marsquakes can be detected and located with only one seismic station, seismic and thermal measurements are more effective when performed by a global network of stations to allow for a precise mapping of seismic activity and heat flow inside the planet.

Mars Deploy Mission Profile

The Mars Deploy mission is an ESA M-class mission. It is a complete system, designed to place and support a set of scientific instruments at 10 separate landing sites on the surface of Mars. The system consists of a support stage and a descent stage, which will be launched together on a Falcon Heavy Reusable launch vehicle. The descent stage consists of 10 identical impacting landers, which utilize large impact attenuating structures to ensure that the scientific instruments and its supporting systems survive the high impact loads. The landers have an entry mass of almost 300 kg, half of which can be attributed to the entry capsule. The support stage consists of an orbiter, which will be used to transport the landers to Mars and release them into their respective Mars entry trajectories. The orbiter will then remain in orbit to act as a relay between the landers and ground stations on Earth.

Table 1: Summary of Mars Deploy system characteristics

	Value	**Unit**
Total mission lifetime	5	Years
Scientific phase duration	3	Years
Amount of landers	10	[-]
Total mission cost	390	M€
Total launch mass	4345	kg
Launch vehicle	Falcon Heavy Reusable	[-]

Eight and a half months after launch, the spacecraft, consisting of the orbiter with the 10 attached entry capsules, will arrive at Mars. Before the spacecraft inserts itself into Mars orbit, the capsule release sequence is started. This sequence consists of making small ΔV adjustments to the spacecraft and releasing the capsules one by one. This entry sequence is compliant with Planetary Protection guidelines, to ensure that the spacecraft does not crash into Mars in case of failure. Table 1 shows several key system characteristics.

Since all entry capsules are unguided, the orbiter will ensure that the probes impact in their desired landing zones. After separation, the probes will take between 48 and 52 hours to impact in the chosen areas. The entry capsules will enter the Martian atmosphere with a velocity of 5.7 km/s. The heat shield will reduce this velocity to 430 m/s, after which the parachute will be deployed to jettison the heat shield. This reduces the velocity even further, after which the impactor is released from the back shell and enters a free fall. Right before impact, two tethered bullets are shot into the ground from the impactor, which deploy the heat flow probe. The impactor will impact with a maximum velocity of 230 m/s, enduring a shock of up to 10000 g.

Orbiter Design

The Mars Deploy orbiter has as primary mission to safely deliver the 10 landers to Mars, after which it will enter a low, circular orbit around the planet and act as a relay. After the 3 year nominal scientific phase, the orbiter is designed to remain operational for at least two more years to act as a general relay for other Mars missions. A set of key design parameters for the orbiter is shown in Table 2, and a render of the spacecraft is shown in Figure 1.

Table 2: Orbiter design parameters

Orbiter	Value	Unit
Wet mass	4345	kg
Payload mass	2901	kg
Payload fraction	67	%
Propellant mass	1065	kg
Dry mass (no PL)	380	kg
Total ΔV budget	3250	m/s
Nominal power consumption	243	W
Peak power consumption	867	W
DSN transmission rate	200	kbit/s
Battery size	895	Wh
Solar array size	2.07	m^2
Engine thrust	425	N
Engine specific impulse	317	s
Cost	118	M€

Table 3: Lander design parameters (given for one lander)

Lander	Value	Unit
Entry mass	290	kg
Entry capsule diameter	1.5	m
Entry capsule height	1.4	m
Parachute size	14.27	m^2
Impact velocity	230	m/s
Lander mass	158	kg
Scientific payload mass	17.4	kg
Payload fraction	11	%
Nominal power consumption	44	W
	909	Wh/sol
Peak power consumption	97	W
Orbiter transmission rate	100+	kbit/s
DSN transmission rate	300	bit/s
Total cost	18	M€

Impactor Design

In order to set up a network of measurement stations for seismic activity and heat flow, delicate scientific instruments must be delivered to the surface of Mars. This is done by using a set of 10 identical landers, outfitted with a suite of scientific instruments, including a novel bullet-type heat flow probe. Based on the heritage HP3 instrument, the bullet solves HP3's shortcomings by deploying the probe at a high velocity from the bottom of the impactor, right before impact. This ensures an uncertainty in the heat flow measurement of only 1 mW/m^2. The network of heat flow probes that the Mars Deploy mission creates will be able to validate current heat flow models of Mars, and give insight into the current geothermal state of the planet.

Next to the heat flow probe, every lander carries a shock-resistant seismometer. This seismometer, based on InSight's seismic package, will be able to detect marsquakes with a magnitude of 1.6 within a distance of 1500 km, and marsquakes of magnitude 3.0 within a distance of 3350 km. The seismic network that is set up covers a large portion of the surface of Mars. Table 3 shows key design parameters for one impactor. The impactor consists of cylindrical outer structure, with an elevated mounting plate for all hardware on the inside. As can be seen in Figure 2, the elevated plate rests on top of a honeycomb crumple zone. After impact, the four circular solar panels will rotate outward to start generating power. Finally, an array of 42 aerodynamic fins is placed around the impactor to ensure aerodynamic stability during descent.

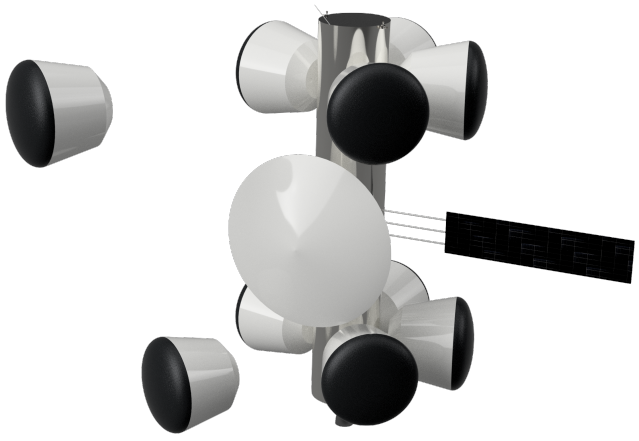

Figure 1: Spacecraft (orbiter with 10 entry capsules) shown mid-separation

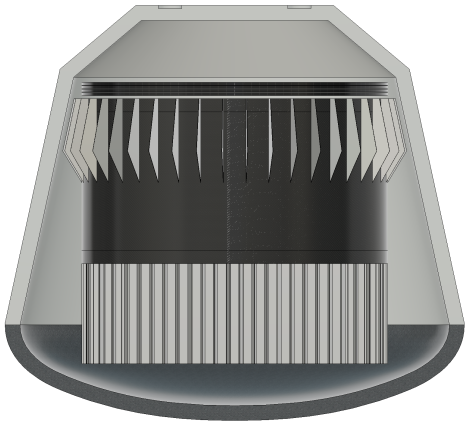

Figure 2: Lander shown in its entry capsule

Nomenclature

Table 4: Nomenclature

Acronym	*Definition*
A	Arrival at Mars
ADCS	Attitude Determination & Control System
AE	Aerodynamics
AU	Astronomical Unit
BROOT	Dr. Ir. Bart Root
CC	Course Correction
CDH	Command and Data Handling
CFNH	Carbon Fiber - Nomex Honeycomb
CNSA	China National Space Administration
CoG	Center of Gravity
CoP	Center of Pressure
COSPAR	Committee on Space Research
DESR	Design Restrictions
DMD	Design Synthesis Exercise Mars Deploy
DoD	Depth of Discharge
DSE	Design Synthesis Exercise
DSN	Deep Space Network
EDL	Entry, Descent and Landing
EOL	End-of-Life
EOSC	European Space Operations Centre
EPO	Earth Parking Orbit
EPS	Electric Power System
ESA	European Space Agency
FBS	Functional Breakdown Structure
FFD	Functional Flow Diagram
GHS	Globally Harmonized System of Classification and Labelling of Chemicals
GNC	Guidance, Navigation, and Control
GPS	Global Positioning System
HB	Hellas Basin
HFE	Heat Flow Experiment
HP3	Heat Flow and Physical Properties Package
IBM	Intercontinental Ballistic Missile
IMO	Initial Mars Orbit
ITO	Interplanetary Transfer Orbit
IPS	Instructions per second
ISRU	In-Situ Resource Utilization
ISS	International Space Station
L	Launch
LGA	Low Gain Antenna(s)
LMO	Low Mars Orbit
LV	Launch Vehicle
MAH	Mars Arrival Hyperbola
MGS	Mars Global Surveyor
M−Class	Medium-Class
MB	Mega Byte
MISC	Miscellaneous
MOI	Mars Orbit Injection
MRO	Mars Reconnaissance Orbiter
MUPUS	Multi Purpose Sensors for Surface and Subsurface Science
NASA	National Aeronautics and Space Administration
NP	Northern Plains
OM	Orbital Maintenance

Continued on next page

Table 4 – continued from previous page

Acronym	*Definition*
OR	Outflow Region of Valleys Marineris
PAY	Payload
PDS	Power Distribution System
PERF	Performance
PF	Powered Flight
PL	Payload
PROP	Propulsion System
PSE	Passive Seismic Experiments
PT	Project Team
RDT	Requirements Discovery Tree
RM	Risk Manager
SARR	Safety, Reliability & Regulation
SC	Scientific Community
SEIS	Seismic Experiment for Interior Structure
SF	Safety Factor
SMO	Secondary Mars Orbit
SNR	Signal to Noise Ratio
SLOC	Source lines of code
SO	Safety Officer
SO	Sustainability Officer
SSD	Sample Standard Deviation
STRUC	Structure and mechanisms subsystems
SWOT	Strengths, Weaknesses, Opportunities and Threats
SUST	Sustainability
TC	Tharsis Complex
TGO	Trace Gas Orbiter
THERM	Thermal Control Subsystem
T.B.D.	To Be Determined
TRL	Technology Readiness Level
TRN	Terrain Relative Navigation
TTC	Telemetry, Tracking and Command
UN	United Nations
WBS	Work Breakdown Structure
WFD	Work Flow Diagram

List of Symbols and Constants

Table 5: List of symbols

Symbol	*Definition*
A	Area
A_e	Emitting area
A_i	Incident area
C_D	Drag coefficient
F_g	Gravitational force
I_{sp}	Specific impulse
K	Ballistic coefficient
k	Conductivity
m	Mass
P	Power
p	Pressure
Q	Heat
S	Cross-sectional area
S_{const}	Parachute constructed area
S_{infl}	Parachute inflated area
T	Temperature
t	Thickness
V_e	Entry velocity
α	Absorptivity
ε	Emissivity
γ	Flight path angle
ρ	Density

Table 6: List of constants

Symbol	*Definition*	*Value*	*Unit*
AU	Astronomical Unit	1.46e11	m
g_0	Gravitational acceleration at sea level	9.81	$m \cdot s^{-2}$
J_{a_e}	Albebo effect at Earth	590.7	$W \cdot m^{-2}$
J_{IR_e}	Infrared radiation Earth	239.7	$W \cdot m^{-2}$
J_{IR_m}	Infrared radiation Mars	110.5	$W \cdot m^{-2}$
J_{s_e}	Solar constant at Earth	1361	$W \cdot m^{-2}$
J_{s_m}	Solar constant at Mars	586.2	$W \cdot m^{-2}$
$T_{atmosphere_{max}}$	Maximum atmospheric temperature on Mars	270.15	K
$T_{atmosphere_{min}}$	Minimum atmospheric temperature on Mars	177.15	K
T_e	Internal temperature Earth	255	K
T_m	Internal temperature Mars	210.1	K
$T_{soil_{max}}$	Maximum soil temperature on Mars	298.15	K
$T_{soil_{min}}$	Minimum soil temperature on Mars	228.15	K
T_{space}	Temperature space	3	K
σ	Stefan-Boltzmann constant	$5.67 \cdot 10^{-8}$	$W \cdot m^{-2} \cdot K^{-4}$
μ_m	Standard gravitational parameter of Mars	$4.282837 \cdot 10^{13}$	$m^3 \cdot s^{-2}$
R_m	Radius of Mars	3389.5	km

Contents

Introduction

Before humans can set foot on the surface of Mars in the near future, a detailed understanding of the workings of the interior of Mars needs to be developed. Next to that, knowing the location of aquifers (underground water wells) and geo-heating sources is crucial for sustained human presence on the Red Planet. The mission need statement for this DSE project is therefore to **"Investigate the tectonic and geologic behaviour of Mars to benefit the search for heat and water sources in preparation of human exploration of the planet"**.

Prior missions have shown that seismometers and surface heat flux measurement system can aid in gaining that understanding. However, these measurements work best if they are conducted at different locations around the planet simultaneously. The project objective statement for this DSE project states: **"Design with ten students in ten weeks, a distributed geologic measuring system for the surface of Mars, without using thrusters to aid the descent"**. After a careful trade-off of concepts, based on scientific return, sustainability, technical risk, and total mission cost, it was decided that Mars Deploy will be an unmanned scientific multi-probe impactor mission. Not only does this configuration carry less risk than the others due to it is inherent simplicity, it also yields the most scientific knowledge for its cost.

This report will focus on the design of the individual subsystems of the vehicles. For each subsystem, a different method has been devised. These individual subsystem designs are then merged and integrated. The initial design of the multi-probe mission is now complete, where ten Mars probes will be accompanied by an orbiter, serving as a deployment vehicle and communications relay. After the unguided entry capsules are released at 500.000 km from the surface and slowed down in the atmosphere, the challenge of landing arises. The impactor is designed to hit the surface at a velocity of 230 m/s and decelerate at 10,000 g in order to deploy the measurement systems. Bullet shaped heat probes are ejected at impact using a pyrotechnic cartridge to maximise the kinetic energy they carry. These bullets are designed to penetrate at least 4 m deep and remain connected to the impactor via a scientific tether which is covered in heat flow sensors.

This report is divided into five parts: Part I Mission Outline, where the project itself is explained and where it fits in the existing market; Part II Mission Design, where general mission design is carried out as well as astrodynamical planning; Part III Orbiter Design, here the design process specific to the orbiter is explained; Part IV Lander Design, here the design process specific to the lander portion is explained; and Part V Mission Evaluation, where the mission is analysed as a whole. A conclusion is provided in at the end of the report.

Part I

Mission Outline

1. Mission Profile

Concept and Challenges

In order to fulfill the scientific goal of the Mars Deploy mission, a total of ten landers shall be brought to the surface of Mars. Every lander carries a scientific instrument suite to gather data on seismic activity, heat flow and atmospheric properties. To provide the necessary coverage of Mars, the landers are intended to be distributed over the surface and impact on different terrains. During the transfer to Mars, the ten landing probes are attached to the cylindrical support stage, also called the orbiter. The design solution for the descent stage is an impactor concept landing on Mars at a high velocity. Upon impact two bullets are deployed, penetrating the surface to deploy a heat flow probe.

The main challenges for the proposed design are Mars entry, descent and landing (EDL) as well as the design of the lander structure to survive the impact. In terms of EDL, a requirement is to not use propellant below an altitude of 10 km for the descent stage. As it was deemed infeasible to perform a soft landing without thrusters, the lander will impact the ground only decelerated by a parachute. The impactor is designed with an impact attenuator which will take up the majority of the loads. It is designed such that the payload is able to survive the high deceleration.

Timeline

The spacecraft will be delivered to Cape Canaveral 30 days before launch for preparation and fairing integration. The Mars Deploy mission will launch on a Falcon Heavy Reusable vehicle provided by Space X on April 11th 2033. Shortly after launch, the spacecraft will leave its parking orbit and is injected into an interplanetary transfer orbit. 10 days after launch the first course correction manoeuvre is performed. The landers will be released sequentially from the support stage 258 days after launch and enter a Mars entry trajectory. The support stage provides the necessary orientation and velocity for the landers to reach their designated landing spots. The landers are released from hyperbolic orbit, so before the Mars orbit insertion of the support stage is performed. After travelling for 48 to 52 hours, the landers will enter the Martian atmosphere and impact on the surface. The orbiter then inserts itself in a low Mars orbit 260 days after launch. The mission timeline is summarised in Figure 1.1.

After initializing, the landers are designed to work nominally on the surface for three years and upload their scientific measurement data to the orbiter. The orbiter relays the collected data to Earth via the NASA Deep Space Network (DSN). The lifetime of the orbiter might exceed that of the landers and can be used as a relay for other landing probes on Mars. The total mission duration is scheduled for five years. An end-of-life (EOL) deorbiting manoeuvre will be performed by the orbiter and the landers will be shut down.

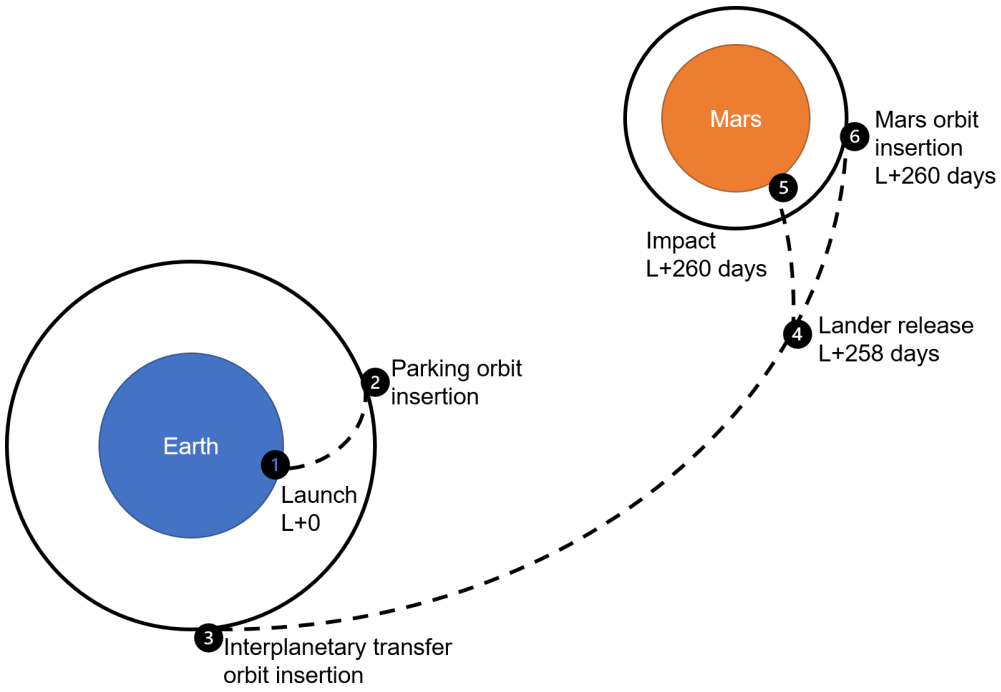

Figure 1.1: Mission steps during the Mars Deploy transfer phase

2. Requirements and Compliance

The mission characteristics given in Chapter 1 translate into a list of stakeholder and system requirements given in Table 2.1, including their origin and compliance. All active requirements were defined in the Baseline Report [1], while new requirements were determined in this final design phase. If a requirement is "Met", the compliance column gives the section or chapter where this will be verified. Some requirements were verified by considering the performance of similar design choices in the past. However, the compliance of these requirements in the specific design of the Mars Deploy systems is therefore not entirely verified. In this case, its compliance status is Verification Pending ("V.P."), indicating that the compliance is achievable in the current design, but not fully verified.

The compliance of other requirements was either Not Applicable ("N.A."), Not Verified ("N.V.") or "Not Met". In the system requirements, a naming transformation was performed with respect to previous reports. This changed each occurrence of "support" or "support system" into "orbiter", and each occurrence of "descent" or "descent system" into "lander".

All stakeholder requirements are met or have a verification pending, whereas some system requirements were scrapped, not verified or not met. Next, the explanation for scrapping, not verifying or not meeting specific requirements is given.

Scrapped requirements

- [DMD-ORBITER-16]: This requirement was scrapped as the mission profile no longer necessitates this capability. The requirement of deploying landers in the correct landing sites is included in [DMD-ORBITER-23-A].
- [DMD-ORBITER-26]: This requirement was scrapped because this functionality falls under the lander system, which includes the entry capsule. For the relevant subsystems, this requirement was translated into subsystem requirements.

Non-verified requirements

- [DMD-ORBITER-14]: This requirement was not verified as it is included in the subsystem requirements of the subsystems most critical for radiation.
- [DMD-ORBITER-18]: This requirement was not yet verified, as the structural analysis for launch was conducted for static loads only.
- [DMD-LANDER-09]: This requirement was not yet verified, as the structural analysis for launch was conducted for static loads only.

Non-met requirements

- [DMD-ORBITER-22]: This requirement was not met, as no investigation was conducted into the required payload to perform this function. Furthermore, the detection of dust storms is included in the lander system.
- [DMD-LANDER-15]: This requirement was not met, as no specific definition of "hibernation mode" was determined. The design of the lander EPS did not include this functionality.

Table 2.1: Stakeholder and system requirement compliance matrix

ID	*Requirement*	*Status*	*Origin*	*Compliance*
Stakeholder requirements				
DMD-PERF-BROOT-01	The system shall provide seismic data sensitive to marsquakes of magnitude MW = 1.6.	Active	Project description [2]	V.P., Section 16.5
DMD-PERF-BROOT-02	The system shall provide heat flow data with an accuracy of 1 mW/m2.	Active	Project description [2]	V.P., Section 16.5
DMD-PERF-BROOT-03	The system shall provide heat flow data with a range of 0-50 mW/m2.	Active	Project description [2]	V.P., Section 16.5

Continued on next page

Table 2.1 – continued from previous page

ID	*Requirement*	*Status*	*Origin*	*Compliance*
DMD-PERF-BROOT-04	The system shall provide location data with an accuracy of 10 m.	Active	Project description [2]	Met, Section 16.5
DMD-PERF-BROOT-05	The system shall provide temperature data with a relative accuracy of 0.1 °C.	Active	Project description [2]	Met, Section 16.5
DMD-PERF-BROOT-06	The system shall provide pressure data with a relative accuracy of 1 Pa.	Active	Project description [2]	Met, Section 16.5
DMD-PERF-BROOT-07	The system shall provide humidity data with a relative accuracy of 0.1%.	Active	Project description [2]	Met, Section 16.5
DMD-PERF-BROOT-08	The system shall provide air composition data with a relative accuracy of 0.1%	Active	Project description [2]	Met, Section 16.5
DMD-PERF-BROOT-09	The system shall have a mission lifetime of five years from the moment of launch.	Active	Project description [2]	Met, Chapter 23
DMD-PERF-BROOT-10	The system shall conduct measurements from the surface of Mars for at least three years.	Active	Project description [2]	Met, Chapter 23
DMD-PERF-BROOT-11	The system shall provide at least two measurement points on all the following Martian areas: Northern Plains, Southern Highlands, Tharsis Complex, outflow region of Valley Marineris and Hellas Basin.	Active	Project description [2]	Met, Chapter 14
DMD-PERF-BROOT-12	The orbiters and landers shall communicate in accordance with the Deep Space Network system.	Active	Project description [2]	Met, Section 16.6
DMD-SARR-BROOT-01	The system shall comply with international space laws as set by the United Nations.	Active	Project description [2]	Met, Chapter 4
DMD-SARR-BROOT-02	The system shall comply with European Space Agency regulations.	Active	Project description [2]	Met, Chapter 4
DMD-SARR-BROOT-03	The system shall not land within 100 km of current and planned landing sites of other missions.	Active	Project description [2]	Met, Chapter 14
DMD-SARR-BROOT-04	The system shall use a Safety Factor (SF) of 1.4 on the EPS subsystem needs.	Active	Project description [2]	Met, Section 10.7
DMD-SARR-BROOT-05	All on-board science instruments shall have technology level TRL 9.	Active	Project description [2]	Met, Section 16.5
DMD-SARR-BROOT-06	The system shall have three redundant communication systems.	Active	Project description [2]	Met, Section 10.5
DMD-SARR-BROOT-07	80% of the system shall operate nominally during the nominal mission phase.	Active	Project description [2]	Met, Chapter 18
DMD-SUST-BROOT-01	The system shall mitigate Earth-based microbial contamination in accordance with European Space Agency standards.	Active	Project description [2]	Met, Chapter 24
DMD-SUST-PT-01	The orbiter and support system shall be de-orbited at EOL.	Active	Baseline Report [1]	Met, Chapter 8

Continued on next page

Table 2.1 – continued from previous page

ID	*Requirement*	*Status*	*Origin*	*Compliance*
DMD-SUST-PT-02	No orbital space debris shall be created in the circumstellar habitable zone during the de-orbiting manoeuvre.	Active	Baseline Report [1]	Met, Chapter 8
DMD-DESR-BROOT-01	The system shall be viable for a proposal to the M-class missions of the European Space Agency.	Active	Project description [2]	Met, Chapter 21
DMD-DESR-BROOT-02	The system shall be submitted to the European Space Agency call for M-class mission proposals of 2025.	Active	Project description [2]	Met, Chapter 21
DMD-DESR-BROOT-03	The system shall not use propellant below 10 km above the Martian surface.	Active	Project description [2]	Met, Chapter 16
DMD-DESR-BROOT-04	The system shall be compatible with different payloads for future missions.	Active	Project description [2]	V.P., Section 15.1
DMD-DESR-SC-01	All scientific measurements performed by the system shall be made available to the scientific community.	Active	Baseline Report [1]	Met, Section 16.5
Orbiter system requirements				
DMD-ORBITER-01	The orbiter shall be able to move with a minimum rotation speed of 0.4 deg/s about all three axes.	Active	Requirements discovery [1]	Met, Section 10.3
DMD-ORBITER-02	The orbiter shall have a pointing accuracy of at least 0.1 deg in all directions.	Active	Requirements discovery [1]	Met, Section 10.3
DMD-ORBITER-03	The orbiter shall have a rotational acceleration of at least 112.5 arcsec/s^2 about all three axes.	Active	Requirements discovery [1]	Met, Section 10.3
DMD-ORBITER-04	The orbiter shall be able to communicate with a bitrate of <tbd> Mbit/s.	Replaced	Functional analysis [1]	Replaced in Section 10.6
DMD-ORBITER-05	The orbiter shall be able to have a nominal power consumption of at least 225 W at all times for the duration of the mission lifetime.	Active	Functional analysis [1]	Met, Section 10.7
DMD-ORBITER-06	The orbiter shall have a maximum peak power consumption of 740 W for the duration of the mission lifetime.	Active	Functional analysis [1]	Met, Section 10.7
DMD-ORBITER-07	The orbiter shall be able to provide location data with an accuracy of at least 10 m.	Active	Functional analysis [1]	Met, Section 10.4
DMD-ORBITER-08	The orbiter shall be able to inject into Martian orbit.	Active	Functional analysis [1]	Met, Section 10.9
DMD-ORBITER-09	The orbiter shall be able to perform a de-orbiting sequence at end of life.	Active	Functional analysis [1]	Met, Section 10.9
DMD-ORBITER-10	The orbiter shall be able to keep all subsystems within their respective operational temperature ranges.	Active	Functional analysis [1]	Met, Section 10.8
DMD-ORBITER-11	The orbiter shall not collide with foreign objects in space.	Active	Functional analysis [1]	Met, Section 10.9

Continued on next page

Table 2.1 – continued from previous page

ID	*Requirement*	*Status*	*Origin*	*Compliance*
DMD-ORBITER-12	The orbiter shall be able to withstand a maximum longitudinal launch acceleration of 6 g.	Active	Launch vehicle [3]	Met, Section 10.2
DMD-ORBITER-13	The orbiter shall be able to withstand a maximum lateral launch acceleration of 2 g.	Active	Launch vehicle [3]	Met, Section 10.2
DMD-ORBITER-14	The orbiter shall be able to shield its subsystems from radiation.	Active	Requirements discovery [1]	N.V.
DMD-ORBITER-15	The orbiter shall be able to have contact with the ground station <tbd>% of one Earth day.	Replaced	Functional analysis [1]	N.A.
DMD-ORBITER-15-A	The orbiter shall be able to have contact with DSN.	New	Replaces [DMD-ORBITER-15]	Met, Section 10.5
DMD-ORBITER-16	The orbiter shall be able to identify the landing locations.	Scrapped	Functional analysis [1]	N.A.
DMD-ORBITER-17	The orbiter shall have a maximum total wet mass of 4345 kg.	Active	Requirements discovery [1]	Met, Section 9.2
DMD-ORBITER-18	The orbiter shall be able to withstand launch vibrations of at least <tbd> Hz.	Active	Launch vehicle [3]	N.V.
DMD-ORBITER-19	The orbiter shall be able to initiate the lander for landing.	Active	Functional analysis [1]	Met, Chapter 8
DMD-ORBITER-20	The orbiter shall be able to compute its trajectory.	Active	Functional analysis [1]	Met, Section 10.4
DMD-ORBITER-21	The orbiter shall be able to correct its trajectory.	Active	Functional analysis [1]	Met, Section 10.9
DMD-ORBITER-22	The orbiter shall be able to detect Martian (global) dust storms at least <tbd> hours before affecting the landers.	Active	Functional analysis [1]	Not Met
DMD-ORBITER-23	The orbiter shall process and assess the feasibility and safety of lander deployment windows.	Replaced	Functional analysis [1]	N.A.
DMD-ORBITER-23-A	The orbiter shall be able to deploy the lander at the correct position and time.	New	Replaces [DMD-ORBITER-23]	Met, Chapter 8, Section 10.9
DMD-ORBITER-24	The orbiter shall have an overall reliability of 80%.	Active	Follows from [DMD-SARR-BROOT-07]	Met, Chapter 12
DMD-ORBITER-25	The orbiter shall have a bioburden level of $\leq 5x10^5$ spores.	Active	Planetary protection [4]	Met, Chapter 24
DMD-ORBITER-26	The orbiter shall protect the landers against radiation.	Scrapped	Risk assessment [1]	N.A.
DMD-ORBITER-27	The orbiter shall be able to communicate with all landers.	Active	Functional analysis [1]	Met, Section 10.5
DMD-ORBITER-28	The orbiter shall be able to offload all collected information to the Earth.	New	Follows from [DMD-PERF-BROOT-11]	Met, Section 10.5

Continued on next page

Table 2.1 – continued from previous page

ID	*Requirement*	*Status*	*Origin*	*Compliance*
Lander system requirements				
DMD-LANDER-01	The lander shall be able to land at the predefined landing sites.	Active	Functional analysis [1]	Met, Chapter 8
DMD-LANDER-02	The lander shall be able to communicate with a bitrate of <tbd> Mbit/s.	Replaced	Functional analysis [1]	Replaced in Section 16.7
DMD-LANDER-03	The lander shall be able to store at least 1479 hours of scientific data.	Active	Functional analysis [1]	Met, Section 16.7
DMD-LANDER-04	The lander shall be able to have a nominal power consumption of at least 36 W at all times for the duration of the mission lifetime.	Active	Functional analysis [1]	Met, Section 16.8
DMD-LANDER-05	The lander shall be able to have a maximum peak power consumption of 73 W per Earth day for the duration of the mission lifetime.	Active	Functional analysis [1]	Met, Section 10.7
DMD-LANDER-06	The lander shall be able to provide location data with an accuracy of at least 10 m.	Active	Functional analysis [1]	Met, Section 16.6
DMD-LANDER-07	The lander shall be able to withstand a maximum longitudinal acceleration of 6 g.	Active	Launch vehicle [3]	Met, Section 16.4
DMD-LANDER-08	The lander shall be able to withstand a maximum lateral acceleration of 2 g.	Active	Launch vehicle [3]	Met, Section 16.4
DMD-LANDER-09	The lander shall be able to withstand launch vibrations of at least <tbd> Hz.	Active	Launch vehicle [3]	N.V.
DMD-LANDER-10	The lander shall be able to withstand Martian dust storms of velocities up to <tbd> km/h.	Replaced	Functional analysis [1]	N.A.
DMD-LANDER-10-A	The lander shall be able to withstand Martian dust storms of velocities up to 100 m/s, after landing.	New	Replaces [DMD-LANDER-10], value from [1]	Met, Section 16.4
DMD-LANDER-11	The lander shall have a maximum mass of 291 kg, including the entry capsule.	Active	Requirements discovery [1]	Met, Section 15.2
DMD-LANDER-12	The lander shall be able to communicate with ground stations for <tbd>% of an earth day.	Replaced	Functional analysis [1]	N.A
DMD-LANDER-12-A	The lander shall be able to communicate with DSN.	New	Replaced [DMD-LANDER-12]	Met, Section 16.6
DMD-LANDER-13	The lander shall be able to withstand impact at the landing on Mars of maximum 10000 g.	Active	Functional analysis [1], Section 16.1	Met, Section 16.4
DMD-LANDER-14	The lander shall be able to be troubleshoot remotely.	Active	Functional analysis [1]	Met, Section 16.7
DMD-LANDER-15	The lander shall be able to enter hibernation mode during a Martian dust storm.	Active	Functional analysis [1]	Not Met

Continued on next page

[1] https://mars.nasa.gov/news/1854/the-fact-and-fiction-of-martian-dust-storms/, Accessed [14-06-2021]

Table 2.1 – continued from previous page

ID	*Requirement*	*Status*	*Origin*	*Compliance*
DMD-LANDER-16	The lander shall be able to detect dust storms which decrease power generation by at least 50%.	Active	Functional analysis, risk assessment [1]	Met, Section 16.8
DMD-LANDER-17	The lander shall have an overall reliability of <tbd>.	Active	Follows from [DMD-SARR-BROOT-07]	Met, Chapter 18
DMD-LANDER-18	The lander shall have a surface bioburden level of $\leq$ 30 spores.	Active	Planetary protection [4]	Met, Chapter 24
DMD-LANDER-19	The lander shall have a total bioburden level of $\leq$ 30 $\pm$2x10^5 spores.	Active	Planetary protection [4]	Met, Chapter 24
DMD-LANDER-20	The lander shall be able to offload all collected information to the orbiter.	New	Functional analysis [1]	Met, Section 16.6
DMD-LANDER-21	The lander shall be able to operate in the scientific phase of the mission for three years after landing.	New	Follows from [DMD-PERF-BROOT-10]	Met, Section 16.7

3. Market Analysis

According to the requirement [DMD-DESR-BROOT-01], the Mars Deploy mission shall be viable for an ESA M-class mission. Performing a market analysis is crucial in identifying the competition in the market and areas were it is possible to make profit from the design. After performing a thorough market analysis it is clear that there is minimum competition for the Mars Deploy mission in the near future.

3.1. ESA M-class missions

As mentioned before, the mission shall be designed to qualify for an M-class mission proposal. Analysing the current proposals for this mission category may provide an insight on similar mission types and therefore potential competition. Currently, 5 ESA medium class mission proposals have been accepted, one of which has launched. The missions can be seen in Table 3.1.[1]

Table 3.1: Existing M-class mission proposals

M-Class Mission	Name	Launch Date	Cost [M€]
M1	Solar Orbiter	Feb 2020	1500 [2]
M2	Euclid	July - Dec 2022	606 [3]
M3	PLATO	2026	600 [4]
M4	Ariel	2029	500 [5]
M5	EnVision	2031	500 [6]

These missions are part of ESA's Cosmic Vision campaign, which focuses on the exploration and understanding of the solar system and beyond. Currently, no proposal for a mission to Mars has been confirmed. This is beneficial for the Mars Deploy mission, as it will be a proposed for the post-2025 M-class round. With the estimated mission cost of 385.7 M€ (Chapter 21), the Mars Deploy mission is a suitable candidate for an M-Class mission and well below the mission cost of the current competitors.

[1] https://sci.esa.int/web/cosmic-vision/-/59977-missions-of-opportunity, Accessed [20-06-2021]
[2] https://spacenews.com/atlas-launches-solar-orbiter-mission/, Accessed [22-06-2021]
[3] https://spacenews.com/esa-panel-gives-final-approval-euclid-space-telescope/, Accessed [22-06-2021]
[4] https://www.bbc.com/news/science-environment-26267918, Accessed [22-06-2021]
[5] https://www.space.com/40042-ariel-alien-planet-mission-european-space-agency.html, Accessed [22-06-2021]
[6] https://spacenews.com/esa-selects-venus-mission, Accessed [22-06-2021].

3.2. Mars Missions

There have been several missions with similar scientific goals over the past years. The main goal of the Mars Deploy is to measure marsquakes as well as find aquifers and geothermal heat sources. No other mission to date has been able to find these underground aquifers under the Martian surface. While numerous past missions have confirmed the existence of water on Mars, the uncertainty of what lies under the Martian surface still remains. The Mars Deploy impacting landers will attempt to answer this question. In order to compare the Mars Deploy mission and its market position to other missions to Mars, a list of past missions and their respective costs was compiled.

Table 3.2: Past missions to Mars

Mission	Mission Date	Approximate Cost M€
Perseverance Rover	2021	2289
Insight	2018	835
ExoMars (TGO) / Schiaparelli EDM	2016	1300
MAVEN	2013	563.64
Mars Orbiter Mission	2013	62
Mars Science Laboratory / Curiosity Rover	2011	2559
Mars Reconnaissance Orbiter	2005	848
Phoenix Lander	2005	455
Mars Express Orbiter / Beagle 2 Lander	2003	431
Spirit & Opportunity Rover	2003	1025
Mars Odyssey Orbiter	2001	386
Mars Polar Lander / Deep Space 2 impactors	1999	151
Mars Climate Orbiter	1998	177
Mars Global Surveyor (MGS) orbiter	1996	225
Mars Pathfinder Lander & Sojourner Rover	1996	388

Note that the only similar mission style was the Deep Space 2 mission from 1999, which had a relatively low mission cost of 151 M€. With the estimated mission cost of 385.7 M€, this mission is more than twice as expensive, but has five times as many impactors. The main difference between the two missions is the impact style as well as the scientific return. The Mars Deploy impactor aims to have an impact attenuator that will attempt to ensure a successful landing, while the Deep Space 2 probes were aimed to survive in one piece without any means attenuation. Mars Deploy aims to deliver four scientific instruments per lander, while Deep Space 2's main payload was the heat flow probe which was designed to measure potential heat sources.

One other lander that is actively measuring marsquakes and looking for aquifers is NASA's InSight. However, due to a malfunction in its heat flow probe mechanism, it was not able to fully deploy and make accurate heat flow measurements. Given that this part of the mission has failed, and if it succeeded, would only have one sample location, the Mars Deploy impactors will provide global coverage as well as accurate heat flux measurements with a 1 mW/m^2 accuracy. Mars Deploy will be a valuable addition to the active scientific measurements from InSight and its predecessors. It will have scientific results of similar accuracy and from multiple landing locations, for a lower estimated mission cost.

3.3. Future of Mars Deploy

As of now, the future of the exploration of Mars is bright. There will be more missions in the future, not only by ESA and NASA, but also by other countries like China, India and the United Arab Emirates. American companies such as SpaceX have their first crewed mission planned to Mars as early as 2026. [7] Additionally, NASA is planning a crewed mission in the 2030's.

Finding water sources at relatively low depth is essential for future crewed mission to succeed. As launch costs of vehicles such as the SpaceX Falcon Heavy run up to 90 M$, consistently launching enough supplies to Mars is financially unsustainable. As the average adult male needs at least 3.7 L of water and an average adult female needs at least 2.7 L of water per day, this means that an astronaut will need on average 1170 L of water per year which translates to roughly 1170 kg per person per year [5]. With average launch cost per kg of the Falcon Heavy being at least 5358$ per kg, supplying the astronauts with water will be an expensive task. Besides water, they will need food and other supplies as well. As the Mars Deploy mission is aiming to locate aquifers at sufficient depths, these can be used to supplement the food and water supplies from Earth, reducing the re-occurring supply costs with upwards of 6.3 M$ per astronaut per year if water would be sourced completely from Mars.

Next to aiding a potential crewed mission, the orbiter supporting the Mars Deploy landers can be used as a relay satellite for future Martian probes as well. The landers have a designed functional lifetime of 3 operational years,

[7] https://observer.com/2020/12/elon-musk-says-spacex-will-land-humans-on-mars-in-a-few-years-if-theyre-lucky/, Accessed [20-06-2021]

after which the impactors might still function as well as the relay satellite itself. However, some of the probes might malfunction after this time period, which leaves bandwidth for other Martian probes. Future rovers and landers from NASA and ESA can connect to the relay satellite and possibly purchase bandwidth for a certain time period.

This allows future Mars landers to be designed with an intention of using the orbiter as a relay. This can potentially decrease the overall cost of that mission, as it would need less powerful telemetry equipment, which results in a decrease in required power, which might lead to a smaller mass.

3.4. Stakeholders

The Mars Deploy mission will have several stakeholders that can both actively and passively benefit from a mission success. It is important to identify these stakeholders as their interest can provide the Mars Deploy mission with a place in the current space market.

ESA
One of the main stakeholders is ESA. As mentioned before, this mission will be a proposal for ESA's M-Class mission category, and therefore shall abide by the predetermined M-Class mission requirements. ESA will be the institution that is responsible for the mission funding, therefore, it is of great importance to them that the mission is well constructed and that mission success can be guaranteed as much as possible.

Customer
As the customer will be responsible for payment of the Mars Deploy project team, it is of main importance that the project team shall deliver a viable mission proposal that has potential to be one of the next scheduled ESA M-Class mission. Therefore, a quality project is of best interest to the customer.

Launch Vehicle Companies
The current launch vehicle that was chosen to launch the Mars Deploy mission is the SpaceX Falcon Heavy. SpaceX will therefore be a stakeholder of the mission.

Future Mars Missions
Even though there have been numerous missions to Mars, there are still a lot of unknowns that can result in a degree of uncertainty. As the Mars Deploy mission aims to impact the red planet with ten landers at several locations, they can provide additional information about the soil types on these locations that can lay the groundwork for future missions.

Furthermore, as the current cost estimate of the Mars Deploy mission is relatively low at 385.7 M€ for multiple landers, compared to the previous Mars missions in Table 3.2, this lander concept may prove to be a cost efficient approach to landing multiple probes at multiple locations for other scientific missions. Next to this, as previously mentioned in Section 3.3, the future generation of crewed missions to the red planet can benefit enormously if Mars Deploy is able to locate multiple aquifers and sources of geothermal heat.

Scientific Community
The scientific results from the impactors will be beneficial for further studies of the formation of Mars and helps humanity in understanding the origins of the solar system. It will allow academics to further study the red planet and provide valuable information for the interior mapping of Mars.

Humanity
Finally, one of the main stakeholders of the Mars Deploy mission is humanity itself. According to the Fermi Paradox, named after Italian-American physicist Enrico Fermi, humanity must be able to travel beyond Earth and eventually past the solar system in order for human kind to persist in the galaxy. As Mars is likely to be the next destination for human space exploration, Mars Deploy will be contributing to this by locating water sources on this extraterrestrial body and potentially aid the foundation of a future Martian colony.

4. Sustainability Strategy

The sustainability strategy of the Mars Deploy design process has been developed in previous reports and was an integral part of the concept trade-off process in the Midterm Report [6]. In general, the Mars Deploy design team understands that to be sustainable, the design should not compromise the economic, social and environmental well-being of current and future generations. To clarify the evaluation of sustainability, six sustainability criteria were identified, which are shown in Figure 4.1. These criteria are linked to United Nations Sustainable Development goals and are divided into the three overlapping areas of sustainability: economic, environmental and social sustainability. A more detailed explanation of each criterion can be found in the Baseline Report [1].

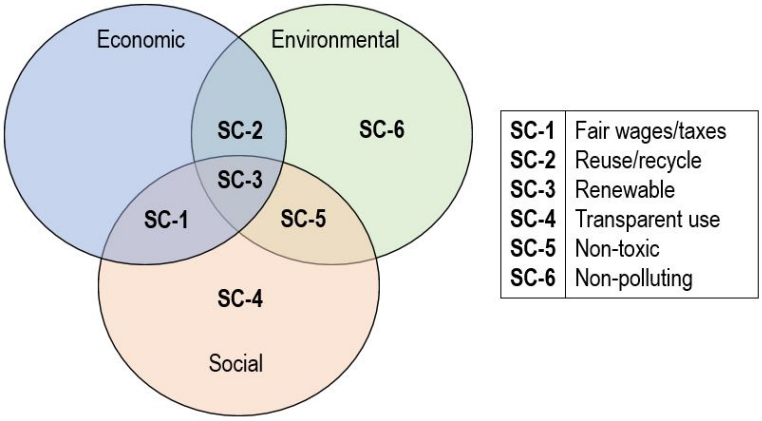

Figure 4.1: Diagram of sustainability criteria.

In the Midterm concept trade-off, each concept was given a sustainability score which combined the concept's performance on each of the six sub-criteria. In this scoring, the selected Impactor concept scored second best, mainly due to its use of a reusable launch vehicle and recyclable alloys. However, the trade-off also indicated that many of the sustainability concerns would be difficult to legitimately address in the limited conceptual design of the mission. Therefore, the sustainable development strategy in this report will be to evaluate the sustainability of each subsystem, using the six sub-criteria. Based on the evaluation, recommendations for future sustainable design steps will be given.

5. Verification and Validation

In this chapter, the verification and validation procedure will be discussed. It is meant to provide a baseline for each subsystem engineer to consistently base their respective verification and validation on, as well as show the procedure undertaken to verify results. Subsystem specific verification and validation is documented in the respective sections of each subsystem.

5.1. Verification

The same procedure as in the Midterm Report [6] is used. Verification will be split in two categories, code and calculation verification. The following main important steps will be undertaken by each respective subsystem engineer to verify the code that has been used.

1. Verify code by solving syntax errors and checking for programming logic.
2. Verify calculations by performing code unit tests and larger system tests on a simplified problem with a known solution.
3. Check accuracy of the results
4. Document results

The verification procedure is broken down in a functional flow diagram which is displayed in Figure 5.1.

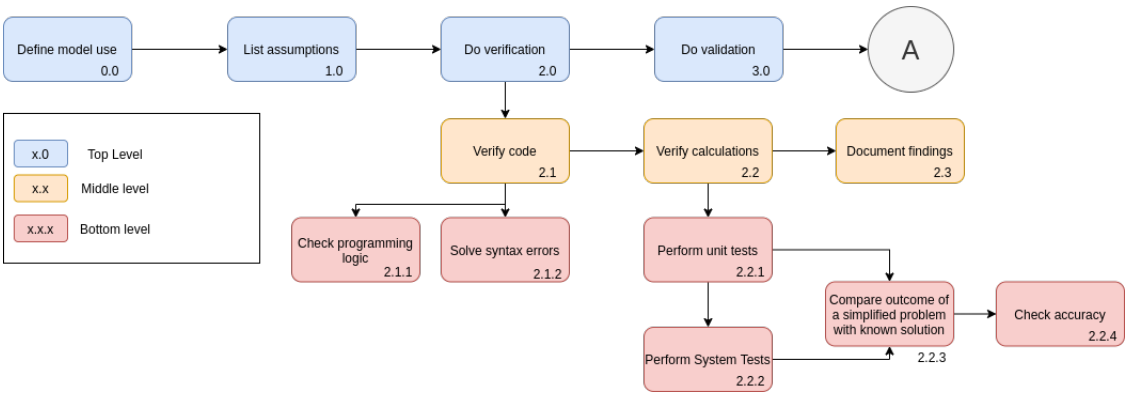

Figure 5.1: Verification functional flow diagram [6]

Specific tests and an explanation on these tests are discussed in Chapter 10 and Chapter 16 at the respective subsystem sections.

5.2. Validation

Similar to the Midterm Report [6], the following procedure is followed to validation. It must be done with the use of well validated software or a validation data set which resulted from a well defined test or measured outcomes. The validation process can be dissected in the following steps.

1. Data Acquisition
2. Testing the model with identical variables
3. Comparing the model to the acquired validation data
4. Determining errors
5. Model calibration

In the functional flow diagram in Figure 5.2, the validation procedure is displayed.

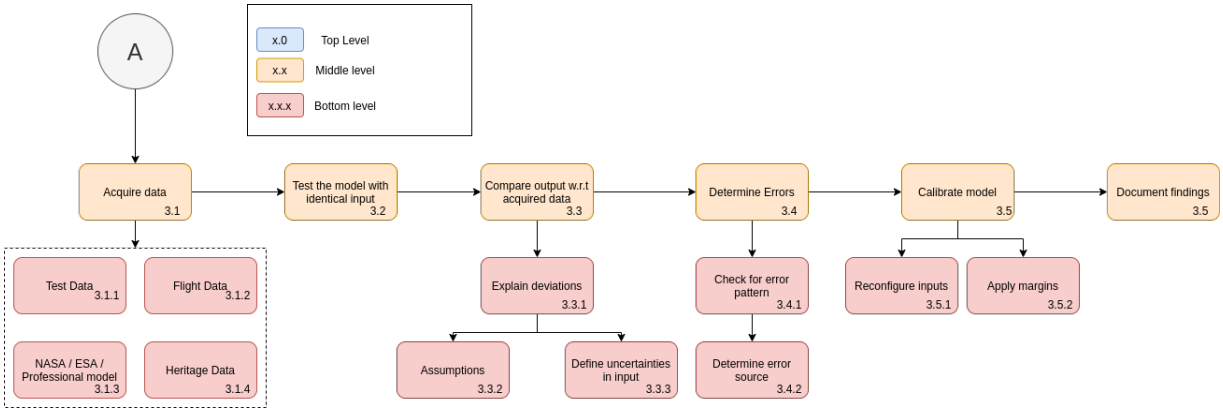

Figure 5.2: Validation flow diagram

When applicable, the specific steps undertaken to validate code is documented under the respective subsystem sections in Chapter 10 and Chapter 16.

Part II

Mission Design

6. Functionality

When addressing the complex design procedure, there are multiple tools used to assist this process. Functional analyses are one of these essential tools, which help analyse and create subsystem requirements. Once functions of systems are clear, these are distributed to their appropriate subsystems, which in turn results in requirements. Below, two ways of presenting results of functional analyses are given.

6.1. Functional Breakdown Structure

A functional breakdown structure (FBS) groups functions of the entire mission. This allows for an easier split between the subsystems. It is important to mention that only functions directly related to the design are presented, such as sustaining launch loads. Being launched is a function of the launcher and not of the design itself. The FBS is presented in Figure A.3.

6.2. Functional Flow Diagram

Similarly, the functional flow diagram represents the same information, but includes dependencies order and iteration loops in a chronological order. The FFD is presented in Figure A.1 and continued on Figure A.2.

7. Interfacing

Most of the interfaces will be mentioned throughout the description of the subsystems for landers and orbiter in Part III and IV respectively. When designing the lander subsystems, the N2 interfacing diagram in Figure A.4 was used to assist and ease the design flow. This diagram proved particularly useful, as it summarised physical interfaces between the subsystems, and provides and overview for the subsystem requirements.

Once the subsystem designs were completed, the interfaces and necessary software blocks were examined. The following diagrams will provide a clear overview of the software interactions necessary for a functional system. Moreover, as internal data rates for most of the components have been established when designing CD&H subsystem in Section 10.6 and Section 16.7, a software diagram which summarises these can be seen Figure 7.2 and Figure 7.1.

These figures should be read from top to bottom. For the orbiter, the software diagram is presented in Figure 7.1. First, the system will need to be initialized, which will happen after launch. This will activate all of the on-board sensors, which will create a steady data flow to the on-board storage, so that it can be prepared for relay to the ground stations.

For the impactor in Figure 7.2, the system starts by getting an initialization command from the orbiter at the point of separation. This will activate the appropriate sensors to compute attitude and altitude of the impactor, once it starts entering the Martian atmosphere. From these computations, commands to deploy the parachute, jettison backshell and detach heatshield can be given. These commands will need to be programmed in the on-board software. After the impact, scientific sensors and payload may be initialized, which marks the start of the scientific phase.

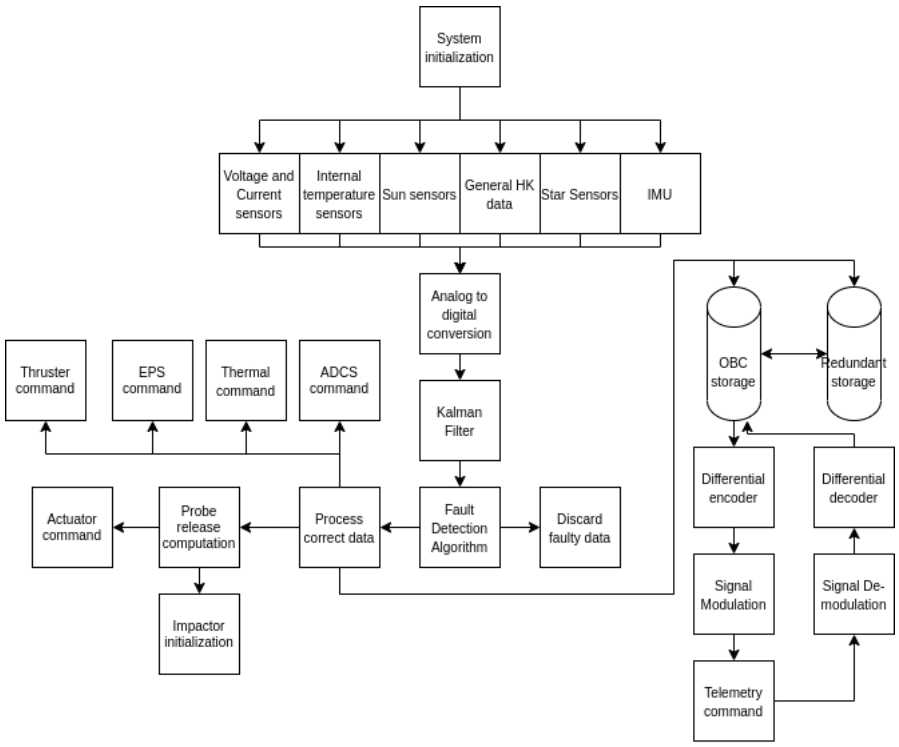

Figure 7.1: Software Diagram Orbiter

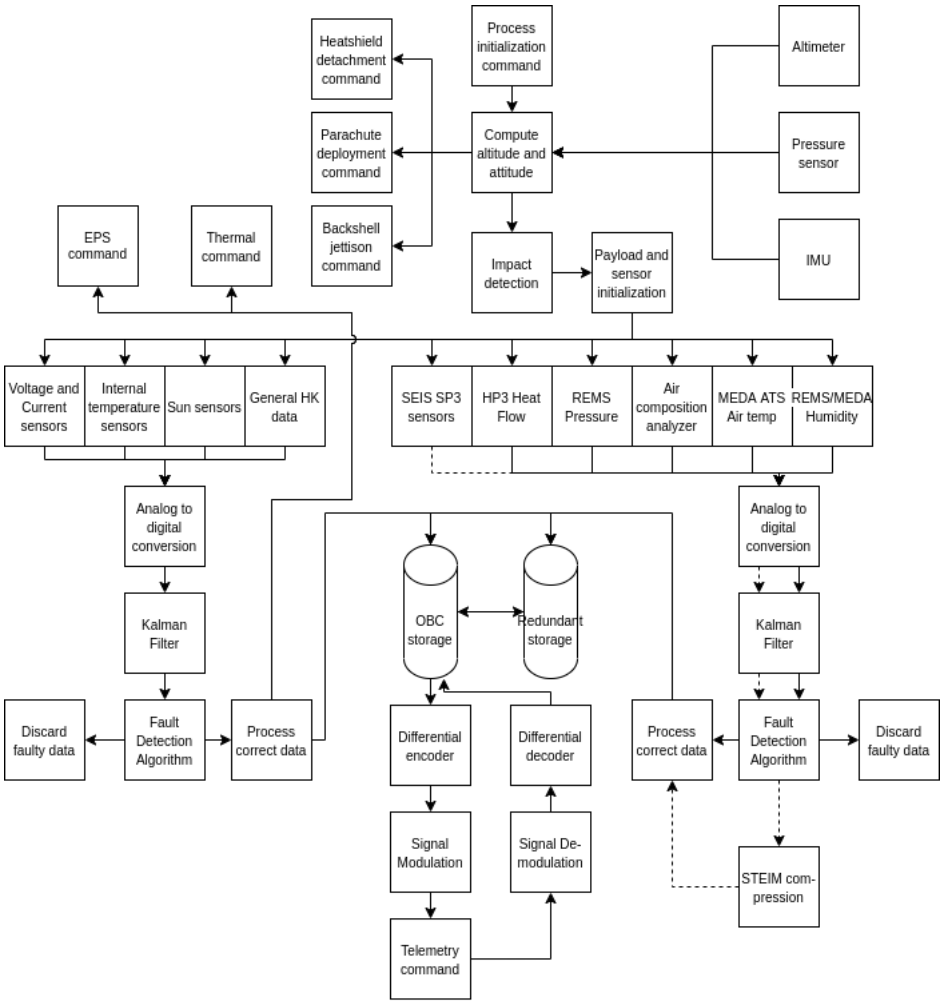

Figure 7.2: Software Diagram Impactor

Finally the hardware components can be interlinked and summarized in Figure 7.3. This diagram summarizes all the interactions between the available subsystems.

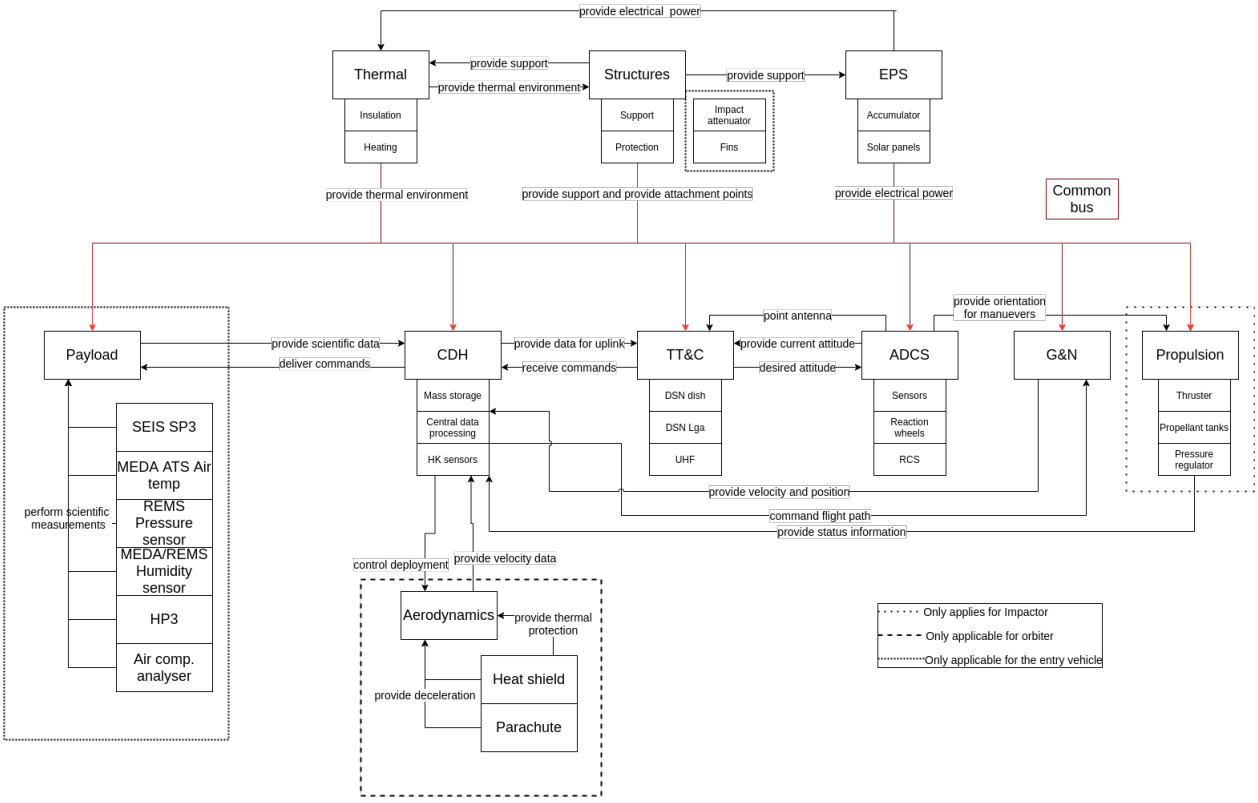

Figure 7.3: Hardware diagram of the lander, orbiter and entry vehicle

8. Astrodynamics

To reach Mars and deploy the landers successfully, astrodynamic modelling was required, which is presented in this chapter. Requirements related to astrodynamics are given in Table 8.1, after which the complete mission profile from launch to end-of-life is presented in the following sections.

Table 8.1: Requirements on astrodynamical mission characteristics

ID	*Requirement*	*Status*	*Origin*	*Compliance*
DMD-ASTRO-01	The launch vehicle shall inject the system into a Mars Transfer Orbit.	Active	-	Met
DMD-ASTRO-02	The probability of impact on Mars by any part of the launch vehicle shall be $\leq$ 1E-4 for a time period of 50 (Earth) years after launch.	Active	Planetary protection	Met
DMD-ASTRO-03	The Interplanetary Transfer Orbit shall ensure the system misses Mars for the first 130 (Earth) days.	Active	Planetary protection	Met
DMD-ASTRO-04	The Interplanetary Transfer Orbit shall ensure the system is headed towards the first landing site after the first 130 (Earth) days.	Active	Purpose of mission	Met

Continued on next page

Table 8.1 – continued from previous page

ID	*Requirement*	*Status*	*Origin*	*Compliance*
DMD-ASTRO-06	The Mars Arrival Hyperbola shall ensure all landing sites are reachable by the landers.	Active	Purpose of astrodynamics	Met
DMD-ASTRO-07	The Mars Arrival Hyperbola shall facilitate the the insertion into Initial Mars Orbit in a single manoeuvre.	Active	Purpose of astrodynamics	Met
DMD-ASTRO-08	The Initial Mars Orbit shall facilitate the adjustment of the argument of the ascending and descending node in a single manoeuvre.	Active	Purpose of astrodynamics	Met
DMD-ASTRO-09	The Secondary Mars Orbit shall facilitate the adjustment of the apoapsis in a single manoeuvre.	Active	Purpose of astrodynamics	Met
DMD-ASTRO-10	The final Low Mars Orbit is continuously sun lit.	Active	EPS	Met
DMD-ASTRO-11	The final Low Mars Orbit shall be sun-synchronous.	Active	EPS	Met

The astrodynamical profile of the mission can be divided in five common phases, explained in Section 8.1: Launch; Earth Parking Orbit (EPO); Interplanetary Transfer Orbit (ITO); Mars Arrival Hyperbola (MAH); and the Lander Release Sequence (LRS). From this point, the orbiter and landers are separated and follow their own mission profile. The orbiter will follow six additional phases, further discussed in Section 8.2: Divert Manoeuvre; Mars Orbit Injection (MOI) and Initial Mars Orbit (IMO); Secondary Mars Orbit (SMO); Low Mars Orbit (LMO); Operation; and End of Life (EOL). The profile of the lander consists of the following five phases explained in Section 8.3: Approach; Entry, Descent and Landing (EDL); Deployment; Operation; and EOL.

8.1. Pre-Release

Launch and Earth Parking Orbit

The first main function of the launch service provider is to put the orbiter and lander combination in a trajectory that will reach Mars. Traditionally, this is done by first achieving a low EPO after which the system is accelerated to escape velocity.

An estimated ΔV = 7.8 km/s needs to be provided by the launcher to reach a 500 km EPO from the equator. This was found by adding the orbital velocity vector to the gravity loss vector using the Pythagorean theorem. Relevant parameters are shown in Table 8.2. An additional ΔV = 3.62 km/s is needed from the launch provider to escape to Mars. Assuming Earth and Mars follow co-planar, circular orbits and using a Hohmann style transfer, the orbital parameters can be quantified in Table 8.2. For this transfer, C3 = 8.67 km^2/s^2 is required, which corresponds with the required ΔV at EPO.

Considering the total launch mass and volume, out of the considered launch service providers, the Falcon Heavy from SpaceX is the best suited launch vehicle, as was investigated in the Midterm Report [6]. [1]

Table 8.2: Orbital parameters EPO & ITO

Orbit	a	e	P	ΔV_{req} (km/s)
EPO	6871 km	0.0	1.58 hrs	7.8
ITO	1.26 AU	0.207	1.42 yrs	3.62

$$r = \frac{h^2}{\mu}\frac{1}{1+e\cos(\Theta)} \xrightarrow{\Theta=0^\circ} r_p = \frac{r_{release}^2 V_{tan}^2}{2\mu} \quad (8.1)$$

$$\text{as } h = rV_{tan} \text{ and where } V_{tan}^2 = V_X^2 + V_Y^2$$

Interplanetary Transfer Manoeuvres

After launch, several manoeuvres are planned. Their purpose and epochs are summarised in Table 8.3. The Course Correction (CC) manoeuvre's main function is to correct for errors or perturbations. CC1 aims the trajectory to miss Mars by some margin to comply with [DMD-ASTRO-02] and CC2 will aim the spacecraft towards the first landing site to simplify LRS.

[1] https://www.spacex.com/media/falcon_users_guide_042020.pdf, Accessed [21-06-2021]

The requirement on Planetary Protection, [DMD-ASTRO-02], can be shown to be able to be met [7]. However, exact calculations at this stage of the design process are not considered to be useful without further detailed design of the trajectory.

Table 8.3: List of Planned Course Corrections.

Manoeuvre	Time	Description
CC1	L+10 d	Correct for errors from transfer injection and aim for planetary protection.
CC2	L+130 d	Correct for errors from CC1 and aim for first landing site.
CC3	MOI-60 d	Correct for errors from CC2.
CC4	MOI-10 d	Correct for errors from CC3.
LRS	MOI-52 hrs	Release sequence of the lander probes.
MOI	MOI	Inject into Mars orbit.

Lander Release Sequence

8.5 months after launch, the spacecraft will arrive at Mars with an excess arrival velocity V_∞ = 2.65 km/s. Starting at practical infinity, once the orbiter has reached a distance to Mars of $r_{release} = 0.5 \times 10^6$ km, the release sequence starts. This figure was chosen keeping in mind the sphere of influence of Mars and the accuracy of ΔV changes the propulsion system can provide, this should however be further analysed in future stages of the design.

As each lander probe is unguided, it must be released already heading towards its landing site. To this end, the orbiter itself must target itself towards each of the landing sites and release the lander. After CC2, the orbiter already aims towards the first landing site to release the first set of landers. After releasing the first set of landers, the propulsion system is used to adjust the tangential velocity components V_X and V_Y. The orbiter now follows a new trajectory towards a new landing site to release the next set of landers. A schematic showing the trajectory of the orbiter-lander combination is shown in Figure 8.1. At this stage, a pair of entry capsules are released before the orbiter takes on a new trajectory.

Using the relation between true anomaly and orbital radius shown in Equation 8.1, V_X and V_Y can be directly related to the periapsis distance r_p. If this distance is assumed to be the target distance r_{max} and r_{MOI}, it now is a function of the controllable velocities.

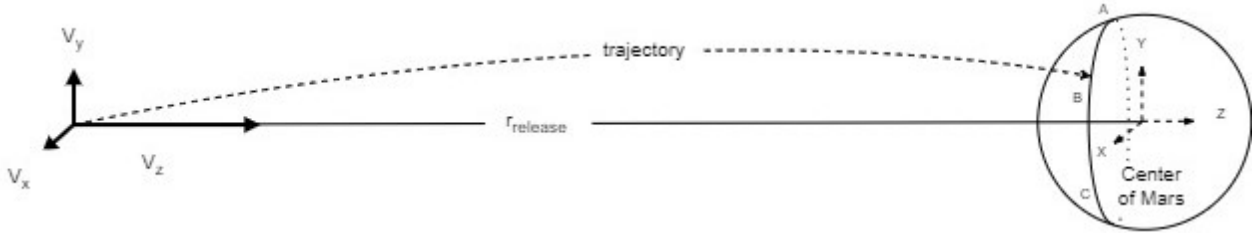

Figure 8.1: Schematic of the targeting method of the orbiter. (Side view)

To estimate the amount of ΔV needed for the LRS, the worst case scenario is chosen. This happens when the five landing zones A through E are furthest away from each other as shown on the left of Figure 8.2. MOI is also positioned furthest away from any landing zone at LMO orbital radius from Mars, further discussed in Section 8.2. The distance between landing zones can then be expressed as a ΔV increment, or the effort needed to change the trajectory of the orbiter from one target to the next. By 'walking' from zone to zone, releasing a pair of landers at every target, the ΔV increments can be added to yield a total ΔV estimate.

The middle schematic in Figure 8.2, shows how these ΔV increments are calculated. The first increment is from A to B. From the figure, it can be seen that vector addition leads to Equation 8.2 and due to point symmetry and for the present configuration, it holds that $\Delta V_{A\to B} = \Delta V_{B\to C} = \Delta V_{C\to D} = \Delta V_{D\to E} = 40.65$ m/s.

$$\Delta V_{A\to B} = V_{tan}(r_{max}) \sqrt{\cos^2(18°) + (1 - \sin(18°))^2} \tag{8.2}$$

Besides these increments, an additional 100 m/s is reserved to increment V_Z to change the coast time and make use of Mars' rotation to allow for the spread of the entry capsules released towards the same target point. This is enough to delay the time of arrival of the landers by almost two hours. This corresponds to Mars Drift of 25°. This figure was found using Kepler's Laws of Planetary Motion to find the time-to-periapsis from $r_{release}$.

The minimum and maximum reachable radii, r_{min} and r_{max}, are determined by the entry angle, which is restricted by requirement [DMD-EDL-05] from Section 16.1, which states that the minimum and maximum entry

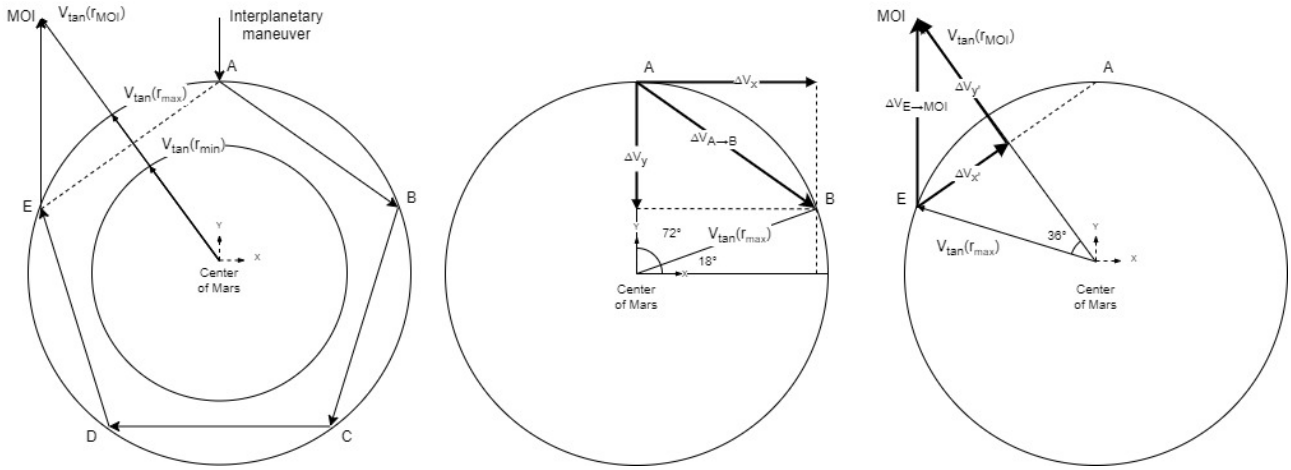

Figure 8.2: ΔV worst-case calculation schematic. (Spacecraft point of view)

angle, $\gamma_{max,min}$, are –12° and –18°, respectively. This results in the minimum and maximum radii, $r_{min,max}$, of 78° and 72°. By assuming the trajectory to be straight, from the left of Figure 8.3 it can be seen that the radii can be expressed as $r_{min,max} = r_{atm}\cos(\gamma_{max,min})$ where r_{atm} is the atmospheric radius. This results in a reachable range d_{entry} through the difference in entry location. On the right of the figure, taking into account the Down Range Distance (DRD) of each entry angle and the rotation of Mars due to different arrival times (Mars Drift), this results in a total reachable range $d_{landing}$. All landing zones must fall within this $d_{landing}$ along some axis on Mars, which is free to choose. This realisation becomes important in choosing landing locations in Chapter 14.

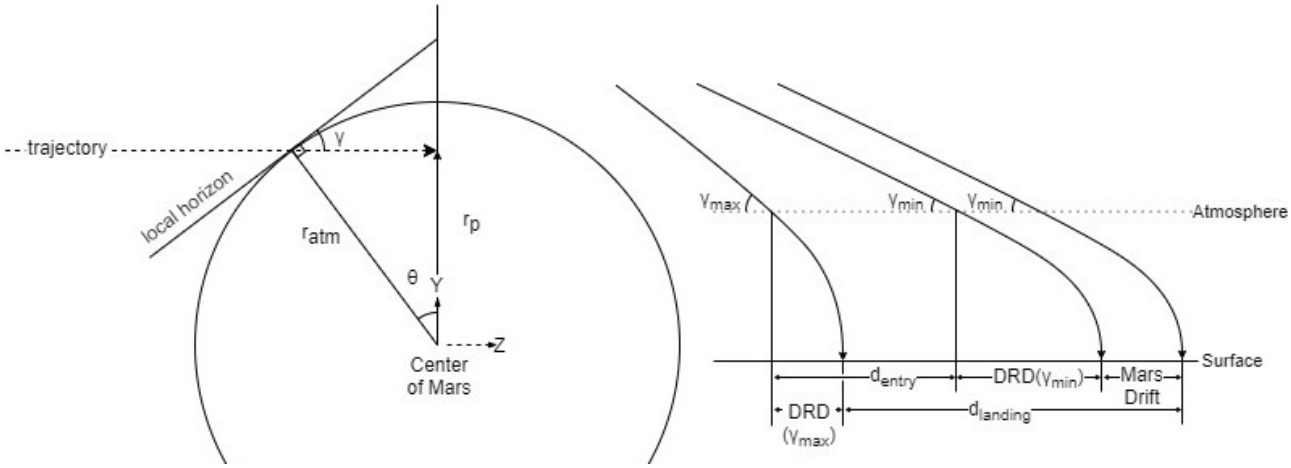

Figure 8.3: Entry angle constraints. (Side view)

8.2. Orbiter Post-Release

Divert and Mars Orbit Injection

After the LRS, the orbiter must divert to not impact Mars. In a similar fashion as in Equation 8.2, it can be seen on the right of Figure 8.2 that the divert manoeuvre budget can be estimated through vector addition shown in Equation 8.3 which results in ΔV_{divert} = 54.3 m/s. The orbiter coasts towards the periapsis to perform the MOI manoeuvre.

$$\Delta V_{E\rightarrow MOI} = \Delta V_{divert} = \sqrt{\left(V_{tan}(r_{max})\sin(36°)\right)^2 + \left(V_{tan}(r_{MOI}) - V_{tan}(r_{max})\cos(36°)\right)^2} \tag{8.3}$$

This manoeuvre will take 1.00 km/s. This was chosen to enter a highly elliptical orbit. This is favourable as at apoapsis, the ΔV needed to correct for angle changes is relatively low. Preferably, a more elliptical orbit would be chosen, but keeping in mind an orbital period of 204.3 hrs, this was deemed sufficient. The properties of both the MAH and IMO are listed below in Table 8.4. These figures were found using Kepler's Laws of Planetary Motion.

Table 8.5 shows the properties of the final two orbits. First, the SMO serves to allow for cheap change of orbital parameters as it brings the spacecraft far away from the planet. Together with the choice of MOI location, the right ascension of the ascending node and inclination can be adjusted to be able to reach the required LMO from any MAH with the ΔV figures provided. This should be investigated further, but the ΔV budget will be sufficient in any case.

Table 8.4: Orbital parameters MAH & IMO.

Orbit	a [km]	e [-]	P [hrs]	ΔV_{req} [km/s]
MAH	-6593.5	1.8	-	-
IMO	83710	0.91	204.3	1.00

Table 8.5: Orbital parameters SMO & LMO.

Orbit	a [km]	e [-]	P [hrs]	ΔV_{req} [km/s]
SMO	83710	0.91	204.3	0.221
LMO	7674.6	0.0	5.67	0.901

Low Mars Orbit

Finally, LMO will be reached. It will be a continuously sun-lit orbit with the parameters mentioned above in Table 8.5. The LMO design was limited by two main requirements: [DMD-EPS-O-08] which mandates the orbiter is sun-lit and the TTC requirements which mark the need to optimize for contact time.

Sun-lit

Several parameters of the LMO are clear from the start. The line connecting the argument of the ascending and descending node is perpendicular to the direction to the Sun. Furthermore, [DMD-EPS-O-08] indicates the orbiter needs to stay out of the umbra of Mars throughout its orbit around Mars, but also throughout the orbit of Mars around the Sun. As the J2 perturbation is centered around the rotational axis of the planet, this means seasonal change have to be taken into account in the design of the LMO. For Mars, this means a solar declination anywhere between $-25.2° \leq \delta \leq 25.2°$ should not cause an eclipse.[2] Figure 8.4 shows the eclipse limits of various semi-major axis and inclination combinations.

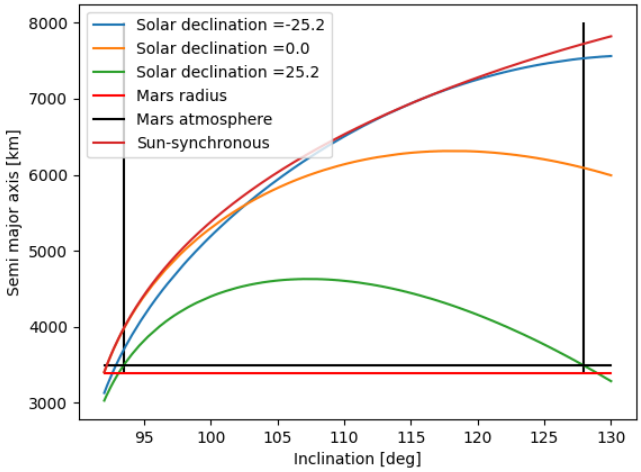

Figure 8.4: Limitations for selection of orbit

Contact Time

Once the orbit limitations were set, the final orbit was optimized for several parameters of interest: contact time and frequency of contacts with the probes. As per EPS requirement [DMD-EPS-L-08], all the landers would be located within a +- 35° band around the equator. As no orbiters would be on higher altitudes, it would be logical to limit the ground track of the orbit to the band of the interest. For a sun synchronous orbit with inclination above 90°, the maximum altitude of ground track is (180-inclination)°. As visible from Figure 8.4, the maximum possible inclination is 127.95°, which result in maximum altitude of 52.06°, which is already higher than ideally desired.

Finally, the inclination had to be lowered in order to accommodate for a reasonable repeat orbit period. To compute possible repeat orbits, the following was required: orbital angular velocity n, the planet's angular velocity $\dot{\Omega}_T$, nodal precession $\dot{\Omega}$ [8, p. 192], apsidal precession $\dot{\omega}$ [8, p. 192] and mean motion n_d [8, p. 204]. Finally, the orbital recurrence frequency k could be computed [8, p. 265]. The recurrence frequency takes into account the orbit's inclination, direction of planet's rotation and J2 perturbation. In order to get a repeat orbit, orbital parameters had to be adjusted so that recurrence frequency becomes a whole number, every X required number of days.

As a result, the orbit was lowered from a maximum possible sun-lit inclination of 127.96° to 126.98 °, with a three days orbital repeat time, during which the orbiter will perform thirteen revolutions around the planet. The ground track of these revolutions is presented on the Mercator map shown in Figure 8.5. By definition of a ground repeat orbit, the provided pattern will repeat in exactly thirteen orbits, or three sols [8, p. 293]. Red dotted lines represent the maximum possible lander latitude, and red dots represent planned lander locations, which will be detailed in Chapter 14. It is important to mention that the orbit was kept perfectly circular, as no clear advantage of highly a elliptical orbit was found, while keeping eccentricity zero greatly simplifies the calculation process.

[2] https://nssdc.gsfc.nasa.gov/planetary/factsheet/marsfact.html, Accessed [21-06-2021]

Finally, the idealized contact time was computed, from an assumption that the orbit passes exactly on top of the lander. A maximum elevation above the horizon of 20° was taken for the landers, as even though isotropic antennas will be used (described in detail in Section 16.6), there is uncertainty of landing angles. The idealized contact time is then computed as visibility time from the fraction of total orbital time by using basic trigonometric relations. The orbital parameters are summarised in Table 8.6.

Special attention was paid to contact time calculation, as the number presented in Table 8.6 is an idealized value, assuming the satellite passes exactly on top of the lander. In reality however, this of course will never be the case, and thus actual contact time will be lower. On the other hand, as visible in Figure 8.5, multiple orbital ground tracks surround each of the landers. Due to relative high view angle of 140° (180° minus 20° above horizon limitation from each side), as well as high orbital altitude, the visibility range of the satellite is very high. Although it proved to be difficult to construct a graphical visibility map, it was clear that actual contact times are much higher, due to the satellite connecting to the same lander over multiple passes. As a result, even though an idealized time estimate is not a real time representative, it is a very good approximation for the minimum possible contact time, as in reality, it will be higher.

a [km]	**height [km]**	**e [-]**	**inclination [deg]**	T_{orbit} **[min]**	$T_{contact}$ [min]
7674.6	4285.6	0	126.98	340.95	86.15

Table 8.6: Final orbit's parameters

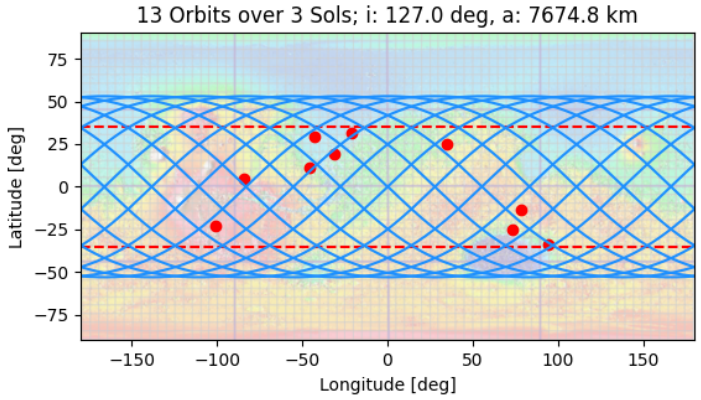

Figure 8.5: Ground track of the selected orbit and planned landers' locations

End of Life

At the end of the mission, the orbiter performs an EOL maneuver where the orbit periapsis is lowered to the surface of Mars. By letting the orbiter descend through the atmosphere and burn up, no space debris is left after the mission's end which is necessary to comply with [DMD-SUST-PT-01] and [DMD-SUST-PT-02].

This manoeuvre will take an approximate 513 m/s of ΔV. It could be argued this figure is higher than needed as it is only necessary to lower the orbit to ensure atmospheric entry and not all the way to the surface. However, considering the uncertainties in the atmosphere of Mars and the strict requirement to guarantee safe entry, this consideration was chosen.

8.3. Lander Post-Release

After LRS, each individual lander will take between 48 and 52 hrs to reach Mars. At each targeting point of the LRS, two landers are released, with a time delay. The delay is necessary to allow for the spread of landers in the deployment zones as stated in [DMD-PERF-BROOT-11]. The selection of the landing sites is closely related to LRS, yet it is highly dependent on scientific considerations as well. Therefore, it is explained in Chapter 14, before the design of the lander itself. At 100 km above the Martian surface, the EDL sequence starts, which will be explained further in Section 16.1.

Part III

Orbiter Design

9. System Characteristics

This chapter summarises general characteristics of the design of the orbiter. Additionally, it provides the orbiter's configuration overview and layout of internal and external components, as well as the orientation of the spacecraft in Martian orbit in Section 9.1. The mass, data rates, and power budgets presented in Section 9.2 are a summary of the detailed and iterative design process. The details of this design process, as well as origin of these numbers, may be found in the respective subsystem sections in Chapter 10.

9.1. Configuration

The configuration of the orbiter at launch and during capsule separation can be seen in Figures 9.1-9.2. The orbiter bus is a long and slender cylinder, around which two rows of 5 entry capsules are connected. In the middle of the cylinder, the parabolic antenna dish, 2 UHF patch antennas and the solar panel are attached. In total, 4 pairs of RCS thrusters and 2 low gain isotropic antennas are placed on the top and bottom of the orbiter. As can be seen in Figure 9.4, the orbiter has a constant orientation with respect to Mars. This allows the solar panel and UHF antennas to be stationary and always pointing towards the Sun and Mars, respectively. The antenna dish always points in the general direction of Earth, but needs to be able to rotate at most 30° around two axes, in order to have accurate pointing. During launch, the orbiter is connected to Falcon Heavy with a truncated conical launch vehicle adapter.

Figure 9.1: The orbiter's configuration at launch

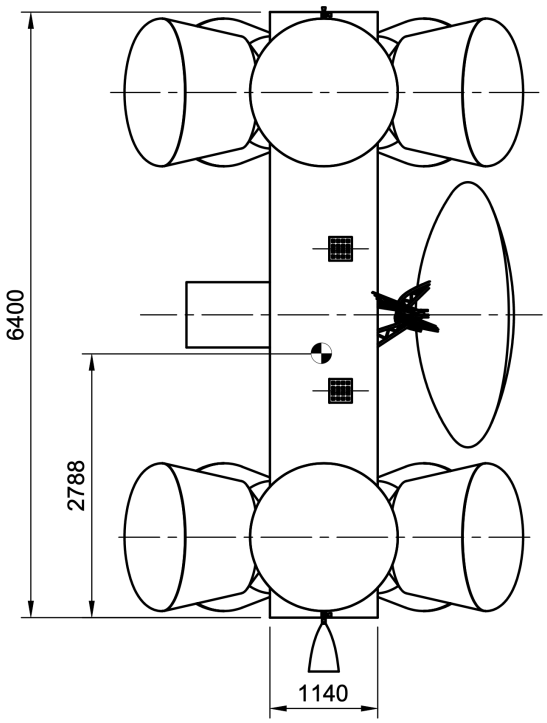

Figure 9.2: Overview of the orbiter's general dimensions. The CoG of the launch configuration can be seen as well. For a detailed overview of the relevant dimensions, please refer to Figure C.1 in Appendix C.

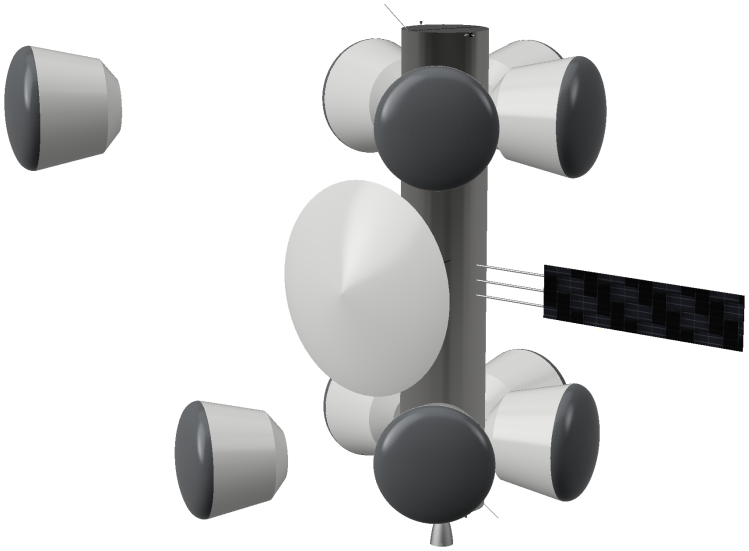

Figure 9.3: The orbiter's configuration during entry capsule separation

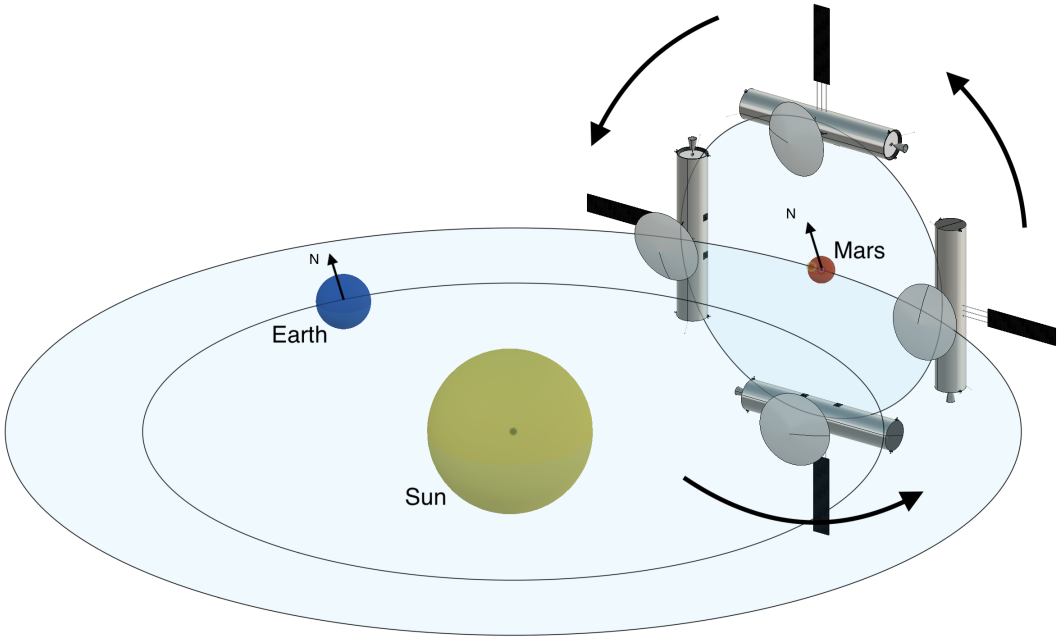

Figure 9.4: Simplified view of the orbiter in orbit around mars (not to scale). North is up.

In Figure 9.5, an overview of the orbiter's subsystem layout can be seen. As the bus is very slender, the two propellant tanks and Helium tanks are placed on top of each other, on top of the propulsion system, followed by the ADCS system (electronics, reaction wheels) and the remaining subsystems. In Figure 9.6, a more detailed overview of these subsystems can be seen. A large part of the orbiter is empty. This extra length is needed to be able to attach all entry capsule to the bus, without interfering with other components, such as the antennas. This opens up the opportunity for taking along payloads from external clients such as the novel rover from Team Tumbleweed.[1] The additional structural weight would be negligible compared to the total launch weight. Finally, a technical drawing of the orbiter can be seen in Figure C.1.

[1] https://www.teamtumbleweed.eu/our-rover/, Accessed [22-06-2021]

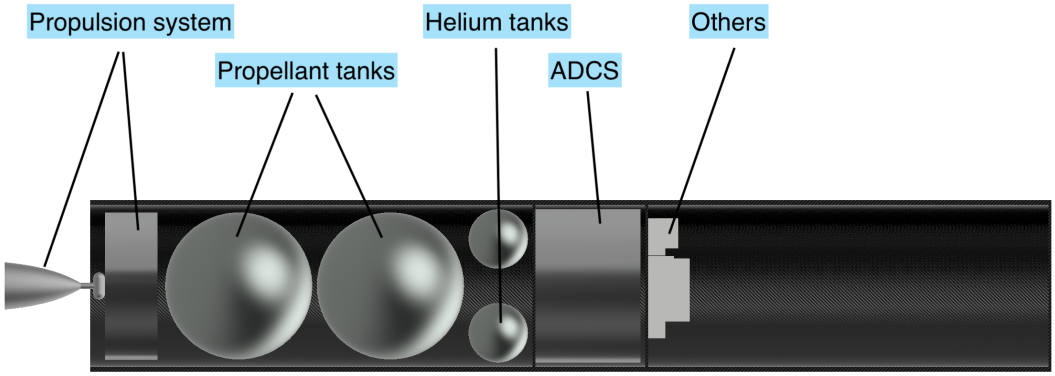

Figure 9.5: Overview of the orbiter's subsystems

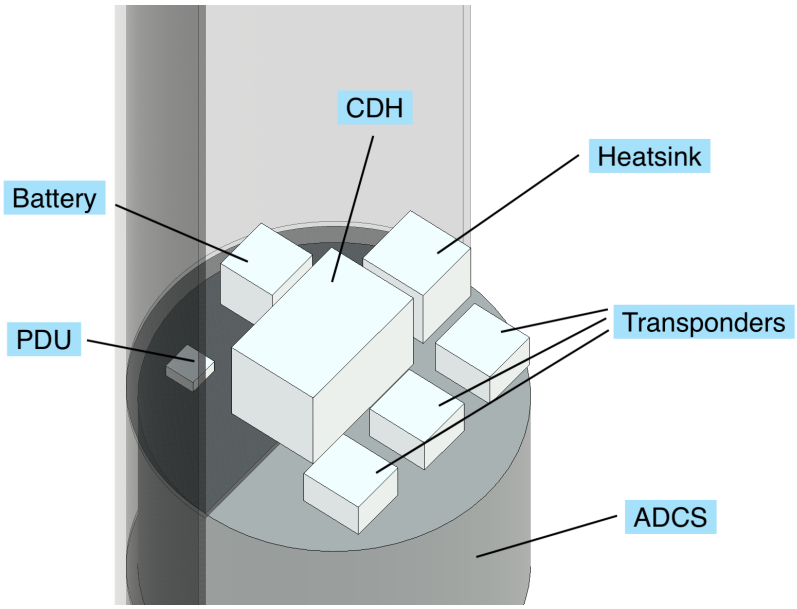

Figure 9.6: Overview of the orbiter's subsystems

9.2. Budgets

In this section, the budgets for the orbiter are presented. The budgets are a summation of the designed subsystem characteristics. This chapter includes the power budget in Table 9.1, mass budget in Table 9.2, internal data rate and ΔV budget in Table 9.3. The following subsystem chapters of the orbiter will be providing the calculations for these budgets. The link budget table of the orbiter, Table 10.17, can be found in Section 10.5.

In the power budget table, a differentiation is made between nominal operations and pre-nominal operations. The pre-nominal operations, depicted in red, result in the necessary amount of energy the battery should be able to provide in the time between launch and operational solar arrays. In black, the nominal operation budgets have been depicted.

Table 9.1: Orbiter power budget with nominal operations in black and pre-nominal operations in red

Subsystem		Nominal power use [W]	Additional peak power [W]	Peak power duration [s/sol]
ADCS		132.3	410.1	4392
CDH				
	OBC	40	20	1700
	Mass storage	0.275	0.34	1700
EPS				
	Distribution system	2.24		
	Deployment		20	60
Payload		7.9	26.1	300
Propulsion				
	Thrusters		35	-
	Tanks/Lines		151.41	-
Thermal		45.22		
TTC				
	DSN dish		60	17755
	DSN LGA		2.5	26632
	UHF		15	62142
Total power:		225.7W	740.5W	-
Total Energy per sol:		5.566kWh	1.09kWh	-
Total Energy required before nominal operations:			0.00033kWh	

Table 9.2: Orbiter Mass Budget

Subsystem		Mass [kg]
ADCS		58.3
CDH		
	OBC	16
	Mass storage	1.45
EPS		
	Distribution system	0.24
	Solar Array	7.1
	Battery	14.4
Structures		46.48
Payload	10 Landers	2901
Propulsion		
	Thrusters	4.3
	Tanks/Lines	133.44
	Propellant	1063.94
Thermal		42.96
TTC		
	DSN dish	50
	DSN Lga	0.3
	UHF	5
Total Mass:		4344.9

Table 9.3: Orbiter ΔV budget

Phase		ΔV [m/s]
Release		262.58
MOI		
	Divert	52.261
	MOI	1000
	Correction	221.7
	Circularisation	901
EOL		513.3
CC		
	SF - 5%	147.64
OM		
	SF - 5%, ESA guideline	147.64
Total ΔV:		3248.2

Table 9.4: Orbiter internal data rate budget

Sensor	Amount [-]	Resolution [bits]	Sampling Frequency [Hz]	Data rate [bit/s]
ADCS				
Star sensors	2	8	10	160
Sun senors	6	8	5	240
IMU	1	8	400	3200
Thermal				
Temperature sensors	25	8	0.2	40
EPS				
Current Sensors	6	8	1	48
Voltage Sensors	6	8	1	48
Propulsion				
Thruster	1	16	100	1600
Pressure transducer	6	16	10	960

10. Design Process

In this chapter, the design process of the orbiter is documented. After the trajectory to Mars was computed in Chapter 8, the orbiter can be sized accordingly. First of all, the payload for the orbiter is defined as the ten landers which will be further discussed in Part IV. To accommodate for the payload and launch, a structure has been designed first, this is discussed in Section 10.2. In order to control the orbiter once in orbit, a control system is required, detailed in Section 10.3. The attitude control system will need guidance and navigation in order to ensure a correct trajectory, this is discussed in Section 10.4. To communicate the trajectory and control sequences to ground control, the orbiter uses the communication subsystem, presented in Section 10.5. In order for the data processing to take place, and for the commands to be properly received, a command and data handling subsystem must be designed. This is discussed in Section 10.6. In order for the aforementioned systems to function, an electrical power system must be present, this is designed and discussed in Section 10.7. Finally the orbiter must remain within an operational temperature to function nominally, this is achieved by the thermal subsystem which is discussed in Section 10.8.

Based on the budgets and preliminary calculations made in the Midterm Report [6], each subsystem engineer designed their respective subsystem further to meet the set requirements. A bottom-up design route was chosen for this project due to the limiting scientific requirements on the payload. The bottom-up design started with the scientific payload on Mars and required this to be finalized. The lander system was then designed around this, after which the orbiter could be designed based on the impactor design.

Before each iteration, all subsystem engineers adjusted and updated the values and performed the design process that will be discussed in the following sections. After these values were discussed and adjusted, the following iterative process from Figure 10.1 commenced, based on the N2 chart in Figure A.4, to converge to a consistent orbiter design.

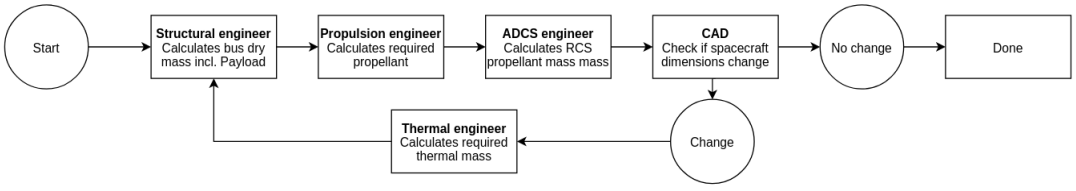

Figure 10.1: Iterative process for the orbiter design

After weekly iterations of each engineer updating and adjusting subsystem values a final design was settled upon. The following graph shows the results of the main spacecraft after each iteration.

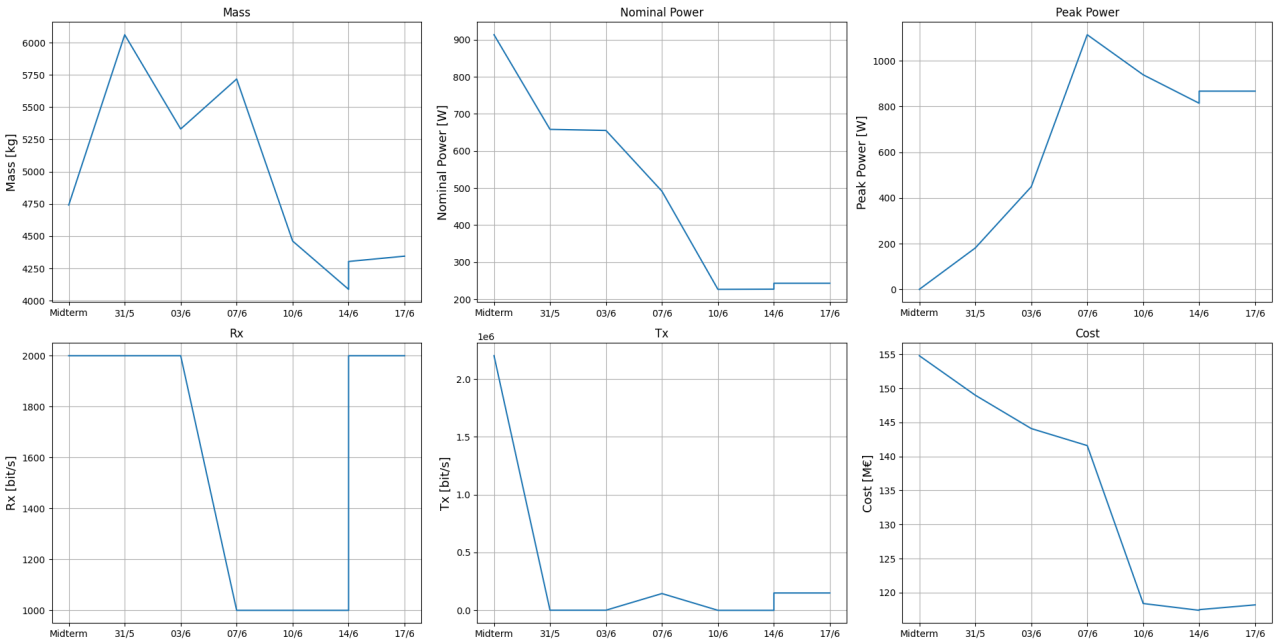

Figure 10.2: Orbiter iterations of main design budgets

10.1. Payload

The payload which will be carried by the orbiter consists of the 10 impactors in their entry capsules, with a total weight of 2901 kg. The origin for this number can be found in Part IV.

10.2. Structure

In this section, the design of the orbiter's structure will be presented. First, an overview of the subsystem requirements is given, followed by the design process. Then, the verification and validation method is presented, followed by an overview of the system performance and characteristics. Finally, some recommendations for future developments will be given.

Requirements

Table 10.1: Requirements on the orbiter's structures subsystem.

ID	*Requirement*	*Status*	*Origin*	*Compliance*
DMD-STRUC-O-01	The structures subsystem shall be able to support all orbiter subsystems.	Active	Purpose of structures subsystem	Met
DMD-STRUC-O-02	The structures subsystem shall be able to shield the orbiter's electronic subsystems from radiation.	Active	Subsytem specifications	N.V.
DMD-STRUC-O-03	The structures subsystem shall be able to support all lander systems.	Active	Launch configuration	Met
DMD-STRUC-O-04	The structures subsystem shall be able to deploy all lander systems.	Active	Launch configuration	Met
DMD-STRUC-O-05	The structures subsystem shall be able to withstand longitudinal launch vibrations of <tbd> Hz.	Active	Launch vehicle specifications	N.V.
DMD-STRUC-O-06	The structures subsystem shall be able to withstand lateral launch vibrations of <tbd> Hz.	Active	Launch vehicle specifications	N.V.

Continued on next page

Table 10.1 – continued from previous page

ID	*Requirement*	*Status*	*Origin*	*Compliance*
DMD-STRUC-O-07	The structures subsystem shall be able to withstand longitudinal propulsion system engine vibrations of <tbd> Hz.	Active	Propulsion system specifications	N.V.
DMD-STRUC-O-08	The structures subsystem shall be able to withstand lateral propulsion system engine vibrations vibrations of <tbd> Hz.	Active	Propulsion system specifications	N.V.
DMD-STRUC-O-09	The structures subsystem shall be able to withstand a maximum longitudinal launch acceleration of 6 g.	Active	Propulsion system specifications [3]	Met
DMD-STRUC-O-10	The structures subsystem shall be able to withstand a maximum lateral launch acceleration of 2 g.	Active	Launch vehicle specifications [3]	Met
DMD-STRUC-O-11	The structures subsystem shall be able to withstand the operational temperatures of <tbd>.	Active	Launch vehicle specifications	N.V.
DMD-STRUC-O-12	The structures subsystem shall have a maximum mass of 47 kg.	Active	Mass budget	Met
DMD-STRUC-O-13	The structures subsystem shall be able to withstand the Martian radiation.	Active	Material specifications	N.V.
DMD-STRUC-O-14	The structures subsystem shall have at least 4 attachment points for each entry capsule.	New	Launch configuration	Met

Design Process

The orbiter was chosen to be a singular cylindrical tube, as this was deemed to be the most efficient shape for both the structural integrity and the compatibility with the launch vehicle fairing. The orbiter has a length of 6.4 m, and an outer diameter of 1.14 m. It is made of a cylindrical shell and 3 plates. Each of the plates are made of a Carbon Fiber - Nomex Honeycomb (CFNH) sandwich, of which the properties are shown in Table 10.2. During launch, the orbiter will need to endure static axial and lateral accelerations of $a_{ax} = 6$ g and $a_{lat} = 2$ g, respectively. A safety factor of SF = 2 is applied to both accelerations.

	E-Modulus (GPa)	**Tensile Strength [MPa]**	**Compressive Strength [MPa]**	**Density [kg/m3]**
Carbon fiber fabric + Epoxy ($V_f = 0.5$)[1]	70	600	570	1600
Nomex Homeycomb[2]	ignored	N/A	1.15	32

Table 10.2: Relevant material properties of the orbiter's structure.

Cylindrical shell

The critical load case of the cylindrical shell of the orbiter is the compressive load on the carbon fiber skin. For this, both axial compression and bending stresses are investigated. The carbon fiber skin is assumed to bear all compressive loads and the horizontal plates are assumed to have no significant effect on the bending stresses of the shell. The Nomex honeycomb core is thus ignored in all calculations. The maximum compressive stress caused by the axial launch accelerations is calculated using Equation 10.1, where m_{tot} is the total mass of the orbiter, including all lander capsules, and A is the cross-sectional area of only the carbon fiber skin. The maximum compressive stress due to the bending loads caused by the lateral launch accelerations can be calculated using Equation 10.2, where M_{max} is the maximum internal moment in the walls, i.e. at the bottom, and I is the second moment of area of only the carbon fiber skin. A safety factor of 2 is applied to both accelerations.

[1] fabrichttp://www.performance-composites.com/carbonfibre/mechanicalproperties_2.asp, Accessed [17-06-2021]
[2] https://www.honeycombpanels.eu/en/products/honeycomb/nomex-aeronautical-grade-en, Accesssed [17-06-2021]

$$\sigma = \frac{F_{max}}{A} = \frac{SF \cdot m_{tot} \cdot a_{ax}}{A} \quad (10.1) \qquad \sigma = \frac{M_{max}}{I} \quad (10.2)$$

The resulting compressive stresses due to the load as well as the allowable compressive stress for the orbiter, with a 1 mm thick carbon fiber skin, can be seen in Table 10.3. A graphical representation of the bending loads can be seen in Figure 10.3. This figure also shows the internal shear forces caused by the lateral launch accelerations.

	Maximum endured compressive stress [MPa]	**Allowable stress [MPa]**
Axial load	129	-
Bending	409	-
Total	538	570

Table 10.3: Internal compressive stresses in the orbiter due to axial and bending loads.

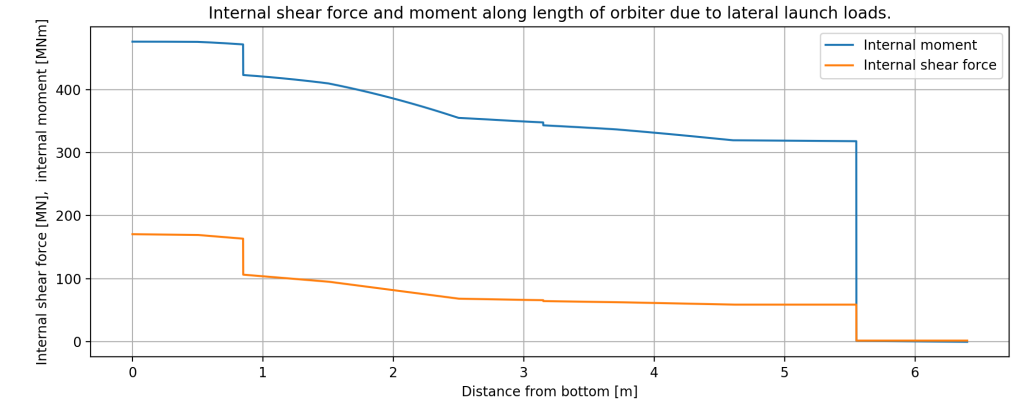

Figure 10.3: Internal shear forces and moment in the orbiter caused by the lateral launch accelerations.

To prevent buckling and to ease the attaching of the subsystems such as the propellant tanks, a 30 mm thick Nomex honeycomb core is used in the sandwich panel. A margin of 50% is applied to the total mass to account for local stiffening and subsystem attachment points. This results in a cylindrical shell mass of 24 kg.

Plates

The orbiter uses three plates that separate the different sections of the bus and support some of the subsystems. Each plate can be idealised as a circular plate that is clamped around its circumference and is acted upon by a uniformly distributed load. This load is easily found by multiplying the mass of the supported components by the longitudinal launch acceleration, again including a safety factor of 2, and dividing by the area of the plate. The critical load case that is evaluated for the orbiter is bending. The maximum bending stress σ and deflection w of a plate with radius R, thickness t, Young's modulus E and pressure load p can be calculated using Equation 10.3 and Equation 10.4, where the flexural rigidity D can be found using Equation 10.5.[3]

$$\sigma = 0.75 p R^2/t \quad (10.3) \qquad w = \frac{pR^4}{64D} \quad (10.4) \qquad D = \frac{Et^3}{12(1-\nu^2)} \quad (10.5)$$

Just like the shell, each plate is made of a CFNH sandwich panel. The Young's modulus of the plate can be calculated using the classical laminate plate theory, where the Young's modulus of the honeycomb is assumed to be zero, as the honeycomb carries negligible bending load. For this, a Microsoft Excel tool is used, made by ESP Composites.[4] With this tool, the Young's modulus can be calculated by orienting plies. To prevent over-complication and to achieve semiisotropy, the carbon fiber has been equally distributed over eight directions. Additionally, compression of each of the plates is evaluated in order to find the required honeycomb strength.

Capsule attachments

In order to safely attach the entry capsules to the orbiter, four attachment points will be used per capsule. A total of 2 kg per lander will be allocated for this in the mass budget.

[3] http://freeit.free.fr/Case,Chilver,Ross_Strength_of_Materials&Structures,1999/19206_19.pdf, Accessed [14-06-2021]
[4] https://www.espcomposites.com/software/download.html, Accessed [14-06-2021]

Verification & Validation

For the structural design of the orbiter, Excel, Python and manual calculations were used. Calculations in Excel and Python are verified by performing manual calculations. A comparison of several values computed by these tools and their manually calculated counterparts can be seen in Table 10.4.

Python code verification is performed using the procedure explained in Chapter 5. The tools have been checked on correct programming logic and do not give any syntax errors.

Table 10.4: Calculation verification results

Equation	Input	Output tool	Output hand calculation	Error[-]
Moment equation: M_{max}	Table 9.2, Section 9.1	475.77 MNm	475.55 MNm	0%
Equation 10.3: top plate	Table 10.6	216.181 kPa	216.102 kPa	<0.1%

System Performance and Characteristics

A brief overview of the orbiter's structural elements is presented in Table 10.5. A more detailed overview of the plates can be seen in Table 10.6.

	Mass [kg]	Material
Shell	24	Carbon fiber - Nomex honeycomb
Plates	2.84	Carbon fiber - Nomex honeycomb
Attachments	20	N.A.

Table 10.5: Overview of orbiter's structural elements.

	Supported subsystems	Supported mass [kg]	Total thickness [mm]	Plate mass [kg]
Top plate	N.A.	0	10.3	0.65
Middle plate	EPS (excl. solar array), CDH, TTC (exl. antennas), Thermal	76.35	14.6	1.13
Bottom plate	ADCS	58.3	12.6	1.06

Table 10.6: Detailed overview of the orbiter's structural plates.

Recommendations

Recommendations can be made for future development of the orbiter's structure. First of all, several requirements could not be verified at this stage of the design, such as those related to the launch and propulsion system vibrations. The radiation resistance and thermal requirements should be investigated further as well. Second, 2 kg of attachment structures per lander has been assumed as a conservative estimate. However, detailed design of these attachments may result in an increase or decrease of weight. Additionally, while utilizing CFNH panels results in an extremely light orbiter structure, it results in a more complex production and attachment method. Therefore, it is recommended to look into conventional materials as well, such as metal isogrids. Finally, as mentioned in Section 9.1, the orbiter has a significant amount of unused volume. This is due to the extra length required to attach all entry capsules. This volume can be used to accommodate additional payload, such as scientific instruments, in order to increase the scientific return of the mission. Alternatively, if the propellant tanks and ADCS subsystem are adjusted accordingly, the space can be used to store and deploy cubesats or a smaller version of a so-called "Tumbleweed" lander.[5]

[5]https://www.teamtumbleweed.eu, Accessed [22-06-2021]

10.3. Attitude Determination and Control

The Attitude Determination and Control System (ADCS) is responsible for controlling and detecting the orbiter orientation. The corresponding requirements are listed in Table 10.7, after which the design process is presented. Manoeuvres for the release of the lander and course correction, as well as counteracting disturbance torques are analysed. Verification is performed with an example design from [9]. Finally, the necessary hardware is selected and recommendations for future design iterations are given.

Requirements

Table 10.7: Requirements on the orbiter's Attitude Determination and Control subsystem

ID	*Requirement*	*Status*	*Origin*	*Compliance*
DMD-ADCS-01	The system shall be able to determine the attitude of the spacecraft throughout all phases of the mission.	Active	Purpose of ADCS	Met
DMD-ADCS-02	The pointing accuracy shall be better than 0.1 degrees.	Scrapped	Already a system requirement (DMD-ORBITER-02)	N.A.
DMD-ADCS-03	The system shall be able to control the attitude of the spacecraft for course correction, orbit insertion and orbit maintenance.	Active	Functional analysis of manoeuvres	Met
DMD-ADCS-03-01	The system shall be able to counteract a maximum disturbance torque of 0.26 mNm occurring during the mission.	Active	Estimation of disturbance environment	Met
DMD-ADCS-03-02	The spacecraft shall have a maneuvering rate of at least 0.4 degrees/second.	Scrapped	Already a system requirement (DMD-ORBITER-01)	N.A.
DMD-ADCS-03-03	The system shall provide a slew rate of at least 0.075 degrees/second.	Active	Functional analysis of manoeuvres	Met
DMD-ADCS-03-04	The system shall be able to generate a control torque of 18.5 Nm around all three axis.	Active	Functional analysis of manoeuvres	Met
DMD-ADCS-04	The system mass shall be below 58.3 kg.	Active	Hardware specifications	Met
DMD-ADCS-05	TThe system shall have a nominal power consumption of 132.3 W.	Active	Hardware specifications	Met
DMD-ADCS-06	The system shall have no single points of failure.	Active	Risk mitigation	Met
DMD-ADCS-07	The reaction control thrusters shall be able to provide a thrust of at least 9.3 N.	New	Analysis of required thrust level	Met
DMD-ADCS-08	The reaction control thrusters shall be able to perform 1159 thruster pulses during the mission lifetime.	New	Estimation of disturbance environment	Met
DMD-ADCS-09	The system dimensions shall fit within a cylinder of radius 510mm and a height of 700mm.	New	Hardware specifications	Met

Design process

The design process of the ADCS is as follows. First the manoeuvres are defined and the disturbance environment is quantified, after which the ADCS components like actuators and sensors are selected and sized.

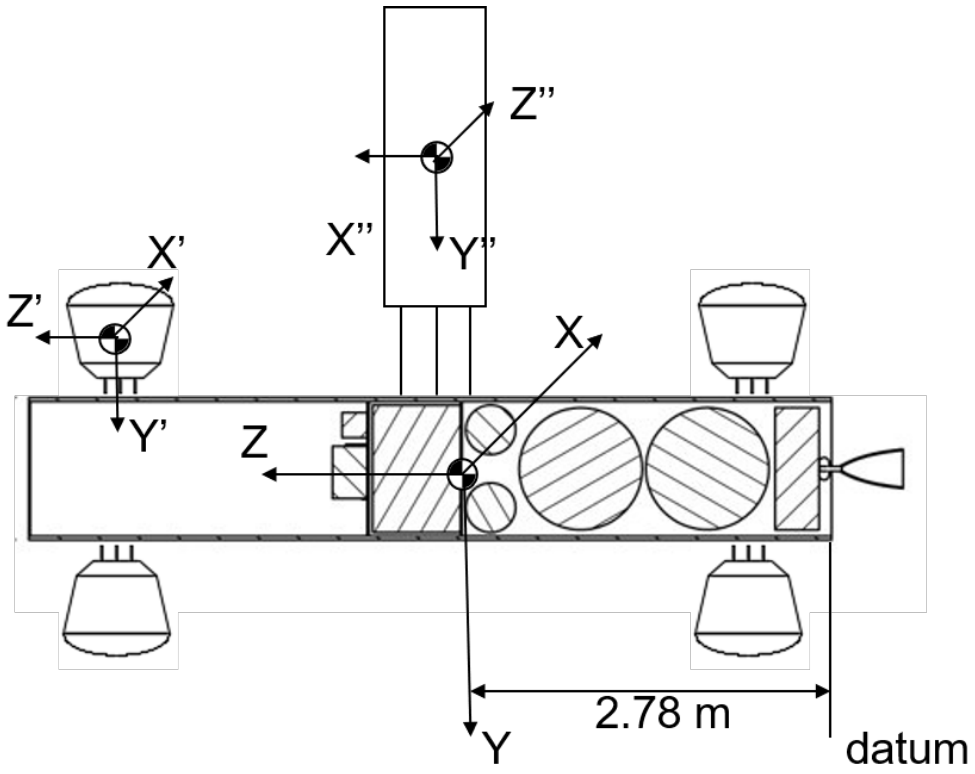

Figure 10.4: Axis system for mass moment of inertia calculation of the orbiter and centre of mass location

The moment of inertia of the orbiter and the center of mass are input parameters for the ADCS design process. The orbiter is modelled as a cylinder with the lander capsules being represented by spheres and the solar array modelled as a flat plate. The moment of inertia of the appendages is calculated using the analytical solutions for these simple shapes, after which they are added to the cylinder's moment of inertia using the parallel axis theorem. The results of this approach is given in Table 10.10 and the axis system is defined in Figure 10.4.

Based on the orbiter configuration and the subsystem mass, the center of mass of the orbiter is calculated. The datum is placed at the bottom of the cylinder where the propulsion system is attached. The distance of the center of mass to this datum is 2.78 m, shown in Figure 10.4. Because of the circular arrangement of the capsules and the comparably lower mass of the solar array and the antenna dish, the shift in center of mass location is in the order of less than a millimeter in x-y-direction and deemed negligible. When all landers are released the center of mass distance changes to 1.96 m.

Certain manoeuvres are defined that the ADCS has to perform during the mission. During Mars transfer a total of 5 correction maneuvers are required to keep the orbiter on its nominal trajectory. When the landers are ejected, the entire orbiter has to be rotated in order to release the capsules in the right orientation. The parameters of theses manoeuvres are listed in Table 10.9. After Mars orbit insertion, a number of disturbance torques will act on the orbiter. The ADCS system must be able to counteract these. The UHF antennas of the orbiter need to be pointed towards the surface of Mars and the whole orbiter has to make a full rotation during one orbit.

The disturbance torques which will be designed for are the magnetic torque, gravity gradient torque, aerodynamic torque, and solar radiation torque. Simplified expressions for these are compiled in Table 10.8. The magnetic torque is the resultant of the tendency of the spacecraft to align its residual magnetic moment with the magnetic field of the planet. Mars does not have a global magnetic field and the magnetic torque is small compared to a satellite in low Earth orbit. In Martian orbit, the gravitational field will attempt to align the minimum principal axis of the spacecraft with the local vertical, creating a gravity gradient torque. Since the centre of pressure of the orbiter is not perfectly aligned with the centre of mass, the atmospheric drag force will cause a disturbance. Finally, the solar radiation pressure of the sun acting on the orbiter results in a torque, assuming a uniform reflectivity of the orbiter's surface.

The gravity gradient and solar torque are calculated to be the most critical as listed in Table 10.8. In addition to the external disturbance torques, rotating masses inside the orbiter also cause disturbances. This is modelled for the antenna dish, which is rotated to allow for communication with the DSN.

Based on the manoeuvres required and the magnitude of the disturbance torques, a 3-axis control system is selected. The control actuators consist of reaction wheels for on-orbit manoeuvres, disturbance counteracting and antenna pointing, and a reaction control system (RCS) with thrusters for moment-dumping, course correction

Table 10.8: Internal and external torques modelled for the orbiter [9]

Disturbance torque	Equation	Value [Nm]
Magnetic	$T_m = D\frac{M}{a^3}$	$4.6 \cdot 10^{-10}$
Gravity gradient	$T_g = \frac{3\mu}{2a^3}(I_z - I_y)\sin(\vartheta)$	$8.1 \cdot 10^{-05}$
Aerodynamic	$T_a = \frac{1}{2}\rho V^2 S C_D (c_p - c_m)$	$-5.7 \cdot 10^{-164}$
Solar radiation	$T_s = \frac{J_s}{c} A_s (1+q)(c_s - c_m)\cos(\varphi)$	$1.3 \cdot 10^{-05}$
Internal disturbance	$h = I\omega$	

manoeuvres, and reorienting the spacecraft for lander deployment. The parameters of the ADCS manoeuvres are given in Table 10.9. With a required pointing accuracy of 0.1 degrees, resulting from [DMD-ORBITER-02] and a relatively large spacecraft mass, spin-stabilization or gravity gradient control are not considered feasible.

Table 10.9: List of manoeuvre characteristics for the ADCS design

Parameter	Symbol	Value	Unit
Rotation for lander release	ϑ_r	72	degrees
Time for release manoeuvre	t_r	300	s
Number of rotations for release	n_r	5	-
Rotation for course correction	ϑ_{cc}	15	degrees
Time for correction manoeuvre	t_{cc}	200	s
Number of course corrections	n_{cc}	5	-
Rotation during a single orbit	ϑ_o	360	degrees
Time for a full rotation	t_o	5.67	hrs

The cyclic disturbance torques require continuous correction from the reaction wheels. As the momentum storage is limited, the reaction wheels are desaturated by an external torque provided by the reaction control system (RCS). Based on the disturbance environment estimate, the desaturation interval is 22 hours. The input for the reaction wheel sizing is therefore the required control torque, and the maximum momentum storage as calculated by Equation 10.6 [9]. Here, T is the maximum cyclic disturbance torque, P the orbital period and $h_{internal}$ the disturbance caused by internal rotating masses.

$$h = \frac{\sqrt{2}}{2} T \frac{P}{4} + h_{internal} \tag{10.6}$$

The thruster sizing is based on the worst case moment of inertia and moment arm. Since the orbiter configuration is a long cylinder, one of the thruster pairs will be the least effective and is selected as the basis for sizing. The thrust level for reorientation, lander release, and momentum dumping are calculated and the thruster hardware is selected accordingly. A total of 1159 thruster pulses are necessary for momentum dumping during the lifetime of the orbiter. The relevant moments of inertia and the control characteristics are summarised in Table 10.10.

Table 10.10: Control actuator parameters of ADCS

Parameter	Symbol	Value	Unit
MMOI about x-axis	I_x	37594.5	kgm^2
MMOI about y-axis	I_y	37789.7	kgm^2
MMOI about z-axis	I_z	5937.5	kgm^2
Specific impulse of RCS	I_{sp}	220	s
Control torque of reaction wheels	T_C	0.1	mNm
Torque for orbit rotation	T_o	2.3	mNm
Thrust for release manoeuvre	T_r	9.3	N
Thrust for course correction	T_{cc}	0.5	N
Thrust for momentum dumping	T_m	4.3	N

Verification and Validation

The tool developed for the ADCS design is verified with an example solution provided in [9]. The results of the verification is divided in thruster sizing and reaction wheel sizing. The functions of the tool to calculate system parameters are fed with the input values of an example satellite, and the deviation is recorded. Table 10.11

summarises the result of the unit tests. As the deviation from the text book solution for each function is zero, it is verified that the code does not include syntax or calculation errors.

Table 10.11: Verification of ADCS design functions

Parameter	Expected	Tool output	Error [%]
Thrust for slew manoeuvre	0.145	0.145	0
Propellant mass for RCS	0.049	0.049	0
Thrust for momentum dumping	2.0	2.0	0
Torque to counter-act disturbance	$2.1 \cdot 10^{-5}$	$2.1 \cdot 10^{-5}$	0
Momentum storage in reaction wheel	0.039	0.039	0

System Performance and Characteristics

The main performance characteristics are summarised in Table 10.12. The momentum storage is limited by the hardware characteristics of the reaction wheel. A 20% contingency is included in the propellant mass.

Table 10.12: Summary of ADCS performance characteristics

Parameter	Symbol	Value	Unit
Maximum disturbance torque	T_D	$9.22 \cdot 10^{-5}$	Nm
Momentum stored after one orbit	h	10.58	Nms
Maximum momentum storage	h_{max}	50	Nms
Desaturation interval	t_s	22.68	hrs
Number of lifetime thruster pulses	n_p	1159	-
Propellant mass	m_p	6.96	kg

The ADCS configuration is listed in Table 10.13. A combination of a star tracker, sun sensors, and an inertial measurement unit (IMU) is used to provide full three-axis pointing knowledge. For the star tracker and IMU, a primary and secondary unit are included for redundancy. Four reaction wheels are installed at an angle such that in the case of failure, the remaining three can provide control over all axis. Six sun sensors are distributed over the surface of the orbiter to ensure a line of sight with the sun, no matter the orientation of the spacecraft. The RCS thrusters are rated for 20N, which in excess of the 9.3 N maximum calculated thrust they have to provide. The reaction wheels are rated for 0.1 Nm of torque, which is sufficient for the 2.3 mNm they have to provide for rotation of the spacecraft.

Component	Commercial component	Quantity	Mass [kg]	Power [W]
Thruster	Ariane Group 20N Monopropellant Thruster [10]	12	0.65	-
Reaction wheel	Honeywell HR14 [11]	4	8.5	84
Star tracker	Sagitta Star Tracker [12]	2	0.25	0.225
Sun sensor	NewSpace Sun Sensor [13]	6	0.04	2
Inertial measurement unit	Northrop Grumman LN-200S [14]	2	0.75	24

Table 10.13: Components and configuration selected for ADCS

Recommendations

In further stages of the design, the preliminary sizing should be extended by considering control algorithms and the necessary computational power. The estimation of the moment of inertia can be improved by setting up a detailed CAD model, when the masses of the subsystems and components are exactly known and the configuration is defined in detail. Furthermore, proper validation has to be performed by testing the components in combination with each other and validate the pointing accuracy in a controlled environment.

10.4. Guidance, Navigation, and Control

The orbiter will have a limited GNC subsystem, mainly to know the point at which trajectory corrections are required and to fulfill stakeholder requirement [DMD-PERF-BROOT-04], locating the landers with an accuracy of 10 m.

Requirements

Table 10.14: Requirements on the GNC subsystem

ID	*Requirement*	*Status*	*Origin*	*Compliance*
DMD-GNC-O-01	The orbiter system shall be able to know its velocity.	Active	Purpose of GNC	Met
DMD-GNC-O-02	The orbiter system shall be able to know its position.	Active	Purpose of GNC	Met
DMD-GNC-O-03	The orbiter system shall be able to perform corrective maneuvers.	Active	Purpose of GNC	Met
DMD-GNC-O-04	The orbiter system shall be able to put the landers in a trajectory towards their landing zone with an accuracy determined by the landing ellipse.	Active	Landers will be unguided	Met

Design Process

The Guidance, Navigation, and Control subsystem (GNC) has three purposes: navigation, to gain knowledge on where the spacecraft is and what its course is; guidance, to determine the target heading; and control, to provide corrective commands to adjust the course of the spacecraft.

To start the design process, it was first investigated what navigation capabilities would be required. For the orbiter, it is useful to know its position for communication and sequencing purposes. Next to that, to predict the course of the spacecraft, the velocities are needed.

Next, the guidance segment can be pre-determined for the scenarios the orbiter might encounter. Finally, the control aspect will use the navigation data to perform propagation. Combining this with guidance, it can find a deviation. If this is deemed large enough, a command must be provided to the propulsion subsystem, to correct for it.

System Performance and Characteristics

The navigation aspect depends mainly on the DSN to provide ephemeris data. Using radio wave ranging, the position and velocity of the satellite can be determined. The accuracy of this system is in the order of magnitude of m and cm/s for range and range-rate, respectively. An angular position accuracy in the range of tens of meters can be expected with further improvements expected in the coming years. This data is received by the communications subsystem. [15]

Even though the DSN can provide these ephemeris, it does so only three times a day. There exists however a need to know its position and velocity between transmissions. To this end, next to the DSN transmissions, the IMU sensors from Section 10.3 will be used. They measure the acceleration which can be used to generate positional data when the DSN is not available. This this entire process is shown in Figure 10.5.

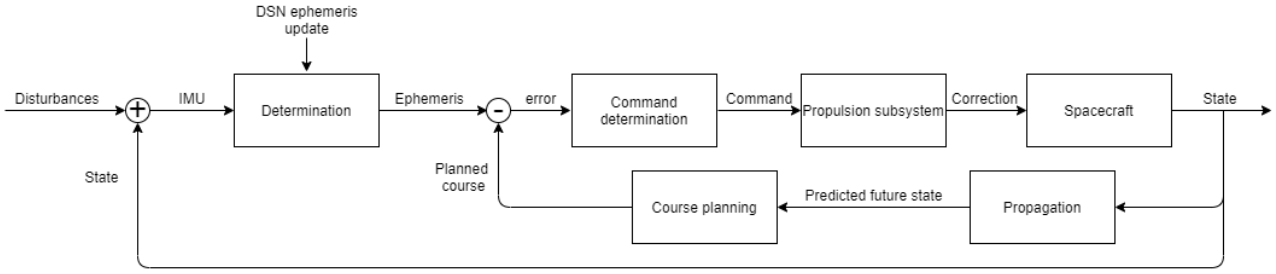

Figure 10.5: GNC schematic for the orbiter

Recommendations

As small errors in the IMU ephemeris data will accumulate until new data is received from the DSN, it should be investigated what the effect of long loss of contact with DSN is, for instance in the case where the path between Earth and Mars is blocked by the Sun.

10.5. Communication

The telemetry, tracking and command (TT&C) subsystem of the orbiter is responsible for delivering all collected scientific data back to Earth, as well as receiving mission commands. In this mission, the orbiter acts as a relay

between the landers and Earth for both uploading scientific data and downloading commands.

Requirements

Table 10.15 presents the TTC subsystem level requirements, derived from system and stakeholder requirements. The designed system is compliant with all of the requirements shown below.

Table 10.15: Requirements on the Tracking, Command & Communication

ID	*Requirement*	*Status*	*Origin*	*Compliance*
TT&C Requirements				
DMD-TTC-ORB-1	The orbiter shall be able to receive emergency commands from DSN.	Active	Flows from [DMD-PERF-BROOT-11]	Met
DMD-TTC-ORB-2	The orbiter shall be able to receive emergency commands at any orientation & direction.	Active	Purpose of TT&C	Met
DMD-TTC-ORB-3	The orbiter shall be able to offload all collected information to Earth.	Active	Purpose of TT&C	Met
DMD-TTC-ORB-4	The orbiter shall have UHF downlink speed of at least 100kbit/s.	Active	Dictated by C&DH & contact time	Met
DMD-TTC-ORB-5	The orbiter shall have DSN uplink speed of at least 150kbit/s.	Active	C&DH & contact time dictate bit rate	Met
DMD-TTC-ORB-6	The orbiter shall have DSN uplink for at least 20% of a sol.	Active	Design decision	Met
DMD-TTC-ORB-7	The orbiter TTC shall be DSN compliant.	Active	Flows from [DMD-PERF-BROOT-11]	Met
DMD-TTC-ORB-8	The orbiter's communication system must not use prohibited frequencies.	Active	Flows from [DMD-SARR-BROOT-01]	Met
DMD-TTC-ORB-9	The orbiter's UHF antennas must be electronically steerable.	Active	Design decision	Met
DMD-TTC-ORB-10	The orbiter's UHF antennas must support at least two simultaneous connections.	Active	Dictated by C&DH & contact time	Met
DMD-TTC-ORB-11	The orbiter's DSN antenna shall not be bigger than 2.8 meters.	Active	Structural limitation	Met
DMD-TTC-ORB-12	The orbiter shall have repetitive and predictable communication pattern.	Active	Purpose of TT&C	Met

Design Process

The following section will first describe and explain the governing equations and computational approach for the design and sizing of the TT&C subsystem. Following this, key design decisions and assumptions will be explained.

Governing Equations

To start the design process, a number of governing equations was collected from various sources, and link budget tools were developed following the approach given in [9]. The main for the link budget is Equation 10.7, where E_b/N_o is the received signal to noise ratio (SNR), P is the antenna power in Watt, G_t and G_r are the gains of transmitting and receiving antennas, L_a is the transmission path loss, L_s is the space loss, L_t is the transmitter to antenna line loss, k is the Boltzmann constant and R is the data rate [9]. The gain of isotropic antennas is simply 1, while the gain of parabolic antennas was computed using Equation 10.8, where η_l is antenna's efficiency, D_r antenna's diameter and λ the wavelength of the signal used. Space loss was computed using Equation 10.9 where S is the distance between transmitter and receiver, loss L_s and is inversely proportional to the transmitting frequency. In this formula, space loss is expressed as a space gain, which simplifies calculations. The system temperature T_s estimation is relatively complex, and requires knowledge of specific component properties, such as amplification factors and noise figures. Therefore, a statistical estimate of a worst case scenario was found to be 614 K [9, p.558]. Similarly, due to the high complexity of specific calculations, L_t and L_a were ignored. Finally, the required SNR could be computed. This parameter depends on bit error probability, the modulation type, as

well as coding and codecs used. Again, empirical methods were used here, as according to [9, p. 546], modern technology allows for achieving the typically required $10^{-}10$ bit error rate (BER) with just 5dB of SNR.

For the simplicity of calculations and iterations, a Python program was constructed to automate the process. Within it, numbers were converted to decibels for an easy interpretation. The program takes antennas sizes, frequency, distance and data rate as input, and computes the required power, taking into account the required SNR margin. It is important to mention that frequencies of the bands slightly alter depending on whether system is in download or upload configuration. Exact frequencies for each of the configurations were taken from NASA's DSN configuration sheet.[6] Finally, a number of assumptions was made during calculations:

1. L_t and L_a are minimal (order of 0.05 dB, from year two estimation techniques), thus ignored, as cannot be computed accurately without knowing exact path parameters
2. Orbital height compared to Mars-Earth distance is minimal, thus ignored
3. Mars and Earth are always at the furthest possible distance of 1+1.54 AU
4. Antennas have 100% efficiency

$$\frac{E_b}{N_o} = \frac{PL_tG_tL_sL_aG_r}{kT_sR} \qquad (10.7)$$

$$G_r = \frac{\pi^2 D_r^2 \eta}{\lambda^2} \qquad (10.8)$$

$$L_s = \frac{\lambda}{4S\pi}^2 \qquad (10.9)$$

System Architecture
As will be explained in detail in Section 16.6, it was decided to use the orbiter as a communication relay between Martian landers and the Earth, which resulted in requirement [DMD-TTC-ORB-3]. As per stakeholder's requirement [DMD-TTC-ORB-7], the orbiter shall communicate over NASA's Deep Space Network, and have three redundant systems. As only two systems are required for this mission's profile, lander-orbiter and orbiter-Earth, the third system would be an emergency communication system using an isotropic antenna, which in turn, resulted in requirement [DMD-TTC-ORB-2].

First, this independent emergency system was designed. The most powerful way of communication with Earth is through NASA's DSN, which operates using Ka, S and X bands. Ka bands are relatively new, designed for high speed transfer, and have stricter pointing requirements, as at higher frequencies the half power beam width becomes smaller. [7] Therefore, X and S bands were considered for this system. Based on historical data, as well as off-the-shelf available components, it was decided to use an S band receiver. This was to be equipped with two isotropic LGAs, positioned on opposite sides of the orbiter, such that there would be a direct line of sight with the Earth regardless of the orbiter's orientation.

Next, the main DSN orbiter-Earth communication subsystem was designed. Similarly, available bands are Ka, S and X. In the early stages of the design, the X band was used following heritage. However, at later stages it was decided to switch to the Ka band. This was done due to the fact that the Ka band operates at around 32 Ghz, instead of around 8 Ghz for X band. Space loss (negative gain in dB) is inversely proportional to frequency (directly proportional for gain in dB), so a lower frequency is preferred. On the other hand, the gain of a parabolic antenna is directly proportional to the frequency, so higher is preferred. Therefore, if system has one parabolic antenna, frequency factors cancels out in Equation 10.7, and link budget becomes frequency independent. In case where parabolic antennas are used on both sides of the transmission line, link budget once again is positively correlated to frequency, thus higher frequency is preferred. This approach was demonstrated by the MRO, which has both X and Ka bands, and achieves much higher data rates with less power with the latter .[8]. In order to minimise the power consumption, the largest possible parabolic antenna was selected, which was 2.8 m in diameter and was limited by the combination of the orbiter structure and the launch vehicle fairing size. It was found that with a 34 m receiving antenna, a 20% contact time was possible, resulting in the [DMD-TTC-ORB-5] requirement. Together with C&DH storage requirements, this resulted in the bit rate of 150 kbit/s, documented in [DMD-TTC-ORB-5]. Since frequency, data rate and dish size were then fixed, only power required was left to be computed. It is important to mention that the 34 m antenna was assumed for DSN, as there are only three 70 m antennas around the world. Their availability is assumed to be limited, and only comes at a steep price [16].

The third and final communication system is the orbiter-lander system. As per historical data, Martian rovers and landers operate in the military designed UHF spectrum, which ranges around 400 Mhz. For increased compatibility in case of orbiter's failure, as well as for increased scientific return of future possible missions, it was decided to use the same standard for the orbiter-lander communication. The next choice was between HGA and LGA both aboard the landers and the orbiter. As there is a high amount of landers, and a simplified system was preferred, which in addition must survive much higher impact loads than traditional systems, it was decided

[6] https://deepspace.jpl.nasa.gov/dsndocs/810-005/201/201C.pdf, Accessed [14-06-2020]
[7] https://www.tutorialspoint.com/antenna_theory/antenna_theory_beam_width.htm, Accessed [22-06-2020]
[8] https://mars.nasa.gov/mro/mission/instruments/kaband/, Accessed [15-06-2020]

to go for a simple, isotropic LGA on the lander. The orbiter would take a much more complex, redundant HGA. Like with any TT&C system, the data rate requirement, [DMD-TTC-ORB-4] in this case, is the main limiting factor. As lander's antenna would be LGA, the only free variable would be orbiter's antenna size/gain, and input power to transmitter of the lander. The orbiter's power requirement was not considered as an issue, since the orbiter's power budget was less restricted, and in addition the majority of traffic would be scientific data upload, as the commands download requires much lower and less frequent data rates. A balance between the antenna gain of the orbiter and the power consumption of the lander was made. Initially, 0.4 m in diameter dish on orbiter was assumed.

However, it was desired to have two redundant system for two reasons: redundancy in case of failure, as this is one of the critical subsystems, and secondly in order to have ability to connect to two landers at the same time. Although this is not technically required, as the bit rate was sized for the worst case scenario of one contact per repeat orbit, this will allow for a greater communication margin. This however, will not just require a pointing mechanism for one antenna, but for two. In addition, this will complicate the structural layout, thus it was decided to go for two phased array antennas instead. This approach was considered by NASA before for high frequency communication [9], and is already being used in space by SpaceX's Starlink, specifically because of its benefits of being electronically steerable.[10] Such an antenna is a flat square, which will allow very fast and simple change in orientation, and eliminates a mechanical pointing system. Due to the lack of specific information on these types of systems, for estimating mass a classical 0.4 m parabolic dish was taken, with a 100% safety margin.

Component Selection
Once the setup for three systems was done, the radiated power required was computed using the mentioned Python code. The summary of results is given in Table 10.16. From there, it was required to do actual power and mass sizing. For the first iterations, an empirical approach based on statistics was used, where the mass of main dish, as well as transceiver were computed from linear regression, while cost was taken from estimates of cost as a fraction of the whole mission. During next iterations, components for the orbiter's TT&C were partially picked: specifically, the DSN LGA emergency system will consist of an off-the-shelf available S band receiver, for which the technical specs were provided by Endurosat.[11] For the DSN Ka band transceiver, it was found that tube amplifiers are often used due to their high efficiency. However, these amplifiers are heavy, with a mass estimated from SMAD of around 25 kg [9]. Finally, due to very limited information on phased array antennas, no actual device could be picked. Instead, the mass of an equivalent antenna of 0.4 m^2 in terms of gain was computed. With a 100% safety margin, this resulted in 2.75 kg. Two more kilograms were added for the transceiver device.

Verification and Validation
As the above mentioned calculations were implemented in Python script, verification and validation of the script was required. Verification was done against an existing validated spreadsheet-based model for link budgets. The spreadsheet-based program has a similar structure to the Python code and uses the same governing equations, but its implementation greatly differs. This tool has previously been validated against existing missions, and is assumed to be accurate.

The tool was run was a number of configurations:

1. Earth - Mars connection. Simulates emergency commands download, over S-band isotropic antenna
2. Earth - Mars connection. Simulates commands download, over Ka band parabolic antenna of the orbiter
3. Mars - Earth connection. Simulates data upload, over Ka band parabolic antenna of the orbiter

Initially, the spreadsheet calculations did not align with the Python code output. Further investigation showed that this difference lies in the additional antenna pointing loss, which was included by spreadsheet as a rough estimate based on known antenna parameters, but was omitted in the Python code. The maximum difference was found to be 0.18 dB. As the main parabolic antenna of the orbiter was computed based on statistical estimates, rather than existing components, no accurate information on half beam power angle was available. Therefore, it was decided to apply a safety margin of two, and subtract an additional 0.4 dB from the SNR values for Ka band antenna to account for this, as this system is the most sensitive to antenna pointing loses.

System Performance and Characteristics
The general communication layout, as well as detailed bit rate, frequencies and bands information for both the orbiter and lander TT&C subsystems are summarised in the communication diagram, given in Figure A.5.

Table 10.17 presents the link budgets for the three communication subsystems. System 1 budget is given only for transmit configuration (orbiter-Earth), as data rate is limited by the orbiter's radiated power. Similarly for System 2, link budget is given for transmit, as receive configuration is limited by lander's radiated power, and will be

[9] https://ntrs.nasa.gov/api/citations/20060051746/downloads/20060051746.pdf, Accessed [22-06-2020]
[10] https://hackaday.com/2020/11/25/literally-tearing-apart-a-spacex-starlink-antenna/, Accessed [15-06-2020]
[11] https://www.endurosat.com/cubesat-store/cubesat-communication-modules/s-band-receiver/, Accessed [18-06-2021]

Table 10.16: Summary of orbiter's communication systems

	Type	Antenna	Size	Bitrate		P(Radiated)	P(Supply)	Mass
Units			[m]	Rx [bit/s]	Tx [bit/s]	[W]	[W]	[Kg]
System 1	DSN	HGA	2.8	200,000+	200,000	25	60	50
System 2	UHF	HGA	0.4	100,000+	100,000+	3	15	5
System 3	DSN	LGA	-	300	-	-	2.5	0.3

presented in Section 16.6. Finally, System 3 is emergency receive only system, so only receive link budget is presented. All three systems have positive SNR margin, meaning that they were properly implemented.

Table 10.17: Orbiter's communication system link budgets

Parameter		Units	System 1 TX	System 2 TX	System 3 RX
Radiated power	P	dB	14.0	10.8	43.0
TX antenna gain	G_r	dB	58.4	4.5	0
RX antenna gain	G_t	dB	81.1	0	57.5
Space Loss	L_s	dB	-294.0	-159.8	-270.5
Data Rate	1/R	dB	-53.2	-50	-24.8
Boltzmann constant	1/k	dB	228.6	228.6	228.6
System Noise (Temp)	T_s	dB	-27.9	-27.9	-27.9
Received SNR	Eb/No	dB	6.9	6.2	6
Required SNR	Eb/No	dB	5	5	5
Verification correction		dB	0.4	0	0
Implementation error		dB	0.5	0.5	0.5
SNR Margin		dB	1	0.7	0.5

Recommendations

Now that the link budget has been completed and required radiated powers have been computed, the design iteration can be taken one step further. The largest uncertainty in the current design is the phased array configuration for the UHF antenna of the orbiter. It would be recommended to further study this concept, and detail the layout of the phased elements. Another recommendation would be a deeper study into Doppler effect positioning technique which will be used in this mission. As described in Section 16.3, currently a dedicated radar-style antenna will be installed on the orbiter. However, phased arrays antenna can be used for radar as well, thanks to their beam scanning ability.[12] It might be therefore possible to combine these two systems into one, eliminating the need for an additional antenna and dedicated transceiver. Finally, it may be considered adding additional DSN transceiver to operate over the main dish, for upload redundancy. Currently, system is three times download redundant, but has a single point of failure in upload mode, which is the Ka band transceiver. As the parabolic antenna is non-foldable, and failed pointing mechanism could be compensated by ADCS of the spacecraft itself, only weak point it the back-end electronics.

10.6. Command and Data Handling

The Command and Data Handling subsystem consists of a double redundant processor configuration, with an extra external mass storage configuration to ensure enough storage will be present for all the scientific data relayed from the Martian surface. It will be able to process this data together with the housekeeping data for transmission to the Deep Space Network. Furthermore it shall provide sufficient storage capacity for the data.

Subsystem requirements & compliance

[12] https://www.ll.mit.edu/sites/default/files/publication/doc/development-phased-array-radar-technology-fenn-ja-7838.pdf, Accessed [18-06-2020]

Table 10.18: Requirements on the Command & Data Handling

ID	*Requirement*	*Status*	*Origin*	*Compliance*
C&DH Requirements				
DMD-CDH-L-01	The CDH shall be able to communicate with all operational subsystems.	Active	Nominal system function	Met
DMD-CDH-L-02	The CDH subsystem shall have a minimum throughput of 10 MIPS.	Active	Memory budget [6]	Met
DMD-CDH-L-03	The CDH subsystem shall be able to track time with an accuracy of at least <tbd> ms/day.	Active	EDL & G&N	T.B.D
DMD-CDH-L-04	The CDH subsystem shall have a maximum mass of 16 kg.	New	Mass budget	Met
DMD-CDH-L-05	The CDH subsystem shall have a maximum power consumption of 40 W.	New	Power budget	Met
DMD-CDH-L-06	The CDH subsystem shall have 2.6 MB of memory for the operating system and interfaces.	Active	Memory budget [6]	Met
DMD-CDH-L-07	The CDH subsystem shall be able to withstand radiation levels of at least 100,000 $\pm$50%.	New	Due to risk [R-CDH-O-04]	Met
DMD-CDH-L-08	The CDH subsystem shall be able to store at least 60 sols of scientific data.	New	Due to risk [R-CDH-O-01]	Met
DMD-CDH-O-09	The CDH subsystem shall have at least one redundant processor.	New	Due to risk [R-CDH-O-03]	Met
DMD-CDH-O-10	The CDH subsystem shall have a safe-boot option in case of system errors.	New	Due to risk [R-CDH-O-02]	N.V.
DMD-CDH-O-11	The CDH subsystem shall be able to process at a bitrate of at least 127.3 kbit/s	New	Replaces [DMD-ORBITER-04]	Met
DMD-CDH-O-12	The CDH subsystem shall have at least 17.4 GByte of mass storage.	New	Memory budget	Met

Design Process

This subsection will provide all relevant equations and calculations to characterize the C&DH subsystem of the orbiter. Furthermore a model on the mass storage will be displayed and described.

Data rates & Data Handling

Estimations and calculations on expected data rates of the orbiter are made from which the memory size and throughput can be computed. First a list of required sensors will be compiled with their accompanying data and sampling rates, after this the incoming telemetry from Mars and Earth will be analysed. From ADCS requirements in Section 10.3 it stems that the sun and star sensors are necessary as well as an inertial measurement unit to fully establish an inertial frame of reference which can be utilised for location calculation and analysis. Temperature sensors will be placed throughout the orbiter bus to keep track of the temperature distribution. A redundant pair of voltage and current sensor will be placed on the solar panel as well as on the accumulator to measure the voltages and currents. The resolution for these sensors will be 8 bits per sensor. An 8 bit integer will be able to provide a resolution of 128 decimals unsigned or 127 decimals signed. For the propulsion subsystem the a datarate for thruster control as well as for a pressure transducer is required for full control of this subsystem. Resolution and of both components and amounts are picked by the propulsion engineer.

Storage & Transmission

Other than the sensor data, the orbiter is meant to act as a relay for the Martian probes, according to the contact times provided in Section 8.2, the worst case scenario is that the orbiter is only able to connect to each probe in clusters of five, once every three sols, for a duration of 5100 seconds. The system will be designed for this particular case. All further assumptions made for the sizing of the subsystem are listed below:

- Every probe will be transmitting at 100 kbit/s to the orbiter.
- The orbiter is connecting to the Deep Space Network 20% per sol, as per Section 8.2
- All data received before transmission to the Deep Space Network has been processed and is available for transmission.
- Sensors will be generating data 100% of the time at the bitrates from Table 9.4
- The orbiter is able to receive probe data and transmit to the Deep Space Network at the same time.
- All contact windows are assumed to be at the end of a sol.

Given this contact window and the transmission rate per lander of 100 kbit/s as given in Section 16.6. The following step Equation 10.10 can be derived to calculate the storage pattern.

$$S(t) = DR_{hk}t + Tx_{probe}\langle t - t_{probe_{connect}}\rangle - Tx_{probe}\langle t - t_{probe_{disconnect}}\rangle - Tx_{DSN}\langle t - t_{dsn_{connect}}\rangle + Tx_{DSN}\langle t - t_{dsn_{disconnect}}\rangle \tag{10.10}$$

Equation 10.10 is similar to a McCauley step function where parts of the equation turn on and off at the given time between the angle brackets. This function is valid when the start and end of a sol is taken as a frame of reference. The storage stability will dictate the required transmission data rates for the TT&C subsystem. The point where Equation 10.11 is satisfied, the storage of the system is stable.

$$\sum\left(DR_{hk}t + Tx_{probe}t_{probe_{connect}}\right) \leq \sum Tx_{DSN}t_{dsn_{connect}} \tag{10.11}$$

Given the sensor data rates as well as the transmission rates of the probes the minimal data rate required for storage stability can be calculated as shown in Equation 10.12. The orbiter will be able to upload data once every sol with the aforementioned assumptions. This means that there will be a window of three sols where data uplink to orbiter and downlink to DSN will take place. All data generated in this time frame will need to be uploaded for the storage to be stable.

$$Tx_{DSN} = \frac{(6296 * 88775 * 3) + (100{,}000 * 10 * 5100)}{0.2 * 88775 * 3} = 127.227\text{kbit/s} \tag{10.12}$$

This transmission rate of the orbiter to the DSN will set the lower limit of design for the TT&C subsystem. Furthermore the required minimal storage for nominal operation can be calculated as follows

$$S_{req.} = (6296 * 88775 + 100{,}000 * 10 * 5100) = 5659\text{Mbit} = 707.37\text{Mbyte} \tag{10.13}$$

From the Midterm Report [6] the amount of storage budgeted for firmware is 2.6 MByte, this needs to be added which results in a storage of 709.97 MByte. However in order to satisfy requirement [DMD-CDH-B08], the storage must allow for at least 60 sols of storage. As the probes upload data once every three sols, it is expected that they will have uploaded at least 20 times during this time period. Which results in 17 Gbyte required for mass storage to fulfil [DMD-CDH-B08]. Applying a safety margin of 20%, this will result in a final storage of 20.33 GByte needed by the system.

Storage Model
To model the storage of the orbiter Equation 10.10 can be computed using a numerical propagator and the minimum uplink speed from Equation 10.12, this will result in the storage pattern as well as the maximum amount of mass storage utilised for nominal operations. For modelling purposes and simplicity, forward Euler is used as a numerical propagator. This results in the graph shown in Figure 10.6. With the transmission rate calculated in Equation 10.12.

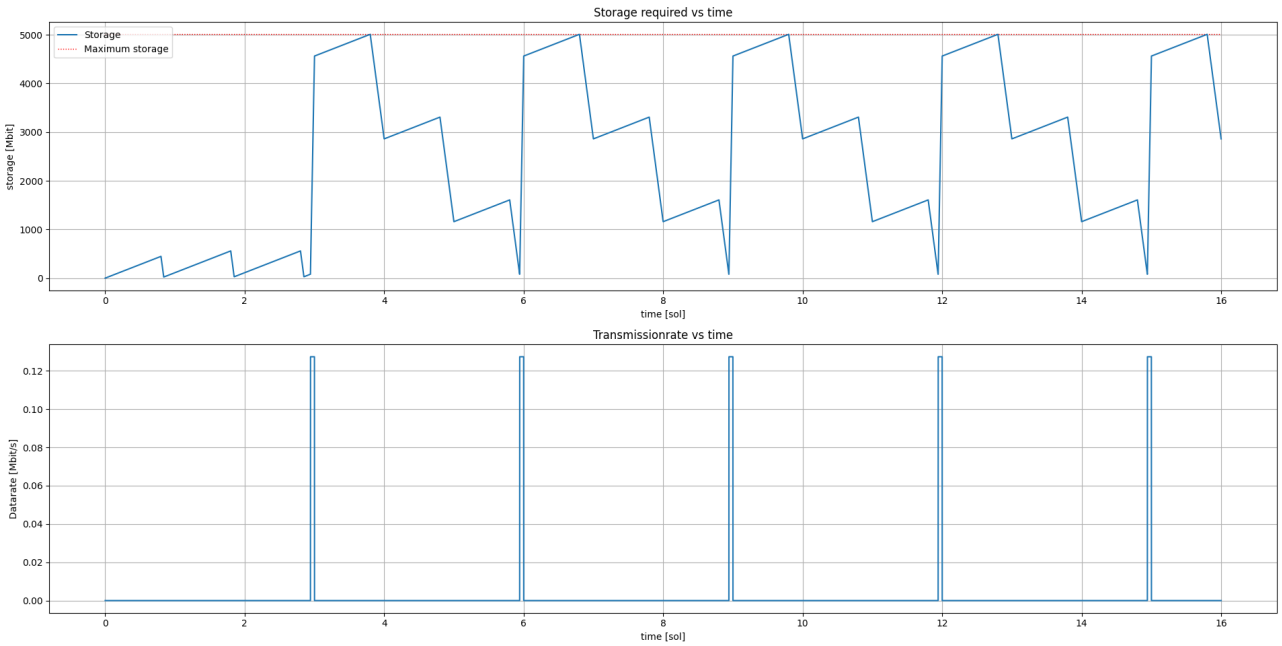

Figure 10.6: Storage model of the orbiter mass storage

In Figure 10.6 the storage model is displayed. The x-axis shows the amount of time passed in sols and y-axis shows the amount of storage in Mbit.

Verification & Validation

Code Verification

The model in Figure 10.6 is verified according to the procedure as prescribed in Chapter 5. The model does not have syntax errors and does abide by the correct programming logic, namely the forward Euler propagator. This is confirmed by the back up Command & Data Handling engineer that it is applied correctly. Furthermore the boundaries of the step function have been evaluated and confirmed to be correct.

Calculation Verification

For the purposes of calculation verification the inputs and data rates are defined as follows. The total sensor data rate from Table 9.4 is 6296 bit/s, the uplink from a probe to the orbiter is 100 kbit/s and finally the uplink to DSN is defined as 150 kbit/s as per Section 10.5. The model consists of one major functions for which the calculation must be verified:

1. *storage_bus* : Computes the storage with a forward Euler propagator based on Equation 10.10.

The following unit and system tests in Table 10.19 have been performed to verify the model.

Test	Expected [Mbit]	Result [Mbit]	Deviation
Nominal sensor data generation without up or down link	700.9674	700.9674	0%
Nominal data generation with connection from probes for 3 sols	7202.9022	7202.8943	0.00011%
Nominal data generation with connection to DSN and probes for 3 sols	5035.9674	5035.9674	0%

Table 10.19: Performed verification tests on the storage model of the orbiter

The second test had a slight deviation from the performed calculation but it is deemed to be insignificant enough. As a final integration test the storage shall be stable when the transmission speed is equal or larger than the aforementioned minimal transmission rate in Equation 10.12. As can be seen in Figure 10.6 the maximum utilised storage does not exceed 5111.305 Mbit after several storage cycles which is indicative of stable behaviour. Every step from Chapter 5 has been followed and the model is therefore verified.

Validation

As the model is purely intended as a calculation tool in order to estimate the amount of required storage, validation can not be applied properly. Therefore verification will provide sufficient evidence of the correctness of the

calculations. A validation test however would be to simulate the read and write sequences in a test setup on Earth. The same amount of data would be up and down linked to validate whether or not the mass storage is sufficient and stable under the given circumstances.

System characteristics & Performance

As a reference C&DH unit, a unit from RUAG Space[17] is picked as a suitable on board computer as it is radiation tolerant, has a storage capacity of 32 Gbyte BOL and has a double redundant processor layout with the correct interfacing for the subsystems mentioned in Chapter 10. The following table will summarize the results obtained in this section will be displayed.

Table 10.20: System budget

Characteristic	Value	Unit
Minimum required storage	20.33	Gbyte
Minimum required transmission rate	127.3	kbit/s
Mass	17.45	kg
Nominal Power	40	W
Radiation Tolerance	100,000	rad

Furthermore as scientific return is of main importance to the mission. It is opted to use an extra redundant external storage device in case of failure, or overload of the main mass storage of the OBC. As a reference, the TRRUST-Stor® VPX RT6U VPX from Mercury Systems is used [18]. This will allow for a fully redundant data storage design. Furthermore the C&DH system shall be able to encode and decode data for transmission using a differential encoding algorithm. This ensures that so called bit-flips do no affect the quality of the relayed signal [19]. The on board software is also equipped with a Kalman filter to reduce incoming noise from sensor data to get a more reliant reading. These software blocks and other system software architecture will be displayed in Chapter 7.

Furthermore during the mission of 5 years there is cosmic radiation that poses potential problems for the on board components as they could be damaged. Because of this, the chosen hardware shall be radiation tolerant. Typical values of radiation tolerant components are in the range of 10-100 kRad.

In Figure 10.7 the data handling of the C&DH subsystem of the orbiter is displayed. It visualizes the interaction between sensors and the on board computer hardware.

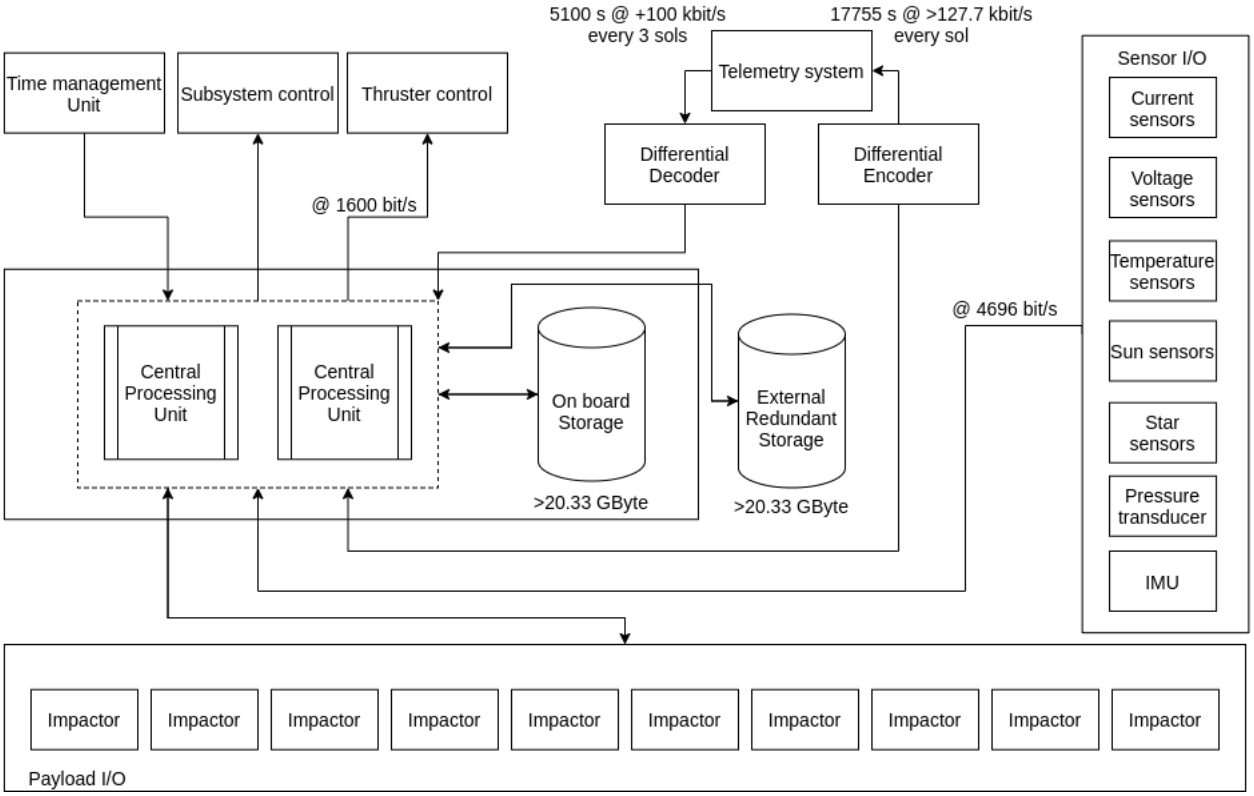

Figure 10.7: Data handling block diagram of the orbiter

Recommendations
As per risk [R-CDH-O-02] there is a chance that due to some software or system error the on board software will return errors making the system unusable, therefore it is recommended to make a separate piece of software the orbiter can boot to in case of system failure, which allows for remote troubleshooting. This software would have no other function other than to allow for remote access by ground stations on Earth, and thus would not have to manage the attached interfaces besides EPS and TT&C to limit sources of error. This recommendation will need to be fulfilled to meet requirement [DMD-CDH-O-10].

10.7. Electrical Power
The Electrical Power System (EPS) provides power to the subsystems of the orbiter for the duration of the mission. It does this via a Power Distribution System (PDS). The energy is generated by solar arrays and stored in a battery.

Requirements and Compliance

Table 10.21: Requirements on Orbiter EPS

ID	*Requirement*	*Status*	*Origin*	*Compliance*
General requirements				
DMD-EPS-O-01	The EPS system of the support shall have a power budget of 0.333Wh for deployment operations.	New	Power Budget	Met
DMD-EPS-O-02	The EPS shall control the power distribution to subsystems.	New	Nominal operation	Met
DMD-EPS-O-03	The EPS shall be able to store 0.64 kWh of energy.	New	Power Budget	Met
DMD-EPS-O-05	The EPS shall be able to provide additional 0.5 kWh of energy in case of emergency.	New	Operational redundancy	Met
DMD-EPS-O-06	The solar array shall be able to point towards the sun.	New	Nominal operation	Met
DMD-EPS-O-07	The EPS shall be able to provide additional 0.138 kWh for undefined pre-nominal operations.	New	Power Budget	Met
DMD-EPS-O-08	The orbiter will always be sun lit.	New	Nominal operation	Met
DMD-EPS-O-09	The energy accumulator should be rechargeable.	New	Nominal operation	Met

Design Process
In order to design the Electrical Power System (EPS) for the orbiter, the environment and hardware have to be clarified first. The environment consideration and mitigation as well as the hardware characteristics are described in this chapter. Later, in the lander's EPS design in Section 16.8, the same information is used as well. This critical information is used to size the EPS, and should provide a clear overview of the considerations taken into account.

Environment
During hardware considerations it should be taken into account that Mars is further away from the Sun than Earth is. Due to the larger distance, the solar irradiance is lower. The solar irradiance at 1.524 AU is 43.1% of the solar irradiance at 1 AU. The solar irradiance at Mars is therefore 586.2 W, on average.[13]

Hardware
To size the EPS, hardware sizing details are considered. As requirement [DMD-SARR-BROOT-05] states, the hardware should be space flown, i.e. Technology Readiness Level (TRL) 9. In the initial phase, a trade-off was done for the EPS, where Radioisotope Thermoelectric Generators (RTGs) as well as unconventional energy accumulators have been considered. For interest in these topics and results one can refer to the Midterm Report [6]. In this subsection, solar arrays, battery and power distribution system(PDS) are covered.

[13] https://nssdc.gsfc.nasa.gov/planetary/factsheet/marsfact.html, Accessed [15-06-2021]

Currently on the market, TRL 9 solar arrays can have efficiencies reaching up to 32% [20]. Some space flown references such as the MMa Design's eHaWK[14][20], which was flown in the MarCO mission, and the Spectrolab XTJ prime solar cells[15] are used for their characteristics. These typical characteristics are used for the EPS design and are listed in Table 10.22. As mentioned in the environment section above, the characteristics are translated to what their characteristic would be at Mars.

Table 10.22: Typical solar array characteristics [20]

Characteristic	value	unit
Efficiency	30	%
Specific power	52	W/kg
Specific cost	3480	€/W
EOL degradation	66	%

The solar arrays require a deployment system. This system would require unfolding the solar arrays around one axis. For the sizing of actuators, torque has to be considered. As the deployment will take place in free floating space, there is no gravitational force to overcome when opening the solar array. The required torque is thus only dependant on the acceleration, which is undefined, but should not be so fast the solar array breaks. Using the Moog Type 1 rotary incremental actuator as a reference actuator size, a peak torque of 7.7 Nm is achieved at an assembly mass of 454 g.[16] Further analysis should be performed on the rotational torque.

During three instances there is a necessity for more power than the solar array can provide; pre-nominal operations power, peak power and nighttime. The energy accumulator should be rechargeable, and preferably have a high specific energy. Li-ion batteries have been vastly used in the past, proving their efficiency and high energy capacity [20]. For reference of typical characteristics, LG ICR18650 B3 Li-ion cells are considered.[17] The 18650 cell type is a cylindrical battery cell. Due to its shape, the packing efficiency is not the most optimal. Some of the characteristics of the LG B3 cells are given in Table 10.23. A very conservative Depth-of-Discharge (DoD) rate has been considered. A higher DoD has a negative effect on the battery lifetime [21]. A DoD of 60% has been decided upon. An added benefit is that the battery could provide more energy by discharging to a larger depth, in the case of an emergency.

Table 10.23: Typical 18650 Li-ion cell characteristics.

Characteristic	value	unit
Specific energy	191[20]	Wh/kg
Specific volume	250[20]	Wh/liter
specific cost	600[20]	€/kWh
EOL capacity	70[21]	%
DoD	60	%

The last hardware to consider is the power distribution system (PDS). The PDS controls the flow of electricity between subsystems. When comparing the different systems, the amount of power it can control, the weight, and the efficiency is important. For sizing purposes, an off-the-shelf PDS has been considered. The Ibeos 150-W SmallSat Electric Power System is one of the suggested power systems by NASA and suits the system needs [20]. It weighs 0.15 kg, has a typical consumption of 1.4 W and an efficiency of 95%.[18] As this is an off-the-shelf product, the product does not have to be developed, thus it is assumed the cost will be relatively low at 50000 €.

Power Budget

The power budget given in Table 9.1 provides the necessary power consumption of all the systems in the orbiter. In the table, a differentiation is made between nominal operations and pre-nominal operations. The pre-nominal operations, depicted in red, result in the necessary amount of energy that the battery should be able to provide in the time between launch and operational solar arrays. In black, the nominal operation budgets have been depicted. For the orbiter, the pre-nominal operations have not been defined, this is dependant on the launch. To prevent underestimating, a conservative 0.139 kWh energy budget has been taken into account.

[14] https://mmadesignllc.com/product/ehawk-27as112/, Accessed [15-06-2021]
[15] https://www.spectrolab.com/photovoltaics.html, Accessed [15-06-2021]
[16] https://www.moog.com/products/space-mechanisms/rotary-actuators.html, Accessed [16-06-2021]
[17] https://datasheetspdf.com/pdf-file/1418726/LG/ICR18650-B3/1, Accessed [15-06-2021]
[18] https://satsearch.co/products/ibeos-150w-smallsat-electric-power-subsystem Accessed [16-06-2021]

Verification & Validation

Code Verification

The calculation tool has been verified according to the method described in Chapter 5. The tool has been checked on correct programming logic and does not give any syntax errors.

Calculation Verification

In order to ensure the correctness of the code, input is given to the tool which results in an output. The input that is given is the power budget presented in Table 9.1. The same calculation have been done by hand and the resulting output should match the output of the tool.

Table 10.24: Calculation verification results

Equation	Input	Output tool	Output hand calculation	Error
Equation 10.14	Table 9.1	0.8946 kWh	0.8946 kWh	0%
Equation 10.15	Table 9.1	339.94 W	339.89 W	0.02%

As the small error is probably due to rounding errors, the code is considered to be verified.

Validation

The program that is written for this subsystem is purely intended as a calculation tool. No validation is applicable. The verified tool can be trusted on correctness of the calculations.

Results

Method

Finally, the EPS sizing has been performed via the method depicted in Figure 10.8. A Python program was written that calculates the system characteristics from the power budget. The environment, hardware characteristics and requirements stated in this chapter form the parameters that make up the calculation.

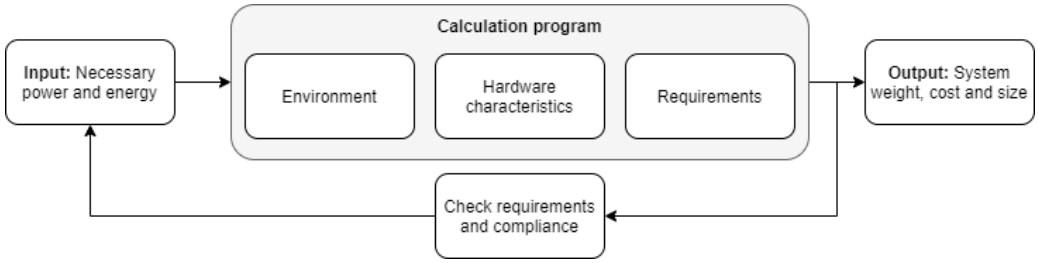

Figure 10.8: EPS sizing method

Calculations

The sizing of the system can be done based on two main parameters; the required energy that has to be stored and the required power the solar array should generate. The equations have been worked out for the parameters given in Table 9.1. During calculations the safety factor (SF) of 1.4 is applied as required by [DMD-SARR-BROOT-04].

The required amount of stored energy is calculated for a worst case scenario. For the orbiter, this is when the system has to perform peak power right after pre-nominal operations. This can be calculated using Equation 10.14.

$$E_{req} = (E_{pre-nominal} + E_{peak}) \cdot SF = 0.895 kWh \tag{10.14}$$

The required power generation by the solar array can be calculated using Equation 10.15.

$$P_{req} = (P_{total} + \frac{E_{req}}{sol * 3600}) \cdot SF / \eta_{PDS} = 339.9 W \tag{10.15}$$

The parameter P_{total} is the nominal power as given in Table 9.1.

The final EPS characteristics are then determined by using the hardware characteristics given in Table 10.22 and Table 10.23. For example, the battery mass is the required energy divided by the specific energy density of the battery.

System Characteristics

By using the method that is depicted above, the characteristics that are given in Table 10.21 and the budget that is given in Table 9.1, the resulting system characteristics are as given in Table 10.25. Also the electrical block diagram for the orbiter is given below in Figure 10.9.

Table 10.25: System characteristics of the Orbiter EPS.

Hardware	Mass [kg]	Power use [W]	Cost [M€]	Size	Performance
Battery	14.4		0.001	7.7 L	0.895 kWh
Solar array	7.1		1.3	2.07 m^2	339.9 W
PDS	0.24	2.24	0.05	0.28 L	
total	21.74	2.24	1.351	-	-

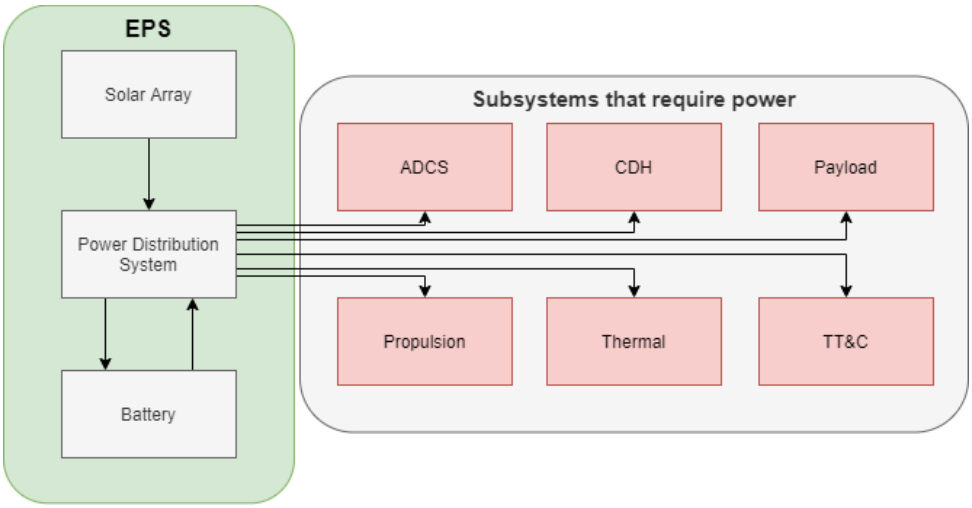

Figure 10.9: Electrical block diagram for the orbiter.

Recommendations

The EPS subsystem for the orbiter could be improved in design accuracy if pre-operational energy consumption is developed better. Besides that, the exact battery effectiveness and degradation, in combination with DoD, can be studied more. The structure of the solar array is included in the weight estimate of the solar array, but an actual structural analysis of solar array structural integrity can be performed as well. Lastly, the launch method should be able to put a better estimate on the pre-nominal operation budget.

10.8. Thermal Control

The thermal control system will keep the orbiter and its subsystems in the required temperature range. Exact control is sometimes necessary, as the survival temperature range for subsystems such as EPS and propulsion are quite narrow, even more so for their operational temperatures [9, p.428]. Therefore, the thermal control system shall be able to add or reject heat from the orbiter subsystems. The thermal control subsystem requirements are given in Table 10.26.

Requirements

Table 10.26: Requirements on the thermal control subsystem

ID	*Requirement*	*Status*	*Origin*	*Compliance*
DMD-THERM-O-01	The thermal control subsystem shall keep electronic power system within the operational temperature range of 273.15-313.15 K.	Replaced	EPS (Orbiter)	N.A.
DMD-THERM-O-01-A	The thermal control subsystem shall keep the electronic power system within the operational temperature range of 273.15-318.15 K.	New	Replaces [DMD-THERM-O-01]	Met

Continued on next page

Table 10.26 – continued from previous page

ID	*Requirement*	*Status*	*Origin*	*Compliance*
DMD-THERM-O-02	The thermal control subsystem shall keep lander within the operational temperature range of <tbd> K.	Replaced	EPS (Lander)	N.A.
DMD-THERM-O-02-A	The thermal control subsystem shall keep the landers within the survival temperature range of 253.15-333.15 K.	New	Replaces [DMD-THERM-O-02]	Met
DMD-THERM-O-03	The thermal control subsystem shall be able to generate heat to increase the internal temperature of the lander to nominally 293.15 K.	Replaced	Critical temperature range (excluding EPS)	N.A.
DMD-THERM-O-03-A	The thermal control subsystem shall be able to generate heat to increase the internal temperature of the orbiter to above nominally 263.15 K.	New	Replaces [DMD-THERM-O-03]	Met
DMD-THERM-O-04	The thermal control subsystem shall be able to radiate heat to decrease the internal temperature of the lander to nominally 293.15 K.	Replaced	Critical temperature range (excluding EPS)	N.A.
DMD-THERM-O-04-A	The thermal control subsystem shall be able to radiate heat to decrease the internal temperature of the orbiter to below nominally 313.15 K.	New	Replaces [DMD-THERM-O-04]	Met
DMD-THERM-O-05	The thermal control subsystem shall have a maximum power consumption of <tbd> W.	Replaced	Power budget	N.A.
DMD-THERM-O-05-A	The thermal control subsystem shall have a nominal power consumption of 45 W.	New	Replaces [DMD-THERM-O-05]	Met
DMD-THERM-O-06	The thermal control subsystem shall have a mass of 44 kg.	Active	Mass budget	Met
DMD-THERM-O-07	The thermal control subsystem shall be designed to allow for degradation.	Active	Stakeholder requirement [DMD-PERF-BROOT-09]	Met
DMD-THERM-O-08	The thermal control subsystem shall keep the propellant within the survivable temperature range of 278.15-313.15 K.	New	Propulsion	Met
DMD-THERM-O-09	The thermal control subsystem shall be able to store 2.4 MJ of heat.	New	Cooling requirements	Met

Design Process

The thermal control subsystem consists of active and passive control, where the main design goal is to limit the active control, thus limiting the power usage.[19]

Governing equation

The governing equation, being the heat equilibrium, is given in Equation 16.31. Time derivatives are excluded because changes slowly occur over time. On the left side, the heat added to the system is given. It consist of the heat absorbed by direct sunlight and other outside sources of radiation. Next, it includes the power dissipated by the internal subsystems. Furthermore, Q_{heat} represent the heat added to the system by heaters, the design

[19] https://www.nasa.gov/smallsat-institute/sst-soa-2020/thermal-control, Accessed [19-06-2021]

parameter. Notice that if this turns out negative, heat must be rejected from the system, in other words 'cooling'. On the right side, the heat emitted from the system is given, which occurs in the infrared spectrum.

$$Q_{absorbed} + \sum P_{dissipated} + Q_{heat} = Q_{emitted} \tag{10.16}$$

The absorbed heat by the system is threefold. It consists of the heat absorbed due to direct sunlight, the albedo effect and infrared radiation, shown in Equation 10.17. The direct sunlight is represented by the solar constant J_s, the albedo effect by J_a, and infrared radiation by J_{IR}. All terms are multiplied by the absorptivity, denoted as α. Notice the symbol ε (emissivity) for the infrared radiation. In this spectrum, the absorptivity equals the emissivity. To prevent any confusion, α_{IR} is called ε instead. Lastly, all terms include the incident area A_i.

The emitted heat is given in Equation 10.18. It includes the emissivity ε, which represents the emitted heat in the infrared region. Furthermore, the total emitting area A_e should be taken into account. Lastly, the difference in temperature between the system and its environment (Space) is present. For the orbiter in space, T_1 is neglected as it only measures approximately 3 K.[20]

$$Q_{absorbed} = \alpha J_s A_i + \alpha J_a A_i + \varepsilon J_{IR} A_i \tag{10.17}$$

$$Q_{emitted} = \varepsilon \sigma A_e (T_2^4 - T_1^4) \tag{10.18}$$

Critical scenarios

The orbiter is designed towards the critical scenarios according to risk [R-THERM-O-05]. This ensures it will be thermally stable at all times. The orbiter experiences two critical scenarios, that is at Earth or at Mars. This covers the warmest and coldest case respectively. For Earth, this means all three radiation terms: direct sunlight, the albedo effect and infrared radiation. On the other hand, for Mars, it is known that the orbit is always in direct sunlight, according to requirement [DMD-ASTRO-10]. This was required due to the risk [R-THERM-O-02]. Therefore, all three radiation terms are also included. Notice that for all constants, a subscript 'e' or 'm' is used to denote Earth or Mars respectively. These constants, as well as symbols, are listed in Chapter 4.

Passive and active control

A Python program was written which calculates the nominal power, the weight of the coating or paint and insulation, and the weight of the active heating and cooling devices. It uses the radius and height of the orbiter, the nominal power, and the mass of the EPS subsystem and propellant as an input. Furthermore, the orbiter is divided into two parts for the modelling. One side will point towards the significant radiation sources at Earth and the other side which would point to those at Mars, denoted by 'insul' and 'open' respectively. This is done so that the heat absorption can be minimised at Earth and maximised at Mars. The program then calculates the optimal values for the absorptivities (2x) and emissivities (2x), that result in the least amount of active cooling and heating. In Equation 16.31, a negative value for Q_{heat} means cooling, whereas a positive value indicates heating. For each new combination of alpha and epsilon, the following three statements were checked. $Q_{heat_{max}}$ and $Q_{heat_{min}}$ represent the heat Q_{heat} to be added at the maximum and minimum heat received respectively. Again, if Q_{heat} turns to be negative, it indicates cooling.

$$|Q_{T_{max}} + Q_{T_{min}}|_{new} < |Q_{T_{max}} + Q_{T_{min}}|_{old} \tag{10.19}$$

$$|Q_{T_{max}}|_{new} < |Q_{T_{max}}|_{old} \tag{10.20}$$

$$|Q_{T_{min}}|_{new} < |Q_{T_{min}}|_{old} \tag{10.21}$$

Each time, the program updates the heating and cooling needed, as well as the absorptivities and emissivities. Next, suitable coatings/paints where chosen that best fit the optimal absorptivity and emissivity. For the 'insul' area, a silver vapor deposited coating was chosen, where $\alpha = 0.04$ and $\varepsilon = 0.02$. On the other hand, for the 'open' area, a buffed aluminium coating was the best choice, with $\alpha = 0.16$ and $\varepsilon = 0.03$ [22].

Moreover, risks [R-THERM-O-03] and [R-THERM-O-04] led to requirements [DMD-THERM-O-01-A] and [DMD-THERM-O-08] respectively. Both the EPS and propellant are insulated with Mutli-layer insulation (MLI) to comply with these.

The program was run again with the exact values for the absorptivities and emissivities, which returned the updated heating and cooling required, as well as the weight of the coatings/paints and MLI. Then, patch heaters were selected that can heat up the system, as well as a heat sink that can store excessive heat. There are plenty of options for a heater, provided by Minco [23]. A final decision has not yet been made. For cooling, a heat sink based on phase change materials (PCM) is chosen.[21][22] This fulfils requirements [DMD-THERM-O-03-A] and [DMD-THERM-O-04-A] respectively.

[20] https://science.nasa.gov/science-news/science-at-nasa/2014/30jan_coldspot, Accessed [19-06-2021]
[21] https://www.heat4cool.eu/pcm-storage/, Accessed [19-06-2021]
[22] https://kulrtechnology.com/ara-thermal-capacitor/, Accessed [19-06-2021]

For the 10 landers, a different coating material is needed, split into a heat shield and a backshell. The heat shield consists of PICA, where $\alpha = 0.94$ and $\varepsilon = 0.9$. The backshell uses a different coating, namely OSO-H White Paint 63W, where $\alpha = 0.27$ and $\varepsilon = 0.83$ [22]. The program calculates that the landers are passively stable, fulfilling requirement [DMD-THERM-O-02-A].

Verification and Validation

The Python code was mainly written by the lead thermal control engineer. To aid in the verification process, the back-up engineer reviewed the code for syntax errors. No direct mistakes were found in the code in its final form.

In addition, unit tests were done for crucial parts in the code. While the code is rather elaborate, many parts of it estimate the required power and mass of the thermal control components. Furthermore, the most intensive part of the code is the determination of the optimal α and ε, found by Equation 10.19 to Equation 10.21. This part of the coding was only used to determine the approximate range for the values, after which the parameters of existing coatings were entered in the code. The main calculation of the code then reduces to the implementation of the heat equilibrium equation. This calculation step was verified by hand, using a simplified input, as shown in Table 10.27. As the results show, there is an error of 0% in these calculations, which is to be expected for a rather simple implementation.

Table 10.27: Manual verification of heat equilibrium calculation

Input	Value	Output	Value (manual)	Value (Python)
α_{open}, ε_{open}	0.05	Q_{abs} max. (W)	131.04	131.04
α_{insul}, ε_{insul}	0.1	Q_{emit} max. (W)	80.06	80.06
Radius (m)	0.1	$P_{T_{max}}$ (W)	43.98	43.98
Height (m)	5	-		
P_{diss} (W)	7	-		

On the other hand, the validation was performed by inserting actual data of the MAVEN orbiter.[23] Running the code, it is difficult to compare both cases, because there exist various thermal solutions. However, the desired absorptivity and emissivity that the program returned, were close to the actual coating.[24] This is an indication that the crucial part of the code is correct, thereby validating the code.

System Performance and Characteristics

Taking into account safety factors of 1.5 for the mass, and setting the required power equal to the nominal power is conservative. This fulfills requirement [DMD-THERM-O-07]. Lastly, Table 10.28 shows the performance characteristics of the thermal control subsystem, which indicates that requirements [DMD-THERM-O-05-A], [DMD-THERM-O-06], [DMD-THERM-O-09] are met. To conclude, system requirement [DMD-ORBITER-10] is met.

Table 10.28: Summary of thermal control subsystem performance

Component	Description	Mass (kg)	Nominal power (W)
Heaters	Minco	0.0264	44.06
Heat sink	PCM	20.2	
Paint/Coatings	Silver Vapor Deposited & Buffer Aluminium	8.98	
Insulation	MLI	13.9	
Heat sensors	Minco	Unknown	Unknown
Total power			44.06
Total mass		43.1	

Recommendations

The next design step would be to look into peak power. When the moons of Mars cause the orbiter to be in eclipse, an extra amount of power would be necessary, or the heat sink could be a solution. This would resolve risk [R-THERM-O-01]. Further recommendations include investigating a hibernation mode. Internal conduction between subsystems can also be considered. Finally, it is recommended to look into the necessity of radiators. The orbiter currently only uses the heat sink for heat ejection, assuming the heat can be reused later, thus leading to a limited required capacity for the heat sink. However, if the maximal amount of heat in the heat sink cannot

[23] https://www.nasa.gov/mission_pages/maven/spacecraft/index.html, Accessed [21-06-2021]
[24] https://spaceflight101.com/maven/spacecraft-information/, Accessed [21-06-2021]

be reused during its lifetime, radiators are required. Given that the orbiter requires nearly constant heating at Mars, this is unlikely however.

10.9. Propulsion

The propulsion subsystem of the orbiter will serve to meet the Δ V requirements set in Chapter 8. Because of stakeholder requirement [DMD-DESR-BROOT-03], the use of propellant on the landers below 10 km is prohibited. It was previously decided to design the landers without any propulsion system, as a result of the trade-off performed in the Midterm Report [6]. The propulsion subsystem is therefore only designed for the orbiter. The propulsion subsystem requirements are given in Table 10.29.

Requirements

Table 10.29: Requirements on the propulsion subsystem

ID	*Requirement*	*Status*	*Origin*	*Compliance*
DMD-PROP-O-01	The propulsion subsystem shall provide a total ΔV of 1000 m/s for Mars orbit insertion.	Active	Astrodynamics	Met
DMD-PROP-O-02	The propulsion subsystem shall provide a total ΔV of 147.6 m/s for orbit maintenance.	Active	Astrodynamics	Met
DMD-PROP-O-03	The propulsion subsystem shall have a restart capability of at least 100 cycles.	Active	Astrodynamics	Met
DMD-PROP-O-04	The propulsion subsystem shall provide a thrust of at least 424 N.	Active	Thruster specifications	Met
DMD-PROP-O-05	The propulsion subsystem shall have a maximum dry mass of 138 kg.	Active	Mass budget	Met
DMD-PROP-O-06	The propulsion subsystem shall have a maximum power use of 186 W.	Active	Power budget	Met
DMD-PROP-O-07	The propulsion subsystem shall have a minimum vacuum specific impulse of 317 s.	Active	Astrodynamics	Met
DMD-PROP-O-08	The propulsion subsystem shall have a maximum volume of 1220 m^3.	New	Structures	Met
DMD-PROP-O-09	The propulsion subsystem shall have a maximum internal data rate of 2560 bit/s.	New	Memory budget	Met
DMD-PROP-O-10	The propulsion subsystem shall provide a total ΔV of 147.6 m/s for transfer orbit course corrections.	New	Astrodynamics	Met
DMD-PROP-O-11	The propulsion subsystem shall provide a total ΔV of 262.5 m/s during the deployment sequence.	New	Astrodynamics	Met
DMD-PROP-O-12	The propulsion subsystem shall provide a total ΔV of 513.3 m/s for a deorbit manoeuvre.	New	Astrodynamics	Met

Design Process

The first design choice is propulsion type where the two high-level options are chemical or electric propulsion [9]. Electric propulsion provides high efficiency, with large values for specific impulse (Isp). However, the mission requires relatively short burn times, to allow for the accurate orientation during the lander deployment. Therefore, the low thrust capabilities of electric propulsion make it unfit for the requirements of the Mars Deploy orbiter.

Next, within chemical propulsion, the two conventional options for orbiters with large and restartable ΔV requirements are liquid monopropellant and bipropellant systems. In the Midterm Report, a literature study was performed on heritage Mars orbiter missions, including four NASA and two ESA missions [6]. In this study, it was found that the only feasible space-flown options for high performance space propulsion are hydrazine monopropellant systems or dinitrogen tetroxide (NTO)/ monomethylhydrazine (MMH) bipropellant systems. Following the propulsion systems of the ESA Mars Express and Trace Gas Orbiter (TGO), it was decided to use an Arianegroup S400-15 thruster as the main engine [24]. This is an NTO/MMH bipropellant system, with a vacuum Isp of 317 s and a nominal thrust of 425 N.[25]

Propellant Mass

As the orbiter releases a pair of entry probes after each orientation manoeuvre, thereby decreasing its dry mass, the estimation of propellant mass has a somewhat staged approach. The general procedure of calculating the propellant mass and sizing the propulsion system is visualised in Figure 10.10. A Python code was written which implements this structure. The main calculation step is implementing the Tsiolkovsky rocket equation, which is rearranged for starting mass in Equation 10.22.

$$M_s = M_f \cdot e^{\left(\frac{dV}{Isp \cdot g_0}\right)} \tag{10.22}$$

As the diagram in Figure 10.10 shows, the total propellant mass is determined by working backwards from the de-orbit manoeuvre. The three computational blocks find the propellant mass required for the respective ΔV requirements of 2838, 40.6 and 148 m/s for each phase in which dry mass is constant. Using Equation 10.22, the script starts with the orbiter dry mass of 390 kg, with all probes released and the ΔV of 2838 m/s required for MOI, orbit maintenance and the de-orbit burn. The script then finds that 611 kg of propellant is required for these conditions. At the end, a 5 % safety margin is added to the propellant mass, to account for unknown performance deviations, leading to a total propellant mass of 1054 kg.

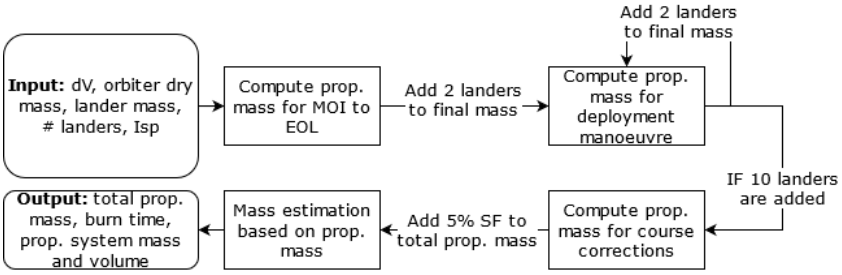

Figure 10.10: Diagram of the calculation procedure for the propulsion subsystem

System Architecture and Components

The sizing of the propellant tanks is based on existing components, produced by Arianegroup.[26] With a mixture ratio of 1.64, the required NTO and MMH have roughly the same volume, at 498 L, including an 8% ullage [9]. The propellant tank is then assumed to be a spherical titanium tank, with a radius of 49 cm.

As the same propellant type and thruster are used, the system architecture of the TGO is used to determine the required components, which also mitigates risks [R-PROP-O-01] and [R-PROP-O-02].[27] This system is a regulated pressurised system, using helium. The same choice is made for the Mars Deploy orbiter and doubly redundant helium tanks are included. A ratio of 0.0655 of the total propellant volume is used from the Mars Express propulsion system and two Northrop Grumman 36.1 L titanium helium tanks are included [24].[28] To estimate the mass of other components such as valves and pipes, the masses of components in the NASA Mars Global Surveyor (MGS) propulsion system are used [25].

[25] https://www.space-propulsion.com/spacecraft-propulsion/apogee-motors/index.html, Accessed [16-06-2021]
[26] https://www.space-propulsion.com/spacecraft-propulsion/bipropellant-tanks/index.html, Accessed [16-06-2021]
[27] https://spaceflight101.com/exomars/trace-gas-orbiter/, Accessed [16-06-2021]
[28] https://www.northropgrumman.com/space/pressurant-tanks-data-sheets-sorted-by-volume/, Accessed [16-06-2021]

Verification and Validation

The simple code to estimate propellant mass was verified by performing the same calculations by hand, for a simplified input. First, the single calculation of the rocket equation was checked, with ΔV of 1000 m/s and a dry mass of 9000 kg. The solution of 3925.627 kg of propellant was found exactly when calculating by hand. The staged calculation, shown in the first three computational blocks of Figure 10.10, was calculated for a dry mass of 9000 kg, a probe mass of 100 kg, and ΔV values of 1000, 20 and 150 m/s for the three blocks respectively. The manual outcome for propellant mass of 4339.08 kg differs from the Python solution of 4340.60 kg by 0.03%, thus the code is verified.

For validation, the propulsion system of the MGS was considered [25]. A total ΔV of 1124.11 m/s was provided by the main engine with Isp 318 s and a ΔV of 155.84 m/s was provided by smaller engines with Isp 229 s.[29] [30] To achieve this, the orbiter included 387.4 kg of propellant [25]. Using the Python script, the propellant mass is estimated to be 390.6 kg, translating to a conservative error of 0.8 %, thereby validating the code.

System Performance and Characteristics

The main propulsion system parameters are summarised in Table 10.30. The main engine, pressurant tanks and miscellaneous components were adapted from existing applications, respectively the Arianegroup S400-15 thruster, the Northrop Grumman 80314-201 helium tank and the system components from the MGS. However, the propellant tank was assumed to be sized as a titanium spherical tank, similar to those produced by Arianegroup.

Table 10.30: Summary of propulsion subsystem performance

Component	Description	Mass (kg)
Main engine	Isp: 317 s, T: 425 N	4.3
Propellant	NTO/MMH, Total ΔV: 3248.2 m/s	1053.82
Propellant tank	2x spherical Ti, V: 995.23 L	68
Pressurant gas	Helium, 330 bar	3.66
Pressurant tank	2x spherical Ti, V: 72.2 L	32
Miscellaneous	26x pyro valve, 6x latch valve, 17x fill & drain valve, 6x pressure sensor, 7x filter, 4x check valve, 2x pressure regulator, propellant lines	29.6
Total wet mass		1191.6

Recommendations

The next steps in the design would be to investigate the exact implications of the system architecture on the orbiter mass moment of inertia, taking into account propellant sloshing. While the two tanks have the same volume, NTO has a higher density, therefore it's tank will be heavier. As is visible in Figure 9.5, the two tanks are currently placed on top of each other. However, with the orbit orientation shown in Figure 9.4, it is possible that sloshing and the decrease in propellant mass will create undesired moments about the orbiter's center of mass. To balance this, the second propellant tank could be placed above the other subsystems, while this will lead to more complex connections and longer propellant lines.

Another interesting recommendation is to look into the feasibility of replacing NTO/MMH by a bipropellant hydrogen peroxide (HP)/ethanol system. From a sustainability perspective, this change would result in a less toxic system, which has less handling costs. Furthermore, it addresses risk [R-PROP-O-05]. At this conceptual design phase, the more conventional hydrazine system was chosen so that existing components can be found easily. After an interview with Dr. Botchu Jyoti, it was confirmed that a HP/ethanol system could be imposed on an existing hydrazine architecture, as the propellant properties are similar. Furthermore, HP/ethanol propulsion systems have been produced and tested experimentally, but mostly in the thrust range of 1 to 10 N [26]. Higher thrust capabilities are expected in the very near future. Other promising results are related to different HP/carbohydrate systems in the range of 500 and 1200 N [27][28].

11. Sustainability

After the orbiter subsystems have been designed, an evaluation of the design's sustainability is made in this chapter. The evaluation will go over each of the six sustainability criteria, identifying the most important concerns

[29] http://www.astronautix.com/m/mr-111.html, Accessed [16-06-2021]
[30] http://astronautix.com/l/leros-1c.html, Accessed [16-06-2021]

across all subsystems. It is therefore important to note that the main focus will be the weak points of the system's sustainability. The intention is to find recommendations and other important factors to keep in mind in the future design of the subsystems.

11.1. SC-1: Fair Wages and Taxes

In many of the orbiter subsystems, electronic components are used. This is especially true for the C&DH, EPS and TTC subsystems. An important factor in this regard is the use of rare Earth elements (REE) or other precious minerals that are crucial in the functionality of many electronic components. The intensive exploitation of these materials brings many sustainability issues, the first being worker conditions.

95 % of the worldwide REE are produced in China, with a priority of keeping costs low, leading to a poor treatment of workers and the environment.[1] Furthermore, China often uses its REE advantage as a geopolitical leverage, which can destabilize the global economy.[2] Other elements that are vital for the production of batteries and capacitors are coltan and cobalt, which are predominantly sourced from the Democratic Republic of Congo. In these mines, working conditions are often inhumane: minors are used as modern slaves, workers are extorted and exposed to heavy and unsafe labour [29].[3]

Another concern in the orbiter design related to SC-1 is the use of off-the-shelf components produced by young start-up companies. While these companies push forward innovation in the industry, the competitive nature of the start-up space industry can lead to a demanding workload and office environment that can lead to undesirable conditions.[4] [5]

11.2. SC-2: Reuse and Recycle

In the Reuse and Recycle criterion, the use of REE has implications as well. While REE can be recycled, currently only around 1% are recycled from end products [30]. This means that REE can currently be considered as a depletable resource, leading to economic, environmental and social tensions. Furthermore, the structure of the orbiter is primarily made up of carbon fiber reinforced polymers and a honeycomb structure of Nomex, which is an aramid polymer. Aramid fibers are already recycled on an industrial scale, whereas carbon fiber recycling is still more experimental, struggling to achieve competitive costs.[6] [7]

Concerning the reuse of components, the orbiter has little potential, besides its use of a reusable launch vehicle in the SpaceX Falcon Heavy. The propulsion system of the orbiter itself is more recyclable, as all propellant and pressurant tanks are constructed in titanium.[8]

11.3. SC-3: Renewable

For the pre-operation renewability of the orbiter, the point of focus is how energy intensive the production of all subsystems is. The use of renewable energy mostly depends on the energy mix of the country where the component is produced. As most countries still only produce a small percentage of energy from renewable sources, it is assumed that the production of any component or material can be more renewable if less energy is used. Again, the use of REE is a major issue, as the mining is very energy intensive and mostly conducted in less industrialized countries with a more fossil energy mix.[9] [10] When the carbon fiber structure is not produced with recycled components, the production of new carbon fibers is also about 14 times more energy intensive than conventional steel production [31].

The orbiter itself uses renewable energy in the form of solar energy, but its current NTO/MMH propellants cannot be acquired from renewable sources. However, if the propulsion system is replaced by a HP/ethanol bipropellant system, the two propellants result a in much more renewable energy source, as both can be obtained from quasi-renewable materials and produced with renewable energy [32][33].

11.4. SC-4: Transparent Use

In space engineering, some issues with the transparent use or sourcing of components relate to the fact that many space companies are contracted by militaries across the world. The propulsion system uses components built by the Airbus group and C&DH uses components produced by Innoflight, which produces avionics for the US

[1] https://e360.yale.edu/features/boom_in_mining_rare_earths_poses_mounting_toxic_risks, Accessed [17-06-2021]
[2] https://worldview.stratfor.com/article/geopolitics-rare-earth-elements, Accessed [17-06-2021]
[3] https://www.cfr.org/blog/why-cobalt-mining-drc-needs-urgent-attention, Accessed [17-06-2021]
[4] https://spacenews.com/from-the-pandemic-to-going-public-space-startups-face-hiring-challenges/, Accessed [17-06-2021]
[5] https://www.washingtonpost.com/technology/2020/06/25/tesla-plant-firings/, Accessed [17-06-2021]
[6] https://www.brentindustries.com/aramid/, Accessed [17-06-2021]
[7] https://www.compositesworld.com/articles/the-state-of-recycled-carbon-fiber, Accessed [17-06-2021]
[8] https://globemetal.com/metals/titanium/, Accessed [17-06-2021]
[9] https://e360.yale.edu/features/boom_in_mining_rare_earths_poses_mounting_toxic_risks, Accessed [17-06-2021]
[10] https://e360.yale.edu/features/china-wrestles-with-the-toxic-aftermath-of-rare-earth-mining, Accessed [17-06-2021]

Army and Lockheed Martin, among others.[11] [12] Prohibiting the cooperation between the Mars Deploy mission and companies with military applications is most likely unfeasible and unreasonable. However, it is important to keep in mind that by cooperating with these companies, problematic constructs such as the US military industrial complex and the further development of high-tech warfare are upheld.

11.5. SC-5: Non-toxic

Evaluating the toxicity of Mars Deploy pre-operation, the use of REE has large implications yet again. The mining of REE exposes workers to toxic and radioactive waste, which leads to an increased risk of cancer.[13] Secondly, hydrazine is used in the propulsion system and ADCS. This fuel is carcinogenic and fatal when inhaled, leading to very cautious and expensive handling procedures [34]. The alternative propulsion system with HP and ethanol is the best solution to solve this issue, as these two propellants are relatively harmless.

11.6. SC-6: Non-polluting

Finally, the final sustainability criterion evaluates the air, land and water pollution of the design pre-, in- and post-operation. REE mines have many negative effects on the surrounding environment, causing water and land pollution due to the chemicals used in excavation methods. In China, the long-term effects and costs of the cleanup of these sites have become clear.[14]

Furthermore, the orbiter design includes two less obvious choices to reduce pollution. Firstly, the orbiter is launched to initially "miss" Mars, thereby reducing how critical the decontamination requirements for the orbiter are, following the Planetary Protection guidelines [4]. However, during the deployment, the orbiter is pointed towards Mars five times, to deploy the entry capsules. If the propulsion system fails at this moment, the orbiter is on a trajectory to impact Mars, thus the chance of contaminating the planet is increased. Secondly, by using a phased array system, the TTC subsystem reduces the frequency pollution that will be created by the orbiter.

11.7. Conclusion

Concluding the sustainability evaluation of the orbiter, Table 11.1 gives an overview of the most important sustainability considerations for all subsystems. The two key recommendations are to make a conscious effort to ethically source REE and to replace the NTO/MMH propulsion system by the more sustainable HP/ethanol system.

Concerning the first recommendation, there already exist REE mining companies, such as Lynas Rare Earths, that make a conscious effort to include sustainability.[15] When purchasing off-the-shelf electronic components, the Mars Deploy project should investigate where the manufacturer sources its REE. The second recommendation has already been treated in Section 10.9, where it was found that viable HP/ethanol thrusters are still in an experimental research phase.

Table 11.1: Evaluation of sustainability criteria for each orbiter subsystem. REE denotes rare Earth elements, CF denotes carbon fiber.

SC	ADCS	CDH	EPS	GNC	PROP	STRUC	TCS	TTC
SC-1		REE, startup comp.	REE, coltan and cobalt					REE, startup comp.
SC-2		REE	REE		Recycled Ti, launch vehicle reused	CF not recycled		
SC-3			Solar energy		NTO/MMH non-renewable	CF production		
SC-4		Military use			Military use			
SC-5	Hydrazine toxicity	REE	REE		Hydrazine toxicity		Non-toxic materials used	REE
SC-6		REE	REE	Orbit misses Mars, EOL deorbit	Launch vehicle pollution	CF production		Less freq. pollution, REE

[11] https://www.airbus.com/defence.html, Accessed [17-06-2021]
[12] https://www.innoflight.com/, Accessed [17-06-2021]
[13] https://e360.yale.edu/features/boom_in_mining_rare_earths_poses_mounting_toxic_risks, Accessed [17-06-2021]
[14] https://e360.yale.edu/features/china-wrestles-with-the-toxic-aftermath-of-rare-earth-mining, Accessed [17-06-2021]
[15] https://lynasrareearths.com/sustainability/our-commitment-to-sustainability/, Accessed [17-06-2021]

12. Risk

The technical risks of the orbiter are discussed in this chapter. First, Section 12.1 describes the approach to assessing and managing the risks. Then, Section 12.2 lists all the risks and their mitigation strategy per subsystem. Lastly, a concise conclusion is given in Section 12.3.

12.1. Technical Risk Assessment and Management

Each design contains technical risks. This section describes the assessment and management of these risks. To ensure the validity of the approach, a consistent approach to assess and manage risk is used. First, the risk manager, in consultation with each engineer, identifies the technical risks of their respective subsystem. Some environmental risks are added too, which are respectively grouped with the subsystem they have the most significant effect on. Then, each risk is given a score to reflect the severity. The scoring method incorporates both the probability and impact. Both are assigned a score between one and five. The reasoning behind this is given below.

Probability

- **Very low (1):** Failure chance between 0-0.1%.
- **Low (2):** Failure chance between 0.1-1%.
- **Moderate (3):** Failure chance between 1-5%.
- **High (4):** Failure chance between 5-25%.
- **Very high (5):** Failure chance above 25%.

Impact

- **Negligible (1):** No significant effect on the system requirements.
- **Low (2):** One system requirement is not met.
- **Marginal (3):** Multiple system requirements are not met.
- **Critical (4):** One or more stakeholder requirements are not met.
- **Catastrophic (5):** The project objective statement is not fulfilled.

After identifying all risks and scoring them, a strategy was developed to manage all risks. The common method is to mitigate each risk. This can range from including safety factors, to testing. The mitigation is either 'done' already, or 'planned' to do in the upcoming phases of the design. After mitigation, the severity was reassessed. It had either reduced the probability, impact or both. Moreover, two other possibilities to manage risks are either to completely delete or ignore them, indicated by 'DEL.' and 'NO MITIGATION INCLUDED' respectively. After mitigation, the risks are revised and checked upon to see whether they are critical. A combined score (probability + impact) above six is deemed too severe.

12.2. Subsystems

Each risk per subsystem is archived in Table 18.1, where every single risk is listed on one row. The table contains five columns; the ID uniquely assigns a tag to each risk. Next, a concise description of the risk is provided. Then, the severity before mitigation (RBM) is given as 'probability, impact'. Furthermore, a mitigation strategy is shortly discussed. Lastly, an updated score for the severity is given as RAM. Notice the colouring system, this is added to see the decrease in severity, as well as to visually identify critical risks. These require specific attention and should be carefully mitigated. The colouring system is based on the addition of probability & impact, and is given below. As a combined score above six is too high, orange indicates the risk needs extra attention.

- Score = 2, 3, 4: Green
- Score = 5, 6: Yellow
- Score = 7, 8: Orange
- Score = 9, 10: Red

Elaborating on the scoring method before mitigation, the impact is fairly easy to assess based on the requirements. On the other hand, the probability is more difficult to assign a score to. First, the total amount of successful

orbiters to Mars was determined. Out of 18 missions, 12 were successful, counting from the year 1975.[1] This equals a failure rate of 1/3. Then, for each subsystem the overall failure chance was retrieved from a research paper [35]. Furthermore, this paper gives the failure rate for the main subsystem components. For instance, the electrical power subsystem (EPS) includes solar array, battery, power regulator, etc. The failure rate for each category is given and each risk can be assigned to one of these categories. To obtain the probability, the three aforementioned failure chances were multiplied. When a risk could not easily be grouped into a category, it was compared to similar, known risks that were already listed in Table 18.1. If little information was available in [35], further research was done, and a source is given at the 'mitigation' column. Notice that environmental risks are indicated by '(Environmental)' behind the 'Description'.

Table 12.1: Identified technical risks. RBM is the probability and impact before mitigation, RAM is the probability and impact after mitigation.

ID	*Description*	*RBM*	*Mitigation*	*RAM*
ADCS				
R-ADCS-O-01	Reaction wheel fails.	2, 2	*Done:* Forth reaction wheel added for redundancy and installed at an angle.	2, 1
R-ADCS-O-02	Inertial measurement unit (IMU) delivers faulty data.	4, 3	*Done:* Secondary IMU installed with 3 accelerometers and 3 gyroscopes each.	4, 1
R-ADCS-O-03	Star tracker fails to deliver attitude information.	2, 3	*Done:* Secondary star tracker included for redundancy.	2, 1
R-ADCS-O-04	Sun sensor is blocked by the spacecraft bus or appendages.	2, 3	*Done:* 6 sun sensors distributed over the spacecraft surface to ensure line of sight with the sun.	1, 3
R-ADCS-O-05	Firing of RCS thrusters introduces transverse velocities disturbing the trajectory.	3, 2	*Done:* Thrusters are installed in pairs to provide a couple moment.	2, 2
R-ADCS-O-06	RCS thruster fails.	3, 4	*Done:* A total of 12 thrusters are installed. If one thruster is lost, the other can still provide rotation with reaction wheels counter-acting the instabilty.	3, 1
R-ADCS-O-07	Fuel tank leakage.	2, 4	*Done:* A safety margin of 20% is added to the propellant mass for RCS. *Planned:* Nondestructive testing (NDT) of the fuel tank.	1, 2
C&DH				
R-CDH-O-01	The orbiter C&DH system will run out of storage space for scientific data.	2, 4	*Done:* The storage will be designed such that it is able to store 60 sols without contact to the relay orbiter.	1, 4
R-CDH-O-02	System errors making the orbiter not usable.	2, 5	*Planned:* Implementing a back up system from which the error can manually or automatically be resolved.	2, 2
R-CDH-O-03	The system will not have enough throughput to process all the gathered data.	3, 4	*Done:* Have multiple processing units on board to spread the load.	1, 4
R-CDH-O-04	Radiation will damage the electronics in the on board computer.	2, 4	*Done:* Use space grade radiation hardened components that are guaranteed to survive the radiation environment.	1, 4
EPS				

Continued on next page

[1] https://westeastspace.com/encyclopedia/missions-to-mars/, Accessed [14-06-2021]

Table 12.1 – continued from previous page

ID	*Description*	*RBM*	*Mitigation*	*RAM*
R-EPS-O-01	The moons of Mars cause the orbiter to be in eclipse. (Environmental)	1, 4	*Done:* Bring batteries.	1, 1
R-EPS-O-02	Energy storage system failure.	3, 4	*Planned:* Careful production process.	1, 4
R-EPS-O-03	The solar array deployment mechanism fails to deploy.	3, 5	*Done:* Two actuator per axis for redundancy.	1, 5
R-EPS-O-04	Space debris impact on arrays. (Environmental)	3, 3	*Planned:* Solar arrays are only deployed after a clearance of 2000 km from Earth.[2]	1, 3
G&N				
R-GN-O-01	No ephemeris data is received from the DSN.	2, 4	*Done:* Use the IMU to determine position and velocity.	2, 1
R-GN-O-02	dV increment isn't accurate enough.	2, 3	*Done:* The release point of the lander probes is brought closer to Mars.	2, 2
R-GN-O-03	Disturbances (aerodynamic or gravity pull) change the course of the orbit around Mars. (Environmental)	2, 3	*Done:* A 5% dV margin is added.	2, 1
Propulsion				
R-PROP-O-01	A pyro valve fails to activate.	2, 5	*Done:* All valves have double redundancy.	2, 2
R-PROP-O-02	A propellant latch valve malfunctions.	2, 5	*Done:* All valves have double redundancy.	2, 2
R-PROP-O-03	The thruster Isp is lower than its specified value.	2, 4	*Done:* A 5% safety margin of propellant is included.	2, 2
R-PROP-O-04	One of the propellant tanks leaks.	2, 4	*Done:* A 5% safety margin of propellant is included. *Planned:* Nondestructive testing (NDT) of the fuel tank.	1, 2
R-PROP-O-05	The use of hydrazine is banned before the planned mission start.[3] (Environmental)	4, 5	*Planned:* Alternative systems with HP/ethanol bipropellants are used.	DEL.
R-PROP-O-06	The thruster is misaligned with respect to the orbiter.	2, 3	*Done:* The ADCS counteracts induced moments and a 5% safety margin is added to propellant mass.	2, 1
R-PROP-O-07	The propellant is contaminated and starts decomposing before use.	2, 4	*Planned:* Additional precautions are followed during tank cleaning and orbiter fueling.	2, 1
Structures				

Continued on next page

[2] https://www.britannica.com/technology/space-debris, Accessed [18-06-2021]
[3] https://echa.europa.eu/candidate-list-table/-/dislist/details/0b0236e1807da31d, Accessed [15-06-2021]

Table 12.1 – continued from previous page

ID	*Description*	*RBM*	*Mitigation*	*RAM*
R-STRUC-O-01	The structure damages due to shear and bending loads caused by the capsules.	2, 4	*Done:* 50% extra support structure mass accounted for to reinforce structure. *Done:* Safety factor of 2 is applied to the applied loads. *Planned:* Local reinforcement can be designed, such as capsule attachment ring.	1, 4
R-STRUC-O-02	The capsule-orbiter attachments fail due to launch accelerations.	2, 5	*Planned:* Design more rigid connections.	1, 5
R-STRUC-O-03	Production flaws in the honeycomb structure.	2, 4	*Planned:* Use isogrid shell instead. *Planned:* Perform thorough testing.	1, 4
R-STRUC-O-04	The structure buckles during launch.	2, 4	*Done:* Safety factor of 2 is used on the loads. *Done:* Sandwich panel is used. *Planned:* Perform thorough testing.	1, 4
R-STRUC-O-05	The sandwich panel's skin delaminates from the core.	2, 4	*Planned:* Perform thorough testing. *Planned:* Use isogrid or conventional structure instead.	1, 4
R-STRUC-O-06	The structure damages due to launch vibrations.	2, 4	*Planned:* Perform vibrational analysis. *Planned:* Use stiffer structure.	1, 4
R-STRUC-O-07	The capsule-orbiter attachments fail due to launch vibrations.	2, 5	*Planned:* Perform vibrational analysis. *Planned:* Design larger and stiffer attachments.	1, 5
Thermal Control				
R-THERM-O-01	The moons of Mars cause the orbiter to be in eclipse, resulting in no direct sunlight (Environmental).	1, 4	*Planned:* Design for peak power.	1, 1
R-THERM-O-02	Mars causes the orbiter to be in eclipse, resulting in no direct sunlight (Environmental).	5, 4	*Done:* The orbiter is always in direct a direct sunlight orbit.	DEL.
R-THERM-O-03	The electrical power system experiences temperatures outside its operational range.	2, 5	*Done:* Use MLI to diminish fluctuating temperatures and provide heating and cooling.	1, 5
R-THERM-O-04	The propellant experiences temperatures outside its survivable range.	2, 5	*Done:* Use MLI to diminish fluctuating temperatures and provide heating and cooling.	1, 5
R-THERM-O-05	The orbiter experiences different conditions close to Earth and Mars, which causes the orbiter to exceed its temperature limits.	2, 5	*Done:* Design for the two worst case scenarios.	1, 5
TTC				
R-TTC-O-01	The main dish fails to orient.	2, 4	*Done:* Have backup system with isotropic antenna for commands.	2, 2
R-TTC-O-02	The UHF phased array fails.	2, 5	*Done:* Design two smaller antennas instead of one large antenna, for redundancy.	2, 2

Continued on next page

Table 12.1 – continued from previous page

ID	*Description*	*RBM*	*Mitigation*	*RAM*
R-TTC-O-03	The antenna loses location of landers.	3, 2	*Done:* Use DSN backup system to obtain coordinates and contact times.	3, 1
R-TTC-O-04	Data inflow/storage failure.	2, 2	*Done:* Keep data for at least 2 repeat orbits, so in case of corrupted connection it may be resent.	2, 1

All risks are mitigated within the allowable severity. No risk has a higher combined probability and impact than six. In many instances, the probability is very small, whereas the impact indicates failure of the entire mission. This shows how impactful some risks are, and that they should be carefully mitigated by reducing their probability.

To clearly indicate the transformation in severity of risks, a risk map before and after mitigation is shown in Table 12.2 and Table 12.3 respectively. This also allows to easily identify remaining critical risks.

Table 12.2: Technical risk map before mitigation, green and yellow is considered acceptable.

	Probability of occurrence				
Impact	*Very Low (1)*	*Low (2)*	*Moderate (3)*	*High (4)*	*Very High (5)*
Catastrophic (5)		**R-CDH-O-02, R-PROP-O-01, R-PROP-O-02, R-STRUC-O-02, R-STRUC-O-07, R-THERM-O-03, R-THERM-O-04, R-THERM-O-05, R-TTC-O-02**	**R-EPS-O-03**	**R-PROP-O-05**	
Critical (4)	**R-EPS-O-01, R-THERM-O-01**	**R-ADCS-O-07, R-CDH-O-01, R-CDH-O-04, R-GN-O-01, R-PROP-O-03, R-PROP-O-04, R-PROP-O-07, R-STRUC-O-01, R-STRUC-O-03, R-STRUC-O-04, R-STRUC-O-05, R-STRUC-O-06, R-TTC-O-01**	**R-ADCS-O-06, R-CDH-O-03, R-EPS-O-02**		**R-THERM-O-02**
Marginal (3)		**R-ADCS-O-03, R-ADCS-O-04, R-GN-O-02, R-GN-O-03, R-PROP-O-06**	**R-EPS-O-04**	**R-ADCS-O-02**	
Low (2)		**R-ADCS-O-01, R-TTC-O-04**	**R-ADCS-O-05, R-TTC-O-03**		
Negligible (1)					

Table 12.3: Technical risk map after mitigation, green and yellow is considered acceptable.

	Probability of occurrence				
Impact	*Very Low (1)*	*Low (2)*	*Moderate (3)*	*High (4)*	*Very High (5)*
Catastrophic (5)	**R-EPS-O-03, R-STRUC-O-02, R-STRUC-O-07, R-THERM-O-03, R-THERM-O-04, R-THERM-O-05**				
Critical (4)	**R-CHD-O-01, R-CHD-O-03, R-CHD-O-04, R-EPS-O-02, R-STRUC-O-01, R-STRUC-O-03, R-STRUC-O-04, R-STRUC-O-05, R-STRUC-O-06**				
Marginal (3)	**R-ADCS-O-04, R-EPS-O-04**				
Low (2)	**R-ADCS-O-07, R-PROP-O-04**	**R-ADCS-O-05, R-CHD-O-02, R-GN-O-02, R-PROP-O-01, R-PROP-O-02, R-PROP-O-03, R-TTC-O-01, R-TTC-O-02**			
Negligible (1)	**R-EPS-O-01, R-THERM-O-01**	**R-ADCS-O-01, R-ADCS-O-03, R-GN-O-01, R-GN-O-03, R-PROP-O-06, R-PROP-O-07, R-TTC-O-04**	**R-ADCS-O-06, R-TTC-O-03**	**R-ADCO-02**	

12.3. Conclusion

All individual risks are below the threshold of seven. Therefore, all risks are mitigated to an acceptable level. It is apparent how some risks have a very high impact, but their probability is reduced to such a low extent, that it is acceptable. To know the total risk of the orbiter to fail, the following was done: each probability of the risks having an impact higher or equal to two were added. This is because an impact equal to 1, has no significant effect on the system requirements. This then returned an orbiter success chance of 90.1%.

13. Sensitivity Analysis

After finishing the subsystem design it has to be quantified how sensitive the design methodology is to a change in input parameters. Every subsystem engineer developed a design tool. The main inputs and outputs of those tool are identified. Every input value is changed by 5% and the corresponding output is recorded. The percentage change of the output value is an indication for the sensitivity of the design. The input parameters are x_1 and x_2, with x_1 being the original value and satisfying the following relation.

$$x_2 = 1.05 \cdot x_1 \tag{13.1}$$

The sensitivity parameter ε represents the percentage change in the output y and is then calculated by

$$\varepsilon = \frac{y_2(x_2) - y_1(x_1)}{y_1(x_1)} \tag{13.2}$$

A percentage change of 5% is applied to the input parameter and was chosen based on the difference in system parameters per iteration. In case of the orbiter, the mass and power increased by about 5% for the last major

iteration. For the very last iterations the percentage change is way less than this value but it was selected to represent the worst case difference. For comparability, the same percentage is applied to every input parameter.

The results are listed in Table 13.1 for the orbiter subsystems. A colour code is used as a visual aid. Blue stands for no change in the output. Green indicates that the change is between 0% and 5%, which means that the difference in output is smaller or equal to the difference in input. Red indicates that the output value decreased or increased by more than 5%.

Table 13.1: Result of the sensitivity analysis of the orbiter for an input change of 5% and ε being the sensitivity parameter

Subsystem	Input	Output	ε
Structures	Orbiter Mass [kg]	Structural mass [kg]	0.00%
ADCS	Orbiter Mass [kg]	Subsystem mass [kg]	0.00%
		Maximum thrust force [N]	2.05%
TTC	Contact time [s]	Power [W]	3.20%
		Data rate [kbits/s]	5.00%
CDH	Nominal data rate [kbits/s]	Memory [MBytes}	0.61%
		Transmission rate [kBits/s]	1.40%
EPS	Nominal power [W]	Subsystem mass [kg]	1.84%
		Solar array size[m^2]	4.83%
THERM	Emitting area [m^2]	Power consumption [W]	24.06%
		Subsystem mass [kg]	-6.25%
	Incident area[m^2]	Power consumption [W]	-3.43%
		Subsystem mass [kg]	9.28%
Propulsion	ΔV [m/s]	Propellant mass [kg]	6.92%
	Dry mass orbiter [kg]	Propellant mass [kg]	3.58%

Structures
Investigating the results of the sensitivity analysis in Table 13.1 and starting from the top, the structural mass of the spacecraft does not increase due to a change in total mass. This is explained by the fact that the cylindrical structure of the orbiter is carefully overdesigned for the load cases it will endure. It is therefore not sensitive to a change in input. The risk is that the structure includes contingencies which are too large making the design heavier than necessary. However, at a mass of 46.48 kg the structure makes up only 1.1% of the total launch mass. The mass increase of the structure is therefore insignificant. As a further investigation the input was increased by 10%, which shows an effect of 3.7% of structure mass increase.

ADCS
Moving on, the ADCS components are selected to meet the requirements including contingencies, so a change in orbiter mass does not require selecting different actuators. The orbiter mass is a critical input for the thrust force of the RCS system, since an increase in mass increases the mass moment of inertia and therefore the torque required to rotate the spacecraft. This is important for the release manoeuvre of the landers, as the whole spacecraft with all probes attached has to be rotated. The increase in force is still less than 5 %, so an acceptable sensitivity.

TT&C
For TT&C the transmitting power increases by 3.2% when the contact time is decreased by 5%. This makes sense since the system has less time to transmit the same amount of data. A linear relationship is found for data rate as a function of contact time. A decrease in contact time results in the same percentage increase of reuired data rate.

C&DH
The parameters of the C&DH subsystem depend on the nominal data rate. The transmission rate is more sensitive to a change in data rate than the required memory.

EPS
In case of the electrical power system the nominal power of the orbiter is identified as an input and the subsystem mass as well as the solar array size as relevant outputs. The solar array size increases by 5%, showing a more sensitive behaviour than the subsystem mass. The subsystem mass includes the battery. As the required power increases the battery capacity has to be larger, resulting in a heavier battery, so this effect is also accounted for by investigating the subsystem mass as an output.

THERM
For the THERM the subsystem parameters mainly depend on the emitting and absorbing area of the orbiter. The power consumption of the THERM is very sensitive to a change in emitting area, increasing by 24%. Since

an increase in emitting area means more heat loss and a lower temperature, the orbiter has to be heated. A heating system has a lower mass than active cooling, therefore the subsystem mass decreases. The opposite effect is true for an increase in incident area. The subsystem mass critically increases by 9.3%, while the power consumption decreases by 3.4%.

Propulsion
The main inputs for the propulsion system are the required ΔV and the dry mass of the orbiter. The design tool developed for propulsion returns the propellant mass as a function of both of these inputs. In general it is more sensitive to a change in ΔV than a change in dry mass.

Results and Recommendations
The values highlighted in red indicates that the output is sensitive and might not meet the corresponding requirement anymore. This is analysed for the following parameters.

- THERM power consumption
- THERM subsystem mass
- Propellant mass

The first point of interest is power consumption of THERM. It is increased by 24% to 56.1 W. The requirement [DMD-THERM-O-05-A] states that the nominal power shall be 45 W. The design of the thermal control system is therefore sensitive enough to violate the requirement, which is therefore suggested to be labeled as a driving requirement. The same is true for the mass decrease due to a change in emitting area, which violates the requirement [DMD-THERM-O-06].

The other sensitive subsystem is propulsion, specifically the propellant mass. There is no requirement on propellant mass, but the increase in mass might kick off a snowball effect in future iterations.

In conclusion, the sensitive subsystems still meet their respective requirements but the mentioned requirement IDs shall be considered as driving requirements for the following design process. The structure and ADCS have to be investigated further to make sure they are not overdesigned since the sensitivity analysis revealed their corresponding subsystem mass is independent of the input parameters.

Part IV

Lander Design

14. Landing Locations

According to stakeholder requirement [DMD-PERF-BROOT-12], at least two landers shall be placed in the Northern Plains (NP), the Tharsis Complex (TC), the outflow region of Valley Marineris (OR), the Hellas Basin (HB), and the Southern Highlands. The first four of these areas are shown in Figure 14.1 , while the Southern Highlands consist the region around TC, OR and HB below the Northern Plains. In addition to this requirement, more requirements with regards to landing site selection have been created by the different subsystem engineers. Of course, the scientific goals of the mission must always be considered when selecting suitable landing locations. This chapter will describe the landing site selection procedure, starting with the relevant requirements in Table 14.1.

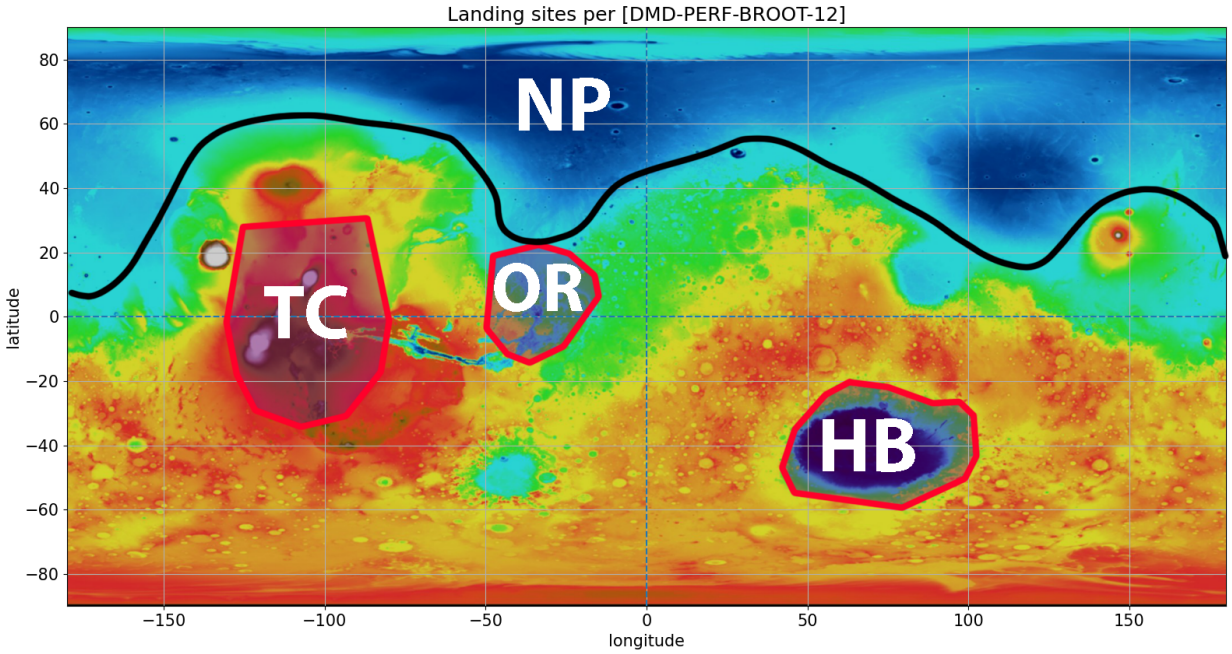

Figure 14.1: Map of Mars with areas of interest, altitude map obtained from MOLA [36]

14.1. Requirements

Table 14.1: Requirements relevant to landing site selection

ID	*Requirement*	*Status*	*Origin*	*Compliance*
DMD-PERF-BROOT-12	The system shall provide at least two measurement points on all the following Martian areas: Northern Plains, Southern Highlands, Tharsis Complex, outflow region of Valley Marineris and Hellas Basin.	Active	Customer	Met
DMD-SARR-BROOT-03	The system shall not land within 100 km of current and planned landing sites of other missions.	Active	Customer	Met
DMD-EDL-03	The system shall deliver the lander up to an elevation of 3000m.	New	EDL	Met
DMD-EPS-L-08	The impactors shall not land more than 35 degrees in latitude from the equator.	New	EPS	Met

14.2. Scientific Considerations

Next to the requirements stated in Section 14.1, certain areas on Mars are more interesting from a scientific point of view than others. One of the primary mission goals is to investigate the possibility of near-surface water

or ice on the planet. Current models show that water ice is likely to be present on Mars 1 - 2 meters below the surface, especially at high latitudes [37, p. 1]. Recently, observations made by ESA's Mars Express spacecraft have proven the existence of subglacial lakes of liquid water near the south pole [38, p. 2].

Due to limitations imposed by EPS and EDL, the Mars Deploy landers will be mostly focused around the equator. In order to find areas that are of high scientific value with regards to water, hydrated mineral data from the ESA's Mars Express OMEGA and NASA's Mars Reconnaissance Orbiter CRISM instruments is used.[1] These mineral sites are indicated in green in Figure 14.2. While these hydrated mineral sites indicate the past presence of liquid water in these areas, they do not necessarily indicate current presence of water. However, Wilson et al. (2018) hypothesized based on data from the Mars Odyssey Neutron Spectrometer, that water ice is currently buried below the ground near the equator near the Tharsis Montes and the Medusae Fossae Formation [39]. This indicates that the equator region is certainly interesting to study in terms of subsurface water or ice.

Next to water, the presence of geothermal heat sources shall also be investigated. Current models put the surface heat flow of Mars between 14 and 25 mW/m^2, with an average value of 19 mW/m^2 [40, p. 3]. The lowest values can be found in giant basins such as Hellas, while the highest heat flow is seen in the Southern Highlands, and the Tharsis region in particular. Even though current models can predict the heat flow on Mars, measuring the heat flow in-situ is needed to check the validity of the model. Generally, the young volcanic regions on Mars are the most interesting when looking for geothermal heat sources [41, p. 31]. Fogg (1996) describes some candidate regions for geothermal heat sources, including the Tharsis Complex and the Vallis Marineris [42]. Potential geothermally active regions as described in [41] are shown in orange in Figure 14.2.

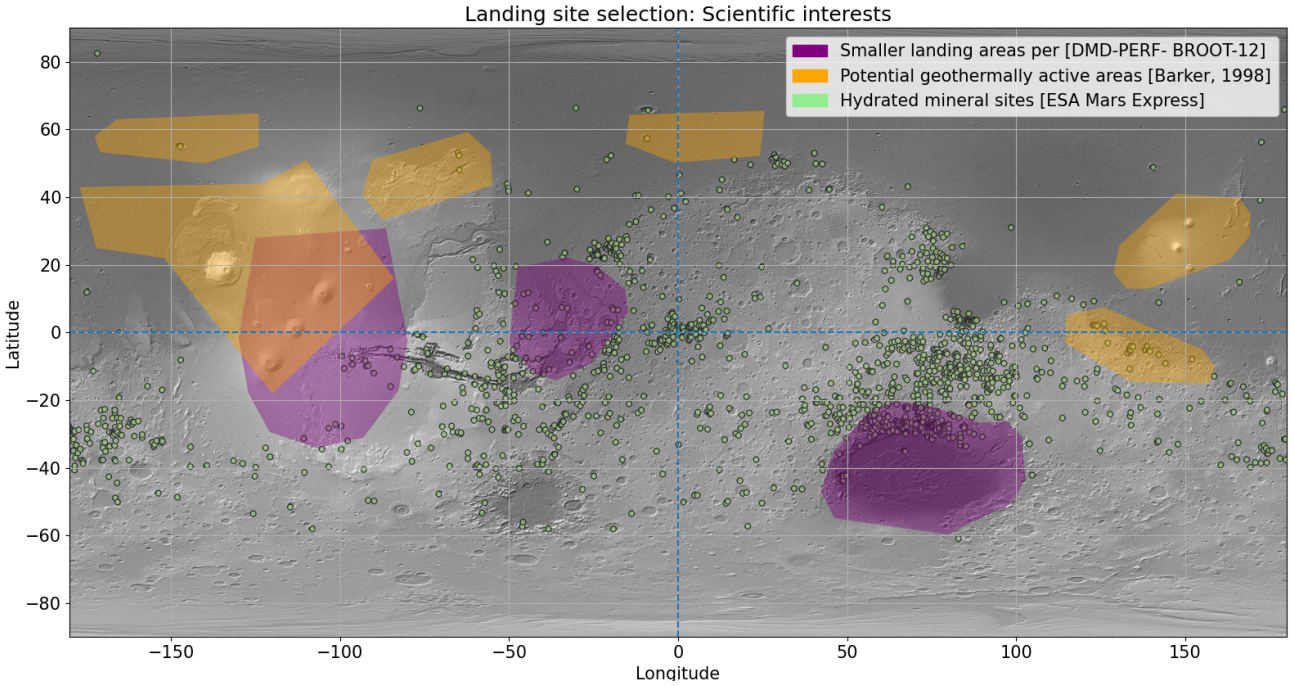

Figure 14.2: Map of Mars showing scientifically interesting regions in orange and green, and the smaller required landing areas of the Tharsis Complex, Outflow Region of the Valley Marineris, and Hellas Basin (left to right)

Figure 14.2 shows regions which are of scientific interest. It is clear that the Tharsis region should be on the list of landing sites due to its geothermal potential, which is also reflected in customer requirement [DMD-PERF-BROOT-12]. Next to this, the region above the Hellas Basin shows a high concentration of hydrated mineral sites, indicating that liquid water once existed there.

14.3. Technical Constraints

As with any planetary mission, there is a set of limitations on the landing sites that are purely technical in nature. These limitations are imposed by the scientific payload (Section 16.5), the entry, descent and landing (EDL) procedure (Section 16.1), and the lander's electric power system (Section 16.8). These will be discussed in the following subsections, after which the landing site selection procedure will be described.

Seismic Coverage

As one of the primary objectives of the mission is to sense marsquakes, the coverage of the seismic network must be considered during landing site selection. As the SEIS Short Period (SP) seismometer will be used on

[1] https://sci.esa.int/web/mars-express/-/51857-mars-hydrated-mineral-map, Accessed [18-06-2021]

the Mars Deploy landers, as mentioned in Section 16.5, it is useful to look at the marsquakes detected by InSight to determine the performance of the instrument. As InSight carried a set of low-frequency Very Broad Band (VBB) sensors in addition to the high-frequency SP sensors, the high-frequency marsquakes detected are particularly interesting. In [43], the high-frequency events as recorded by InSight are analysed and discussed. In this report, a high-frequency event is defined as having a frequency between 1 and 10 Hz [43, p. 1]. Figure 14.3 shows the magnitude of high-frequency marsquakes plotted against their calculated distance in degrees.

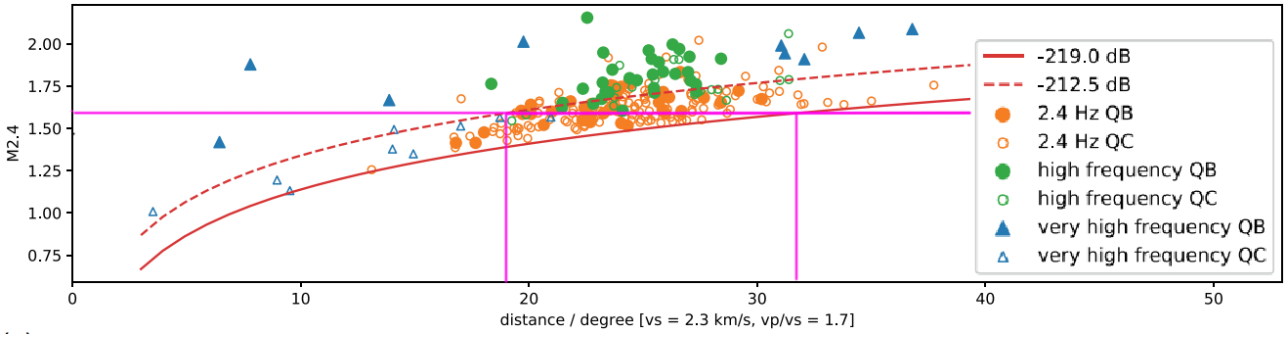

Figure 14.3: Marsquake magnitude versus epicenter distance in degrees, for high-frequency events recorded by InSight. Adapted from [43, p. 10]

In Figure 14.3, the solid red line corresponds to the detection thresholds in the ideal case, during times with the least background noise. The red dashed line indicates the threshold for the worst case with the most background noise [43, p. 10]. QB and QC stand for quality B and C respectively, where a quality B is better than C, with less detected noise. Finally, 2.4 Hz events are those which are characterised by their resonance around the 2.4 Hz band. It is clear from the pink line that for the desired minimum magnitude of $M_W = 1.6$, the detectable distance ranges between 18.5 and 32 degrees. It is therefore safe to assume that a marsquake with magnitude $M_W = 1.6$ can be detected by the SP sensors at an average distance of 25 degrees, especially for the 2.4 Hz events.

Next to the seismic events exceeding 1 Hz, InSight has also detected low-frequency events which are below 1 Hz, but still within the SP's frequency range of 0.1 - 50 Hz [45, p. 27]. According to [46, p. 15], all low-frequency events recorded in the first seven Earth months of operation fall within a frequency range of 0.17 Hz and 0.85 Hz. If we assume that the SP sensors have an accuracy close to the VBB sensors in the 0.1 - 1 Hz frequency range, data from [44] can be used to determine the the range of the seismometer for low-frequency events as well. Table 14.2 shows the predicted minimum detectable marsquake magnitudes for different distances in degrees. From this table, it can be seen that a larger marsquake of magnitude 3 would be detectable within a range of 60 degrees.

Table 14.2: Minumum detectable magnitudes for marsquakes for different distances, given in degrees. Adapted from [44, p. 13].

Distance (°)	M_{min}
25	2.6
45	2.9
60	3.0
90	3.2
150	3.5

EDL Limitations

The methods chosen for interplanetary travel and Mars entry, descent, and landing impose restrictions on the possible landing sites. As explained in Section 8.1, the landing sites are restricted to be within a circular band around a target point on Mars, with an inner diameter of 72 degrees and an outer diameter of 78 degrees. The target point around which this landing band is taken is not subjected to any restrictions and may be freely chosen. By using the rotation of Mars, the width of the landing band could be increased in the longitudinal direction. The amount of allowed shift in longitudinal direction was determined to be 25.5° eastward. The main challenge here proved to be choosing a target point which allowed all the required landing sites to be covered, as per [DMD-PERF-BROOT-12]. After trial and error, the best target point was found to be 18.0° W, 45.0° S. This particular target point allowed the landing band to cover all five required landing sites. In Figure 14.4, the target point can be seen in the Southern Hemisphere as the magenta "X". The white dashed lines around this point then indicate the inner and outer landing zone limits with radii of 72 and 78 degrees respectively. The white dashed lines are then shifted east, since the rotation of Mars is used to expand the possible landing area. This results in the cyan dashed lines. As the dashed lines indicate the boundaries of the landable region, any zone between the leftmost and rightmost dashed line can be landed in.

Another limitation imposed by EDL is [DMD-EDL-03], which states that the landers shall land at an altitude not exceeding 3 km. In order to take this restriction into account during landing site selection, altitude data from Mars Global Surveyor's MOLA instrument was used [36]. Using a custom Python image processing tool, pixels corresponding to an elevation above 3000 m were colored black and applied to Figure 14.4. In can be seen that requirement [DMD-EDL-03] heavily restricts the Tharsis region in particular.

EPS Limitations

As mentioned earlier, requirement [DMD-EPS-L-08] limits the distance of the landing sites from the equator to a maximum of 35 degrees. This limit has been set in order to keep the received amount of solar energy to an acceptable level. These bounds are shown in Figure 14.4 as yellow lines.

Finally, Figure 14.4 shows the full site selection map with all the considerations and constraints mentioned above. It can be seen that the landing band stemming from the astrodynamic manoeuvres is by far the most limiting. The map also shows several areas where a Mars mission is currently active or is planned to land, indicated in pink. To comply with stakeholder requirement [DMD-SARR-BROOT-03], landing in these areas is prohibited.

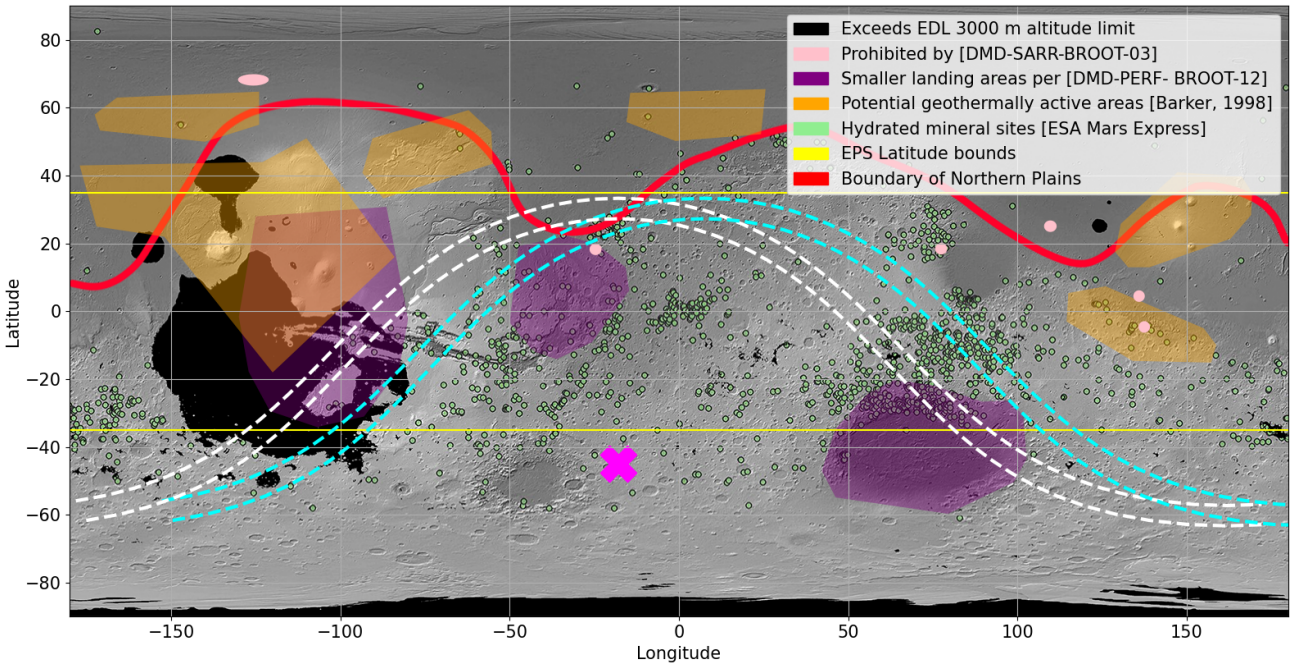

Figure 14.4: Map of Mars with all requirements and constraints visualised. Target point from astrodynamic manoeuvre is shown in magenta. White and cyan dashed lines represent the EDL landing band.

14.4. Landing Site Selection Procedure

With Figure 14.4 as a foundation, approximate locations for landing sites could be selected. With ten probes carried to Mars by the orbiter and requirement [DMD-PERF-BROOT-12] in place, the objective was to put two landers in all five required areas, while maximizing the seismic coverage as much as possible. This led to a set of preliminary landing sites.

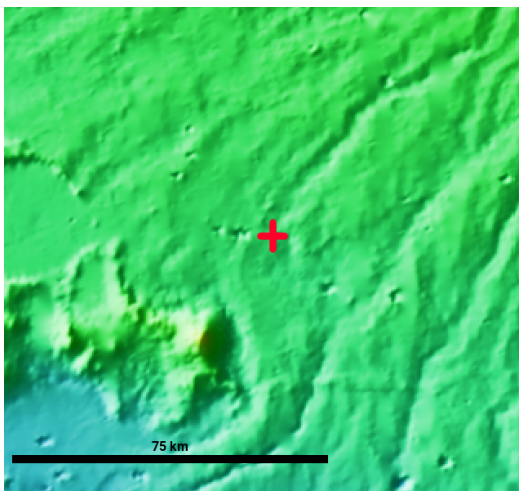

Figure 14.5: Preliminary landing site Hellas East shown using JMARS

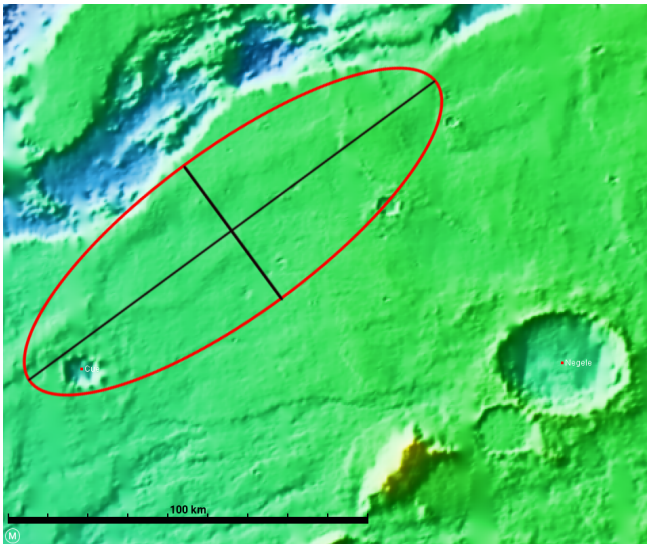

Figure 14.6: Final Hellas East landing site shown with landing ellipse

As an example, the preliminary coordinates for the Hellas East landing site were -32.9° N, 90.75° S. Using the JMARS software package, this area was then analysed in greater detail than Figure 14.4 would allow. In

Lander	Coordinates
Hellas East	-34.08°N, 94.04°E
Hellas West	-24.86°N, 73.24°E
Outflow East	18.86°N, -31.40°E
Outflow West	11.17°N, -45.55°E
Tharsis South	-23.0°N, -101.10°E

Lander	Coordinates
Tharsis North	4.71°N, -83.91°E
NP East	31.67°N, -21.38°E
NP West	29.14°N, -42.97°E
SH East	-13.20°N, 78.40°E
SH West	25.21°N, 35.0°E

Table 14.3: Final landing sites

Figure 14.5, the landing site is shown in red. It can be seen that the landing region is not smooth, with some large mountains to the southwest of the landing site.

Therefore, a new region was searched close to the preliminary landing site, where the landing ellipse of size 127.2 km $\times$ 42.2 km would fit. The new landing site was found to be to the southeast with respect to the old landing site, with new coordinates -34.08°N, 94.04°E. The new landing site with its landing ellipse is shown in Figure 14.6. For the remaining 9 landing sites, a similar approach was taken. This resulted in the final landing sites given in Table 7.3.

With the landing sites finalised, the seismic coverage maps could be created. Figures 14.7 and 14.8 show the coverage maps for a marsquake magnitude of $M_W = 1.6$ and 3.0 respectively. On these maps, the locations of the landers are indicated as red triangles. In Figure 14.7, two seismic hot spots can be identified: one near the Outflow region, and one near the Hellas Basin. In these areas, good triangulation of seismic activity is possible. All three smaller required landing zones can be seen to be relatively well covered. In Figure 14.8, the same effect can be seen but magnified. The regions near the Outflow Region and the Hellas Basin where triangulation would be possible has significantly increased in size. Due to the fact that all landers must lie within the landing band, a blind spot remains around the magenta "X". This is inherent to the method with which the landers are delivered to the surface.

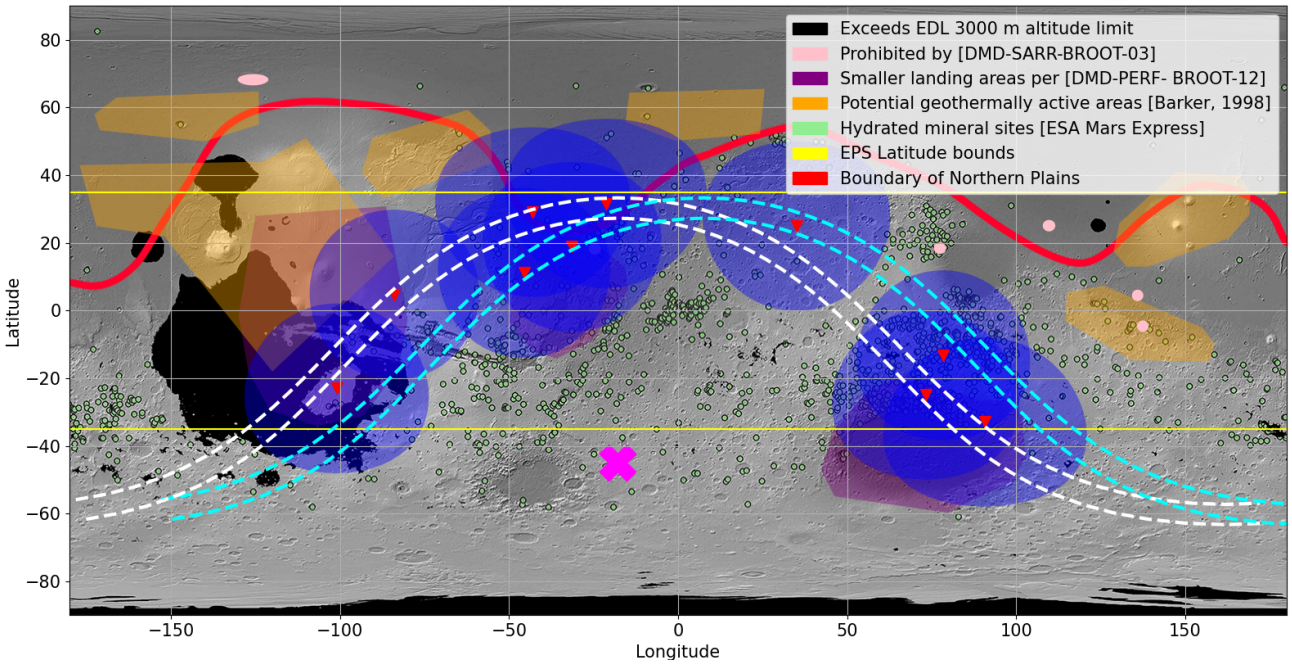

Figure 14.7: Seismic coverage map for a marsquake magnitude of $M_W = 1.6$

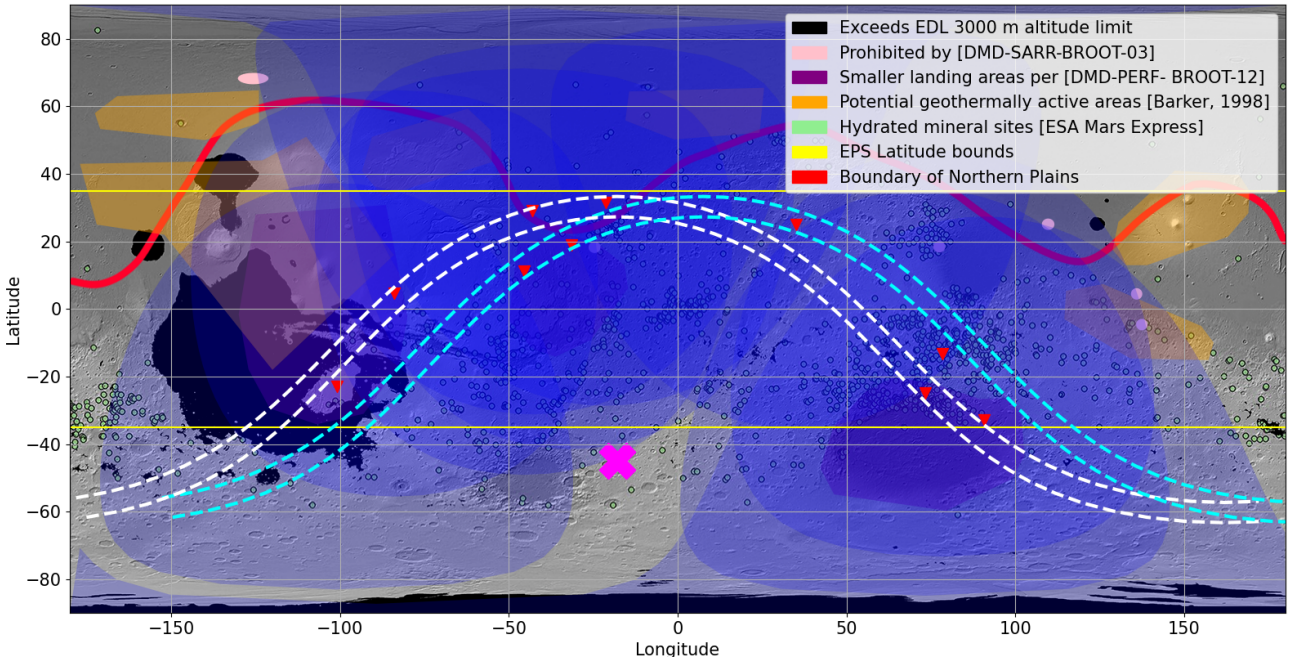

Figure 14.8: Seismic coverage map for a marsquake magnitude of $M_W = 3.0$

15. System Characteristics

This chapter will give an overview of the lander design and system characteristics. Additionally, it provides the lander's configuration overview and layout of internal and external components in Section 15.1. The mass, data rate, and power budgets presented in Section 15.2 are a summary of the detailed and iterative design process, which is explained in more detail in Chapter 16.

15.1. Configuration

The outside layout of the lander can be seen in Figure 15.1 and Figure 15.2. The structure of the lander consists of a cylindrical support structure, with an elevated plate on the inside. The cylindrical honeycomb crumple zone is attached to the bottom of the lander and has the same diameter as the support structure. Four solar panels are used, which rotate outwards after landing. In order for the impactor to fit as compactly as possible in the entry capsule, the aerodynamic fin area is distributed across 42 small fins. On top of the impactor, two helical low-gain antennas and two UHF patch antennas are placed. The locations of the center of gravity and center of pressure can be seen in Figures 15.3 and 15.4. A more detailed CAD drawing of the lander showing all relevant dimensions can be seen in Figure C.2 in Appendix C.

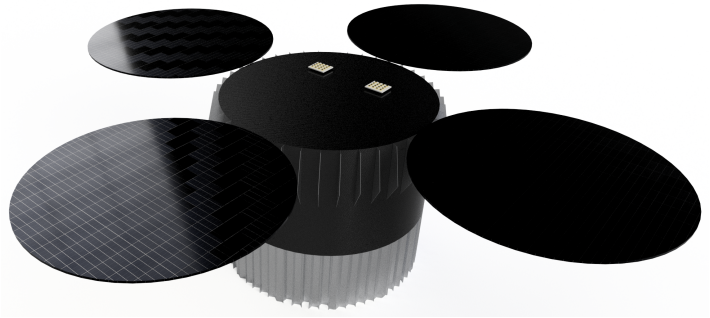

Figure 15.1: Outside layout of the lander.

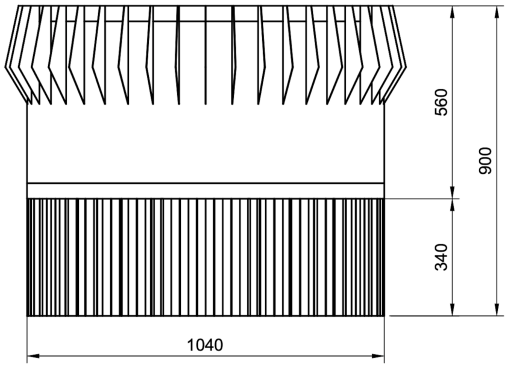

Figure 15.2: Overview of the lander's general dimensions. For a detailed overview of the relevant dimensions, please refer to Figure C.2 in Appendix C.

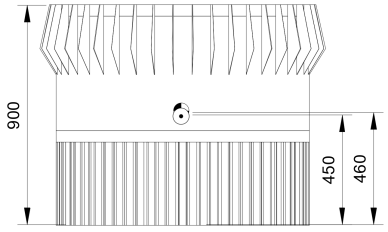

Figure 15.3: Old CoG and CoP locations of the lander, excluding aerodynamic fins

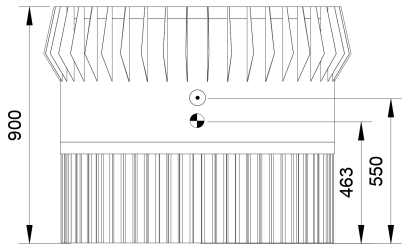

Figure 15.4: New CoG and CoP locations of the lander, including aerodynamic fins

A cross-sectional view of the impactor in the entry capsule can be seen in Figure 15.5. Along the bottom and sides of the outer support structure, 15 cm of aerogel insulation is placed. Because of this, some of the subsystems are attached to a middle plate.

The weather station and air composition analyser are attached to the top plate, which has small openings, as they need access to the Martian atmosphere. This can also be seen in Figure 15.5. The remaining subsystems are placed on the middle plate. An overview of these subsystems can be seen in Figure 15.6. In order to ensure accurate measurements, the seismometer assembly is placed in the middle of the plate. As the added energy of the bullets is 20 kJ and 6.3 kJ, the lander might rotate before the landing if their moment arms are the same. To mitigate this, the bullets are placed at a different distance from the center of gravity of the lander in order for their applied moments to cancel out. These distances are 32 cm and 100 cm for the 20 kJ and 6.3 kJ bullet, respectively. The center of gravity is assumed to be the geometric center of Figure 15.6.

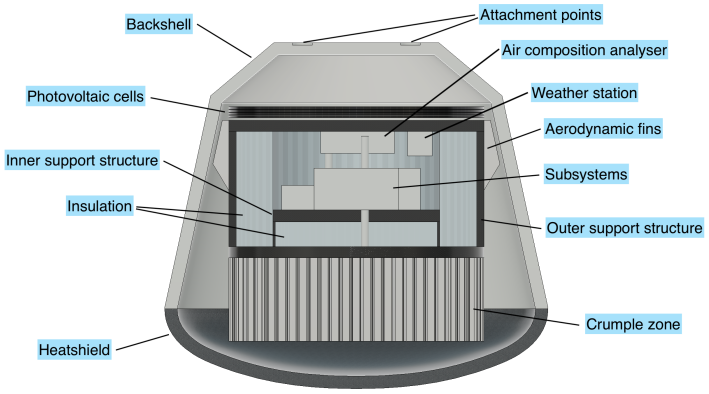

Figure 15.5: Cross-sectional view of lander within the entry capsule

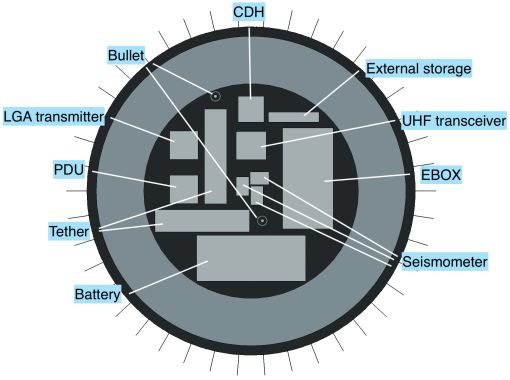

Figure 15.6: Overview of the lander's inside configuration

15.2. Budgets

In this section, the budgets for the lander are presented. This chapter includes the power in Table 15.2, mass in Table 15.3 and internal data rate budget in Table 15.1. The following subsystem sections in Chapter 16 will provide the calculations for these budgets. The link budget table of the orbiter, Table 16.24, can be found in Section 16.6.

Table 15.1: Sensor data rates for the lander

Sensor	Amount [-]	Resolution [bits]	Sampling Frequency [Hz]	Data rate [bit/s]
EDL				
IMU	1	8	400	3200
Pressure Sensor	8	8	1	200
Altimeter	1		1000	400000
Thermal				
Temperature sensors	25	8	0.1	20
EPS				
Current Sensors	6	8	1	48
Voltage Sensors	6	8	1	48
Sun senors	3	8	5	240

In the power budget table, a differentiation is made between nominal operations and pre-nominal operations. The pre-nominal operations, depicted in red, result in the necessary amount of energy the battery should be able to provide in the time between launch and operational solar arrays. In black, the nominal operation budgets have been depicted.

Table 15.2: Lander power budget with nominal operations in black and pre-nominal operations in red

	Subsystem	Nominal power use[W]	Additional peak power[W]	Peak power duration (per sol)[s]
EDL				
	IMU		5.5	198000
	Pressure sensor		0.015	1800
	Altimeter		1.3	1800
CDH				
	OBC	12		
	Mass storage	0.275	0.34	1723 per sol
	Pre-nominal		5.7	198000
EPS				
	Distribution system	1.4		
	Deployment		20	60
Payload		7.9	26.1	300 per sol
Thermal		15.305	15.305	28800 per sol
TTC				
	DSN dish		15	33734 per sol
	DSN Lga		2.5	26632 per sol
	UHF		7	10400 per sol
Total power:		36.88W	73.06W	-
Total Energy per sol:		0.909kWh	0.304kWh	
Total Energy required before nominal operations:			0.617kWh	

Table 15.3: Lander Mass Budget

Subsystem		Mass[kg]
EDL		
	IMU	0.75
	Pressure Sensor	0.05
	Altimeter	0.022
Aerodynamics		
	Fins	1.33
	Parachute	4.092
	Drogue Parachute	0.33
	Drogue Gun	0.91
	Heat shield	79.74
	Backshell	47.33
CDH		
	OBC	0.25
	Mass storage	1.45
EPS		
	Distribution system	0.15
	Solar Array	10.3
	Battery	16.01
	Dust Clearing	0.15
	Actuator	0.65
Structures		
	Supportive	24.75
	Impact attenuator	50.36
	Bullet	8.4
Payload		17.4
Thermal		
	Heaters	0.02
	Heat Storage	1.87
	Paint/insulation (aerogel)	21.49
TTC		
	DSN dish	1.2
	DSN Lga	0.3
	UHF	0.8
Total Mass:		290.1

16. Design Process

In this chapter the design process of the lander will be documented. After the landing locations have been established in Chapter 14, the entry descent and landing scenario in Section 16.1 can be determined. This will need aerodynamics, which will be discussed in Section 16.2. After this, the guidance and navigation in Section 16.3 will be designed for impact detection. In order to withstand the impact the structure will need to be designed, this is discussed in Section 16.4. The scientific payload that needs to be inside of the lander is described in Section 16.5. The scientific data will need to be sent through a communication system, the design of this system will be discussed in Section 16.6. In order to process and eventually send the data, the lander will need a command and data handling system, which is discussed in Section 16.7. In order for all subsystems to function, the lander will need an electronic power system which is discussed in Section 16.8. Finally, to ensure proper operations, the equipment must be kept within a temperature threshold, which is achieved with a thermal control subsystem, this is discussed in Section 16.9.

Based on the budgets and preliminary calculations made in the Midterm Report [6], each subsystem engineer designed their respective subsystem further to meet the set requirements. Similar to the orbiter design process in Chapter 10 a top-down design route was chosen for this project due to the limiting scientific requirements on the payload. The top-down design started with the scientific payload on Mars and required this to be finalized. The lander system was designed around this specific payload.

Before iteration, all subsystem engineers had adjusted and updated the values and developed their design

process that will be discussed in the following sections. After these values were discussed and adjusted, the following iterative process from Figure 16.1 was commenced based on the N2 chart from the Midterm Report [6], to converge to a consistent lander design.

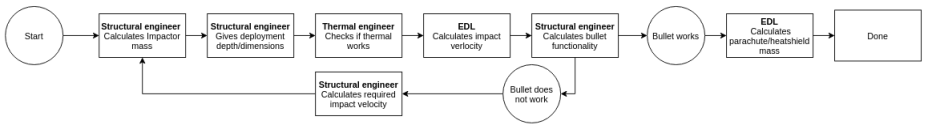

Figure 16.1: Iterative process for the lander design

After weekly iterations of each engineer updating and adjusting subsystem values a final design was settled upon. The following graph shows the results of the main spacecraft after each iteration.

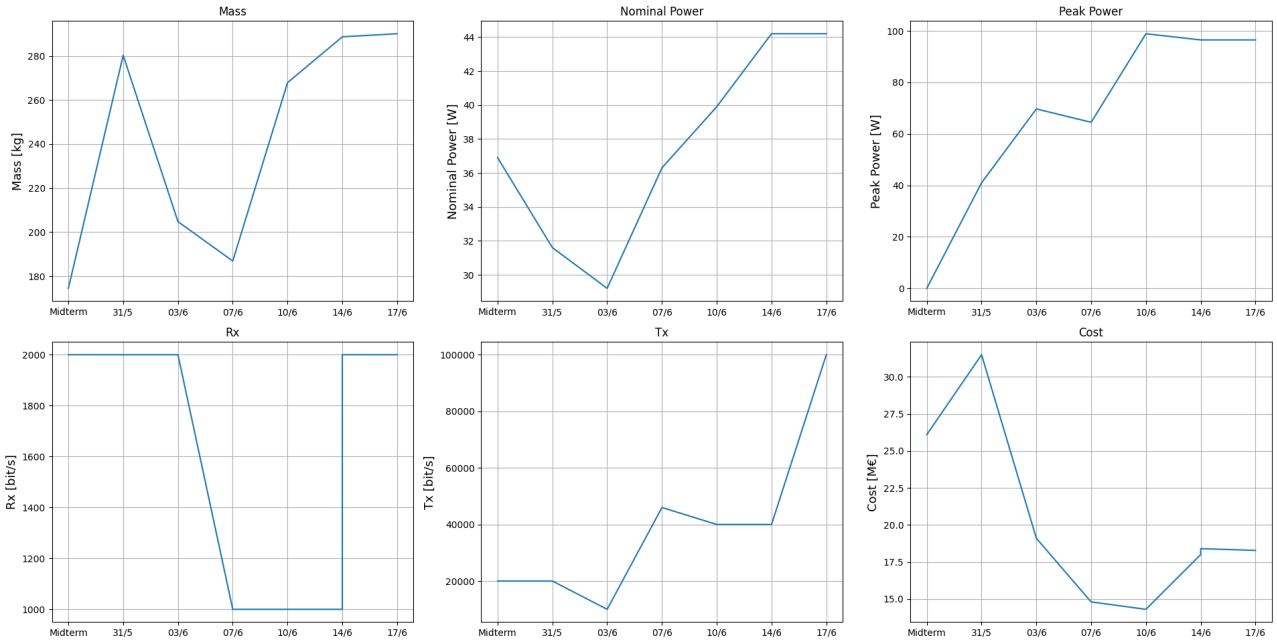

Figure 16.2: Lander iterations of main design budgets

16.1. Entry, Descent, and Landing

The Entry, Descent, and Landing (EDL) for Mars missions has been notoriously difficult as about one third of the attempted landings have failed.[1] The main philosophy in the EDL phase of this mission is therefore simplicity.

Requirements

Table 16.1: Requirements on entry descent and landing

ID	*Requirement*	*Status*	*Origin*	*Compliance*
EDL requirements				
DMD-EDL-01	The entry capsule shall be passively stable during the entry phase.	New	Orientation	Met
DMD-EDL-02	The heat shield shall protect the lander from temperatures up to 1850 K.	New	Entry heating simulation	Met
DMD-EDL-03	The system shall deliver the lander up to an elevation of 3000 m.	New	Landing site selection	Met

Continued on next page

[1] https://westeastspace.com/encyclopedia/missions-to-mars/, Accessed [22-06-2021]

Table 16.1 – continued from previous page

ID	*Requirement*	*Status*	*Origin*	*Compliance*
DMD-EDL-04	The system shall provide an impact velocity between 200 and 230 m/s for all landing sites.	Replaced	Structures subsystem	N.A.
DMD-EDL-04-A	The system shall provide an impact velocity between 200 and 230 m/s for all landing sites.	New	Replaces [DMD-EDL-04]	Met
DMD-EDL-05	The entry angle of the lander shall be between -12 and -18 degrees.	New	Landing site selection	Met

Design Process

The EDL sequence of each lander will be roughly similar and differ only as the different landing sites bring their own challenges. Before the orbiter performs Mars Orbit Insertion (MOI), it releases the landers such that they reach their respective landing sites. The release of each lander will occur at different times to accommodate for the spread of targets. After the coast towards the planet, the landers will encounter the atmosphere at a height of about 100 km and a velocity of around 5.7 km/s. The resultant friction will gradually slow the lander down and heat it up. Before impact with the ground, the lander will have reached a velocity of between 200 and 230 m/s.

The descent phase is simulated and simplified by employing multiple assumptions. The capsule is modelled as a point mass with only drag force and gravitational forces acting on it. This also implies that the entry is purely ballistic as the lift force of the entry vehicle is neglected. The forces acting on the capsule are modelled as point forces acting through the centre of mass of the vehicle. The curvature and rotation of Mars is assumed to be negligible. As the entry speed is in the order of kilometers per second, the influence of wind gusts is deemed negligible. The gravitational force on the point mass is modelled with the inverse square law. A simplified atmospheric model of the Martian atmosphere is used to estimate pressure p in kPa (Equation 16.1), density ρ in $\frac{kg}{m^3}$ (Equation 16.2) and temperature T in degrees Celsius (Equation 16.3) as a function of altitude h.[2]

$$p(h) = 0.699e^{-0.00009h} \quad (16.1) \qquad \rho(p,T) = \frac{p}{0.1921(T+273.1)} \quad (16.2)$$

$$T(h) = \begin{cases} 0.699 - 0.00009 & \text{if } h > 7000 \\ -31 - 0.000998h & \text{if } h < 7000 \end{cases} \quad (16.3)$$

The drag equation is used to estimate the aerodynamic forces on the capsule Equation 16.4 with S being the cross-sectional area and C_D the drag coefficient of the entry vehicle. The gravitational force is modelled as given in Equation 16.5 with R_m the radius of Mars, m the mass of the entry capsule and μ_m the standard gravitational parameter.

$$D = \frac{1}{2}\rho V^2 S C_D \quad (16.4) \qquad F_g = \frac{\mu_m m}{(R_m + h)^2} \quad (16.5)$$

Simulating the velocity and acceleration of the capsule with the initial condition gives a velocity profile for the whole descent phase, shown in Figure 16.5. The design of the EDL sequence was done in compliance with the requirements set by the structures subsystems. Several options were considered for the deceleration method, such as inflatable devices, ballutes and parachutes. Looking at successful heritage missions and available literature, the parachute was selected for further analysis. Important constraints on the EDL system are the impact speed and the dynamic pressure. Due to a high entry speed the parachute can be deployed at low altitudes only as otherwise the dynamic pressure limit is exceeded. One of the functions of the parachute is to support in safely jettisoning the heat shield and backshell of the entry capsule. It provides a velocity difference between the heat shield and the capsule such that the shield can be dropped without colliding with the impactor. The parachute will be jettisoned before impact, as otherwise the impactor would be decelerated too much. The impactor is dropped from a certain height such that it reaches the desired impact velocity at elevation ranging from -6 km to 3 km with respect to zero-elevation level.

Both the parachute area and the deployment height at which the impactor is released from the capsule have an influence on the impact velocity. To find suitable combinations of both parameters, the entry simulation was run for different parachute area and deployment height. Additionally, the impact elevation was changed as an input to

[2] https://www.grc.nasa.gov/www/k-12/airplane/atmosmrm.html, Accessed [15-06-2021]

make sure the impactor can land at high elevations without violating the impact speed requirement. For illustration purposes, the resultant plot is shown in Figure 16.3. If the resultant impact speed is between 200 and 230 m/s, the combination of parachute area and deployment height is feasible. In the simulation, the drag of the parachute is added to the drag of the capsule, given in Equation 16.6.

During descent the probe will encounter severe heating due to the compression effect as it travels at hypersonic velocities [47]. A simplified analytical model is used to determine how severe this heating will be. The two main assumptions are that the trajectory is ballistic and the flight path does not change, and that wall of the spacecraft is much colder than the flow it is in. These assumptions lead to a heating rate proportional to $q \sim \sqrt{\rho}V^3$ and a wall temperature proportional to $T \sim \sqrt[4]{\rho V^3}$. Estimating the necessary constants using heritage data, a maximum heating load between 69.3 and 84.4 W/cm^2 for a flight path angle between -12 and -18 °, respectively. Maximum temperature estimates are between 917 and 1013 K.

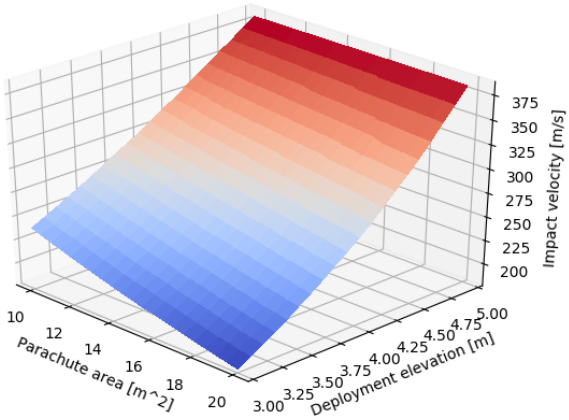

Figure 16.3: Impact speed at an altitude of 3 km as a function of parachute area and deployment height at which the lander is released from the back shell of the entry capsule

$$D_p = \frac{1}{2}\rho V^2 S_p C_{D_p} \tag{16.6}$$

The velocity profile during entry is depicted in Figure 16.5 and the sequence is described in the following. Initially, the capsule enters the Martian atmosphere at an altitude of 100 km with an entry speed of 5.7 km/s at an angle of -15 degrees. During the entry phase, the capsule endures a maximum deceleration of 13.3 g. The entry phase ends as soon as the dynamic pressure falls below 900 Pa and the parachute is deployed. Disk-gap-band parachutes were tested to deploy successfully at dynamic pressures of up to 972 Pa [48]. The parachute design is further explained in Section 16.2. The parachute deployment causes a deceleration spike of 5 g and the velocity is 427 m/s at an altitude of 4.9 km. After deployment of the parachute, the heat shield is jettisoned. The parachute decelerates the capsule to 224.2 m/s. At an altitude of 3450 m the impactor is released from the back shell of the capsule and enters a free fall. The velocities associated with the final deployment steps are shown in Figure 16.4. The impact occurs at a design altitude of 3 km with an impact speed of 230 m/s. The whole sequence lasts for a total of 136 seconds.

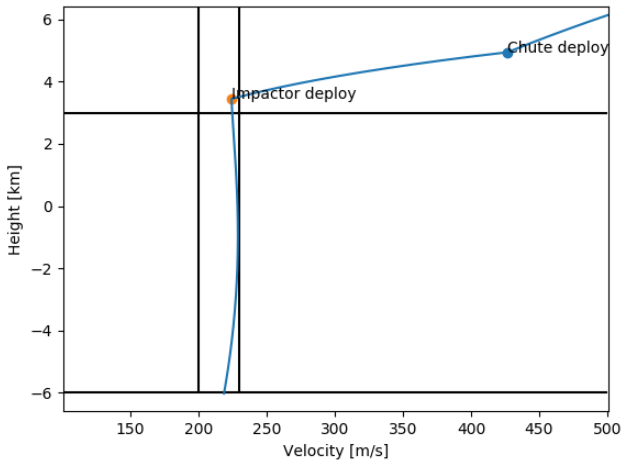

Figure 16.4: Final descent profile for an impact at an altitude between 3 and -6 km, indicated by horizontal lines. The vertical lines indicate the impact velocity bounds of 200 and 230 m/s

Verification and Validation

In order to verify the simulation, an analytical solution for the velocity profile is set up and compared to the simulation result. In order for this comparison to be meaningful, the same initial conditions are selected. As the analytical solution is only capable to model the purely ballistic descent, the final descent phase cannot be verified with this method.

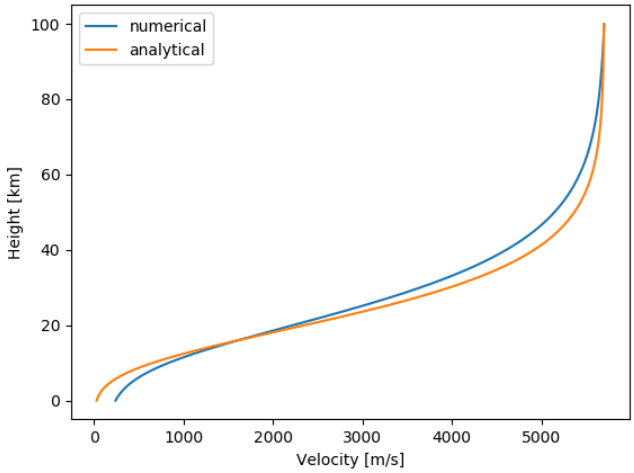

Figure 16.5: Comparison between analytical and numerical velocity profile for the entry phase

An analytical solution for a ballistic entry is described by Dr.Ir. Mooij in [49]. It is once again assumed that the entry capsule is non-lifting. The analytical solution is derived from the general equation of motion and assuming no lift means that the flight path angle is constant. The velocity profile throughout the descent can be calculated using Equation 16.9 with K being the ballistic coefficient (Equation 16.8) and V_e being the entry velocity.

$$\gamma \approx \text{constant} \qquad (16.7) \qquad K = \frac{mg}{C_D S} \qquad (16.8) \qquad \ln\left(\frac{V}{V_e}\right) = \frac{p}{2K\sin(\gamma)} \qquad (16.9)$$

Plotting the resultant velocity profile of Equation 16.9 together with the simulation result yields a comparison between the analytical and numerical result. Figure 16.5 shows that the overall shape of the profile is the same. The numerical method underestimates the velocity up to an altitude of 20 km, while the impact speed is overestimated. The analytical solution is only valid for steep entry angles [49]. Increasing the entry angle in the simulation results in a slightly better solution convergence.

Additionally, the maximum deceleration can be analytically derived, given inEquation 16.10, and is compared to the numerical result. The analytical result is 14.3 g, while the numerical result is 13.3 g, translating in a percentage difference of 7.5%. The deceleration is underestimated but the loads during entry are small compared to the impact loads and deemed non-critical.

$$\bar{a}_{max} = -\left(\frac{dV}{dt}\right)_{max} = -\frac{\beta \sin(\gamma)}{2e} V_e^2 \tag{16.10}$$

To validate the numerical model, data from a previous Mars entry mission is used. The NASA Mars Exploration Rovers are used as they have a similar entry speed of 5.6 km/s and also enter the atmosphere of Mars from a transfer orbit. The peak deceleration experienced by the Mars Exploration Rovers is 6.2 g [50]. Feeding the numerical model with the parameters of the existing capsule gives a peak deceleration of 8.9 m/s. The percentage error is 43.5%. An identified inaccuracy in the simulation is that the drag coefficient of the capsule is assumed to be constant and not a function of Mach number. Furthermore the atmospheric model lacks accuracy at high altitudes.

System performance and characteristics

The EDL sequence is summarised in Figure 16.6. To control the deployment steps a pressure sensor, radar altimeter and an inertial measurement unit are included in the system. The entry capsule is a 70 degree blunt body cone based on the Viking style geometry. Generally, the entry vehicle is stable when the center of mass is upstream of the center of pressure. The geometry of the capsule is designed to be passively stable. The heat shield is made from a phenolic-impregnated carbon ablator and the back shell is alumina-enhanced thermal barrier, as used on the NASA Orion spacecraft.[3] The system characteristics are summarised in Table 16.2. The simulation is run for a range of entry angles from -12 to -18 degrees and the difference in downrange distance, so the major axis of the landing ellipse, is 127.2 km. Applying the same change in angle of 3 degrees in the direction perpendicular to the flight path results in a minor axis of 42.2 km.

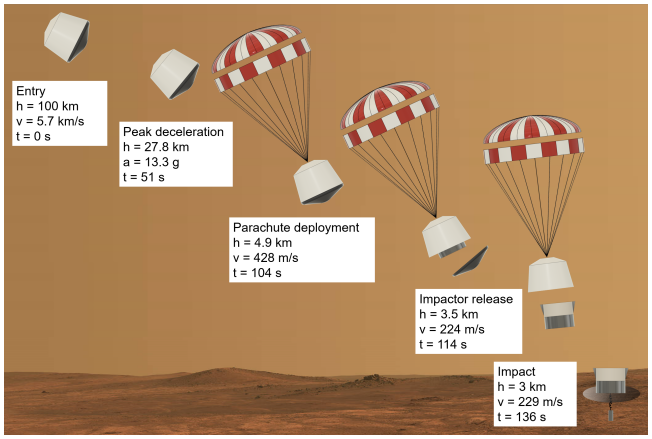

Figure 16.6: EDL sequence for a landing at 3 km elevation with altitude, velocity and time indicated.

Table 16.2: Summary of EDL parameters

Parameter	Parameter value [unit]
Entry mass	288.7 [m^2]
Entry flight path angle	-15 [deg]
Heat shield diameter	1.5 [m]
Heat shield angle	70 [deg]
Entry velocity	5.7 [km/s]
Drag coefficient	1.5 [-]
Peak heating rate	64 [W/cm^2]
Cross-sectional area	1.77 [m^2]

Recommendations

The accuracy of the of the reentry simulation can be improved by utilizing NASA's Mars Global Reference Atmospheric Model. The aerodynamic coefficients are based on heritage data and are assumed constant throughout the descent. Further studies are necessary to model the drag coefficient as a function of Mach number. The stability of the capsule can be assessed by setting up a state space model, which was deemed out of the scope of this report. An altimeter is used to determine the altitude of the entry vehicle during the final descent phase and further research has to show if the sensor can detect the impact reliably.

[3] https://www.nasa.gov/centers/ames/thermal-protection-materials/tps-materials-development/reusable.html, Accessed [16-06-2021]

16.2. Aerodynamics

In this section, the design of the aerodynamic subsystem of the lander will be explained. First in Section 16.2, the requirements of the subsystem are identified. In the next sections 16.3 and 16.3, the method for designing the parachute and the stabilising fins is explained, and the results of the design are given. Finally, the verification and validation of the used codes is performed.

Requirements

In Table 16.3, the requirements of the aerodynamics subsystem are given.

Table 16.3: Requirements on the Aerodynamics subsystem

ID	*Requirement*	*Status*	*Origin*	*Compliance*
Aerodynamics requirements				
DMD-AERO-01	The parachute shall withstand a dynamic pressure up to 900 Pa.	New	EDL	Met
DMD-AERO-02	The parachute shall provide a ΔV of 120 m/s.	New	EDL	Met
DMD-AERO-03	The aerodynamic fins shall provide stability for the lander during descent.	New	EDL	Met

Design Process

In this section the design process behind the two main parts of aerodynamics is discussed. In Table 16.3 the design of the parachute process is explained. In Table 16.3 the design process of the aerodynamic fins is explained.

Parachute

During the descent phase of the lander, a parachute is needed to slow down the capsule and allow for the jettison of the heat shield. More on this process can be found in Section 16.1. The parachute is designed such that it can withstand 900 Pa, if the parachute is opened at a higher dynamic pressure it will fail. A disk-gap-band parachute was therefore chosen which has been tested to withstand a dynamic pressure of up to 970 Pa [51], giving a safety factor of 8%. Furthermore, disk-gap-band parachutes have been used on many previous heritage missions and are designed to be used in lower density atmospheres like that of Mars [52]. Finally, the drag coefficient for a disk-gap-band parachute can be between 0.4 and 0.7, in this case a reasonably low value of 0.5 is assumed, this allows in further studies for an increase in the drag coefficient of the parachute and thus a possible decrease in the size and mass of the parachute subsystem. The drag coefficient is effected by the forebody, in this case the entry capsule, which will be taken into account when choosing the length of the suspension lines [52].

The parachute size is based on the required area needed to slow down the capsule to 219 m/s as required by the EDL design. This parachute area is called the inflated parachute area and can be used to calculate the constructed parachute area by multiplying with sizing constants, given in Equation 16.11, where $\frac{S_{const}}{S_{inf}}$ is known as the constructed to inflation area ratio [52].

$$S_{const} = S_{inf} \cdot \frac{S_{const}}{S_{inf}} \tag{16.11}$$

Once this construction size is found the mass and cost of the canopy can be calculated. This is done by simply calculating the volume of the parachute and then multiplying by the density of the chosen material to get the mass. As shown in Equation 16.12. For the canopy, the chosen material is Nomex, this is chosen as it is lightweight, strong material which has been used in previous missions. [52] In order to accommodate for the parachute and its deployment system a 30 cm gap has been left between the lander and the backshell. The inputs and outputs of this part of the parachute design can be seen in Table 16.4.

$$m_{para} = V_{para} \cdot \rho_{Nomex} \tag{16.12}$$

Input parameter	Value [unit]	Output value	Value [unit]
Inflated parachute size	18 [m^2]	Constructed parachute area	14.27 [m^2]
Inflated to constructed parachute ratio	0.8904 [-]	Parachute mass	4.038 [kg]
Parachute thickness	0.0107 [m^2]	Parachute packed volume	0.0084 [m^2]
Mass density of Nomex [53]	48.06 [kg/m^3]		
Drag coefficient of parachute	0.5		
Pressure pack packing density [54]	480 [kg/m^3]		

Table 16.4: Parachute design: Inputs and outputs

Once the parachute size is acquired, the size, mass and cost of the suspension lines can be calculated. To ensure that the suspension lines can withstand the load, two additional lines will be added after the diameter and length of the suspension lines have been sized. In this case it was chosen that 8 suspension lines will be designed for, therefore 10 in total are used. When designing the length of the suspension lines, the effect of the forebody, the entry capsule, must be taken into account. The entry capsule has an effect on the drag coefficient of the parachute: when the lines are too short, the drag coefficient of the parachute will be reduced. This leads to an increase in the parachute area, which adds weight. To calculate this, there is a relation where a coefficient, $\frac{L_s}{D_{forebody}}$, is multiplied by the diameter of the forebody to get the length of the suspension lines, this coefficient also relates to a second coefficient, $C_{d_{forebody}}$ which is multiplied with the drag coefficient to give the effective drag coefficient after the effect of the forebody on the parachute has been taken into account. These can be seen in Equation 16.13 and Equation 16.14 respectively.

$$L_{sus} = D_{shield} \cdot \frac{L_s}{D_{forebody}} \tag{16.13}$$

$$C_d = C_{d_{para}} \cdot C_{d_{forebody}} \tag{16.14}$$

To ensure that the suspension lines are strong enough, they are designed for the peak load case, this is when the parachute first opens. To find the necessary cross sectional area of the suspension lines the force, in this case the drag, is divided by the tensile strength of the material. This gives the total cross-sectional area of the combined suspension lines, this is then divided by the number of lines to get the cross-sectional area of an individual suspension line. The material chosen for the design of the suspension lines is Kevlar-29 the drag is calculated at a dynamic pressure of 900 Pa, with the drag coefficient after the effect of a forebody presence. This can be seen in Equation 16.15.

$$A_{sus} = \frac{q \cdot (C_d \cdot C_{d_{forebody}}) \cdot S_{inf}}{N \cdot \sigma_{K-29}} \tag{16.15}$$

Input parameter	Value [unit]	Output value	Value [unit]
Dynamic pressure	900 [Pa]	Length of suspension line	10.5 [m]
Effect of fore-body on drag coefficient	0.93 [-]	Area of suspension line	0.347 [mm^2]
Tensile strength of Kevlar	2920 [MPa]	Suspension line mass	0.0524 [kg]
Diameter of fore-body	1.5 [m]	Number of suspension lines	10 [-]
Ratio of suspension line length to fore-body diameter	7.0 [-]		

Table 16.5: Suspension line design: Inputs and outputs

Finally, in the design of the parachute it is necessary to design a deployment mechanism for the parachute. The method of using a drogue parachute is chosen, which is deployed by use of a drogue gun. A drogue gun is lightweight and creates little reaction force when used [55]. The drogue parachute is designed based on the mass of the main parachute as the drogue parachute must create enough of force to pull the main parachute out of its bag. Therefore the drag needed to be provided by the drogue parachute it taken equal to the weight of the main parachute and from this the required area of the drogue parachute is found. This is shown in Equation 16.16.

$$S_{drogue} = \frac{(m_{para} + m_{lines}) \cdot g_{Mars}}{\frac{1}{2} \cdot \rho \cdot V_{deploy}^2 \cdot (C_{d_{drogue}} \cdot C_{d_{forebody_{drogue}}})} \tag{16.16}$$

Furthermore, the suspension lines are designed in the same way as for the main parachute, with the exception that the lines will use a smaller constant for the forebody, hence will have shorter lines and a lower drag coefficient. This design choice has been made to save mass as the increase in size of the parachute due to smaller lines is less than the reduction in weight due to shorter lines and hence leads to a lighter design. Both the material for the canopy and the suspension lines are the same as for the main parachute. The inputs and outputs for the drogue parachute design process can be seen in Table 16.6

Input parameter	Value [unit]	Output value	Value [unit]
Effect of fore-body on drag coefficient	0.7 [-]	Drogue parachute area	0.097 [m^2]
Ratio of suspension line length to fore-body diameter	4.0 [-]	Drogue suspension line length	6.0 [m]
Deployment velocity	298 [m/s]	Drogue parachute and lines mass	0.34 [kg]
Drag coefficient of drogue parachute	0.5	Drogue gun mass	0.91 [kg]
		Number of suspension lines	6

Table 16.6: Deployment system design: Inputs and outputs

Aerodynamic Fins

When the lander impacts the surface it must be ensured that it lands as straight as possible, while wind gusts acting on the lander could affect the descent. This can cause the lander to become unstable and not return to a vertical position. To counteract this, the centre of pressure must be moved above the centre of gravity to ensure stability. To move the centre of pressure up aerodynamic fins have been placed at the top of the lander. These fins increase the area at the top without adding too much weight and thus shift the centre of pressure above the centre of gravity. By defining the desired location of the center of pressure and the placement of the fins, the area of the fins required for this combination is then calculated, as seen in Equation 16.17. The additional mass of the fins is added to the centre of gravity location and compared to the centre of pressure to ensure it remains below.

$$A_{fin} = \frac{A_{cap} \cdot (D_{cap} - x_{cp})}{x_{cp} - x_{fin}} \tag{16.17}$$

The results of this process are shown in Table 16.7. Note that all locations are taken with reference to the bottom of the lander.

Input parameter	Value [unit]	Output value	Value [unit]
Centre of gravity, x_{cg}	0.460 [m]	New centre of gravity	0.463 [m]
Desired centre of pressure, x_{cp}	0.55 [m]	Total surface area of fins	0.489 [m^2]
Density of Aluminum	2710 [kg/m^3]	Total mass of fins	1.33 [kg]
Location of fins	0.75 [m]		

Table 16.7: Aerodynamic fin design: Inputs and outputs

Verification & Validation

For the verification of the code used during the sizing of the parachute, the volume of the canopy and surface area of the suspension lines are checked using the process given in Chapter 5. To check the parachute, two different diameters were used and the expected outcomes were calculated by hand. For the suspension lines different drag forces were used and the expected outcomes were also calculated by hand. In Table 16.8 the results of the verification can be seen.

Component	Input	Expected output	Output from code	Percentage difference
Parachute	D = 1 m	0.00108 [m^3]	0.00108 [m^3]	0%
	D = 10 m	0.0108 [m^3]	0.0108 [m^3]	0%
Suspension lines	Drag = 100 kN	34.25 [mm^2]	34.25 [mm^2]	0%
	Drag = 5 kN	1.71 [mm^2]	1.71 [mm^2]	0%

Table 16.8: Verification: Parachute & Suspension line sizing

For validation, the mass of the parachute is compared to that of heritage data relation, this is a good indicator as to whether the values for the mass of the parachute are accurate. For the results of the validation see Table 16.9.

Input	Code result	Heritage result	Percentage difference
D = 3 m	2.53	2.76	8.33%
D = 10 m	8.44	14.89	43.3%

Table 16.9: Validation: Parachute mass

For the first result the it can be seen that the results are very close together. There is only a difference of 8%. This percentage difference could be due to the relation for heritage data being for much larger parachutes, therefore when scaling down to much smaller parachutes, some differences such as the number of suspension lines or the deployment method may be overlooked, thus causing a higher mass. For the second result, a much larger difference is seen, 43.3%. The first reason for this is that for larger parachutes, the materials required would indeed need to be stronger therefore in most cases heavier, this leads for the same area to much higher mass values. The second reason could be due to the deployment method: larger parachutes require more complex, stronger deployment methods than the one used for the parachute in the code, which could cause higher masses. However as the code deals with much smaller parachutes, it is crucial that the match for smaller diameters is closer. This is indeed the case, thus it is concluded that for the parachute size required, the code is valid. However, if larger parachutes would be required, it is recommended to update the code to ensure it gives valid answers for larger parachutes.

System performance and characteristics

In Table 16.10, the list of all the aerodynamic subsystem characteristics can be seen.

Parameter	Parameter value [unit]	Parameter	Parameter value [unit]
Constructed parachute area	14.27 [m^2]	Parachute mass	4.038 [kg]
Suspension line length	10.5 [m]	Suspension line surface area	0.347 [mm^2]
Suspension line mass	0.0524 [kg]	Drogue parachute area	0.097 [m^2]
Drogue line length	6.0 [m]	Drogue parachute and line mass	0.34 [kg]
Drogue gun mass	0.91 [kg]	Total area of fins	0.49 [m^2]
Total mass of fins	1.33 [kg]		

Table 16.10: Aerodynamic subsystem characteristics

Recommendations

For further development of the aerodynamics subsystems, three aspects are recommended. The first is to research parachutes that can withstand a higher dynamic pressure. The disk-gap-band parachute is currently leading the way with dynamic pressures up to 970 Pa, however developing parachutes that can withstand higher dynamic pressures will increase the altitude at which parachutes can be deployed [51]. This is already being explored by NASA in [56] and will help especially with landing at higher altitudes, such as in the Tharsis region. The final recommendation is looking into the possibility of having moving fins. Having fins that can move would improve the stability of the lander, especially in the case of landing in storms or stronger winds. By having moving fins the lander is able to react better to side winds and improve the ability to land vertically.

16.3. Guidance, Navigation, and Control

Requirements

Table 16.11: Requirements on Attitude Determination and Control subsystem

ID	*Requirement*	*Status*	*Origin*	*Compliance*
DMD-GNC-L-01	The lander system shall determine its velocity with respect to the surface with an accuracy of 5 m/s for the last 40 meters before impact.	Active	Bullet release	Met
DMD-GNC-L-02	The lander system shall determine its altitude above the surface with an accuracy of 0.5 meters for the last 40 meters before impact.	Active	Bullet release	Met
DMD-GNC-L-03	The lander system shall determine the impact time with an accuracy of 0.02 seconds.	Active	Bullet release	Met
DMD-GNC-L-04	The lander system shall determine the dynamic pressure while descending.	Active	Deployment of parachutes	Met
DMD-GNC-L-05	The lander system shall determine when the lander has zero velocty.	Active	Initialisation	Met

Design Process

Similar to the design of the orbiter GNC from Section 10.4, it was first decided what the GNC of the lander needs to do. It serves four functions: determine parachute deployment time; determine bullet ejection time; to determine initialisation time; and to determine the location of the lander.

System Performance and Characteristics

First, for the deployment of the parachute a set of pressure sensors are added. This is because the deployment is restricted by the dynamic pressure acting on the probe. It is therefore necessary to know this pressure. Using a pitot static sensor and a total pressure sensor placed in free flow, the dynamic pressure can be extracted. As the free flow at some point during entry has a velocity of several km/s and a dynamic pressure of over 8980 Pa, the pressure ports need to withstand these loads.

For the ejection of the two bullets, the lander needs to know at what time it needs to set off the cartridges. In order to comply with [DMD-GNC-L-01], [DMD-GNC-L-02] and [DMD-GNC-L-03], the same LIDAR-Lite V3[4] system is used as on the Mars 2020 Ingenuity probe . This sensor generates altitude data for the last 40 meters of descent to an accuracy of 1 cm which can be used to generate velocity data and therefore to predict impact time. There is no need for this TRL-9 rated sensor to survive the landing as it is only needed right up until impact.

The last sensor is an IMU, which will measure the acceleration of the probe. It will register an immense peak in acceleration at landing which signifies impact. Combining this with the altimeter data, the spacecraft will know when it hits the ground. Similar to the altimeter, the IMU does not need to survive the impact either as the system has predicted the timing of impact and can determine the start of the initialisation sequence from that, without knowing the exact impact time.

This is all summarised in below in Figure 16.7.

There are several localisation techniques: optical, using images to find the probe; DSN radio ranging, using the Doppler effect to find the distance to the DSN; DSN-orbiter radio ranging, using the Doppler effect to find the distance to the DSN and the orbiter for increased accuracy. To meet with requirement [DMD-PERF-BROOT-04], an accuracy of 10 m or less should be obtained.

Traditionally, the Doppler effect has been exploited in radio ranging to find the distance to the DSN. This method has been used extensively before and for probes on Mars this can lead to an accuracy of up to around 1 km after only a few days [57].

To improve this figure to meet the requirements, an additional reference point can be utilised: the orbiter [58]. In addition to the DSN radio ranging, radio ranging to the orbiter is used. This can be compared to the method of the Global Positioning System (GPS). The main difference is that GPS uses at least three different satellites at one moment in time, this system uses one satellite at at least three different moments in time. This method can yield an accuracy of up to 0.5 m [59].

[4] https://buy.garmin.com/en-US/US/p/557294/pn/010-01722-00, Accessed [16-06-2021]
[4] https://www.garmin.com/en-US/blog/general/garmin-on-mars/, Accessed [18-06-2021]

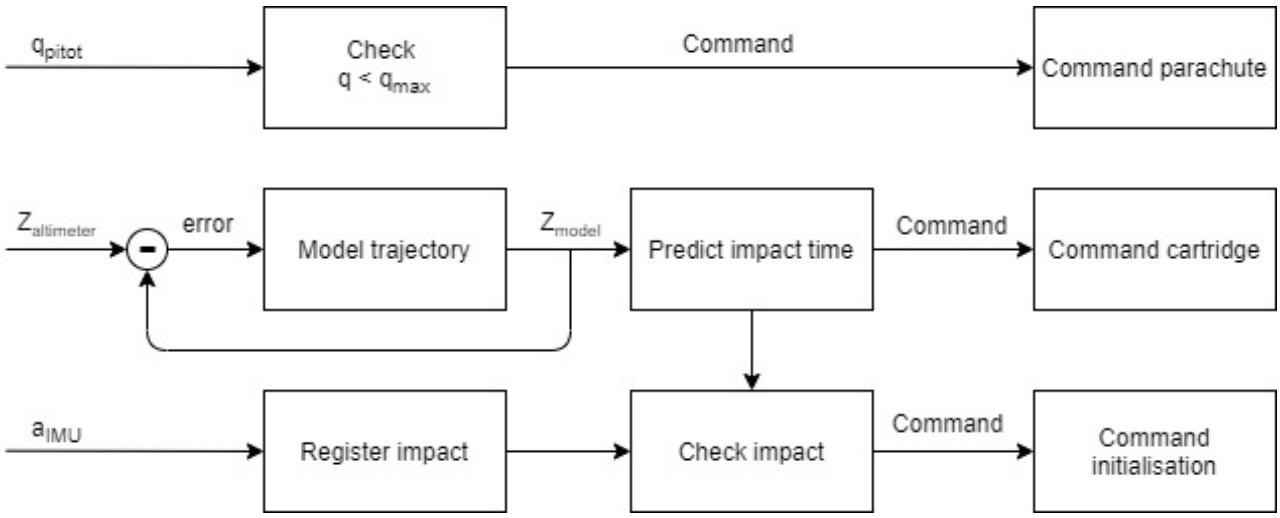

Figure 16.7: GNC for the lander during descent and landing

Even though optical methods have traditionally not been favoured for precise localisation, it can be used for Mars Deploy as a redundant system. For example, using the NASA HIRISE camera on the Mars Reconnaissance Orbiter the location can be found with an accuracy of approximately 0.3 m, considering the resolution of the camera. Especially as the impactor is expected to leave a small crater, it will be visible for the satellite.

Recommendations

As the pressure sensors are in the free flowing stream they are subject to extreme conditions throughout the entry. As the sensors are only needed for the last, less intense phase of the EDL, a deploying pressure probe could be considered. This was initially dismissed for the sake of simplicity but it might make the whole sensor system lighter as less thermal protection is needed.

The LIDAR system was chosen for its weight, and TRL, and most of all accuracy as the cartridge release time is critical. However, it only provides altitude data for the last 40 meters. Even though this is sufficient to determine the impact time, with an impact velocity of around 230 m/s, this distance passes in 0.16 seconds. Even though this was deemed enough for the system to determine an impact time, it leaves little time for diagnosing any problems that might arise. Therefore it is recommended to consider altimeters from other missions with longer ranges, possible in conjunction with the present system.

16.4. Structures

In this section, the structural design of the landers will be presented. First, an overview of the subsystem requirements is given, followed by the design process. Then, the verification and validation method is presented, followed by an overview of the system performance and characteristics. Finally, some recommendations for future developments will be given.

Requirements

The requirements of the structural subsystem of the landers are shown in Table 16.12. Requirement [DMD-STRUC-L-16] has been scrapped, as it coincides with requirement [DMD-STRUC-O-04]. The requirements pertaining to the launch vibrations, radiation and Martian weather have not yet been investigated.

Table 16.12: Requirements on the landers' structures subsystem

ID	*Requirement*	*Status*	*Origin*	*Compliance*
DMD-STRUC-L-01	The structures subsystem shall be able to support all lander subsystems.	Active	Purpose of structures subsystem	Met
DMD-STRUC-L-02	The structures subsystem shall be able to shield the lander's electronic subsystems from radiation.	Active	Subsystems specifications	N.V.

Continued on next page

Table 16.12 – continued from previous page

ID	*Requirement*	*Status*	*Origin*	*Compliance*
DMD-STRUC-L-03	The structures subsystem shall be able to withstand longitudinal launch vibrations of <tbd> Hz.	Active	Launch vehicle specifications	N.V.
DMD-STRUC-L-04	The structures subsystem shall be able to withstand lateral launch vibrations of <tbd> Hz.	Active	Launch vehicle specifications	N.V.
DMD-STRUC-L-05	The structures subsystem shall be able to withstand a maximum longitudinal launch acceleration of 6 g.	Active	Launch vehicle specifications [3]	Met
DMD-STRUC-L-06	The structures subsystem shall be able to withstand a maximum lateral launch acceleration of 2 g.	Active	Launch vehicle specifications [3]	Met
DMD-STRUC-L-07	The structures subsystem shall be able to withstand impact loads of 10000 g.	Active	Payload specifications	Met
DMD-STRUC-L-08	The structures subsystem shall be able to withstand entry loads of 14 g.	Active	EDL	Met
DMD-STRUC-L-09	The structures subsystem shall protect all lander subsystems against impact loads of 10000 g.	Active	Payload specifications	Met
DMD-STRUC-L-10	The structures subsystem shall be able to protect all lander subsystems against Martian weather.	Active	Follows from [DMD-LANDER-21]	Met
DMD-STRUC-L-11	The structures subsystem shall be able to withstand the operational temperatures of <tbd>.	Active	Thermal control subsystem	N.V.
DMD-STRUC-L-12	The structures subsystem shall have a maximum mass of 84 kg.	Active	Mass budget	Met
DMD-STRUC-L-13	The structures subsystem shall be able to withstand the Martian radiation.	Active	Material specifications	N.V.
DMD-STRUC-L-14	The structures subsystem shall be able to withstand Martian dust storms.	Active	Follows from [DMD-DESCENT-21]	N.V.
DMD-STRUC-L-15	The structures subsystem shall have at least 4 attachment points for the orbiter.	Active	Launch configuration	Met
DMD-STRUC-L-16	The structures subsystem shall be able to release the entry capsule.	Scrapped	Launch configuration	N.A.
DMD-STRUC-L-17	The forebody shall be able to reach a depth of at least 4 m.	New	Payload requirements	Met

Design Process

In this subsection, the structural design process will be presented. First, a brief overview of the design given. Then, the design process of the impact attenuator is presented, followed by the support structure and forebody.

Structures Overview

One of the most important components of the lander is the seismometer, which can withstand a maximum load of up to 13000 G, or 10000 G including a safety margin of 3000 G. Additionally, the heat flow probe needs to reach a depth of at least 4 m in order to meet the accuracy requirement. Keeping this in mind, several concepts have been evaluated in a pro-con analysis. Five of these concepts are shown in Figure 16.8. The driving design options

included penetrating through the Martian soil, using a separate fore- and aftbody and using a shock-absorbing impact attenuator. All concepts feature a fully enclosed design in order to protect the internal components from the harsh Martian weather conditions, such as dust storms.

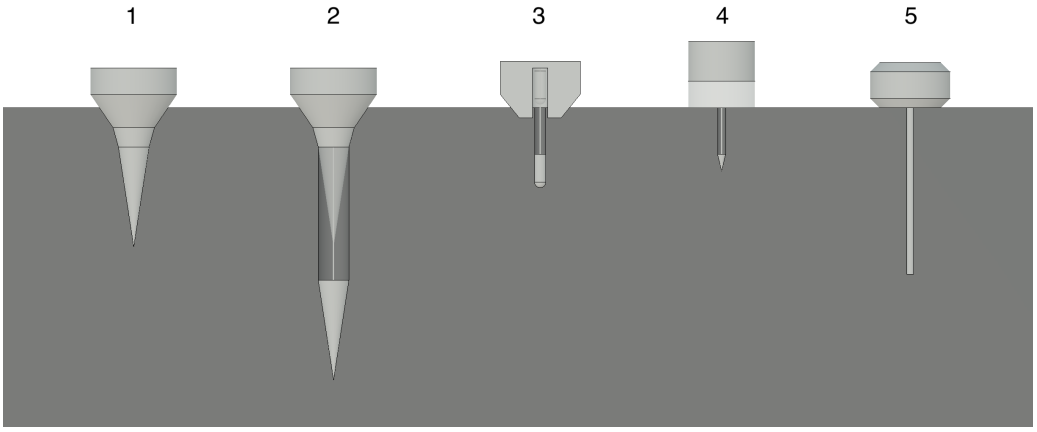

Figure 16.8: Proposed descent system concepts. Left to right: 1) Penetrator 2) Penetrator with forebody 3) Impactor with forebody 4) Impactor with forebody and impact attenuator 5) Body on penetrating stick. Relative dimensions are to scale. Absolute dimensions are arbitrary.

Following the pro-con analysis, the fourth concept in Figure 16.8 was chosen, which consists of a main structure that stays near the surface and contains all subsystems and payload. Upon impact, an aluminium honeycomb impact attenuator absorbs the loads, while a small forebody uses its kinetic velocity to penetrate through the soil. It is connected to the main structure via a carbon fiber tether, along which 14 temperature sensors are distributed. The use of a forebody was chosen, as it allows the lander to be considerably more compact as opposed to a 4 m long lander. Additionally, it allows for a wider top area that can be used to accommodate the solar panels and antennas. The support structure is made of Carbon Fiber - Nomex Honeycomb (CFNH) sandwich. It is worth noting that carbon fiber has been shown to attenuate radiation, thus no additional radiation protection is required [60]. The relevant properties of all materials are shown in Table 16.13.

	E-Modulus (GPa)	**Tensile Strength [MPa]**	**Compressive Strength [MPa]**	**Density [kg/m3]**
Carbon fiber fabric + Epoxy ($V_f = 0.5$)[5]	70	600	570	1600
Nomex Homeycomb[6]	negligible	N.A.	0.70	28
Aluminium Honeycomb[7]	N/A	N.A.	14.4	173
Carbon fiber HMC[8]	370	4400	N.A.	1000

Table 16.13: Relevant material properties of the lander structures

Impact Attenuator

The travel distance d_{req} required to slow down at the constant deceleration of 10000 G can be found by setting the kinetic energy of the lander equal to the work done by the impact attenuator and rearranging the equation. This is shown in Equations 16.18-16.20 and yields a required travel distance of 27 cm, or 32 cm including a 20% safety margin.

$$E = W \qquad (16.18) \qquad \frac{1}{2}mv^2 = Fd_{req} \qquad (16.19) \qquad d_{req} = \frac{v^2}{2a} \qquad (16.20)$$

The impactor not only slows down because of its impact attenuator, but also by partially penetrating through the soil. The penetration depth d_{pen} of an object with weight m, frontal area A and impact velocity V can be calculated for varying soil types by using Equation 16.21. The penetrability factor S is a measure of the soil's impact resistance, where a larger number results in deeper penetration. According to Smrekar et al. (1999), "The S number in general correlates with broad soil categories, with a hard material like frozen soil having an S number

[3] http://www.performance-composites.com/carbonfibre/mechanicalproperties_2.asp, Accessed [14-06-2021]
[4] https://www.honeycombpanels.eu/en/products/honeycomb/nomex-aeronautical-grade-en, Accessed [14-06-2021]
[5] https://www.plascore.com/download/datasheets/honeycomb_data_sheets/PLA_PAMG-XR1-5052_4-6-2021.pdf, Accessed [14-06-2021]

of 2-4, while easily penetrated loose sand or dust deposits might have an S number greater than 20" [61]. Since not much is known about the exact properties of the Martian soil in each of the landing areas, as illustrated by InSight's HP3 instrument failure, a penetrability factor range of 1-35 is assumed.[9]

$$d_{pen} = 6.0 \cdot 10^{-8} S^{0.5} \left(\frac{m}{A}\right)^{0.7} V^2 \tag{16.21}$$

In this range, the penetration depth of the lander is found to be between 12 and 70 cm. As some of the impact is absorbed by the soil, the minimum travel distance can be subtracted from the required travel distance, resulting in a required crumple zone deformation distance of 21 cm. For this crumple zone, a Plascore PAMG-XR1 5052 Aluminium honeycomb is chosen, as it shows constant plastic buckling deformation, and is less prone to fracture than nonmetallic composites, such as Nomex.

Though honeycombs of this type are shown to reach strains of close to 0.8, a conservative strain of 0.6 is assumed [62]. This means that the required height of the honeycomb structure is 21/0.6 = 34 cm.

Next, the required honeycomb strength σ can be found by using the relation $A = \frac{F}{\sigma}$, where A is the cross-sectional area of the crumple zone, and the force F can be easily found by multiplying the impact deceleration by the mass on top of the crumple zone. Since the mass of this crumple zone also weighs down on itself, several iterations are required to converge to a final weight. It is worth noting that, while buckling, some part of the crumple zone becomes stationary and thus does not weigh down on itself. As such, only half of the crumple zone's mass is included in the aforementioned weight.

Finally, the honeycomb density can be estimated based on its compressive strength. Figure 16.9 shows a linear regression of several PAMG-XR1 5052 honeycombs and their corresponding strength and density. From this linear relation, the density can be estimated, and the resulting mass of the impact attenuation structure. In this case, the strength, density and resulting mass are found to be 14.4 MPa, 173 kg/m^3 and 50 kg, respectively.

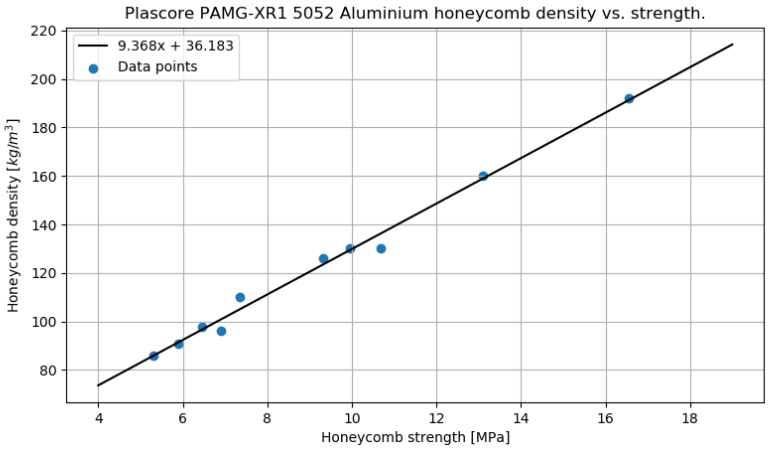

Figure 16.9: Linear least squares regression of Plascore PAMG-XR1 5052 Aluminium honeycomb bare compressive strength vs. density.[10]

It is worth noting that the design is heavily constrained by the frontal area. As mentioned before, the maximum penetration depth in very soft soil is 70 cm, which results in an overlap of 36 cm with the lander's support structure. Decreasing the frontal area results in deeper penetration, thus burying the entire lander in the soil. Similarly, increasing the area results in a wider lander that is heavier and less aerodynamically stable.

Support Structure

The support structure is the structure to which all subsystems are connected. Additionally, it provides a load path for the launch, entry and impact loads. The outer support structure of the lander consists of a cylindrical wall, a bottom plate and a top plate, to which the air composition analyser and weather system are attached. As the lander requires the use of a 15 cm thick aerogel lining, explained in Section 16.9, the remaining subsystems cannot be attached to the bottom plate or walls. Therefore, they are attached to a sub-structure, which consists of a cylindrical wall and middle plate made of CFNH. This structure, along with the impact attenuator and barrels, can be seen in Figure 16.10 and Figure 16.11. Each of these elements are designed using the same methods as the orbiter, which are explained in Section 10.2. A safety factor margin of 40% is used in these calculations.

[9] https://mars.nasa.gov/news/8444/common-questions-about-insights-mole/?site=insight, Accessed [22-06-2021]

[10] https://www.plascore.com/download/datasheets/honeycomb_data_sheets/PLA_PAMG-XR1-5052_4-6-2021.pdf, Accessed [14-06-2021]

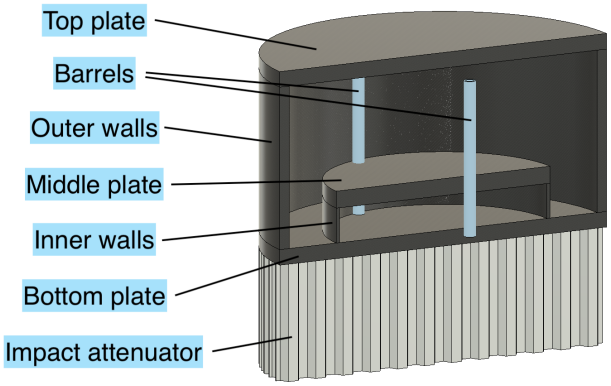

Figure 16.10: Cross-sectional view of the lander's support structure, impact attenuation structure and barrels.

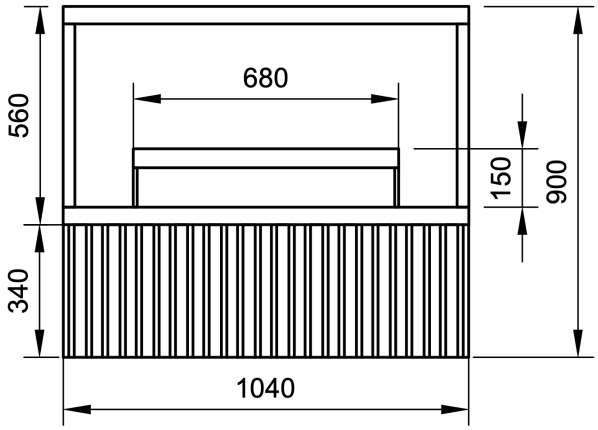

Figure 16.11: Overview of the lander's general support structure dimensions. For a detailed overview of the relevant dimensions, please refer to Figure C.2 in Appendix C.

Forebody

In order to meet the measurement depth requirement of the heat flow probe, a penetrating forebody will be used. This forebody, or bullet, must reach a depth of four meters in every type of soil. In order to reach this depth, the bullet needs to have a high mass and impact velocity, but a small frontal area. Tungsten is used, as it has a high density and strength, and is commonly used in bullets and missiles with comparable energy. Equation 16.21 can again be used to calculate the penetration depth for this bullet. Much like the lander, the bullet is designed for a wide penetrability factor (S) range of 1-35.

At the lander's nominal impact speed of 230 m/s, no bullet within reasonable constraints is found to be able to reach four meters at S = 1. For this reason, the velocity of the bullet must be increased. To achieve this, a firearm cartridge will be used, which will ignite before impact and accelerate the bullet through a 0.45 m long barrel. With this velocity increase, however, the bullet will penetrate too deeply in soft soil types. For this reason, an additional bullet will be used, with a smaller cartridge. This first bullet is designed for hard soil types with S = 1-6, while the second is designed for harder soil types with S = 6-35.

Each of these bullets is attached to the main body of the lander via a tether, which should be able to transfer data from and to the bullets and contains the temperature sensors. The maximum depth that would be reached by the bullets is just below 10 m. The tether has been designed for 11m to include a safety margin of 10%. This margin also accounts for the distance between the tether support structure and the ground, which is at most 53 cm. The tether will be under a significant load during acceleration of the bullet. The tethers have been designed for the first bullet, as its acceleration is the highest.

The tether load has been defined for the worst case. The load can be calculated by multiplying the acceleration times tether total mass. The acceleration is dependant on the barrel length and required ΔV. The resulting Equation 16.22 is simply derived from the kinetic energy equation from Newtonian physics.

$$F_{tether} = m_{tether} \cdot \frac{2 \cdot l_{barrel}^2}{\Delta V} \tag{16.22}$$

By using the material characteristics of a carbon fiber tether, the final sizing can be done. The resulting tether will thus have a mass of 335 g with a maximum tensile stress of 3.74 GPa. This falls within the properties of carbon fiber.

Verification & Validation

For the structural design of the lander, Excel, Python and manual calculations were used. Calculations in Excel and Python are verified by performing manual calculations. A comparison of several values computed by these tools and their manually calculated counterparts can be seen in Table 16.14.

Python code verification is performed using the procedure explained in Chapter 5. The tools have been checked on correct programming logic and do not give any syntax errors.

Table 16.14: Calculation verification results

Equation	Input	Output tool	Output hand calculation	Error[-]
Equation 16.20, excl. SF	Table 15.3, deceleration	0.2696 m	0.2696 m	0%
Equation 16.21	Table 15.3, lander impact velocity, area, S = 1	0.1184 m	0.1185 m	<0.1%
Equation 16.21	Table 15.3, lander impact velocity, area, S = 35	0.7006 m	0.7013 m	<0.1%
Equation 16.22	bullet mass, ΔV, barrel length	3.74 GPa		
Equation 16.21 bullet 1: cartridge energy	Table 16.17, S = 1, d_{pen} = 4 m	19103 J	19101 J	<0.1%
Equation 16.21 bullet 1: d_{pen}	Table 16.17, S = 6	9.798 m	9.800 m	<0.1%

System Performance and Characteristics

A brief overview of the lander's structural elements is given in Table 16.15. A more detailed overview of the support structure's elements and the bullets can be seen in Table 16.16 and Table 16.17.

	Mass [kg]	Material
Support structure	24.01	Carbon fiber - Nomex honeycomb
Crumple zone	50.36	Aluminium honeycomb
Bullets	0.21	Tungsten
Tethers	0.67	Carbon fiber

Table 16.15: Overview of lander's structural elements

	Supported subsystems	Supported mass [kg]	Total thickness [mm]	Plate mass [kg]
Top plate	Solar cells, antennas, air composition analyser, weather station	23.60	47.2	5.47
Middle plate	EPS (excl. solar array), CDH, TTC electronics, Thermal (excl. aerogel), seismometer, heat probes	35.34	49	2.86
Bottom plate	Inner walls, middle plate, aerogel insulation	63.11	51	6.71
Outer walls	Top plate	30.53	33	6.87
Inner walls	Middle plate	38.96	15	2.10

Table 16.16: Overview of the landing system's structural plates and walls

	Bullet 1	Bullet 2
Mass [g]	106	100
Energy added [kJ]	19	6.3
S range [-]	1 - 6	6 - 35
Penetration depth range [m]	4 - 9.8	4-9.64
Impact velocity [m/s]	655	421

Table 16.17: Overview of bullet characteristics

Recommendations

Some recommendations can be made for future development of the lander's structure. Firstly, several requirements have not been verified. These requirements are related to the vibrations, Martian weather, thermal control and radiation. These will need to be investigated in more detail.

Secondly, as the lander is designed to impact at a deceleration of 10000 g, one of the main risks is impact damage of the subsystems. For this reason, it is recommended to perform thorough testing of the honeycomb structure,

to ensure it behaves as expected on various soil types, for different landing conditions. Additionally, a damping system can be designed for the subsystems, excluding the seismometer, to lower the deceleration they will endure during landing. Furthermore, the bullets need to be looked at in closer detail. A proper analysis should be done on whether or not the bullets, tethers and the lander will survive the explosion, and how deep they will penetrate.

Finally, surface wind speeds should be taken into account. During the last phase of descent, the craft will move with the wind and therefore may have a non-zero tangential velocity component. Using a maximum wind speed of 32 m/s [11] and an impact speed of 230 m/s, the maximum impact angle is $\angle_{\text{impact}} = \arctan\left(\frac{32}{230}\right) = 7.4°$. The impact structure should be able to function as intended with this angle in mind.

16.5. Scientific Payload

In order to meet the mission objective, the scientfic payload carried on each lander must be able to help in locating geothermal heat and water sources on Mars. The instruments are subjected to a set of strict requirements, in order to ensure that high quality scientific data is produced. Following these requirements, each impactor shall carry a heat flow probe, seismometer, atmospheric composition analyser, and a weather station. The weather station shall consist of air temperature, pressure and humidity sensors.

These requirements are presented below. Changes in requirements with respect to the Midterm Report [6] are clearly indicated. Note that some requirements originate form instrument specifications. These requirements have been set after the scientific instruments had been designed, in order to set restrictions for future design phases. Performance requirements of form [DMD-PERF-XXX-XX] were driving requirements for the instrument design process.

Requirements

Table 16.18: Requirements on the scientific payload

ID	*Requirement*	*Status*	*Origin*	*Compliance*
General requirements				
DMD-SCI-01	The scientific payload shall have a mass not exceeding 25 kg.	Replaced	Mass budget	N.A.
DMD-SCI-02	The scientific payload shall experience forces not exceeding 10 g during entry, descent and landing.	Replaced	Payload specifications	N.A.
DMD-SCI-03	The scientific payload shall have a mass not exceeding 20 kg.	New	Replaces [DMD-SCI-01] due to updated value	Met
DMD-SCI-04	The scientific payload shall experience accelerations not exceeding 10000 g in the x, y, and z-directions.	New	Replaces [DMD-SCI-02] due to updated value	Met
DMD-SCI-05	The scientific payload shall operate nominally for three years after deployment on Mars.	New	INSERT ORIGIN	Met
Heat Flow Probe Requirements				
DMD-PERF-HF-01	The heat flow probe shall determine Mars's heat flow at the landing site with an accuracy of 1 mW/m^2.	New	Flows from [DMD-PERF-BROOT-02]	Met
DMD-PERF-HF-02	The heat flow probe shall be able to measure heat flows in range 0-50 mW/m2.	New	Flows from [DMD-PERF-BROOT-03]	N.V.
DMD-SCI-HF-01	The heat flow probe shall be unaffected by heat generated by the lander.	Active	To mitigate risk [R-PAYL-3]	N.V.
DMD-SCI-HF-02	The heat flow measurements shall be unaffected by a change in seasons on Mars.	Replaced	To mitigate risk [R-PAYL-3]	N.A.
DMD-SCI-HF-03	The heat flow measurements shall be unaffected by the day-night cycle on Mars.	Replaced	To mitigate risk [R-PAYL-3]	N.A.

Continued on next page

[11] https://airandspace.si.edu/exhibitions/exploring-the-planets/online/solar-system/mars/wind/

Table 16.18 – continued from previous page

ID	*Requirement*	*Status*	*Origin*	*Compliance*
DMD-SCI-HF-04	The heat flow probe shall determine its deployment depth with an accuracy of 4 mm.	Active	Originates from HP3 documentation	Met
DMD-SCI-HF-05	The heat flow probe shall determine the tilt of deployment with an accuracy of 1 degreesin both tilt directions.	Active	To mitigate risk [R-PAYL-4]	Met
DMD-SCI-HF-06	The heat flow probe shall be able to measure over a depth range of 4m.	Active	Follows from [DMD-PERF-HF-01] and [DMD-SCI-05]	Met
DMD-SCI-HF-07	The heat flow probe shall have a nominal measuring time of 1.6 Martian years.	Active	Follows from [DMD-PERF-HF-01] and [DMD-SCI-05]	Met
DMD-SCI-HF-08	The heat flow probe's temperature sensors shall have an accuracy of 0.01 K.	Active	Originates from HP3 documentation	Met
DMD-SCI-HF-09	At least one of the heat flow probe's bullets shall reach a deployment depth of 4 m when landing on soil with a penetrability factor of 1-35.	New	To mitigate risk [R-PAYL-2]	Met
DMD-SCI-HF-10	Data handling and control of the heat flow probe shall be done by the EBOX	New	Originates from HP3 documentation	Met
DMD-SCI-HF-11	The heat flow measurements shall take place over at least one Martian year.	New	To mitigate risk [R-PAYL-2]	Met
Seismic Instrument Requirements				
DMD-PERF-SEIS-01	The seismic instrument shall be sensitive to marsquakes of magnitude $M_W = 1.6$.	New	Flows from [DMD-PERF-BROOT-01]	Met
DMD-SCI-SEIS-01	The seismic instrument shall be able to filter out the vibrations generated by the lander.	Active	This requirement mitigates risk [R-PAYL-8]	N.V.
DMD-SCI-SEIS-02	The seismic instrument shall be deployed on inclinations not exceeding 15°.	Active	Originates from HP3 documentation	Met
DMD-SCI-SEIS-03	Data handling and control of the seismic instrument shall be done by the lander maincomputer.	Replaced	Originates from HP3 documentation	N.A.
DMD-SCI-SEIS-04	Data handling and control of the seismic instrument shall be done by the EBOX.	New	Originates from HP3 documentation	Met
Weather Station Requirements				
DMD-PERF-WS-01	The temperature sensor shall have a resolution of 0.1 ℃.	New	Flows from [DMD-PERF-BROOT-05]	Met
DMD-PERF-WS-02	The pressure sensor shall have a resolution of 1 Pa.	New	Flows from [DMD-PERF-BROOT-06]	Met
DMD-PERF-WS-03	The relative air humidity sensor shall have a resolution of 0.1%.	New	Flows from [DMD-PERF-BROOT-07]	Met
DMD-SCI-WS-01	Control and data handling of the weather station sensors shall be done by the landermain computer.	Active	Originates from design decision	Met
Air Composition Analyser Requirements				
DMD-PERF-GCMS-01	The GCMS shall measure the atmospheric composition with an accuracy of 0.1 vol%.	New	Flows from [DMD-PERF-BROOT-08]	Met
DMD-SCI-GCMS-01	The GCMS shall be protected against dust.	Active	Originates from instrument specifications	Met

Besides the scientific instrument performance requirements, the most driving requirement is [DMD-SARR-BROOT-05] which states that the scientific instruments shall have Technology Readiness Level 9. According to the European Space Agency, TRL9 is reached after successful operation of the system, with performance metrics that satisfy the system and mission requirements [63, p. 28].

Design Process

Due to the strict TRL9 requirement, the four scientific instruments carried by each lander could not be designed from scratch but had to be chosen from existing missions. When simply looking at the scientific objectives of the mission, the most logical comparison is with NASA's InSight mission. InSight is designed to study the inner structure of Mars by measuring the planet's heat flow and listening for marsquakes.

Heat Flow Probe

Since it is the only heat flow probe ever to be deployed on Mars, InSight's Heat Flow and Physical Properties Package (HP3) instrument was the primary candidate to be integrated into the Mars Deploy landers. The HP3 instrument was designed to be a stand-alone device, which would be placed on the surface of Mars by InSight's robotic arm. HP3 would then activate its "mole" to start digging up to 5 m deep, pulling a tether with temperature sensors along with it. The mole contained a heating element in order to measure the thermal conductivity of the Martian soil. By combining the thermal conductivity measurements with the measurements from a set of 14 thermometers on the tether, the planet's heat flow at the lander location could be determined [64, p. 1].

According to HP3 documentation [64, p. 2], the heat flow probe is designed for a target measurement uncertainty of 5 mW/m^2, which does not meet the strict requirement imposed by [DMD-PERF-HF-01]. The same document however states that an accuracy of 2.2 mW/m^2 would be reached for a deployment depth of 3 m and an observation period of 0.6 Martian years, and an accuracy of 1 mW/m^2 could be reached if the mole would reach its maximum depth of 5 m. Since the accuracy of the heat flow measurement depends on the deployment depth and the measurement time amongst others, a simple relation was set up to relate the measurement accuracy to the deployment depth, based on the accuracy data given in [64, p. 28]. This relation was then corrected to account for measurement time as well, given that the measurement error decreases with a factor $1/\sqrt{n}$, where n is the measurement time in Martian years [65, p.6]. This resulted in equation Equation 16.23, with u being the 1-σ measurement uncertainty in mW/m^2, n the measurement time in Martian years and d the final deployment depth.

$$u = \frac{1.704}{\sqrt{n}} \cdot -0.2727d + 1.8181 \tag{16.23}$$

With the measurement time of three Earth years given by [DMD-SCI-05], Equation 16.23 could be used to determine the target deployment depth. In order to meet the 1 mW/m^2 set by [DMD-PERF-HF-01], a deployment depth of 4 meters would be required. This resulted in requirement [DMD-SCI-HF-04], which was used in further stages of the design.

As described in Section 16.4, some major changes had to be made to adapt HP3 to the impactor design. First of all, it must be noted that HP3 never successfully deployed on Mars, only reaching a deployment depth of 43 cm [66, p. 17]. Current data on the soil composition around Mars is very limited, as proven by the failure of HP3. Therefore, a two-bullet design was chosen in which the 4 meter deployment depth requirement is met regardless of soil hardness. This mitigates risks [R-PAYL-1] and [R-PAYL-2], and meets requirement [DMD-SCI-HF-09]. Supporting calculations can be found in Section 16.4. Finally, due to the close integration of HP3 into the impactor, the support structure which would be needed to allow HP3 to stand on the surface of Mars can be discarded. This brings the mass of the instrument down from around 3 kg to 1.7 kg [64, p. 17]. HP3's back end electronics will be stored in the EBOX [64, p. 12], similarly to InSight.

Seismometer

To find a TRL9 seismometer which met the stakeholder performance requirements, the only two seismic instruments on Mars were assessed for their feasibility: the Viking Seismometers and InSight's SEIS. After a trade-off procedure the InSight SEIS instrument was selected to enter the detailed design phase. The main reason for this being that measurements from the seismometer aboard the Viking 2 lander were heavily contaminated by wind, with only one potential seismic activity detected [67, p. 14]. This makes it impossible to verify the performance of the instrument, and prohibits a TRL9 classification. The SEIS instrument however is performing to expectations, and has detected hundreds of marsquakes down to a magnitude of $M_W = 1.3$ [68]. Requirements [DMD-PERF-SEIS-01] and [DMD-SARR-BROOT-05] are therefore considered to be met.

Similar to the heat flow probe, the SEIS instrument had to be adapted to better fit the mission profile and scientific objectives. Like HP3, SEIS was designed to be deployed on the ground, some distance removed from the lander. The deployment strategy of the Mars Deploy landers is much simpler, as the seismometer will be located inside the lander. This means that the wind and thermal protective assembly may be removed entirely.

Furthermore, the Mars Deploy and InSight mission differ in their scientific objectives. While Mars Deploy's mission objective is to benefit the search for heat and water in preparation of human exploration, InSight's scientific

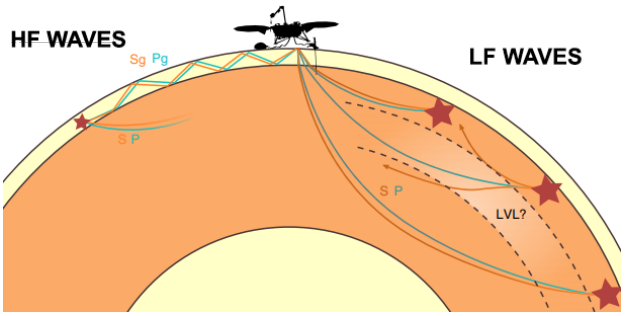

Figure 16.12: Schematic of wave propagation for the different event types [46]

	Mass in kg
VBB Assembly	3.2
SP Assembly	0.46
Levelling System	2
Thermal Blanket	0.84
EBOX	5.2
Cradle	1.7
Windshield	9.5
Tether assembly	6
Total	28.9

Table 16.19: Mass distribution for the SEIS instrument adapted from [45, p. 37]

objectives include "Determining the size, composition and physical state of the core." [45, p. 4]. Mars Deploy's area of interest therefore lies within the upper crust.

In the marsquakes detected by InSight, a distinction was made between low-frequency (LF) and high-frequency (HF) events. LF events were characterised by their sub 1 Hz frequencies, while HF events had a frequency exceeding 1 Hz [46, p. 206]. Table 16.12 shows a schematic of HF waves travelling on the left, and LF waves on the right. The Sg and Pg waves on the left are high-frequency waves which are trapped in the crust [46, p. 212], and would thus produce the most valuable scientific data for the Mars Deploy mission. InSight's SEIS instrument consists of two separate seismometers: the Very Broad Band (VBB) and the Short Period (SP) seismometers. VBB sensors operate in the 0.01 - 5 Hz region while SP sensors detect frequencies between 0.1 and 50 Hz [45, p. 27]. Since the 1+ Hz frequencies are most relevant to the scientific objectives of the Mars Deploy mission, only the SP sensors will be used on the impactors.

Removing the VBB sensors from the system has several other advantages. First of all, the SP sensors are rated for acceleration forces up to 13000 g [69, p. 17]. For the VBB sensors, no shock resistance data is available, although it is believed to be several orders of magnitude worse due to the large size and mass of VBB compared to SP. Following the 13,000 g limit from the SP sensors, requirement [DMD-SCI-04] is formulated which limits the payload's landing shock to 10,000 g, allowing for a sufficient safety margin. Furthermore, removing the VBB sensors removes the need for a precise levelling mechanism, as the SP sensors are designed to operate at inclinations up to 15°. This introduces [DMD-SCI-SEIS-02], which poses restrictions on the EDL procedure.

As mentioned earlier, the 9.5 kg windshield will be removed from the SEIS instrument. Furthermore, the cradle and tether assembly will also not be necessary since the instrument does not need to be lifted off the ground. Then, as discussed only the SP sensors will be kept, and the more heavy VBB sensors are removed. With the removal of the VBB sensors, the EBOX which houses SEIS's supporting electronics also becomes lighter. Since the exact mass distribution of the EBOX is unknown, a conservative weight savings of 1 kg will be assumed. A mass distribution for the SEIS instrument is shown in Table 16.19, where it can be seen that with the removal of the 2 kg levelling system, the total instrument mass becomes 5.5 kg.

Weather Station

Next to the TRL9 requirement, the driving requirements for the selection of the weather station sensors are [DMD-PERF-WS-01], [DMD-PERF-WS-02] and [DMD-PERF-WS-03], which specify the required resolution of the air temperature, pressure, and humidity sensors respectively. Specifications for currently active and previously flown Mars missions were collected in order to find sensors which met the performance requirements. For the air temperature and pressure sensors, the MEDA ATS [70, p. 4] (Perseverance) and REMS PS [71, p. 635] (Curiosity) sensors have been selected as they met their respective performance requirements. No TRL9 relative humidity sensor was found that met requirement [DMD-PERF-WS-03]. Therefore, data points for both the MEDA and REMS humidity sensors was extrapolated to estimate the mass, power draw and data production of a sensor that could meet the performance requirement. A safety factor of 25% was applied since only two data points were used.

It should finally be noted that InSight's seismometers relied on its Auxiliary Payload Sensor Suite (APSS) for active reduction of noise caused by atmospheric effects such as wind [45, p. 3]. While the Mars Deploy impactors are not outfitted with the APSS system, the weather station sensors will be used instead to achieve the same goal.

Air Composition Analyser

In order to analyse the composition of a mixture of gases, gas chromatograph - mass spectrometers (GCMS) are often used. GCMS's have been used on Mars, but have often been integrated into instruments to also determine soil composition, like for the SAM instrument on the Curiosity rover.[12] In order to obtain accurate numbers for

[12] https://mars.nasa.gov/msl/spacecraft/instruments/sam/, Accessed [17-06-2021]

mass, size and power for the GCMS instrument, the GCMS from the Pioneer Venus Large probe was selected instead. With a mass of 10 kg, this instrument meets performance requirement [DMD-PERF-GCMS-01], with a sensitivity of 1 part per million [72, p. 1].

System Performance and Characteristics

The table below presents an overview of the technical and performance specifications for the scientific instruments which will be carried on each impactor. More detail on the data characteristics of the instruments can be found in Section 16.7.

Instrument	Parameter	Value	Unit
HP3	Mass	1.7	*kg*
[33][64]	Nominal power	2.8	*W*
	Peak power	11.8	*W*
	Data production	20	*bps*
	Data upload	1.5	*Mb/sol*
SEIS SP	Mass	5.5	*kg*
[45]	Nominal power	5	*W*
	Peak power	8	*W*
	Data production	990	*bps*
	Data upload	88	*Mb/sol*
GCMS	Mass	10	*kg*
[72]	Nominal power[13]	0	*W*
	Peak power	14	*W*
	Data production	80	*pbs*
	Data upload	72	*kb/sol*

Table 16.20: Key specifications for the heat flow probe, seismometer, and air composition analyser

Sensor	Parameter	Value	Unit
MEDA ATS	Measurement range	150 - 300	*K*
[70, p. 4]	Relative accuracy	0.1	*K*
	Absolute accuracy	1	*K*
	Mass	56	*g*
	Power consumption	21	*mW*
REMS PS	Measurement range	0-1400	*Pa*
[71, p. 635]	Relative accuracy	0.2	*Pa*
	Absolute accuracy	3.5	*Pa*
	Mass	35	*g*
	Power consumption	15	*mW*
HS	Relative accuracy	0.1	*%*
[70][71]	Absolute accuracy	10	*%*
	Mass	120	*g*
	Power consumption	33	*mW*

Table 16.21: Key specifications for the air temperature, pressure, and humidity sensors

Recommendations

In this section some recommendation for the further stages of the design will be given.

Heat Flow Probe

The design decision has been made to deploy the heat flow probe using a gun-like cartridge. This raises some inherent concerns. The most critical area here would be the tiltmeter, which would need to survive the high impact loads on deployment. While the tiltmeter inside HP3's mole had to survive the impacts during the digging process, these are much smaller than being fired from a cartridge. Furthermore, [DMD-SCI-HF-01] could not yet be verified at this stage of the design. It is recommended to create a thermal model of the impactor on Mars with the heat flow probe deployed, to investigate the thermal contamination of the heat flow measurement caused by the impactor. In order to increase the accuracy of the heat flow measurement even further, increasing the accuracy of the thermometers on the tether should be considered as well. Finally, in any future stages of the design a more detailed error budget should be set up which takes into account errors stemming from different sources, like is done in [64, p. 25].

Seismometer

One aspect of the seismometer that should be investigated further is the coupling to the ground. During the EDL phase, the seismometer needs to be as decoupled from the external impactor structure as possible. This must be done to avoid transferring the full impact loads directly to the seismometer, and is in this case achieved by a large crumple zone. When the impactor has landed however, the coupling between the seismometer and the ground should be as strong as possible to allow the seismometer to sense the vibrations. It must therefore be tested whether the crumple zone after landing is stiff enough to allow the seismometer to meet its sensitivity requirements. If not, a system must be created with which the seismometer can be coupled to the ground after impact.

Similarly, the internal vibrations caused by the impactor, and by the effects of wind on the impactor must be further investigated. This would require setting up a precise model of the impactor, with its exact weight distribution. The vibrations caused by all internal components must then also be known. It could for instance be the case that at very low wind speeds the impactor starts resonating heavily, increasing the noise in the seismometer's measurements. This should be avoided.

Finally, further reduction in weight could be achieved by investigating the EBOX further. The EBOX houses the supporting electronics for the heat flow probe and the seismometer, and is a heavily shielded, insulated, heated

enclosure. While no detailed specifications on the EBOX are publicly available, it is believed that some weight could be shaved off since the EBOX will be stored inside the impactor, which will already be shielded and heated.

Air Composition Analyser
For the GCMS, the shock resistance could not be verified due to the very limited data available on the instrument. A proposed solution would be to choose a non-TRL9, miniaturised GCMS, as proposed in [73, p. 6]. This GCMS is said to be more rugged, and much lighter at only 3 kg.

16.6. Communication

TT&C of lander is responsible for the upload of collected scientific data to the orbiter, as well as the download of commands. Moreover, it shall have the ability to directly upload low speed data to DSN, such that it can be tracked, as per stakeholder's requirement [DMD-SARR-BROOT- 06]. First, requirements will be listed as well as their compliance state. Next, similar to orbiter's communication system design, design decisions will be described, and finally, subsystems characteristics will be listed. As the process of computing the data link budget itself has not changed, governing equations and verification and validation will not be presented.

Requirements

Table 16.22 presents the subsystem level requirements, derived from the system and stakeholder requirements. The designed system is compliant with all of the mentioned requirements.

Table 16.22: Requirements on the Telemetry, Tracking & Command

ID	*Requirement*	*Status*	*Origin*	*Compliance*
TT&C Requirements				
DMD-TTC-LNDR-1	Lander shall be able to receive emergency commands from DSN	Active	Stakeholder's requirement	Met
DMD-TTC-LNDR-2	Lander shall be able to receive emergency commands at any orientation & direction	Active	Purpose of TT&C	Met
DMD-TTC-LNDR-3	Lander shall be able to send its ping information directly to the Earth	Active	Stakeholder's requirement	Met
DMD-TTC-LNDR-4	Lander shall be able to send its ping information for up to 38% of the sole	Active	Design decision	Met
DMD-TTC-LNDR-5	Lander shall be able to offload all collected information to the orbiter	Active	Purpose of TT&C	Met
DMD-TTC-LNDR-6	Lander shall have UHF uplink speed of at least 100kbit/s	Updated	C&DH & contact time dictate bit rate	Met
DMD-TTC-LNDR-7	Lander shall have UHF uplink speed of at least 5100 seconds per sole	Active	Orbital	Met
DMD-TTC-LNDR-8	Lander's communication system must be compatible with existing missions	Active	Design decision	Met
DMD-TTC-LNDR-9	Lander's communication system must not use prohibited frequencies	Active	Stakeholder's requirement	Met

Design Process

Governing Equations
Similarly to Section 10.5, the same python code with the same relations was used for calculating data the link budget and power required. However, the selection procedure of the components was different.

System Architecture
As the same three redundant system requirements apply to the lander, it was decided to use an emergency receive only LGA DSN antenna. As these part was already computed, the same S band receiver would be used

[13] GCMS is only active 15 minutes per sol

here [14]. The antenna must be a LGA isotropic, so a 50 cm long wire was assumed for simplicity, with a mass of 100 grams.

Next, the scientific upload channel had to be established. It was computed that a direct DSN upload from a lander with up to 1 m dish will require almost a kilowatt of radiated power in order to transmit 100 kbit/s as per [DMD-TTC-LNDR-6], which is completely unfeasible. Therefore, the only option would be to use satellite as an orbital relay. As already described in the orbiter's communication system, a UHF band would be used at roughly 400 Mhz, with an isotropic antenna on the lander for simplicity of system and increased chance of impact survival. Phased antennas would be used on the orbiter, with a gain equivalent to a 0.4 m dish. For this, off the shelf components from Endurosat were picked, however as their nominal power are lower than required, as a first order estimation, mass and input power was linearly scaled. The UHF transceiver of 1 W radiated power was used [15], and scaled 12 times to archive the required radiated power of 12 W, resulting in the first order estimate of input power of 16.8 W. This is a good side estimate, as provided transceiver have relatively high efficiency of 70%. Once again, a wire type isotropic antenna of 100 grams was assumed. The operational time was taken from 5100 seconds availability of orbiter per repeat orbit, or three sols. However, as may be seen in Chapter 8 ground track plots, it is almost certain that the orbiter will pass very close to the same location at least twice. Therefore, requirement for contact time of 5100 seconds was increased from once in three sols, to once per sol, to allow for possibly higher connection times.

Finally, in order to fulfil [DMD-TTC-LNDR-3], DSN transmitting subsystem was designed. The aim of this system was to ping the lander's information directly to DSN, enabling extensive radio study of the planet's motion, thanks to a high number of distributed transmitters. The challenge was low available power and limited spacing for antennas. It was assumed that even low bit rates of 5 bit/s will be enough to pass on the required information. As using LGA would be completely unfeasible, a small dish of roughly 10 cm in diameter was selected in dish size versus input power trade-off. Part of contribution to this decision was availability of off the shelf components. In order to increase the chance of surviving the impact, a patch antenna was selected instead of parabolic dish, as these are flat and can be glued across the whole surface to the structure, and thus are less delicate than parabolic dishes with pointing mechanisms. Once again components were selected from Endurosat cubesat's catalog, a X band transmitter [16] and a patch antenna with gain of 16 dBi within X band [17] were picked. Similarly to the UHF band, these are not the perfectly suiting devices, but linear scaling was used to approximate characteristics: the equivalent of four transmitters and two antennas will be required. Although the antenna has a gain of 16 dBi, which is equivalent to 7.5 cm in diameter dish, it was limited to just 4 W of radiated power, which is why two had to be used. Finally, the total operational time was assumed from the worst case scenario in terms of power, which is antenna transmitting in a 'dumb' manner, whenever it may see Earth. That is 180° of half planet's visibility, minus twice 20° due to elevation above horizon limitation, resulting in 140/360 of the Sol operational time. However, if the exact position will be computed, this may be limited to just 18/360 of the Sol, as presented antennas have a half power beam angle of just 18°, and no pointing mechanism will be used.

Verification and Validation

As the code for computing the radiated power required is exactly the same as the ones used for orbiter, no additional verification or validation was needed. Verification and validation of the code is already described in Section 10.5.

System Performance and Characteristics

Table 16.23 presents the summary of technical characteristics for all three communication subsystems. It is important to mention, that DSN HGA antenna is not actually a parabolic antenna of 7.5 cm in diameter, but as mentioned above a combination of patch antennas, with a gain of 16 dBi, which is equivalent to that of 7.5 cm ideal dish.

Table 16.23: Summary of lander's communication systems.

	Type	Antenna	Size	Bitrate		P(Radiated)	P(Supply)	Mass
Units			[m]	Rx [bit/s]	Tx [bit/s]	[W]	[W]	[Kg]
System 1	DSN	HGA	0.15	10,000	5	8	15	1.2
System 2	UHF	HGA	-	100,000+	100,000	12	17	0.8
System 3	DSN	LGA	-	300	-	-	2.5	0.3

General communication layout, as well as detailed bit rate, frequencies and bands information from sections both these section as well as Section 10.5 is summarised in the communication diagram, Figure A.5.

[14] https://www.endurosat.com/cubesat-store/cubesat-communication-modules/s-band-receiver/, Accessed [18-06-2020]
[15] https://www.endurosat.com/cubesat-store/cubesat-communication-modules/uhf-transceiver-ii/, Accessed [18-06-2020]
[16] https://www.endurosat.com/cubesat-store/cubesat-communication-modules/x-band-transmitter/, Accessed [18-06-2020]
[17] https://www.endurosat.com/cubesat-store/cubesat-antennas/x-band-4x4-patch-array/, Accessed [18-06-2020]

Table 16.24 presents the link budgets for the three communication subsystems. System 1 budget is given only for transmit configuration (lander-Earth), as data rate is limited by the lander's radiated power. The same applied for System 2. Finally, System 3 is emergency receive only system, so only receive link budget is presented. This system is fully identical to System 3 of the orbiter. All three systems have positive SNR margin, meaning that they were properly implemented. One may notice, that even though both System 1 and System 3 operate over X band, space loss is slightly different. This is due to upload/download frequency difference, which, as described above, was taken from NASA's DSN specification sheet.

Table 16.24: Lander's communication system link budgets

Parameter		Units	System 1 TX	System 2 TX	System 3 RX
Radiated power	P	dB	9	10.8	43.0
TX antenna gain	G_r	dB	16.4	0	0
RX antenna gain	G_t	dB	69.5	4.5	57.5
Space Loss	L_s	dB	-282.5	-159.8	-270.5
Data Rate	1/R	dB	-7.0	-50	-24.8
Boltzmann constant	1/k	dB	228.6	228.6	228.6
System Noise (Temp)	T_s	dB	-27.9	-27.9	-27.9
Received SNR	Eb/No	dB	6.2	6.2	6
Required SNR	Eb/No	dB	5	5	5
Verification correction		dB	0	0	0
Implementation error		dB	0.5	0.5	0.5
SNR Margin		dB	0.7	0.7	0.5

Recommendations

As lander's systems were designed in more detail than orbiter, and real components were selected for each of the systems, the next step would be the detailed design, and manufacturing of the actual components. Additionally, it shall be investigated further to what extend communication redundancy is required. As per stakeholder requirement [DMD-SARR-BROOT-06], system shall have three redundant communication systems. Although technically this requirement is met, as lander may receive commands over three independent subsystems, it may only upload scientific information over one system (UHF System 2). Therefore, adding secondary UHF antenna, transceiver, or a complete system shall be considered.

16.7. Command and Data Handling

Requirements

Table 16.25: Requirements on the Command & Data Handling

ID	*Requirement*	*Status*	*Origin*	*Compliance*
C&DH Requirements				
DMD-CDH-L-01	The CDH shall be able to communicate with all operational subsystems.	Active	Nominal system function	Met
DMD-CDH-L-02	The CDH subsystem shall have a minimum throughput of 8 MIPS.	Active	Memory budget [6]	Met
DMD-CDH-L-03	The CDH subsystem shall be able to track time with an accuracy of at least <tbd> ms/day.	Active	EDL & G&N	TBD
DMD-CDH-L-04	The CDH subsystem shall have a maximum mass of 0.25 kg.	New	Mass budget	Met
DMD-CDH-L-05	The CDH subsystem shall have a maximum power consumption of 12 W.	New	Power budget	Met
DMD-CDH-L-06	The CDH subsystem shall have 2.8 MB of memory for the operating system and interfaces.	Active	Memory budget [6]	Met

Continued on next page

Table 16.25 – continued from previous page

ID	*Requirement*	*Status*	*Origin*	*Compliance*
DMD-CDH-L-07	The CDH subsystem shall be able to withstand radiation levels of at least 30 kRad ±50%.	New	Due to risk [R-CDH-L-04]	Met
DMD-CDH-L-08	The CDH subsystem shall be able to store at least 60 sols of scientific data.	New	Due to risk [R-CDH-L-01]	Met
DMD-CDH-L-09	The CDH subsystem shall have at least one redundant processor.	New	Due to risk [R-CDH-L-03]	Met
DMD-CDH-L-10	The CDH subsystem shall have a safe-boot option in case of system errors.	New	Due to risk [R-CDH-L-02]	N.V
DMD-CDH-L-11	The CDH subsystem shall be able to process at a bitrate of at least 96.3 kbit/s	New	Replaces [DMD-LANDER-02]	Met
DMD-CDH-L-12	The CDH subsystem shall have at least 17.4 GByte of mass storage.	New	Memory budget	Met

Design Process

This subsection will provide all relevant equations and calculations to characterize the C&DH subsystem of the orbiter. Furthermore a model on the mass storage will be displayed and described.

Data rates & Data Handling

Estimations and calculations on expected data rates of the lander are made from which the mass storage size and throughput can be computed. First the data rates from the sensors will be listed. The altimeter, pressure sensor and IMU are necessary for the entry descent and landing of the probe. Furthermore sun sensors are required for the pointing mechanism of the solar panels to optimise power generation. The current, voltage and temperature sensors are necessary to keep track of the status of the probe. All sensors will have a resolution of 8 bits, an 8 bit integer will be able to provide a resolution of 128 decimals unsigned or 127 decimals signed .

The scientific payload as described in Section 16.5 create data to be handled by the C&DH subsystem. Each payload will be evaluated on their respective data generation. According to the article [45] describing the characteristics of the seismometer from NASA's InSight mission. After using STEIM compression [45, p. 38] the expected output of the SP sensors is 9 to 10 bits per sample, which is a reduction of more than 50% with the original bit samples being 24 bit. STEIM compression is regularly used in seismic measurement equipment [74]. This method relies on computing the difference between two consecutive samples. This can be expressed as the following[45].

$$d(n)-d(n-1)=\Delta t\frac{d(n)-d(n-1)}{\Delta t}\approx\frac{\Delta t}{LSB}\gamma \tag{16.24}$$

Where d(n) is the velocity flat output signal in count, γ is the acceleration, Δt the sampling interval in second and LSB the velocity flat output LSB in m/s. This has the benefit that the bytes needed to express a delta measurement is generally less than the original measurement itself. This compression technique is lossless and therefore will not have any negative effects on the accuracy of the measurements.

The seismometer is able to run at 10 Hz nominally with 100 Hz upon request. According to the statistical data the seismometer is running at 100 Hz, 25% of the time with the remainder at 10 Hz. This means that the weighted average of the sampling frequency is 33 Hz, which will be used for further calculations.

Table 16.26: Payload data rates

Instrument	Data rate [bit/s]
Seismometer	990 [45]
Heat flow probe	20 [64]
Air composition analyser	80 [75]
Temperature sensor	24 [70]
Pressure sensor	216 [18]
Humidity sensor	208 [70]

Storage & Transmission
Section 8.2 states that the contact time of the probes with the orbiter is at least once every 3 sols for a duration of approximately 5100 seconds. The following assumptions were made while sizing the subsystem:

- The payload will be generating data 100% of the time at the bit rates from Table 16.26.
- The sensors will be generating data 100% of the time at the bit rates from Table 15.1.
- The EDL sensors are only utilised during descent.
- All the data generated before the point of contact is available for transmission.

Given the data rates from the sensors and payloads and the contact times for the probes from Section 8.2 an equation for the storage of the probe can be made, similar to Equation 10.10.

$$S(t) = (DR_{pay} + DR_{sens})t - Tx_{probe}\langle t - t_{connect}\rangle \tag{16.25}$$

From this equation the storage stability can be derived which results in Equation 16.26.

$$\sum (DR_{pay} + DR_{sens})t = \sum Tx_{probe} t_{connect} \tag{16.26}$$

With the aforementioned data Equation 16.26 results in the following for the required transmission rate of the probe storage to be stable.

$$Tx_{probe} = \frac{1843.6 * 88775 * 3}{5100} = 96.3\text{kbit/s} \tag{16.27}$$

This transmission rate will provide a lower limit to the TT&C subsystem. Furthermore for nominal storage operations the required storage must be able to store at least three sols.

$$S_{req} = 1843.6 * 3 * 88775 = 491\text{Mbit} = 61.4\text{Mbyte} \tag{16.28}$$

Requirement [DMD-CDH-L-06] states that there needs to be at least 2.8 Mbyte free for the operating system and interface firmware [6]. Which results in the minimum required storage to be 64.2 Mbyte. Due to requirement [DMD-CDH-A08] the storage must be sufficient enough to store at least 60 sols worth of data. This results in a final storage capacity of 1.23 Gbyte of storage per probe. During the descent, the EDL sensors are generating data, from Table 15.1 the combined bitrate is 403.4 kbit/s. The landing duration is approximated to be 136 s, however the storage will be sized for a total of 240 s. This amounts to 9.0765 MByte that is needed to store this, totalling the required storage to 1.239 GByte. Finally Applying a safety factor of 50% for additional error analysis and flags and additional data, this will result in a final required storage capacity of 1.859 GByte.

As there will be periods where the payload is going to be offline, this model calculates the worst case scenario of all equipment being online for the entire duration of the mission. It is expected that the storage capacity will not be exceeded.

Storage model
Similar to Section 10.6, a numerical model to calculate the storage pattern of the probes has been made based on the step function seen in Equation 16.25. For modelling purposes and simplicity, forward Euler is chosen as a numerical propagator.

In Figure 16.13 the storage model is displayed. The x-axis shows the amount of time passed in sols and the y-axis the amount of storage in Mbit. The bottom graph shows the transmission rates at times of transmission to the orbiter in Mbit/s.

Verification & Validation

Code Verification
The model in Figure 16.13 is verified according to the procedure as prescribed in Chapter 5. The model does not have syntax errors and does abide by the correct programming logic, namely the forward Euler propagator is applied correctly as confirmed by the back-up Command & Data Handling engineer. Furthermore the boundaries of the step function have been evaluated and confirmed to be correct.

[18] http://cab.inta-csic.es/rems/en/intrument-description/pressure-sensor-ps/, Accessed [15-7-2021]

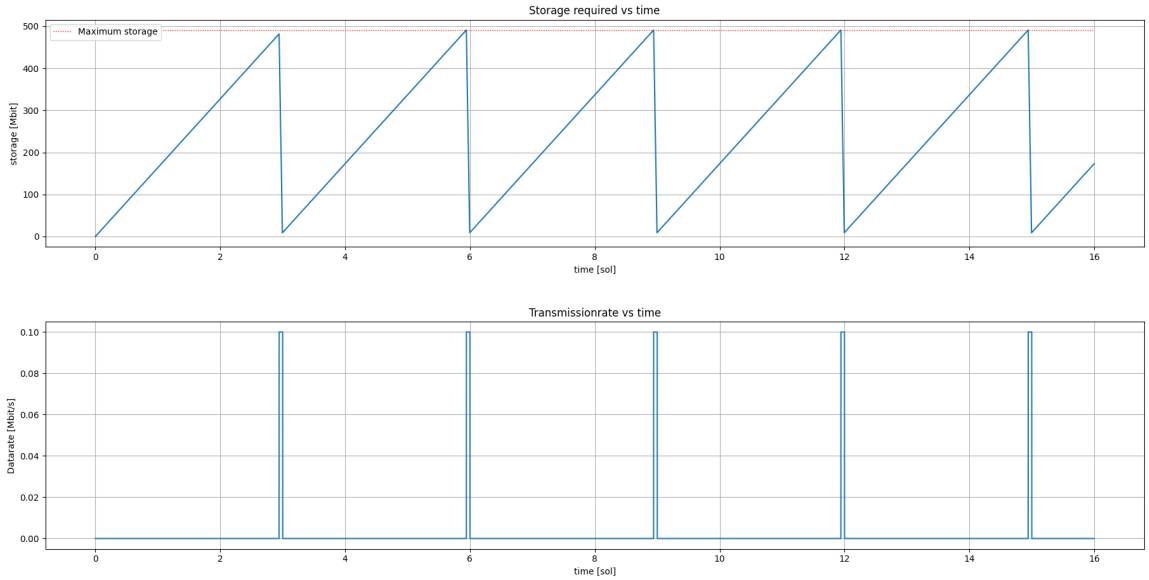

Figure 16.13: Storage model of the Impactor mass storage

Calculation Verification

For the purposes of calculation verification the inputs and data rates are defined as follows. The combined data rate from Table 15.1 and Table 16.26 is 1843.6 bit/s, the uplink from a probe to the orbiter is 100 kbit/s as per Section 16.6. The uplink to orbiter takes place every three sols with a total upload time of 5100 seconds. The model consists of one major functions for which the calculation must be verified:

1. *storage_probe* : Computes the storage with a forward Euler propagator based on Equation 16.25.

The following unit and system tests have been performed to verify the storage model.

Test	Expected [Mbit]	Outcome [Mbit]	Deviation
Maximum storage after 3 sols	481.594	481.593	0.0002%
Maximum storage after 9 sols	490.997	490.997	0%
Residual memory	8.718	8.718	0%

Table 16.27: Unit and System test of the probe storage model

The reason why the storage after 9 sols is more than after the initial upload to the orbiter is because of the assumption that all data before contact with the orbiter is available for sending, this means that after every cycle there is a residual amount of memory left that will need to be sent in the next cycle. The first test shows a slight deviation of 0.0002% which is a negligible deviation and can be due to rounding errors of the computer. Finally in Figure 16.13 can be seen that the storage of the probe shows stable behaviour at the calculated limit from Equation 16.27 which is indicative of stable behaviour as predicted at this datarate. The verification procedure from Chapter 5 has been followed and the model has therefore been verified.

Validation

As the model is purely intended as a calculation tool in order to estimate the amount of required storage, validation can not be applied properly. Therefore verification will provide sufficient evidence of the correctness of the calculations. In order to validate the read and write sequence a test could be performed with a setup that is similar to the probe. Data could be written and read at the same intervals as would be done during the mission.

System characteristics & Performance

The C&DH unit MPSoC CFC-400 from Innoflight [76] is used as a reference for the design as it is suitable for this design. It has a main board with a LEON3FT processor and an Field Programmable Gate Array equipped with an ARM Cortex-A53 that is capable of handling the altimeter throughput for the descent and can act as a back up for the main board during nominal operations. It has sufficient interfacing for the sensors and equipment mentioned in Chapter 16, such as I2C and SPI interfaces for the PDU from Section 16.8. Furthermore FGPA's allow for custom programmable features operating at relatively high frequencies.

Table 16.28: System characteristics C&DH lander

Characteristic	Value	Unit
Minimum Storage	1.859	GByte
Minimum required transmission rate	96.3	kbit/s
Mass	1.7	kg
Nominal Power	12	W
Radiation tolerance	30,000	rad

As with the orbiter in Section 10.6 it is opted to use an extra redundant external storage device in case of failure, or overload of the main mass storage of the OBC. As a reference, the TRRUST-Stor® VPX RT6U from Mercury Systems is used [18]. This will allow for a fully redundant data storage design. Furthermore the C&DH system shall be able to encode and decode data for transmission using a differential encoding algorithm. This ensures that so called bit-flips do no affect the quality of the relayed signal [19]. The on board software is also equipped with a Kalman filter to reduce incoming noise from sensor data to get a more reliant reading. These software blocks and other system software architecture are displayed in Chapter 7.

Because of the lack of atmosphere and weak magnetic field of Mars there is relatively more radiation on the martian surface than there is on Earth. This radiation poses a problem as it can damage silicon components. According to the MSL-RAD experiment from the Curiosity rover [77]. The surface radiation equivalent dose rate was found to be approximately 0.64 ± 0.12 mSv/day. For contrast, the average dose on earth, depending on the location of measurement, is 0.6 to 7 mSv per year[19]. Therefore components will need to be radiation hardened to ensure reliability.

In Figure 16.14 the data handling characteristics of the C&DH is displayed. It shows the interaction between various components and shows the data rates of various sensors and hardware. Do note that the SP sensors of the seismometers are operating at 24 bits at approximately 33 Hz. As mentioned before this data will be compressed once it arrives at the central processing unit to 9 to 10 bits per sample.

Recommendations

Impact Damage

A proposed mitigation strategy for risk [R-CDH-L-05] is to test and further investigate resin coatings. Although the components can withstand a relatively high g-force of sometimes up to several hundreds of g's, the impact forces of the Impactor are above the rating of the on board computer components. Similar to Deep Space 2 where the electronic components were protected by a resin also referred to as "glob-top" [78], to protect them from the impacting forces. Therefore a strong recommendation is to look into electronic resin coatings and the effectiveness of them as well as looking for relevant quality and acceptance tests.

Software Architecture

As per risk [R-CDH-L-02] there is a chance that due to some software or system error the on board software will return errors making the system unusable, similar to the boot problems of NASA's Curiosity Rover which appeared to be stuck in a boot-loop sequence[20], rendering it unusable. A strong recommendation would be to make a separate software that the Impactor is able to boot to in case of said errors to allow for remote troubleshooting, mitigating the risk of complete mission failure. The software would have no other function than to allow for remote access by ground stations on Earth via the orbiter and would only have to manage EPS and TT&C to limit sources of error. This recommendation will need to be fulfilled to meet requirement [DMD-CDH-L-10].

Hibernation Mode

In order to meet system requirement [DMD-DESCENT-15], the system will need to go into hibernation mode when a dust storm is detected. It is recommended that this piece of software is developed as dust storms negatively influence the Impactor. The detection can be done by measuring the current of the solar panels and applying a threshold on current throughput, when this threshold is met, the system enters in hibernation mode which will turn off the scientific instruments. This system has not been implemented at this stage of the design and is therefore a strong recommendation.

16.8. Electrical Power

The Electrical Power System(EPS) provides power to the subsystems of the lander for the duration of the mission. It does this via a Power Distribution System(PDS). The energy is generated by solar arrays and energy is stored in a battery.

[19] https://www.world-nuclear.org/information-library/safety-and-security/radiation-and-health/naturally-occurring-radioactive-materials-norm.aspx,[accessed 29-06-2021]

[20] https://mars.nasa.gov/news/8416/curiosity-resumes-operations-after-switching-computers/, Accessed [17-05-2021]

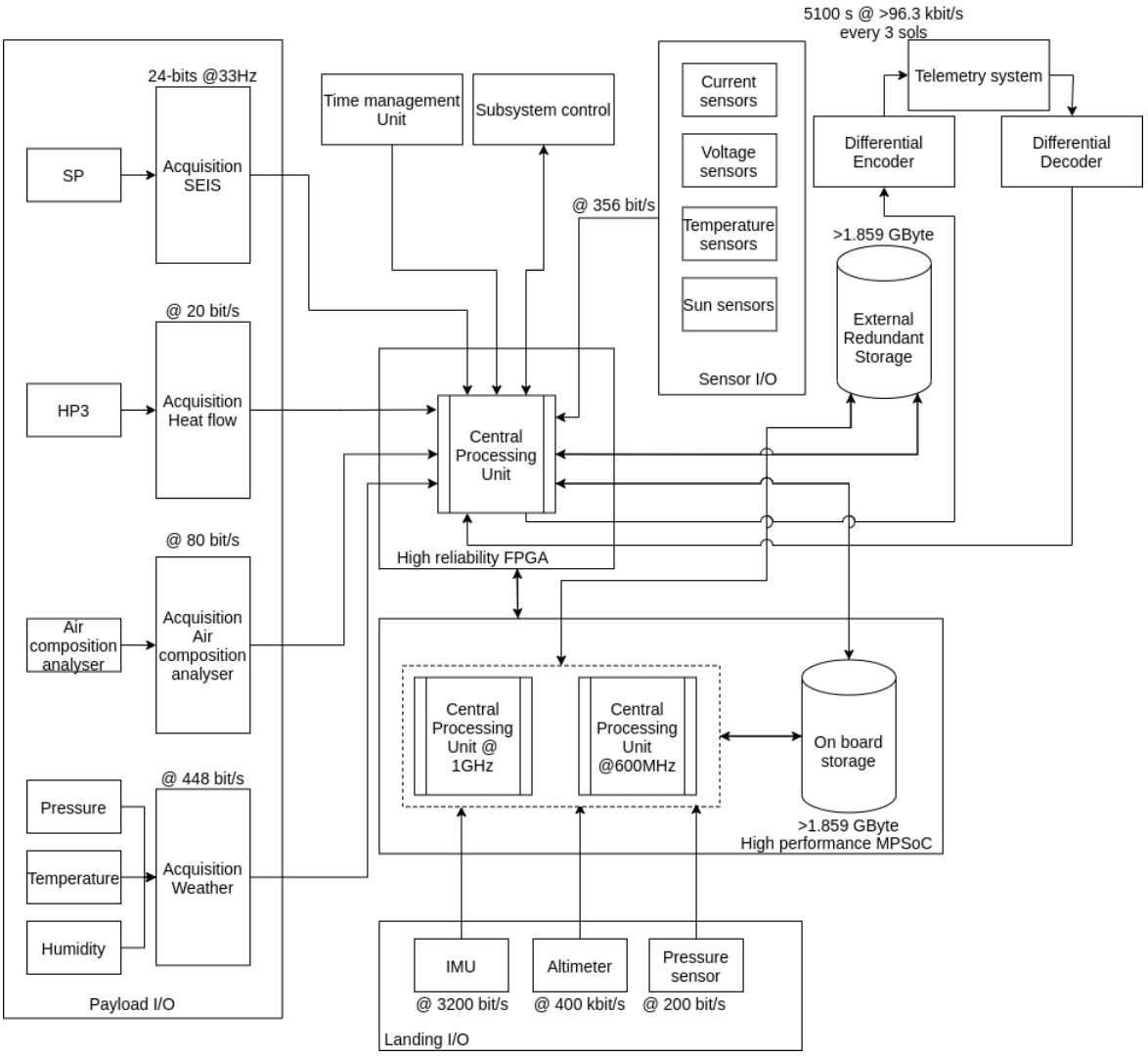

Figure 16.14: Data handling block diagram of the Impactor

Requirements and Compliance

Table 16.29: Requirements on Lander EPS

ID	*Requirement*	*Status*	*Origin*	*Compliance*
General requirements				
DMD-EPS-L-01	The EPS shall account for the dust settlement by using the dust-factor of 0.28%/sol.	New ID	Nominal operation	Met
DMD-EPS-L-02	The EPS can control the power distribution to subsystems.	New	Nominal operations	Met
DMD-EPS-L-03	The EPS shall be able to store 1.1892 kWh of energy.	New	Power Budget	Met
DMD-EPS-L-04	The EPS shall be able to provide 0.617 kWh of energy during pre-nominal operation.	New	Power Budget	Met
DMD-EPS-L-05	The EPS shall be able to provide additional 0.5 kWh of energy in case of emergency.	New	Operational redundancy	Met
DMD-EPS-L-06	The battery shall be able to cycle at least 1067 times.	New	DMD-PERF-BROOT-10	Met

Continued on next page

Table 16.29 – continued from previous page

ID	*Requirement*	*Status*	*Origin*	*Compliance*
DMD-EPS-L-07	The EPS shall be able to point the solar array to the sun path.	New	Nominal operation	Met
DMD-EPS-L-08	The lander shall land at a maximum latitude of +-35 degrees.	New	Nominal operation	Met

Design Process

There is great overlap between the EPS of the orbiter and the EPS of the lander. As the lander is actually landing on the surface of mars, extra environmental considerations have to be taken into account. Furthermore, the hardware specifications will remain the same for both EPS systems, further information on this can be found in Table 10.21.

Environment

This subsection will clarify the surroundings that have been taken into account when designing the EPS for the Lander. The martian atmosphere is known for its dust(storms) thus this is covered as well. And secondly considerations regarding the position on Mars and the resulting incoming light irradiance are covered.

The settlement of atmospheric dust on to the surface of solar arrays is possibly a power system lifetime limiting factor. Martian Dust is expected to adhere to the surface of solar arrays due to Van Der Waals forces [79]. This adhesion has to be broken, and the particles have to be moved off the array. Multiple methods such as brushes, compressed air or vibrations can be considered. Electrostatic dust removal has been chosen, as it has no moving parts, and NASA has proven the effectiveness of it [79]. The effectiveness of the system is decent were it nearly completely removes the dust [79]. For EPS sizing purposes, the dust degradation factor(dust-factor) is assumed to be a loss of 0.28% efficiency per sol [79] [80]. The solar arrays are cleaned whenever the solar arrays lose 20% of its efficiency due to dust, resulting is 16 cleanings in the lifetime. Finally it is assumed not all particles are cleared thus after cleaning efficiency is 95%.

The system requires to charge the surface of the array to 700V [79]. Preliminary system characteristics will be estimated using the following reasoning. The duration that the surface has to be charged is equal to the time it takes for the dust particle to fall off. Over estimating this parameter will make for a redundant system. The expected fall distance is 0.5-1.0m thus the charge duration will be long enough to fall 2.0m. Now assuming peak power output, the amount of energy necessary to clear the array's is 4081J. The system should be purposely build. As mentioned before, NASA has build a space flown test set up, called DART, that also includes this system with 4 other systems [81]. This system weighed 750 grams in total, including the 4 other systems [81]. A basic conductor that can convert up to 700V, is calculated to weigh around 138mg, which is negligible. No further development of the system seems appropriate in this stage of the design. The assumption is made the system weighs 150 grams, which has mostly deducted from DART its weight.

As mentioned and explained in Table 10.21, the solar irradiance at mars is 586.2W. Due to seasons and latitude location, the winters on mars can be short of light. The lower the absolute latitude of the landing site, the more beneficial it is for the weight of the EPS as the amount of light per sol increases. With a maximal latitude of +-35°, all the required landing sites are covered. This is were the requirement DMD-EPS-L-08 originates from. Adding the 25.2°.[21] inclination angle of Mars, the maximum inclination angle of the surface of Mars with the sun is 60.2°. At a latitude of 35°, it can be simply calculated that the sun is only visible for 40% of the sol. During the sol the relative inclination from the Sun with the surface of Mars changes as well as Mars is turning around her axis. At the start and end of the daytime the intensity is lowest, and at the mid of the day the highest. The average fraction of intensity that is received on the shortest day due to this event alone, is 0.637.

Table 16.30: Sun intensity factors

Factor	description	Value
Location	Inclination between sun and martial surface at 35° latitude	0.5
Sun Path	The average fraction of intensity that is received in daytime due to sun path	0.637
Dust	Decreased effectiveness due to dust(after mitigation)	0.8-0.95

The Dust-factor has already been mitigated. The Location-factor can be mitigated by tilting the solar arrays towards the Sun to counter for the latitude and Mars-pitch when deploying them. This would require to be able to

[21] https://nssdc.gsfc.nasa.gov/planetary/factsheet/marsfact.html, Accessed [07-06-2021]

tilt the solar array in two axis, as the landing orientation is not pre-defined. This would thus also set a requirement on knowing the orientation of the lander towards the Sun.

Hardware

The hardware considered for the EPS of the Lander is the same as the hardware considered for the EPS of the orbiter. The hardware characteristics that are used for the design can thus be found in Table 10.21. The effect of the impact deceleration on the solar array is covered in this section.

During landing impact the deceleration can reach up to 10000 g. The EPS should thus be designed to maintain structural integrity and full functionality. In a deployed state the solar array could snap off fairly easily. Therefore during landing the arrays should be folded in safely and deploy after landing. If the arrays would lay on top of each other, on top of the lander, they would only have to be designed for equally distributed stress. This stress is equal to it's own weight/area fraction times the deceleration. Using the before mentioned properties of the solar arrays, the stress would be 437 kpa. This stress level is in the same order of magnitude as worst case vibration analysis of comparable solar array, which endures a maximum stress of 375 kPa [82]. Therefore it is assumed the solar arrays can be designed for the required landing loads.

Power Budget

The power budget given in Table 15.2 provides the necessary power consumption of all the systems in the lander. In the table a differentiation is made between nominal operations and pre-nominal operations. The pre-nominal operations, depicted in red, result in the necessary amount of energy the battery should be able to provide in the time between launch and operational solar arrays on mars. In black the nominal operation budgets have been depicted.

Verification & Validation

Code Verification

The calculation tool has been verified according to the method described in Chapter 5. The tool has been checked on correct programming logic and does not give any syntax errors.

Calculation Verification

In order to ensure the correctness of the code, input is given to the tool which results in an output. The same calculation will be done by hand and the resulting output should match the output of the tool.

Table 16.31: Calculation verification results

Equation	Input	Output tool	Output hand calculation	Error[-]
Equation 16.29	Table 15.2	1.18922 kWh	1.18916 kWh	0.005%
Equation 16.30	Table 15.2	220.51 W	220.51 W	0%

The error is marginal and ignorable, the error is most likely due to rounding errors.

Validation

The program that is written for this subsystem is purely intended as a calculation tool. No validation is applicable. The verified tool can be trusted on correctness of the calculations.

Results

Method

Finally, the EPS sizing has been performed via the same method as the EPS of the Orbiter, depicted in Figure 10.8. A calculating python program has been build to produce system characteristics out of a required power budget. The environment, hardware characteristics and requirements stated in this section and Section 10.7 form the parameters that make up the results.

Calculations

The sizing of the system can be done based on two main parameters; the required energy that has to be stored and the required power the solar array should generate. The equations have been worked out for the parameters given in Table 15.2. During calculations the safety factor (SF) is 1.4 as required by [DMD-SARR-BROOT-04].

The required amount of stored energy is calculated for a worst case scenario, for the Lander this is when the system has to perform peak power during night time. which can be calculated as followed:

$$E_{req} = (E_{nominal} \cdot 0.6 + E_{peak}) \cdot SF = 1.1892 \text{kWh} \tag{16.29}$$

The 0.6 factor originates out of the worst case scenario where there is only 40% daytime per sol.

The required power generation by the solar array can be calculated as follows:

$$P_{req} = (P_{total} + \frac{E_{req}}{sol * 3600 * 0.4}) \cdot SF/\eta_{PDS} = 220.5W \quad (16.30)$$

The 0.4 factor originates out of the worst case scenario where there is only 40% daytime per sol.

The parameter P_{total} is the nominal power as given in Table 15.2.

The final EPS characteristics are then determined by using the hardware characteristics. For example the battery mass is the required energy divided by the specific energy density of the battery.

System Characteristics
By using the method that is depicted in above, the characteristics that are given in Table 10.21 and Table 16.29 and the budget that is given in Table 15.2, the resulting system characteristics are as given in the following Table 16.32. Also the electrical block diagram for the orbiter is given below in Figure 16.15.

Table 16.32: System characteristics of the EPS.

Hardware	Mass[kg]	Power[W]	Cost[M€]	Size	Performance
Battery	16.0		0.0015	8.5l	1.1892 kWh
Solar array	10.3		1.92	3.0m^2	220.5 W
PDS	0.15	1.4	0.05	90x90x20mm	
Dust system	0.15		0.025	0.162l	
Actuator	0.65		0.025	0.35l	
total	27.25	1.4	2.0215	-	-

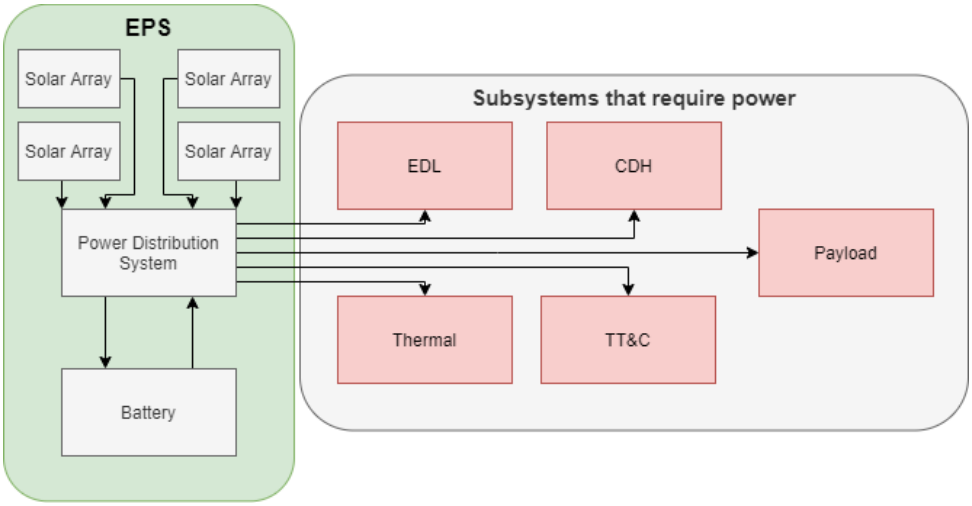

Figure 16.15: The Electrical block diagram for the lander.

Recommendations
The EPS subsystem accuracy could be increased by further developing the following points. The impact load could of course be detrimental to the EPS. The load on the solar array has been shortly covered, and other subsystems would have to be analysed on impact as well. Furthermore the dust clearing system is a proven system to work but would require further development to provide better budget estimates. Developing an efficient dust clearing system could also benefit future mars missions. Furthermore, specific deployment actuation and a deployment strategy has not been covered well, and should be developed.

16.9. Thermal Control
The thermal control system of the lander will keep the impactor and its subsystems in the required temperature range. Therefore, it shall either add or reject heat to comply with this. The design steps taken are similar to the orbiter thermal control subsystem, as explained in Section 10.8. The thermal subsystem requirements are given in Table 16.33.

Requirements

Table 16.33: Requirements on the thermal control subsystem

ID	*Requirement*	*Status*	*Origin*	*Compliance*
DMD-THERM-L-01	The thermal control subsystem shall keep electronic power system within the operational temperature range of 273.15-313.15 K	Replaced	EPS	N/A
DMD-THERM-L-01-A	The thermal control subsystem shall keep the electronic power system within the operational temperature range of 273.15-318.15 K.	New	Replaces [DMD-THERM-L-01]	Met
DMD-THERM-L-02	The thermal control subsystem shall keep the payload within the operational temperature range of <tbd> K.	Scrapped	Payload	N/A
DMD-THERM-L-03	The thermal control subsystem shall be able to generate heat to increase the internal temperature of the lander to nominally 283.15-293.15 K.	Replaced	Critical temperature range EPS	N/A
DMD-THERM-L-03-A	The thermal control subsystem shall be able to generate heat to increase the internal temperature of the lander to above nominally 273.15 K.	New	Replaces [DMD-THERM-L-03]	Met
DMD-THERM-L-04	The thermal control subsystem shall be able to radiate heat to decrease the internal temperature of the lander to nominally 293.15-303.15 K.	Replaced	Critical temperature range EPS	N/A
DMD-THERM-L-04-A	The thermal control subsystem shall be able to radiate heat to decrease the internal temperature of the lander to below nominally 318.15 K.	New	Replaces [DMD-THERM-L-04]	Met
DMD-THERM-L-05	The thermal control subsystem shall have a maximum power consumption of <tbd> W.	Replaced	Power budget	N/A
DMD-THERM-L-05-A	The thermal control subsystem shall have a nominal power consumption of 15.5 W.	New	Replaces [DMD-THERM-L-05]	Met
DMD-THERM-L-06	The thermal control subsystem shall have a mass of 23.5 kg.	Active	Mass budget	Met
DMD-THERM-L-07	The thermal control subsystem shall be designed at end-of-life for all thermal requirements.	Replaced	Stakeholder requirement [DMD-PERF]	N/A
DMD-THERM-L-07-A	The thermal control subsystem shall be designed to allow for degradation.	New	Replaces [DMD-THERM-L-07]	Met
DMD-THERM-L-08	The thermal control subsystem shall be able to store 0.22 MJ of heat.	New	Cooling requirements	Met
DMD-THERM-L-09	The thermal control subsystem shall have a peak power consumption of 31 W.	New	Power budget	Met

Design Process

The thermal control subsystem consists of active and passive control. The main design goal is to limit the active control, thus limiting the power usage from the EPS.[22] In consultation with the scientific engineer, the payloads either have an autonomous thermal control system, or have a wide range of allowable temperatures. Therefore, requirement [DMD-THERM-L-02] was scrapped.

Governing equations

The governing equation is repeated in Equation 16.32. The only additional term is $Q_{conduction}$. This is because the lander makes contact with the Martian soil, resulting in conduction between the two systems.

$$Q_{absorbed} + \sum P_{dissipated} + Q_{conduction} + Q_{heat} = Q_{emitted} \tag{16.31}$$

The conduction equation is given by Equation 16.32. It includes the conductivity k of the insulating material from the lander. Next, it is multiplied by the contact area A between these two systems and by the difference in temperature between them. Lastly, it is divided by the thickness of the insulating material. The soil temperature at the Martian equator ranges between a minimum of 228.15 K and a maximum at 298.15 K [83]. Notice that the temperature of the environment cannot be ignored for $Q_{emitted}$, which was the case for the orbiter. The Martian atmosphere has a minimum temperature equal to 177.15 K, whereas the maximum is 270.15 K.[23]

$$Q_{conduction} = \frac{kA(T_2 - T_1)}{t} \tag{16.32}$$

Critical scenarios

The lander is also designed towards the critical scenarios according to risks [R-THERM-L-02], [R-THERM-L-03] and [R-THERM-L-04]. The impactor experiences either direct sunlight, Martian infrared radiation and soil conduction during daytime, or only Martian infrared radiation and soil conduction during nighttime. Notice that the albedo effect is never included as the reflected sunlight will be minimal at the Martian surface.

Passive and active control

A slightly different Python program was written compared to the orbiter design, but no major changes were made. The core functions are exactly the same. It uses the following inputs: radius, height & depth of the impactor, the nominal power and the thickness & conductivity of the structure. The only noticeable difference is the way that the impactor is modeled. It consists of one paint/coating and is insulated at the bottom and sides. The program calculates the optimal thickness for both these insulations. MLI is deemed inefficient following risk [R-THERM-L-01], and silica aerogel was instead used [84].

The program returned the necessary heating and cooling required, the weight of the paints/coatings, as well as the optimal insulation thicknesses and α and ε values for the outside coating. A silver vapor deposited coating was the best fit, where $\alpha = 0.04$ and $\varepsilon = 0.02$ [22]. Furthermore, both silica aerogel insulations have a thickness of 15 cm. According to risk [R-THERM-L-05], radiators would use too much area and weight too much. Therefore, a heat sink was chosen, as was used for the orbiter. This resulted in requirement [DMD-THERM-L-08]. To conclude, requirements [DMD-THERM-L-01-A], [DMD-THERM-L-03-A] and [DMD-THERM-L-04-A] are fulfilled.

Verification and Validation

The only additional term in the governing equation, compared to the orbiter, is the conduction. It was checked by a simple hand calculation, with the same input parameters, that this formula was implemented correctly in the code. The inputs were as follows: a conductivity of 1.5, area of 5 m^2, temperature difference equal to 6 K, and thickness of 1 mm. This returned both for the hand calculation, and Python program, a conductive heat flow of 45000 W. Apart from this, the verification procedure is the same as for the orbiter, which was elaborated upon in Section 10.8. On the other hand, for validation, no data was directly found that is representative. The reason for this could be due to the uniqueness of the mission, as the lander is highly influenced by conduction with the Martian soil for thermal control.

System Performance and Characteristics

A safety factor of 1.5 is included in the design for the mass. The program is based on the critical scenarios, thus calculating peak power. Therefore, the nominal power is taken as 0.5 of the peak power, whereas the peak power is determined by the longest Martian night. This fulfils requirement [DMD-THERM-L-07-A] and [DMD-THERM-L-09]. Lastly, Table 16.34 lists the performance characteristics of the thermal control subsystem, which also fulfils requirements [DMD-THERM-L-05-A] and [DMD-THERM-L-06].

[22] https://www.nasa.gov/smallsat-institute/sst-soa-2020/thermal-control, Accessed [19-06-2021]
[23] https://mars.nasa.gov/mer/mission/rover/temperature/, Accessed [21-06-2021]

Table 16.34: Summary of thermal control subsystem performance

Component	Description	Mass (kg)	Nominal power (W)	Peak power (W)
Heaters	Minco	0.02	15.3	30.6
Heat sink	PCM	1.87		
Paint/Coating	Silver vapor deposited	Negligible (order $10^{-}6$)		
Insulation	Silica aerogel	21.5		
Heat sensors	Minco	Unknown	Unknown	
Total power			15.3	30.6
Total mass		23.4		

Recommendations

Recommendations include further investigating the heat sink, as it could have some limitations and could undesirably release heat to other subsystems. Furthermore, the aerogel should be able to withstand the high impact loads, which is not yet guaranteed. If an insulation could be found which is able to support more loads than aerogel, this could dampen the impact and remove some structural mass as well. Other possibilities include looking into a hibernation mode.

17. Sustainability

The evaluation of the lander sustainability will follow the same structure as that of the orbiter, going over each of the six sustainability criteria to identify the relevant considerations for each subsystem. For the subsystems that are present in both orbiter and lander, most concerns that were previously mentioned in Chapter 11 are also relevant for the lander subsystems. Especially the issues related to the use of rare Earth elements and carbon fiber are deemed important, but will not be repeated here.

17.1. SC-1: Fair Wages and Taxes

In the lander support structure and parachute, use is made of Nomex and Kevlar materials. These aramid fibers are both patented and produced by the American chemical company DuPont.[1] While alternative aramid fibers with comparable performance are produced by other companies, the broad use of Nomex and Kevlar means that DuPont has a de facto monopoly in the high-performance aramid fiber industry. Because DuPont has less competition in this field, the company has less incentive to keep prices low or to be the most appealing employer in the industry. Anti-trust cases in the past have shown that concerns regarding DuPont's dominance are shared by European and American government.[2]

17.2. SC-2: Reuse and Recycle

The impactor design does not perform well on the reuse criterion. Firstly, the EDL sequence makes use of many single-use components, such as the entry capsule and parachute. These parts will also be jettisoned without guidance after their use, thus retrieving their location could be difficult. The PICA heatshield is ablative, meaning it would not be fit to reuse, even if it was retrieved.[3] The backshell is made with reusable AETB tiles, which could be recovered from a previous mission before being used for Mars Deploy.[4]

The impactor itself is inherently difficult to reuse as well. As the landing impact will be critical for most subsystems, the connections to the support structure will require precise design and assembly. The detailed and robust connections will make later disassembly difficult, as well as the fact that the impactor should be sealed towards the environment, preventing dust from entering the probe. Secondly, the bullet and tether system will ensure that the heat flow probe is securely fixed in the soil, preventing easy removal and reuse.

Furthermore, the impactor structure will be made out of CF Nomex panels, where only the Nomex fibers could realistically be produced from recycled aramid fibers.[5] The impact attenuator is made of aluminium honeycomb, which could be produced with recycled alloys. The TCS uses silica aerogel for insulation, which can also be

[1] https://www.dupont.com/, Accessed [18-06-2021]

[2] https://www.reuters.com/article/du-pont-ma-dow-idUSL1N1JC1R0, Accessed [18-06-2021]

[3] https://www.nasa.gov/centers/ames/thermal-protection-materials/tps-materials-development/low-density-ablators.html, Accessed [18-06-2021]

[4] https://www.nasa.gov/centers/ames/thermal-protection-materials/tps-materials-development/reusable.html, Accessed [18-06-2021]

[5] https://www.brentindustries.com/aramid/, Accessed [17-06-2021]

produced from recycled materials.[6]

17.3. SC-3: Renewable

The impactor solely uses renewable energy during operation, as it is fully powered by solar arrays. However, the energy required to manufacture the impactors will be high, due to its use of CF reinforced polymers. When CF are not used from recycled sources and instead produced from raw materials, the process is very energy intensive [31]. When the production requires large amounts of energy, the likelihood of using purely renewable sources decreases, due to the limited amount available in current energy mixes.

17.4. SC-4: Transparent Use

Similarly to any spacecraft design, the impactor will use components or cooperate with companies that are closely related to the military industry. This is an inevitable issue that most likely has small implications for perception the mission, yet it could prevent the design from being as socially sustainable as possible. For the impactor specifically, the use of Nomex and Kevlar is connected to the protective gear of countless military and law enforcement personnel.

Another concern for the transparent use of the impactor is the inclusion of the penetrating bullet and the cartridge firing it. If the bullet fails to fire, the impactor could pose a danger for future missions. Therefore, a clear "disarming" procedure should be implemented for the cartridge, to ensure that the Mars Deploy mission is safe far past its operational life.

17.5. SC-5: Non-toxic

Apart from the use of rare Earth elements, there are not many toxicity issues for the impactor. The TCS based the heating elements on existing components produced by Minco, which ensures that non-toxic materials are used in all their flexible heaters.[7]

17.6. SC-6: Non-polluting

The main concern for the landers' pollution is the surface pollution of Mars. Firstly, as 10 impactors will enter the atmosphere, 10 EDL subsystems will be jettisoned onto the surface, each including a heat shield and backshell of 1.5 m diameter and a 18 m^2 parachute. Not only will they be difficult to trace, but following COSPAR regulations for Planetary Protection, they should all be decontaminated to a surface bioburden level of ≤ 30 spores and a total bioburden level of $\leq 30 \pm (2 * 10^5)$ spores [4]. The same obviously holds for the impactor itself, for which the spore contamination is even more critical, due to the high impact velocity. The Planetary Protection Policy does not specify clear decontamination requirements for soil penetrating components such as the bullet, but they will most likely be even more stringent.

17.7. Conclusion

The most important sustainability considerations for each subsystem are given in Table 17.1. As mentioned previously, many concerns are shared with the orbiter subsystems. The least sustainable part of the lander design could be the EDL, yet this may be inevitable, considering the characteristics and time frame of EDL procedures. EDL seems to be inherently single-use, as all components need to fulfill their purpose only once during the mission. However, if probes will land on Mars in a future where manned missions are present, developing reusable EDL systems will certainly be worthwhile.

[6] https://www.thermablok.com/thermablok-commercial-construction/, Accessed [18-06-2021]
[7] https://www.minco.com/products/flexible-heaters/, Accessed [18-06-2021]

Table 17.1: Evaluation of sustainability criteria for each lander subsystem. REE denotes rare Earth elements, CF denotes carbon fiber.

SC	CDH	EDL	EPS	PAY	STRUC	TCS	TTC
SC-1	REE, startup comp.	DuPont monopoly	REE, coltan and cobalt		DuPont monopoly		REE, startup comp.
SC-2	REE	Single use, ablative heat shield, reusable tiles	REE	Difficult disassembly or reuse	CF not recycled	Recycled aerogel	
SC-3			Solar energy		CF production		
SC-4	Military use	Military use		Bullet should be disarmed			
SC-5	REE		REE			Non-toxic materials used	REE
SC-6	REE	Surface pollution	REE	Strict decontamination	CF production		Less freq. pollution, REE

18. Risk

The technical risks of the lander are discussed in this chapter. The approach to assessing and managing the risks is the same for the orbiter, as discusses in Section 12.1. In Section 18.1, all the risks and their mitigation strategy per subsystem are listed. To conclude, it is checked upon whether the stakeholder requirement [DMD-SARR-BROOT-07] is complied with in Section 18.2.

18.1. Subsystems

The only difference with the orbiter risk assessment and management is the determination of probability. Out of 17 landers that successfully landed on Mars, counting from 1975, 13 succeeded.[1] This results in a failure rate of 4/17. Furthermore, all possible failures for a lander on Mars were retrieved from [85, p.6], where each risk is connected to their failure category. Multiplying both failure rates returned the probability for each risk before mitigation.

Table 18.1: Identified technical risks. RBM is the probability and impact before mitigation, RAM is the probability and impact after mitigation.

ID	*Description*	*RBM*	*Mitigation*	*RAM*
AERO				
R-AERO-L-01	Parachute will break due to dynamic pressure.	1, 5	*Done:* Dynamic pressure to stay around 900 Pa (maximum tested for is 970 Pa).	1, 5
R-AERO-L-02	Suspension line of the parachute breaks.	1, 4	*Done:* Added two extra suspension lines for redundancy.	1, 2
R-AERO-L-03	Parachute doesnt deploy.	1, 5	*Planned:* Perform thorough testing.	1, 5
R-AERO-L-04	Heat shield fails to jettison.	2, 5	*Planned:* Perform thorough testing.	1, 5
R-AERO-L-05	Backshell fails to let go off lander.	2, 5	*Planned:* Perform thorough testing.	1, 5

Continued on next page

[1] https://westeastspace.com/encyclopedia/missions-to-mars/, Accessed [14/06/2021]

Table 18.1 – continued from previous page

ID	*Description*	*RBM*	*Mitigation*	*RAM*
C&DH				
R-CDH-L-01	The lander C&DH system will run out of storage space for scientific data.	2, 4	*Done:* The storage will be designed such that it is able to store 60 sols without contact to the relay orbiter.	1, 4
R-CDH-L-02	System errors making the lander not usable.	2, 5	*Planned:* Implementing a back up system from which the error can manually or automatically be resolved.	2, 2
R-CDH-L-03	The system will not have enough throughput to process all the gathered data.	2, 4	*Done:* Have multiple processing units on board to spread the load.	1, 4
R-CDH-L-04	Radiation will damage the electronics in the on board computer.	2, 4	*Done:* Use space grade radiation hardened components that are guaranteed to survive the radiation environment.	1, 4
R-CDH-L-05	CDH components will be damaged upon impact.	2, 5	*Planned:* The components can be further tested to verify the load cases. A resin similarly to Deep Space 2 can be applied to protect sensitive electronics.	1, 5
EPS				
R-EPS-L-01	Solar arrays will be covered in dust during a duststorm. (Environmental)	2, 5	*Done:* Dust clearing system.	2, 2
R-EPS-L-02	Energy storage system failure.	3, 5	*Planned:* Careful production process.	1, 5
R-EPS-3	The solar array deployment mechanism fails to deploy.	2, 5	*Done:* Two actuator per axis for redundancy.	1, 5
G&N				
R-GN-L-01	Wind storm on Mars [86]. (Environmental)	5, 4	*Done:* Ratio of impact velocity to wind gusts is about 25.9 at maximum, meaning the impact angle stays below 5 degrees.[2]	DEL.
Payload				
R-PAYL-L-01	HP3 Probe fails to deploy due to the hardness of the soil.	2, 4	*Done:* The mole is replaced by a bullet, which will be shot into the ground at high velocity.	1, 4
R-PAYL-L-02	Due to varying soil composition at different landing sites, not all heat flow probes are deployed to their required depth.	2, 4	*Done:* Two differently shaped bullets are carried per lander, ensuring that at least one of them reaches the required deployment depth.	1, 2
R-PAYL-L-03	The heat flow measurement is disturbed by the heating/cooling of the impactor itself.	2, 4	*Planned:* With accurate heat modelling of the impactor, the heat flow measurement can be corrected for this.	2, 2
R-PAYL-L-04	The heat flow probe(s) are deployed at an angle with respect to the vertical.	2, 3	*Done:* The bullet contains a tiltmeter, which will precisely measure the deployment tilt.	1, 3

Continued on next page

[2] https://airandspace.si.edu/exhibitions/exploring-the-planets/online/solar-system/mars/wind/, Accessed [28/06/2021]

Table 18.1 – continued from previous page

ID	*Description*	*RBM*	*Mitigation*	*RAM*
R-PAYL-L-05	The heat flow measurement is affected by the temperature change due to seasonal effects or the day/night cycle.	2, 3	*Done:* Measuring time will be at least one Martian year to average out seasonal effects and the day/night cycle.	1, 3
R-PAYL-L-06	The seismometer does not survive the high impact loads.	2, 5	*Done:* Only the SP seismometers are used, which have a high resistance to shock.	1, 5
R-PAYL-L-07	The seismometer is deployed at an angle with respect to the horizontal, reducing the quality of seismic measurements.	2, 4	*Done:* Only the SP seismometers are used, which can operate at inclinations up to 15 degrees. Landing sites are also selected carefully to avoid inclinations as much as possible.	1, 2
R-PAYL-L-08	The seismometer has an insufficient SNR due to vibrations induced by other lander subsystems.	2, 4	*Planned:* Careful testing and analysis will be done, and the seismometer will be isolated from other components as much as possible.	1, 4
Structures				
R-STRUC-L-01	The lander penetrates too deeply in soft soil.	2, 5	*Done:* The lander is made taller and wider, the impact speed is decreased.	1, 5
R-STRUC-L-02	The structure fails during impact.	2, 5	*Done:* A honeycomb impact attenuation structure is used.	1, 5
R-STRUC-L-03	The structure experiences too much force on one side due to high impact angle.	2, 4	*Done:* A larger parachute is used, and for a longer period, to decrease the horizontal velocity. Fins are used to stabilise the lander during descent.	1, 4
R-STRUC-L-04	The impact attenuator shows less strain than expected.	2, 5	*Done:* A 20% margin is added to the required deceleration distance. *Planned:* Perform honeycomb deformation tests.	1, 3
R-STRUC-L-05	The impact speed is higher than expected.	2, 5	*Done:* A 20% margin is added to the required deceleration distance.	2, 3
R-STRUC-L-06	The soil type is softer/harder than expected.	2, 5	*Done:* The lander is designed for a wide range of S-factors. *Planned:* Soil types can be investigated in more detail.	1, 3
R-STRUC-L-07	The lander lands on a rock.	2, 5	*Done:* The impact structure is made wider. *Done:* A 20% margin is added to the required deceleration distance. *Planned:* An ADCS system and descent camera can be added to avoid large rocks.	1, 4
R-STRUC-L-08	The lander lands on rough surface.	2, 4	*Done:* The impact structure is made wider. *Done:* A 20% margin is added to the required deceleration distance. (done).	2, 3
R-STRUC-L-09	The support structure walls buckle upon impact.	2, 4	*Done:* A honeycomb sandwich panel is used.	1, 4
R-STRUC-L-10	The support structure shows too much strain upon impact.	2, 5	*Done:* A stiff carbon fiber skin is used. *Done:* A 30% safety margin is taken on the load on the walls.	1, 5

Continued on next page

Table 18.1 – continued from previous page

ID	*Description*	*RBM*	*Mitigation*	*RAM*
R-STRUC-L-11	A payload gets damaged upon impact.	2, 4	*Done:* A 20% safety margin is used on the allowable deceleration.	1, 4
R-STRUC-L-12	Production flaws in the honeycomb support structure.	2, 4	*Planned:* Perform thorough testing.	1, 4
R-STRUC-L-13	The sandwich panel's skin delaminates from the core.	2, 4	*Planned:* Perform thorough testing. *Planned:* Use conventional metal structure.	1, 4
Thermal Control				
R-THERM-L-01	MLI is not effective enough on Mars.	5, 5	*Done:* Use aerogel instead.	DEL.
R-THERM-L-02	The impactors have different deployment depths, causing the lander to undesirably fluctuate in temperature.	2, 5	*Done:* Design for two extreme cases: minimum and maximum deployment depth.	1, 5
R-THERM-L-03	The soil of Mars has fluctuating temperatures during day and night, causing the lander to undesirably fluctuate in temperature.	2, 5	*Done:* Use insulation to diminish the effect of the environment.	1, 5
R-THERM-L-04	The nights on Mars are extremely cold, causing the lander to critically decrease in temperature.	2, 5	*Done:* Design for the worst case scenario and provide peak power.	1, 5
R-THERM-L-05	The radiators require a large area and weigh a lot.	5, 4	*Done:* Use a heat sink instead. This heat can be used during nighttime when the lander requires heating.	DEL.
R-THERM-L-06	Aerogel cannot withstand the high loads upon impact.	5, 5	*Planned:* Find ways to strengthen the aerogel to survive the high impact loads.[3]	2, 5
TTC				
R-TTC-L-01	DSN dish fails to deploy.	2, 4	*Done:* Deployment tests.	1, 4
R-TTC-L-02	UHF antenna fails to deploy.	2, 5	*Done:* Make system as simple as possible: isotropic stick LGA.	1, 5
R-TTC-L-03	UHF Fails to connect to orbiter.	3, 2	*Done:* Have backup system with isotropic antenna for commands.	3, 1
R-TTC-L-04	Misses orbiter contact time.	3, 1	*Done:* Overdesign data rate and storage capabilities, in order to catch up later.	3, 1

[3] https://technology.nasa.gov/patent/LEW-TOPS-20, Accessed [28/06/2021]

Table 18.2: Technical risk map before mitigation, green and yellow is considered acceptable.

	Probability of occurrence				
Impact	*Very Low (1)*	*Low (2)*	*Moderate (3)*	*High (4)*	*Very High (5)*
Catastrophic (5)	**R-AERO-L-01, R-AERO-L-03**	**R-AERO-L-04, R-AERO-L-05, R-CDH-L-02, R-CDH-L-05, R-EPS-L-01, R-EPS-L-03, R-PAYL-L-06, R-STRUC-L-01, R-STRUC-L-02, R-STRUC-L-04, R-STRUC-L-05, R-STRUC-L-06, R-STRUC-L-07, R-STRUC-L-10, R-THERM-L-02, R-THERM-L-03, R-THERM-L-04, R-TTC-L-02**	**R-EPS-L-02**		**R-THERM-L-01, R-THERM-L-06**
Critical (4)	**R-AERO-L-02**	**R-CDH-L-01, R-CDH-L-03, R-CDH-L-04, R-PAYL-L-01, R-PAYL-L-02, R-PAYL-L-03, R-PAYL-L-07, R-PAYL-L-08, R-STRUC-L-03, R-STRUC-L-08, R-STRUC-L-09, R-STRUC-L-11, R-STRUC-L-12, R-STRUC-L-13, R-TTC-L-01**			**R-GN-L-01, R-THERM-L-05**
Marginal (3)		**R-PAYL-L-04, R-PAYL-L-05**			
Low (2)			**R-TTC-L-03**		
Negligible (1)			**R-TTC-L-04**		

Table 18.3: Technical risk map after mitigation, green and yellow is considered acceptable.

	Probability of occurrence				
Impact	*Very Low (1)*	*Low (2)*	*Moderate (3)*	*High (4)*	*Very High (5)*
Catastrophic (5)	**R-AERO-L-01, R-AERO-L-03, R-AERO-L-04, R-AERO-L-05, R-CDH-L-05, R-EPS-L-02, R-EPS-L-03, R-PAYL-L-06, R-STRUC-L-01, R-STRUC-L-02, R-STRUC-L-10, R-THERM-L-02, R-THERM-L-03, R-THERM-L-04, R-TTC-L-02**	**R-THERM-L-06**			
Critical (4)	**R-CDH-L-01, R-CDH-L-03, R-CDH-L-04, R-PAYL-L-01, R-PAYL-L-08, R-STRUC-L-03, R-STRUC-L-07, R-STRUC-L-09, R-STRUC-L-11, R-STRUC-L-12, R-STRUC-L-13, R-TTC-L-01**				
Marginal (3)	**R-PAYL-L-04, R-PAYL-L-05, R-STRUC-L-04, R-STRUC-L-06**	**R-STRUC-L-05, R-STRUC-L-08**			
Low (2)	**R-AERO-L-02, R-PAYL-L-02, R-PAYL-L-07**	**R-CDH-L-02, R-EPS-L-01, R-PAYL-L-03**			
Negligible (1)			**R-TTC-L-03, R-TTC-L-04**		

18.2. Conclusion

For an individual lander, all risks except for R-THERM-L-06 are within acceptable bounds. This requires special attention in the next design phase. It is again apparent how many risks have a very high impact, but a relatively low probability. For each individual lander, the success rate was calculated with the same manner as done for the orbiter in Section 12.3. This resulted in a success rate of 90.6%. The chance of a lander being operational should be at least 80% according to requirement [DMD-SARR-BROOT-07]. For this to hold, the probability of success for the lander has been multiplied with the orbiter its success rate. Doing so, led to a success rate of 81.6%, meaning this stakeholder requirement is met.

19. Sensitivity Analysis

The sensitivity analysis of the lander design is carried out in the same way as for the orbiter in Chapter 13. The method is to change the original design input parameter x_1 by 5% and document the output. The percentage change, or sensitivity parameter ε indicates whether the design is robust and gives a value close to the original output y_1. The equations are repeated here for clarity's sake.

$$x_2 = 1.05 \cdot x_1 \tag{19.1}$$

$$\varepsilon = \frac{y_2(x_2) - y_1(x_1)}{y_1(x_1)} \tag{19.2}$$

The results are listed in Table 19.1. If the sensitivity parameter is highlighted in red, the percentage change of the output is larger than the original change applied to the input parameters. A red cell indicates that the corresponding requirement must be checked whether it is still compliant. Green means that the sensitivity parameter is between 0 and 5%.

Table 19.1: Result of the sensitivity analysis of the lander for an input change of 5% and ε being the sensitivity parameter

Subsystem	Input	Output	ε
EDL	Entry angle [deg]	Impact speed [m/s]	9.75%
	Entry speed [m/s]	Impact speed [m/s]	1.64%
Structures	Total lander mass [kg]	Crumple zone mass [kg]	3.99%
	Impact speed [m/s]	Crumple zone mass [kg]	12.59%
Aerodynamics	Parachute area [m^2]	Subsystem mass [kg]	2.06%
	Heat shield diameter [m]	Heat shield mass [kg]	12.18%
TTC	Contact time [s]	Power [W]	5.00%
		Data rate [kbits/s]	5.00%
CDH	Nominal data rate [kbits/s]	Memory [MB]	5.05%
		Transmission rate [kbits/s]	4.98%
EPS	Nominal power [W]	Subsystem mass [kg]	4.33%
		Solar array size[m^2]	4.21%
THERM	Emitting area [m^2]	Power consumption [W]	1.44%
		Subsystem mass [kg]	-0.60%
	Incident area[m^2]	Power consumption [W]	1.54%
		Subsystem mass [kg]	3.17%
	Max deployment depth [m]	Power consumption [W]	1.55%
		Subsystem mass [kg]	2.74%
Astrodynamics	$r_{release}$ [km]	ΔV [m/s]	-0.35%
		Mars drift [m]	5.53%
		$d_{landing}$ [m]	4.50%

EDL

The Entry, Descent and landing systems employs entry angle and entry speed as the main input parameters. The main output is impact speed, as it poses multiple constraints on the structures subsystem. The impact speed is found to be very sensitive to entry angle, while the entry speed has less of an impact.

Structures
In case of structures, the crumple zone mass is investigated as it is the critical structural component dealing with the entry loads. It is dependent on the total lander mass and impact speed. The crumple zone mass is very sensitive to an increase in impact speed, increasing by over 12%.

Aerodynamics
The aerodynamics design tool outputs the subsystem mass, including parachute, deployment mechanism and miscellaneous items, when given the parachute area. The design process from area to system mass is robust. Looking at the heat shield, its mass is comparably sensitive to a change in diameter. Both relationships make sense from a qualitative standpoint, as an increase in size results in a higher mass.

TT&C
The TT&C subsystem analysis reveals that there is a direct linear relationship between contact time and the outputs power and data rate. Decreasing the contact time by a certain percentage increases both outputs by the same amount. It has to be noted that, unlike for the other inputs, the contact time is decreased, as this is the more critical case for power and data rate.

C&DH
C&DH shows a similar behaviour, although the relation between input and output is not perfectly linear. An increase in nominal data rate causes the memory and required transmission rate to grow.

EPS & THERM
The sensitivity analysis of the EPS and THERM uses the same inputs and outputs as for the orbiter, discussed in Chapter 13. For EPS, the nominal power of the lander has an immediate effect on subsystem mass and solar array size, with both outputs being relatively insensitive. The input of THERM is divided into emitting area and incident area, resulting in a required subsystem power and mass. All of those show a robust behaviour. Additionally the deployment depth, meaning how far the Impactor digs itself into the ground when hitting the surface, is investigated as it changes the thermal environment significantly. The analysis however shows that the sensitivity parameters for the relevant outputs are in the range of 1.6 to 2.7%, meaning that the design method diverges only by a small amount.

Astrodynamics
Lastly, the behaviour of the astrodynamic system is analysed. The main input that can be controlled is $r_{release}$, which is the distance of the orbiter to the centre of Mars at the moment of lander release. To bring the landers to their dedicated landing spots the orbiter slows down and speeds up during release which requires a certain ΔV. It is investigated by how much this ΔV changes when the release distance is altered.

Releasing the probes at a distance 5% larger than the original results in a decrease of 0.35% of total mission ΔV. Other output parameters affected by $r_{release}$ are the Mars drift and $d_{landing}$. Both of them are terms in the calculation of the landing range, which describes the distance on the surface of Mars where the probes can land. Increasing Mars drift and $d_{landing}$ makes the system more versatile when it comes to choosing the landing sites. It is found that both Mars drift and $d_{landing}$ increase, which means that by releasing the capsules further away from Mars the surface range of the landing window can be increased by 4.5%. Since the lander will be travelling independent from the orbiter for a longer time in that scenario, it affects the EPS and THERM since the lander has to be supported for longer without the possibility to deploy solar panels. To sum up, by releasing the landers earlier the possible landing area increases and especially the Mars drift is sensitive to a change in $r_{release}$.

Results and Recommendations
The values indicated in red in Table 19.1 show that the design process of that particular subsystem is sensitive and the corresponding requirements are checked to make sure the design is still compliant. This is analysed for the following parameters.

- EDL impact speed
- Structures crumple zone mass
- Heat shield mass
- C&DH memory size

According to [DMD-EDL-04] the impact speed shall be between 200 and 230 m/s. In the sensitivity analysis it is shown that the impact speed is highly sensitive to a change in entry angle. This problem is solved by tailoring the parachute deployment height and lander release for different entry angles. The requirement [DMD-EDL-05] allows an entry angle between -12 and -15 degrees to reach the designated landing spot, which is a difference of 25%. In conclusion, by altering the entry angle by 5% the impact speed increases to a value outside of the requirement, but this sensitive behaviour is known and tackled by altering parameters of the entry sequence.

Moving on to the structures, the subsystem is limited to a mass of 84 kg according to [DMD-STRUC-L-12]. In the sensitivity analysis the increase in mass of the crumple zone violates this requirement. It is recommended to consider the requirement as driving. A chain of highly sensitive subsystems is identified. The impact speed is very sensitive to the entry angle, while the crumple zone mass reacts heavily to a change in impact speed. Therefore it is recommended to carefully manage the contingencies on these parameters to prevent the design from becoming unacceptable.

The heat shield mass is sensitive to an increase in heat shield diameter. The diameter depends on the internal subsystem configuration and is not expected to change a lot because the subsystem dimensions are designed with contingencies which are expected to decrease during the course of further studies.

Lastly, the required storage on board the lander is sensitive to an increase in nominal data rate. The requirement [DMD-CDH-L-11] sets the maximum storage to 17.4 GB. The sensitivity analysis gives an increase in required memory to 64.5 MB, meaning the requirement is still met.

The main recommendation of the sensitivity analysis of the lander is to further investigate the effect of impact velocity on the design. It has been found that the impact speed is very sensitive to entry angle and moreover has a great impact on the structures subsystems. An increase in entry angle 5% results in an increase of impact velocity from 230 to 250 m/s. All mentioned requirements are recommended to be labeled as driving requirements.

Part V

Mission Evaluation

20. RAMS Analysis

For the design a short analysis on Reliability, Availability, Maintainability, and Safety (RAMS) characteristics is performed. This is done to describe the design's safety functions and to outline the redundancy philosophy applied.

Contingencies

During the design phase, many variables have to be taken into account. In a space mission like such as Mars Deploy, there are many unknowns as well. For the instances were something is not designed for or unknown, the design should take a contingency into account. During the design, every subsystem has taken their respective safety factors. Some certain approaches or calculations deserve some extra contingency management, these will be covered below.

One of the most critical unknowns to cover for was for the impact structure. The impact velocity is not constant for all terrains, therefore the necessary deceleration distance had to be taken with a 20% margin. The surface composition is unknown and could be rougher, so the impact structure is designed for a 10000 g impact, even though the payload is rated for 13000 g. Finally the impact angle to the ground is also considered and mostly mitigated by making sure the parachute will make it descent straight down.

Second, the environment on the surface of Mars can be harsh on the spacecraft, especially the EPS. It is widely known that the dusty environment causes problems as dust accumulated on the solar arrays. The presence of large dust storms poses additional problems for EPS availability. Besides this, thermal conditions on Mars are also far from ideal. All of these considerations combined require significant contingencies for the EPS. Requirement [DMD-SARR-BROOT-04] states that the EPS shall have a safety margin of 1.4. This safety margin has been applied to the amount of energy the system can store, and the amount of power it is able to generate. This already gives a more redundant system. Furthermore, as Li-ion batteries should not be fully discharged as to not decrease their lifetime, the system is designed for a 60% DoD, but the battery does allow for a full discharge in an emergency.

Manufacturing

The decision was made to use carbon fiber sandwich structures for the support structure for both the orbiter and lander. The manufacturing process of such a structure is tedious and difficult. Especially when one would want to attach something to the structure, the internal structure has to be manufactured with care as well. Calculations that have been done on the orbiter and lander structures show that they are currently overdesigned. The exact impact of manufacturing inconsistencies should be evaluated and taken into account for.

Resource Utilization

As not all aspects of the design were of equal importance, it was imperative that tasks were prioritized. Ten weeks with 10 students may sound like much, but due to the large amount of work the time is actually very limited. Due to this, the resource allocation was shifted towards more important topics.

First of all, the main focus of the design was on the landers themselves, as it was deemed the most complex and critical part of the mission. Due to this, the majority of time was spent researching and designing landers and their subsystems, as well as researching Martian weather, soil types, dust storms, and other information which would affect the way lander shall be designed and operate. As a result, it is visible in the report that lander's subsystems are designed to a higher level of detail, with less uncertainties. In the majority of the cases, real subsystem components were picked for the lander, while the orbiter's characteristics in most cases are left at statistical estimates.

Finally, within design of the lander itself, there was a higher importance paid to EDL and structures, rather than any other subsystem. The scientific payload also required more attention than others, as elaborate literature studies had to be done. Unlike auxiliary subsystems such as TT&C, structures required a lot of innovation, an enormous amount of researching, and application of completely new methods and techniques. Results are visible throughout the report, for example in the form of the highly innovative impact-bullet approach with additional explosives, as well as the sandwich shaped impact structure. In order to achieve this, two people instead of one were appointed to the subsystem. They were also cleared from auxiliary tasks such as system diagrams, risk management etc. It is worth mentioning that the EDL group of four people has also produced total work higher than average subsystem, as complex hyperbolic entry patterns had to be considered in addition to the aerodynamic systems, which had tight requirements.

Fault Detection & Resolution

One of the more important aspects of any digital system is self diagnostics and fault detection. Especially critical in space missions without the possibility of physical access to the hardware, it is important that a system can detect its own problems. In Mars Deploy, a number of steps were undertaken to accommodate for this.

First, the lander's power subsystem is able to detect loss of sunlight due to damaged solar cells, or a martian storm. This is done by means of analysing voltage readout and comparing it to expected levels, as well as by analysing sun readout from the sun sensors. If both would hint at decreased sunlight, there is a high chance of an ongoing dust storm, and the lander shall enter hibernation mode until nominal power is restored (Section 16.8). In case the signals from the solar cells and sun sensors disagree, there is a potential damage to the solar cells. In order to mitigate this as much as possible, the landers are equipped with four partially redundant solar cells, which generate 40% more power than required. Failure of one panel will not lead to catastrophic failure of the whole system.

A similar approach to redundancy was taken when designing the most critical communication segment; the UHF receiver on the orbiter. Instead of one big phased array, two smaller are used, thus providing a degree redundancy. This system has been shown to meet requirements and operate at the minimum requested parameters even with just one of the two arrays operational. Detecting antenna malfunctioning would be rather easy, as there will be a high number of errors in information received, or no information will be received at all.

Finally, one of the lander's most critical pieces of payload, the heat flux probe, is present in a quantity of two. Although initially designed in a pair in order to increase variety of soil types suitable for successfully meeting the requirements, the two bullets also provide partial redundancy, as even in case of one failing, the second will provide measurements, although of less than required accuracy.

Maintenance

Due to the specifics of the mission, the majority of maintenance aspects such as hardware replacements and visual inspection are not possible. In turn, this means that special attention shall be paid to the manufacturing and quality control processes. Testing must also be thoroughly performed, as once the hardware is placed in the launcher, there is no possible way to access it anymore for repairs.

Nevertheless, software maintenance possibility was taken into account, and accommodated for. Specifically, both the TT&C and C&DH subsystems were over-designed, to allow for additional commands downloading, prolonged off periods without loss of scientific data, and even over the air software updates.

The TT&C subsystem is mainly limited in Mars-Earth uploads, and has a much higher bandwidth capacity when it comes to downloading from Earth to orbiter or landers (Section 16.6), allowing remote diagnostics and updates to take place. In case with C&DH, space graded solid state drives (SSD) are to be used (Section 16.7, Section 10.6), which are significantly over-designed in terms of storing capacity, which allows to postpone scientific data transmission over the maintenance period, without the need to stop scientific experiments, or lose priceless information collected.

21. Cost

21.1. Cost Breakdown Structure

The following Table 21.1 and Table 21.2 will provide the cost breakdown of the research, development and production (RD&P) cost side of this mission. These two tables provide a break down of the cost for each subsystem, and where possible a breakdown within the subsystem as well. For further explanation on the cost breakdown, one can be referred to the respective subsystem section.

Table 21.1: RD&P Cost budget for the Orbiter

Subsystem		Cost[M€]
ADCS		17.5
CDH		
	OBC	6.1
	Mass storage	0.58765
EPS		
	Distribution system	0.05
	Solar Array	1.3
	Battery	0.001
Structures		1.3
Propulsion		5.5
Thermal		1.641
TTC		84.4
Total Cost:		118.4

Table 21.2: RD&P Cost budget for the Lander

Subsystem		Cost[M€]
EDL		
	IMU	0.1031
	Pressure Sensor	0
	Altimeter	0.00013
Aerodynamics		
	Fins	0.005228
	Parachute	0.12731889
	Drogue Parachute	0.00062147
	Drogue Gun	0.01132
	Heat shield	0.9485718
	Backshell	0.700685
CDH		
	OBC	3.07
	Mass storage	0.58765
EPS		
	Distribution system	0.05
	Solar Array	1.92
	Battery	0.0015
	Dust Clearing	0.025
	Actuator	0.025
Structures		
	Supportive	0.99
	Impact attenuator	1.34
	Bullet	0.62
Payload		3.6
Thermal		1.26
	Insulation(aerogel)	1.7
TTC		1.2
Total Cost:		18.28

The RD&P cost of the lander has been defined such that the research and development cost is split over the ten Landers. Thus this would mean that the RD+P cost for all Landers combined is 10 times 18.28 M€. For the operational cost, the operating costs of the DSN has been considered. NASA provides a formula which can be used to get an estimate on the cost of utilizing the DSN. The report is from 2014 and the latest hourly rate that was given is from 2009, and is adjusted yearly. To account for inflation, the hourly rate is recalculated for 2021:

$$\text{HourlyRate} = 1057 * 1{,}032^{12} = 1542.5\$ = 1264.9 \tag{21.1}$$

The required contact time is given to be 4.8 hours per contact, and there is one contact per day. By utilizing equation 5-1 given in the NASA report [16], hourly aperture fee can be calculated. The resulting total weekly cost is 68.7 k€. Which brings the total DSN operational cost to 10.7 M€.

Table 21.3: Total Cost Breakdown

Cost type	Contribution	CostM€
RD+P cost		%
	Orbiter	118.4
	10 Landers	182.8
	Launch	73.8
Operational cost		
	DSN	10.7
Total		385.7

21.2. Return On Investment

The Return Of Investment (ROI) for a space related mission is generally not intended for the return of money or resources. The ROI that is received due to this mission can mostly be found in the scientific return. There could be

some future financial benefits in this mission as well.

Scientific Return
Finding sustainable sources of heat and or water could speed up the next step in space exploration by a lot. By investigating the tectonic and geologic behaviour of mars to benefit the search for heat and water sources, it will return a habitable landing location where these resources can be harvested. This mission , therefor, compliments the vision from ESA on Mars and human space travel beyond the ISS. Furthermore the spread out system could possibly also return data on how martian dust storms move. This could benefit future missions but also present missions on mars by being able to warn for an incoming storm.

Financial Benefit
As explained in Section 3.3 as well, there could be some financial benefits for this mission as well. The first one is that if the mission would successfully find heat and/or water sources, it could really benefit the cost of future missions. Thus this return would rather safe money in the future than make money. The second possible financial benefit is that the orbiter could still be operational after Mars Deploy is finished, and thus it would be possible to sell the bandwidth to an other mission.

22. Project Design and Development Logic

The project design and development logic was first set up in the midterm report [6] and is expanded upon in the following. The logic describes the steps taken after the end of the DSE. As the mission aims to be selected as an M-class candidate by ESA, the schedule is tailored such that the proposal can be handed in on time. A presentation by the French Space Agency CNES suggests that the call for an M6 mission is cancelled due to budget overruns. [1]. The calls for the missions M1 to M5 were issued in intervals of three to four years. Assuming this planning is not effected by the cancellation of M6, Mars Deploy is expected to be proposed as an M7 candidate in 2025.

The project design phases of Mars Deploy are based on the mission lifetime cycle as defined by ESA.[2] The phases are described below. Phase 0 as well as Phase A and B are part of the Design Synthesis Exercise. The mission phases follow the timeline as shown in Figure 22.1.

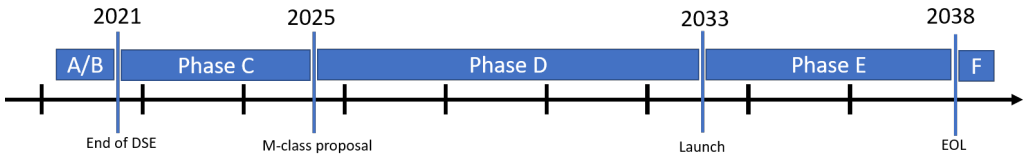

Figure 22.1: Mission timeline

Phase 0
The project commenced with the start of the DSE on 19th of April 2021. At the start of the project the design phase is planned out from a project management standpoint. A Gantt chart and a work breakdown structure is generated to divide the work efficiently. The product of Phase 0 is the project plan [87].

Phase A
Phase A is the feasibility study of the project. It results in the midterm report [6] and investigates different design options suitable for the mission objective. A trade-off was performed and the impactor design was chosen to continue with.

Phase B
The preliminary detailing is performed in Phase B. The technical budgets and configurations are presented in the final report of the DSE. This phase is concluded in on the 1st of July 2021 with the end of the DSE.

[1] http://sf2a.eu/semaine-sf2a/2017/presentations/S00/CNES_2017.pdf, Accessed [20-05-2021]
[2] https://www.esa.int/Science_Exploration/Space_Science/How_a_mission_is_chosen, Accessed [19-06-2021]

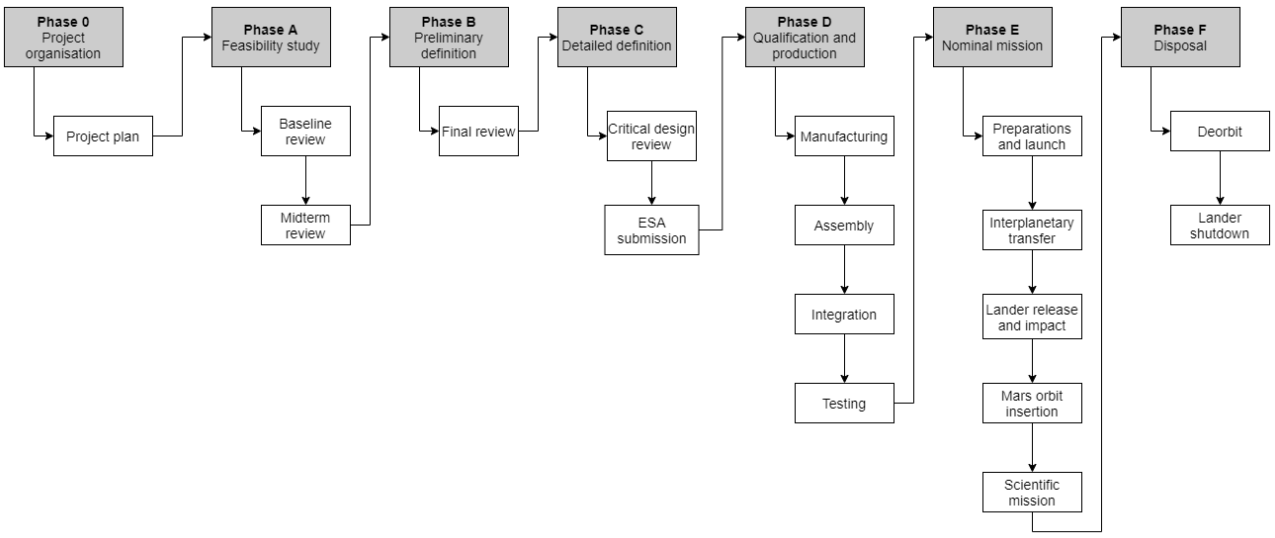

Figure 22.2: Project design and development logic

Phase C

In Phase C the design is detailed on component level which is concluded with the critical design review. The mission is then proposed to ESA as an M-class candidate in 2025. A time frame of 4 years is reserved for Phase C to extend the requirements data base and the detail the design. It also leaves sufficient time to prepare the ESA proposal, as a letter of intent, a proposal submission and a briefing meeting must be completed. The proposal is intended to cover a science theme of the ESA publication "Cosmic Vision" in order to comply with the scientific goals of the agency. Especially the theme "Explore in situ the surface and subsurface of solid bodies in the Solar System most likely to host – or have hosted – life" [88] applies to Mars Deploy and the ESA application shall be tailored such that it is made clear how this scientific goal is achieved.

Phase D

The system is manufactured and assembled in Phase D. Refer to Chapter 24 for the manufacturing plan. It is concluded with rigorous qualification and testing procedures to prepare the orbiter and probes for launch. Phase D includes the production of a qualification model and the flight model of the spacecraft in order to validate the compliance of the system with its requirements. The electrical system is tested to ensure proper communication of the subsystems with the CDH unit and the ground. Every subsystem is tested individually and then integrated into the system. A number of unit tests and system tests are combined to make sure the spacecraft works as intended.

Phase E

Phase E is referred to as utilisation and includes the launch and nominal operation phase of Mars Deploy. The launch preparations for the Falcon Heavy are described in the user's guide [3]. Typically the spacecraft is delivered to Cape Canaveral 30 days prior to launch. 10 days before launch the craft is mounted to the payload adapter and integrated in the fairing in the subsequent days. The launch is scheduled for April 11th 2033. The spacecraft releases the entry capsules eight and a half months after launch. The orbiter enters a Mars orbit shortly after.

Phase F

The mission ends with deorbiting and shutdown of the probes after the end of scientific mission. This is scheduled for 2038, so five years after launch.

A block diagram showing the interconnections and order of the mission phases is given in Figure 22.2. The items of the block diagram are organised and scheduled in the project Gantt chart (Figure 22.3). The Gantt chart is based on the proposed timeline and estimated times to complete all the actions. Fixed dates are launch, following the lander release and Mars orbit insertion.

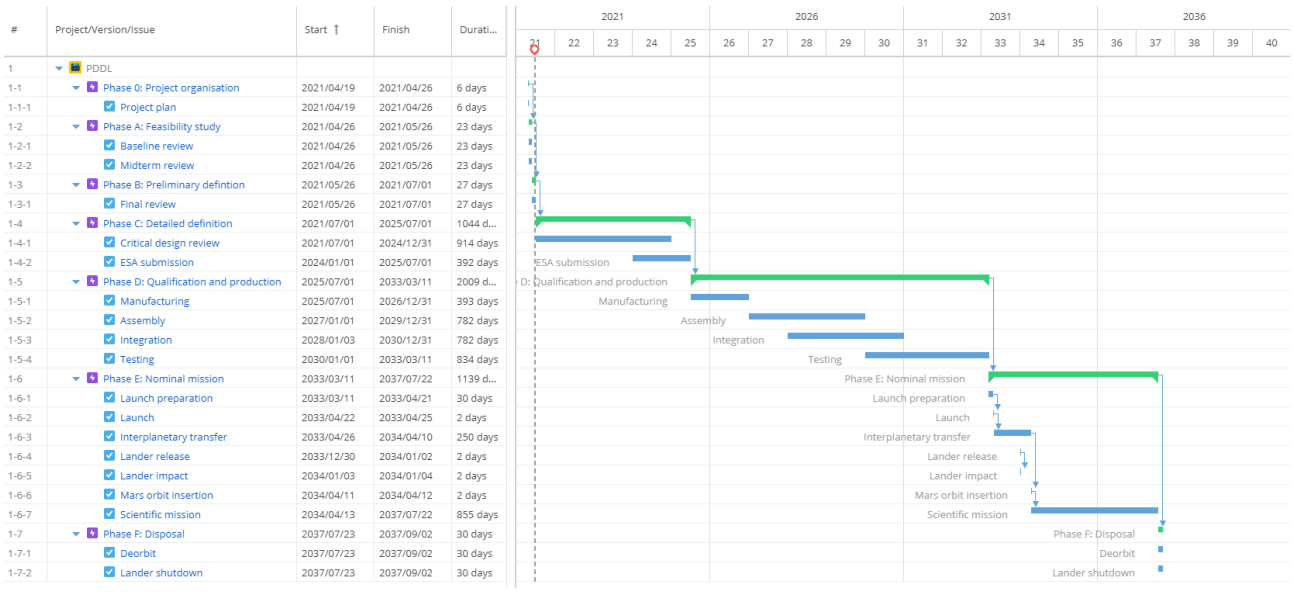

#	Project/Version/Issue	Start	Finish	Durati...
1	PDDL			
1-1	Phase 0: Project organisation	2021/04/19	2021/04/26	6 days
1-1-1	Project plan	2021/04/19	2021/04/26	6 days
1-2	Phase A: Feasibility study	2021/04/26	2021/05/26	23 days
1-2-1	Baseline review	2021/04/26	2021/05/26	23 days
1-2-2	Midterm review	2021/04/26	2021/05/26	23 days
1-3	Phase B: Preliminary defintion	2021/05/26	2021/07/01	27 days
1-3-1	Final review	2021/05/26	2021/07/01	27 days
1-4	Phase C: Detailed definition	2021/07/01	2025/07/01	1044 d...
1-4-1	Critical design review	2021/07/01	2024/12/31	914 days
1-4-2	ESA submission	2024/01/01	2025/07/01	392 days
1-5	Phase D: Qualification and production	2025/07/01	2033/03/11	2009 d...
1-5-1	Manufacturing	2025/07/01	2026/12/31	393 days
1-5-2	Assembly	2027/01/01	2029/12/31	782 days
1-5-3	Integration	2028/01/03	2030/12/31	782 days
1-5-4	Testing	2030/01/01	2033/03/11	834 days
1-6	Phase E: Nominal mission	2033/03/11	2037/07/22	1139 d...
1-6-1	Launch preparation	2033/03/11	2033/04/21	30 days
1-6-2	Launch	2033/04/22	2033/04/25	2 days
1-6-3	Interplanetary transfer	2033/04/26	2034/04/10	250 days
1-6-4	Lander release	2033/12/30	2034/01/02	2 days
1-6-5	Lander impact	2034/01/03	2034/01/04	2 days
1-6-6	Mars orbit insertion	2034/04/11	2034/04/12	2 days
1-6-7	Scientific mission	2034/04/13	2037/07/22	855 days
1-7	Phase F: Disposal	2037/07/23	2037/09/02	30 days
1-7-1	Deorbit	2037/07/23	2037/09/02	30 days
1-7-2	Lander shutdown	2037/07/23	2037/09/02	30 days

Figure 22.3: Project development Gantt chart

23. Logistics and Operations

The development of the Mars Deploy mission will take place across multiple locations across Europe and the rest of the world. Future design work will ideally take place in person, yet the design process until now has shown the feasibility of working online. Once the development of the mission is complete, the mission is not over: the lander, capsule and orbiter must all be manufactured and then launched. Once in operation, data must be received and processed in order to gain results and end-of-life processes will need to be guided. The manufacturing of all parts will take place in Europe and off the shelf products may come from all over the world. Once manufactured, assembly will take place in Noordwijk, Netherlands at ESTEC.[1] During the manufacturing and assembly phase several tests will take place to ensure quality control of the manufactured and assembled products. This way it can be ensure that only the highest quality products are used for the mission reducing the chance of failure. Once the landers and orbiter are assembled they will be transferred to Kennedy Space Center where they will be integrated with the chosen launcher, the SpaceX Falcon Heavy launch vehicle.[2] In Table 23.1 a summary of the dates and duration of the beginning of the mission to the end of mission can be seen.

Mission phase	Duration/date
Launch date	April 11th 2033
Travel from Earth to Mars	0.711 Earth years post launch
Release of entry capsules	0.706 Earth years post launch
Scientific phase	4.289 years
Total mission duration	5 years

Table 23.1: Mission Phase Durations

As can be seen from the table, the orbiter will begin interplanetary transfer to Mars after successful launch. Two days before arrival, the entry capsules will be released and begin their own independent travel and descent towards the Martian surface. During this phase a ground team working at the European Space Operations Centre in Darmstadt, Germany will monitor the proceedings. [3] The ground team will be responsible for over viewing the launch, the transfer obits, as well as collecting and processing the scientific data. Once this is complete, slots for communications will have been reserved and occur through the Deep Space Antenna in Cebreros, Spain. Once the mission has come to an end, the End-Of-Life (EOL) phases will begin, in this process the orbiter will be deorbited and the landers will be powered down. The landers are then left on Mars with reusable parts that could be used for future missions on Mars.

[1] https://www.esa.int/About_Us/ESTEC, Accessed [22-06-2021]
[2] https://www.kennedyspacecenter.com/launches-and-events/events-calendar?pageindex=1, Accessed [18-06-2021]
[3] https://sci.esa.int/web/cluster/-/33308-mission-operations, Accessed [19-05-2021]

24. Manufacturing, Assembly & Integration plan

To produce and assemble a launch-ready product, a Manufacturing, Assembly and Integration(MAI) plan is developed. The MAI plan can be seen in Figure B.1. The MAI is set up such that the chronological order flows from left to right and shows the manufacturing assembly and integration of all components for the landers, entry vehicle and orbiter. Logically, the manufacturing of all products is done before assembly, with the products most expensive to store being manufactured last. Once all parts are manufactured the lander will first be assembled, then the entry vehicle is assembled and the landers integrated. This process is repeated for 10 landers, followed by the assembly of the orbiter, and then integration of the 10 landers. Once all landers are integrated, the orbiter will be integrated into the capsule, and then onto the launcher. As can be seen in plan, components for the next production are ordered during the production of the component phase before them. Furthermore products that will be shop bought will be ordered at the beginning of the production and requested for delivery towards the end of the production phase in order to minimise storage. All components and assemblies will be decontaminated and stored in clean rooms to ensure compliance with the sustainability requirement SC-6. It is crucial for the mission that the MAI plan runs smoothly so that it is completed on time.

Conclusion and Recommendations

Conclusion

After the stakeholder and system requirements were set in the Baseline Report [1] and a concept trade-off was performed in the Midterm Report [6], this Final Report dealt with the preliminary subsystem design of the Mars Deploy mission. Through an iterative process, the subsystems of the orbiter and ten landers were sized and the mass, power, data and cost budgets were estimated. Before this, the mission profile was determined, through the calculation of a deployment and EDL sequence and by the landing site selection. After the design was finalised, considerations regarding future development, mission planning, manufacturing and cost were made.

The mission will be launched on April 11th 2033 in a SpaceX Falcon Heavy rocket. This launch vehicle will bring the orbiter carrying the ten landers to a Mars transfer orbit. Its main structure is a cylinder, made of carbon fiber Nomex honeycomb panels to save weight. On the outside, ten landers are attached, each with four attachment points. The orbiter communicates with DSN and will relay the landers' scientific data back to Earth via this connection. For power generation, the orbiter has a single 2 m^2 solar array, together with a Lithium-ion battery. Thermal control is mostly achieved passively, but also includes patch heaters and a heat sink. The orbiter uses a NTO/MMH bipropellant system and one main thruster, although this configuration could easily be adapted in the future to a more sustainable bipropellant HP/ethanol system. The ADCS uses the same MMH for reaction control thrusters, combined with reaction wheels for precise orientation. The main design parameters are given in Chapter 9.

The orbiter will release the landers two-by-two from the transfer orbit towards the ten predetermined landing locations on Mars, shown in Chapter 14. By deploying the impactors from the transfer orbit, the orbiter requires around 1000 kg of propellant less, leading to a decrease in size and dry mass as well. The entry capsule and disk-gap-band parachute will allow for entry and deceleration in the Martian atmosphere. The impactor itself includes fins to stabilise its final descent after the heat shield, backshell and parachute have been jettisoned. The landing impact of 10000 g is mostly absorbed by a 0.34 m tall crumple zone of aluminum honeycomb. The rest of the Impactor support structure is made of carbon fiber Nomex honeycomb panels.

Each Impactor will carry four scientific instruments: a seismometer, a heat flow probe, a weather station and an air composition analyser. Each of these instruments has TRL 9, following the requirements of the main stakeholder Dr. ir. Bart Root. The heat flow probe will be deployed as a bullet from a cartridge, using the impact velocity to reach at least 4 m of sub-surface depth. The Impactor will be able to communicate at low bit-rates with DSN directly, yet it will use the uplink to the orbiter for the main communications and data transfer. In case no contact is available with the orbiter, the Impactor C&DH system can store at least 60 sols worth of data. The Impactor will generate power using four circular solar arrays, with a total size of 3 m^2. To keep its internal temperature in the operational range, the Impactor uses a silver vapor deposited coating, patch heaters, a heat sink and 15 cm of silica aerogel insulation. The lander configuration and main design parameters can be found in Chapter 15.

Recommendations

There are several recommendations which have resulted from the design process. First the recommendations from the sustainability and risk analyses are mentioned, after which future design plans and subsystem specific recommendations are presented.

Sustainability Analysis

The sustainability analysis of both the orbiter and Impactor design shows that some considerations are common to both systems. Firstly, the electronic components in both systems will make use of rare Earth elements (REE). With this fact come many sustainability issues, ranging from the poor treatment of miners, to the toxicity of the excavation procedure and the resulting pollution for surrounding areas. In the further development of Mars Deploy, components should be selected from companies that have a clear policy regarding these issues. Secondly, the use of carbon fiber in both the orbiter and Impactor structure makes it difficult to use recycled materials during manufacturing. When new carbon fibers are used, this is paired with an energy intensive and polluting process. Therefore, the use of recyclable alloys for both support structures should be considered, or a further investigation into recycled carbon fiber composites.

For more specific sustainability recommendations, the main focus for the orbiter is the selected propulsion system. The current NTO/MMH bipropellant system is highly toxic and should be replaced by a more sustainable HP/ethanol system in the next design phase. This system can be used with renewable propellant and is not toxic for the assembly crew. The main concern for the sustainability of the lander is the contamination of the Martian

surface following the high velocity impact. By assembling the entire system in clean rooms, this concern can be addressed, yet additional attention could be given to the disposal of the EDL components.

Risk Assessment

The technical risk assessment and management for all individual subsystems was performed. In general, both the lander and orbiter subsystems contained risks which are quite impactful, while the probability is not too high. This indicates that more testing should be planned, which will assure that the probability diminishes substantially. This includes testing under similar conditions, NDT, deployment tests, firing tests, simulations etc.

For the orbiter, CDH, structures and thermal control have the most severe risks. On the other hand, the lander contained most critical risks in aerodynamics, CDH, structures and thermal control. It is apparent that these three latter subsystems are crucial for both lander and orbiter. As said, the probability is very low, whereas the impact could be catastrophic. Apart from the safety factors included in the current design, as well as the conservative approach followed, testing should be extensively planned to remove any remaining uncertainties. In addition, the risk tables should also be updated as not every risk has yet been identified. New risks will still appear in the further design stages and should be carefully assessed and managed.

Design Recommendations

Orbiter

The design of each subsystem prompted other recommendations, for future design phases. First of all the mission profile and planning, the current deployment procedure restricts the landing locations by limiting boundaries. To allow for a more flexible landing site selection, the deployment sequence could be revised, by releasing the probes further away from Mars or releasing the probes from orbit instead. Secondly, the launch vehicle selection and the orbiter configuration and mass budget would allow for one additional Impactor to be brought to Mars. This could lead to increased coverage for Martian seismic data. The implications on the sizing of other subsystems would still need to be investigated after the addition of an eleventh Impactor.

The current orbiter configuration has a lot of available volume in its internal structure, as it mostly needs the height to attach all ten impactors. It could therefore be considered to fill this space with secondary payload that needs to be transported to Mars. This could include CubeSats or other simple lander concepts for the Martian surface. Furthermore, it should still be verified whether the orbiter structure can withstand the dynamic loads during launch.

Other orbiter recommendations are related to a more detailed design process for several subsystems. For ADCS, a control algorithm could be developed and a more detailed moment of inertia calculation could be implemented. From TTC, the recommendation arises to further investigate the use of a phased array configuration, potentially to include the lander locating capability, which is currently performed with Doppler ranging. Finally, C&DH recommends including a safe boot system as a separate software component, such that the orbiter could be troubleshot remotely from this mode.

Lander

For the EDL sequence, it is recommended to further investigate parachutes that can be deployed at a higher dynamic pressure, such that parachute deployment could occur sooner in the descent. Secondly, the design of movable fins would provide more stability for the final Impactor descent, however they would also make the system more complex, taking away some of the benefits of the Impactor's mechanical simplicity. The Impactor GNC for EDL currently uses LIDAR for the altitude determination, yet a more accurate and fitting system could be used for the high velocity descent. Furthermore, the EDL simulation could be made more accurate by improving the atmospheric models and by a more detailed investigation of the surface conditions of the selected landing sites.

A very important recommendation is related to the landing impact of the Impactor itself. While the structure has been developed in detail to comply with the 10000 g deceleration, more investigation into the other subsystems' impact resilience is necessary. Not all of the currently selected components will be able to survive this impact, yet by designing an impact absorbing coating or a dampening inner structure, the loads could be decreased. The same concerns hold for the solar arrays which will be mounted to the exterior of the Impactor.

Related to the Impactor payload, the first recommendation is to look more into the deployment of the bullet to serve as the heat probe. Not only should the penetration dynamics be further investigated, but the effect of the cartridge explosion on the tether and other Impactor subsystems is still rather uncertain. Concerning the seismometer, the most important consideration is the coupling with the ground. During impact, the honeycomb crumple zone takes up most of the loads between the seismometer and the ground. However, during operation, it should ideally be in direct contact with the ground, to sense marsquakes accurately. Therefore, an investigation into the secure coupling with the ground through the crumpled honeycomb should be carried out.

System requirement [DMD-LANDER-15] stated the need of a "hibernation mode" in case any of the Impactors is faced with a Martian dust storm during operation. No subsystems were sized with this functionality included. Importantly, for the thermal control subsystem, one could consider a low-power operational mode, in which the heat sink is used to provide all heat necessary, (temporarily) negating the necessity of patch heaters. Critical

subsystems, such as the payload and key electronics could also be additionally shielded and insulated, this was not done in the current design. For EPS, hibernation mode would entail a more detailed battery sizing. Furthermore, the dust storm requirement brings the recommendation of a closer investigation into the dust clearing mechanism for the solar arrays. In case a robust, simple system can be designed, this could be used for future Mars missions as well. For the C&DH subsystem, hibernation mode would entail a separate software mode, in which reduced data rates are to be processed, but housekeeping data should be stored before contact with the orbiter can be restored.

Iterations
Lastly, regarding the entire design process, the preliminary design of the Mars Deploy mission has shown the importance of a structured iterative process. If the design would be further developed, it is therefore recommended to continue in this manner, adding a level of complexity for each iteration and performing subsystem integration after each cycle of a certain amount of iterations. Secondly, it has become clear that the impact structure design is very closely related to the landing site selection, EDL sequence and even the deployment method. Therefore, these four broad design segments should be in close communication with each other. For the design of all subsystems, steps should be taken to create a uniform coding method, using classes in Python, for example, such that the integration and iteration could be more automated.

Bibliography

[1] DSE Group 22, "Mars deploy: Baseline report of the design synthesis exercise," 2021.

[2] B. Root, *Project guide design synthesis exercise*, 2021.

[3] Space Exploration Technologies Corp. (2020). "Falcon user's guide."

[4] G. Kminek, C. Conley, V. Hipkin *et al.*, "Cospar's planetary protection policy," 2017. [Online]. Available: https://cosparhq.cnes.fr/assets/uploads/2019/12/PPPolicyDecember-2017.pdf.

[5] Institute of Medicine, *Dietary Reference Intakes for Water, Potassium, Sodium,Chloride, and Sulfate*. Washington, DC: The National Academies Press., 2005, p. 638, ISBN: 978-0-309-09158-9. DOI: https://doi.org/10.17226/10925.

[6] DSE Group 22, "Mars deploy: Midterm report of the design synthesis exercise," 2021.

[7] J. Barengoltz, "A review of the approach of nasa projects to planetary protection compliance,"

[8] M. Capderou, *Satellites Orbits and Missions*. Springer-Verlag, 2005.

[9] W. J. Larson and W. R. Wertz, *Space Mission Analysis and Design*, 3th ed. El Segundo, California: Space Technology Library, 2005.

[10] Ariane Group. (2020). "Chemical monopropellant thruster family," [Online]. Available: https://www.space-propulsion.com/brochures/hydrazine-thrusters/hydrazine-thrusters.pdf (visited on 21/06/2020).

[11] Honeywell Defense and Space Systems. (2003). "Constellation series reaction wheels," [Online]. Available: https://satcatalog.com/datasheet/Honeywell%5C%20-%5C%20HR14-50.pdf (visited on 21/06/2020).

[12] arcsec Space. (2020). "Sagitta star tracker," [Online]. Available: http://www.arcsec.space/wp-content/uploads/2021/04/arcsec-Star-Tracker-Datasheet.pdf (visited on 21/06/2020).

[13] New Space Systems. (2020). "Nss sun sensor," [Online]. Available: https://www.cubesatshop.com/wp-content/uploads/2020/11/NewSpace-Sun-Sensor_2020-10a.pdf (visited on 21/06/2020).

[14] Northrop Grumman. (2013). "Ln-200s inertial measurement unit," [Online]. Available: https://satcatalog.com/datasheet/Northrop-20Grumman-20-20LN-200S.pdf (visited on 21/06/2020).

[15] S. I. Sheikh, J. E. Hanson, J. Collins *et al.*, "Deep space navigation augmentation using variable celestial x-ray sources," 2009.

[16] "Nasa's mission operations and communications services," *NASA*, Oct. 2014.

[17] RUAG Space AB, *Command & Data Handling*, 405 15 Gothenburg, Sweden. [Online]. Available: https://www.ruag.com/system/files/media_document/2017-12/Command%5C%20and%5C%20Data%5C%20Handling.pdf.

[18] Mercury Systems, *TRRUST-Stor® VPX RT6U VPX Radiation-Tolerant Large Geometry SLC NAND SpaceDrive PCIe/SRIO*, 3601 East University Drive Phoenix, AZ 85034-7217 USA. [Online]. Available: https://www.mrcy.com/application/files/2416/1367/0262/5031.09E_6U-VPX_TRRUST-Stor-VPX-RT_SSD.pdf.

[19] Leon W. Couch, *Digital and Cnalog Communication Systems*, 8th ed. Upper Saddle River,New Jersey: Pearson, 2013, Professor Emeritus.

[20] B. Yost, “State-of-the-art small spacecraft technology,” Oct. 2020. [Online]. Available: http://nasa.gov/smallsat-institute/sst-soa-2020.

[21] S. T. Mayer, J. H. Feikert and J. L. Kaschmitter, “Testing and evaluation of lithium-ion batteries for leo space missions,” *U.S. Department of Energy by Lawrence Livermore National Laboratory*,

[22] J. Henninger, *Solar absorptance and thermal emittance of some common spacecraft thermal-control coatings*, Apr. 1984.

[23] Minco, *Thermal solutions design guide*, 2019.

[24] C. Hunter, “Venus express chemical propulsion system-the mars express legacy,” in *4th International Spacecraft Propulsion Conference*, vol. 555, 2004.

[25] S. Dominick, “Design, development, and flight performance of the mars global surveyor propulsion system,” in *35th Joint Propulsion Conference and Exhibit*, 1999, p. 2176.

[26] A. Woschnak, D. Krejci, M. Schiebl *et al.*, “Development of a green bipropellant hydrogen peroxide thruster for attitude control on satellites,” *Progress in Propulsion Physics*, vol. 4, pp. 689–706, 2013.

[27] S. Jo, S. An, J. Kim *et al.*, “Performance characteristics of hydrogen peroxide/kerosene staged-bipropellant engine with axial fuel injector,” *Journal of Propulsion and Power*, vol. 27, no. 3, pp. 684–691, 2011.

[28] H. Kang, D. Jang and S. Kwon, “Demonstration of 500 n scale bipropellant thruster using non-toxic hypergolic fuel and hydrogen peroxide,” *Aerospace Science and Technology*, vol. 49, pp. 209–214, 2016.

[29] J. W. Mantz, “Improvisational economies: Coltan production in the eastern congo,” *Social Anthropology*, vol. 16, no. 1, pp. 34–50, 2008.

[30] S. M. Jowitt, T. T. Werner, Z. Weng *et al.*, “Recycling of the rare earth elements,” *Current Opinion in Green and Sustainable Chemistry*, vol. 13, pp. 1–7, 2018.

[31] S. Das, “Life cycle assessment of carbon fiber-reinforced polymer composites,” *The International Journal of Life Cycle Assessment*, vol. 16, no. 3, pp. 268–282, 2011.

[32] C. Gong, N. Cao, J. Du *et al.*, “Ethanol production from renewable resources,” *Recent progress in bioconversion of lignocellulosics*, pp. 207–241, 1999.

[33] Y. Ando and T. Tanaka, “Proposal for a new system for simultaneous production of hydrogen and hydrogen peroxide by water electrolysis,” *International Journal of Hydrogen Energy*, vol. 29, no. 13, pp. 1349–1354, 2004.

[34] E. Vernot, J. MacEwen, R. Bruner *et al.*, “Long-term inhalation toxicity of hydrazine,” *Fundamental and Applied Toxicology*, vol. 5, no. 6, pp. 1050–1064, 1985.

[35] S. Tafazoli, “A study of on-orbit spacecraft failures,” *Acta Astronautica - ACTA ASTRONAUT*, vol. 64, pp. 195–205, Feb. 2009. DOI: 10.1016/j.actaastro.2008.07.019.

[36] The MOLA Instrument and Science Team, *Mars topography (MOLA dataset)*. 2000. [Online]. Available: http://svs.gsfc.nasa.gov/stories/MOLA/.

[37] J. L. Bandfield, “High-resolution subsurface water-ice distributions on mars,” *Nature*, vol. 447, no. 7140, pp. 64–67, May 2007, ISSN: 1476-4687. DOI: 10.1038/nature05781. [Online]. Available: https://doi.org/10.1038/nature05781.

[38] R. Orosei, S. Lauro, E. Pettinelli *et al.*, “Radar evidence of subglacial liquid water on mars,” *Science*, vol. 361, no. 6401, pp. 490–493, 2018.

[39] J. T. Wilson, V. R. Eke, R. J. Massey *et al.*, “Equatorial locations of water on mars: Improved resolution maps based on mars odyssey neutron spectrometer data,” *Icarus*, vol. 299, pp. 148–160, 2018, ISSN: 0019-1035. DOI: https://doi.org/10.1016/j.icarus.2017.07.028. [Online]. Available: https://www.sciencedirect.com/science/article/pii/S0019103516306029.

[40] L. M. Parro, A. Jiménez-Díaz, F. Mansilla *et al.*, “Present-day heat flow model of mars,” *Scientific Reports*, vol. 7, no. 45629, 2017.

[41] D. Barker, G. Chamitoff and G. James, “Resource utilization and site selection for a self-sufficient martian outpost,” May 1998.

[42] M. J. Fogg, “The utility of geothermal energy on Mars,” *Journal of the British Interplanetary Society*, vol. 50, p. 187, Jan. 1997.

[43] M. van Driel, S. Ceylan, J. F. Clinton *et al.*, “High-frequency seismic events on mars observed by insight,” *Journal of Geophysical Research: Planets*, vol. 126, no. 2, e2020JE006670, 2021, e2020JE006670 2020JE006670. DOI: https://doi.org/10.1029/2020JE006670. eprint: https://agupubs.onlinelibrary.wiley.com/doi/pdf/10.1029/2020JE006670. [Online]. Available: https://agupubs.onlinelibrary.wiley.com/doi/abs/10.1029/2020JE006670.

[44] W. B. Banerdt, S. E. Smrekar, D. Banfield *et al.*, “Initial results from the insight mission on mars,” *Nature Geoscience*, vol. 13, no. 3, pp. 183–189, 2020.

[45] P. Lognonne, W. B. Banerdt, D. Giardini *et al.*, “Seis: Insight’s seismic experiment for internal structure of mars,” *Space Science Reviews*, vol. 215, no. 1, p. 12, Jan. 2019, ISSN: 1572-9672. DOI: 10.1007/s11214-

018-0574-6. [Online]. Available: https://doi.org/10.1007/s11214-018-0574-6.

[46] D. Giardini, P. Lognonné, W. B. Banerdt *et al.*, "The seismicity of mars," *Nature Geoscience*, vol. 13, no. 3, pp. 205–212, 2020.

[47] C. G. Justus and R. D. Braun, "Atmospheric environments for entry, descent and landing (edl)," 2007, https://ntrs.nasa.gov/api/citations/20070032693/downloads/20070032693.pdf.

[48] J. Cruz and S. Lingard, "Aerodynamic decelerators for planetary exploration: Past, present, and future," *Collection of Technical Papers - AIAA Guidance, Navigation, and Control Conference 2006*, vol. 8, Aug. 2006. DOI: 10.2514/6.2006-6792.

[49] Prof. Dr. Ir. Mooij, *Re-entry systems: Ballistic entry*, 2020.

[50] P. Desai and P. Knocke, "Mars exploration rovers entry, descent, and landing trajectory analysis," *The Journal of the Astronautical Sciences*, vol. 55, Sep. 2007. DOI: 10.1007/BF03256527.

[51] J. R. Cruz and J. S. Lingard, "Aerodynamics decelerators for planetary exploration: Past, present, and future," *American Institute of Aeronautics and Astronautics*, [Online]. Available: https://ntrs.nasa.gov/api/citations/20060028185/downloads/20060028185.pdf.

[52] Juan R. Cruz, *Parachutes for planetary entry systems*, 2006.

[53] (2021). "Rs," [Online]. Available: https://nl.rs-online.com/web/p/thermal-insulation/7757466/?cm_mmc=NL-PLA-DS3A-_-google-_-CSS_NL_NL_Engineering_Materials_%5C%26_Industrial_Hardware_Whoop-_-(NL:Whoop!)+Thermal+Insulation-_-7757466&matchtype=&pla-341996961042&gclid=CjwKCAjwn6GGBhADEiwAruUcKo_Z0RwWCrItXnmrhqO1m7fo4wGlt3Afs0jOQwu8qFs4vi9UCa1eQBoCTWoQAvD_BwE&gclsrc=aw.ds (visited on 18/06/2021).

[54] Narcon. (2000). "Parachute recovery technology," [Online]. Available: https://fruitychutes.com/genes_blog/parachute_recovery_technology (visited on 29/12/2020).

[55] T. W. Knacke, *Parachute Recovery Systems Design Manual*, First edition. Para Publishing, 1991.

[56] J. P. Masciarelli, "Technology development for deployable aerodynamics decelerators at mars," *NASA Johnson Space Center*, [Online]. Available: https://ntrs.nasa.gov/api/citations/20100035224/downloads/20100035224.pdf.

[57] J. Guinn, T. Ely and B. Portock, "Mars surface asset positioning using in-situ radio tracking,"

[58] J. Guinn and T. Ely, "Preliminary results of mars exploration rover in-situ radio navigation," Feb. 2004.

[59] K.-M. Cheung, C. Lee, W. Jun *et al.*, "Single-satellite doppler localization with law of cosines (loc)," pp. 1–12, 2019. DOI: 10.1109/AERO.2019.8742181.

[60] D. Munalli, G. Dimitrakis, D. Chronopoulos *et al.*, "Electromagnetic shielding effectiveness of carbon fibre reinforced composites," *Composites Part B: Engineering*, vol. 173, p. 106 906, 2019, ISSN: 1359-8368. DOI: https://doi.org/10.1016/j.compositesb.2019.106906. [Online]. Available: https://www.sciencedirect.com/science/article/pii/S1359836818343762.

[61] S. Smrekar, D. Catling, R. Lorenz *et al.*, "Deep space 2: The mars microprobe mission," *Journal of Geophysical Research E: Planets*, vol. 104, Nov. 1999. DOI: 10.1029/1999JE001073.

[62] Z. Wang and J. Liu, "Numerical and theoretical analysis of honeycomb structure filled with circular aluminum tubes subjected to axial compression," *Composites Part B: Engineering*, vol. 165, pp. 626–635, 2019, ISSN: 1359-8368. DOI: https://doi.org/10.1016/j.compositesb.2019.01.070. [Online]. Available: https://www.sciencedirect.com/science/article/pii/S1359836818326611.

[63] European Space Agency. (Sep. 2008). "Technology readiness levels handbook for space applications."

[64] T. Spohn, M. Grott, S. Smrekar *et al.*, "The heat flow and physical properties package (hp3) for the insight mission," *Space Science Reviews*, vol. 214, Aug. 2018. DOI: 10.1007/s11214-018-0531-4.

[65] M. Grott, J. Helbert and R. Nadalini, "Thermal structure of martian soil and the measurability of the planetary heat flow," *Journal of Geophysical Research: Planets*, vol. 112, no. E9, 2007. DOI: https://doi.org/10.1029/2007JE002905. eprint: https://agupubs.onlinelibrary.wiley.com/doi/pdf/10.1029/2007JE002905. [Online]. Available: https://agupubs.onlinelibrary.wiley.com/doi/abs/10.1029/2007JE002905.

[66] C. Sorice, K. S. Ali, A. Trebi-Ollennu *et al.*, "Insight robotic arm testing activities for hp3 mole anomaly recovery on mars," in *2021 IEEE Aerospace Conference (50100)*, IEEE, 2021, pp. 1–19.

[67] A. Lazarewicz, D. Anderson, K. Anderson *et al.*, "The viking seismometry," *National Aeronautics and Space Administration Report*, vol. -1, Mar. 1981.

[68] J. F. Clinton, S. Ceylan, M. van Driel *et al.*, "The marsquake catalogue from insight, sols 0–478," *Physics of the Earth and Planetary Interiors*, vol. 310, p. 106 595, 2021, ISSN: 0031-9201. DOI: https://doi.org/10.1016/j.pepi.2020.106595. [Online]. Available: https://www.sciencedirect.com/science/article/pii/S0031920120302739.

[69] B. Pavri, *Requirements review: Seis-sp level 2, 3, 4, 5 requirements*, Sep. 2004.

[70] J. A. Rodriguez-Manfredi, M. de la Torre Juárez, A. Alonso *et al.*, "The mars environmental dynamics

analyzer, meda. a suite of environmental sensors for the mars 2020 mission," *Space Science Reviews*, vol. 217, no. 3, p. 48, Apr. 2021, ISSN: 1572-9672. DOI: 10.1007/s11214-021-00816-9. [Online]. Available: https://doi.org/10.1007/s11214-021-00816-9.

[71] J. Gomez-Elvira, C. Armiens, L. Castañer *et al.*, "Rems: The environmental sensor suite for the mars science laboratory rover," *Space Science Reviews*, vol. 170, pp. 583–640, Sep. 2012. DOI: https://doi.org/10.1007/s11214-012-9921-1.

[72] J. H. Hoffman, R. R. Hodges and K. D. Duerksen, "Pioneer venus large probe neutral mass spectrometer," *Journal of Vacuum Science and Technology*, vol. 16, no. 2, pp. 692–694, 1979. DOI: 10.1116/1.570059. eprint: https://doi.org/10.1116/1.570059. [Online]. Available: https://doi.org/10.1116/1.570059.

[73] B. J. Shortt, M. R. Darrach, P. M. Holland *et al.*, "Miniaturized system of a gas chromatograph coupled with a paul ion trap mass spectrometer," *Journal of Mass Spectrometry*, vol. 40, no. 1, pp. 36–42, Jan. 2005. DOI: 10.1002/jms.768. [Online]. Available: https://doi.org/10.1002/jms.768.

[74] S. Newman, *Seismographic Data Compression*. 2006.

[75] P. T. Palmer and T. F. Limero, "Mass spectrometry in the u.s. space program: Past, present, and future," *Journal of the American Society for Mass Spectrometry*, vol. 12, no. 6, pp. 656–675, 2001, ISSN: 1044-0305. DOI: https://doi.org/10.1016/S1044-0305(01)00249-5. [Online]. Available: https://www.sciencedirect.com/science/article/pii/S1044030501002495.

[76] Innoflight Inc., *CHAMPS Flight Computer (MPSoC CFC-400)*, 9985 Pacific Heights Blvd., Suite 250, San Diego. [Online]. Available: https://satcatalog.com/datasheet/Innoflight%5C%20-%5C%20CFC-400.pdf.

[77] D. M. Hassler, C. Zeitlin, R. F. Wimmer-Schweingruber *et al.*, "Mars' surface radiation environment measured with the mars science laboratory's curiosity rover," *Science*, vol. 343, no. 6169, O. Kemppinen, D. Cremers, J. F. Bell *et al.*, Eds., 2014, ISSN: 0036-8075. DOI: 10.1126/science.1244797. eprint: https://science.sciencemag.org/content/343/6169/1244797.full.pdf. [Online]. Available: https://science.sciencemag.org/content/343/6169/1244797.

[78] G. Arakaki and S. D'Agostino, "New millennium ds2 electronic packaging an advanced electronic packaging "sandbox"," in *1999 IEEE Aerospace Conference. Proceedings (Cat. No.99TH8403)*, vol. 2, Mar. 1999, 205–213 vol.2. DOI: 10.1109/AERO.1999.793162.

[79] P. P. J. Geoffrey A. Landis, "Dust mitigation for mars solar arrays," *NASA John Glenn Research Center, Ohio Aerospace Institute*, 2002.

[80] L. R. D., L. M. T., M. J. *et al.*, "Scientifc observations with the insight solar arrays: Dust clouds and eclipses on mars.," *Earth and Space Science*, 2020. [Online]. Available: https://doi.org/10.1029/2019EA000992.

[81] P. Jenkins, "A dust characterization experiment for solar cells operating on mars," *IEEE*, 2000.

[82] A. T. Daniel Bain Craig Patton, "Deployable solar array structure: G1:3," *Kennesaw State University*, 2019.

[83] J. W. Ells, "Estimate of sub-surface Martian temperatures.," *Journal of the British Astronomical Association*, vol. 79, pp. 280–285, May 1969.

[84] R. Caps and J. Fricke, "Aerogels for thermal insulation," in *Sol-Gel Technologies for Glass Producers and Users*, M. A. Aegerter and M. Mennig, Eds. Boston, MA: Springer US, 2004, pp. 349–353, ISBN: 978-0-387-88953-5. DOI: 10.1007/978-0-387-88953-5_46. [Online]. Available: https://doi.org/10.1007/978-0-387-88953-5_46.

[85] M. Biswal, M. Kumar and R. N. Annavarapu, "A study on mars probe failures," *AIAA Scitech 2021 Forum*, Jan. 2021. DOI: 10.2514/6.2021-1158. [Online]. Available: http://dx.doi.org/10.2514/6.2021-1158.

[86] R. W. Zurek and L. J. Martin, "Interannual variability of planet-encircling dust storms on mars," *Journal of Geophysical Research: Planets*, vol. 98, no. E2, pp. 3247–3259, 1993. DOI: https://doi.org/10.1029/92JE02936. eprint: https://agupubs.onlinelibrary.wiley.com/doi/pdf/10.1029/92JE02936. [Online]. Available: https://agupubs.onlinelibrary.wiley.com/doi/abs/10.1029/92JE02936.

[87] DSE Group 22, "Mars deploy: Project plan of the design synthesis exercise," 2021.

[88] G. Bignami, P. Cargill, B. Schutz *et al.*, "Cosmic vision," 2005.

A. Technical diagrams

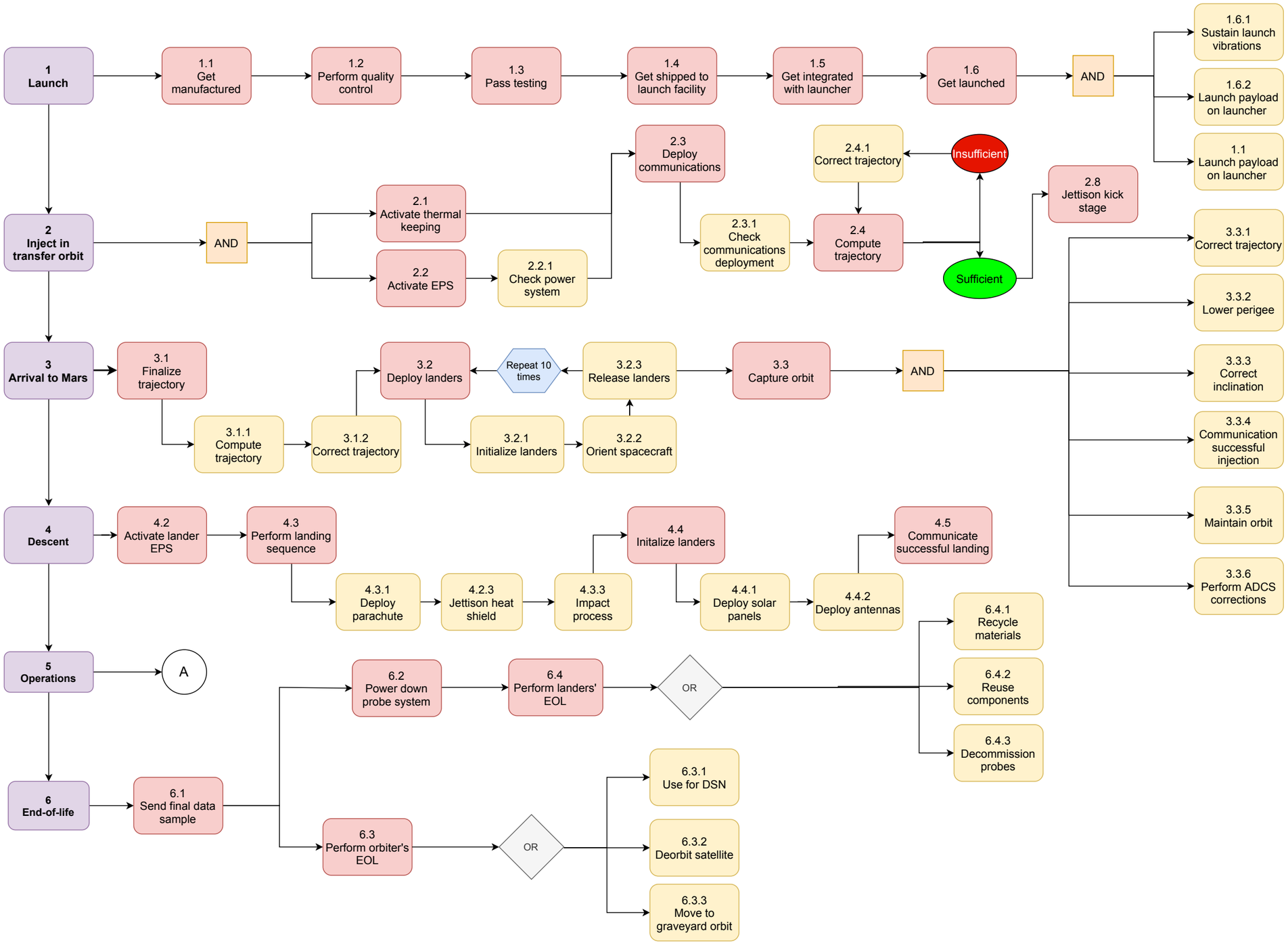

Figure A.1: Functional flow diagram (FFD)

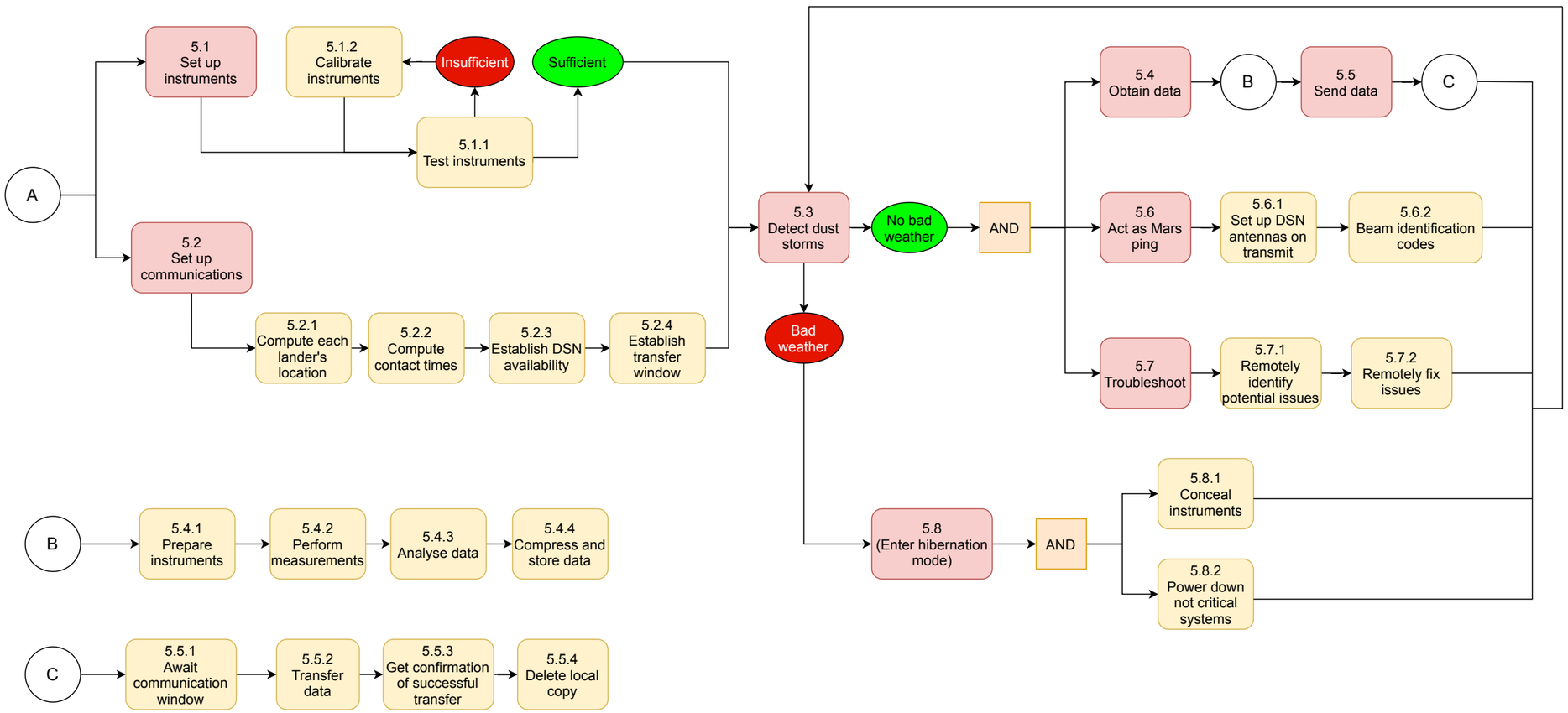

Figure A.2: Functional flow diagram (continued)

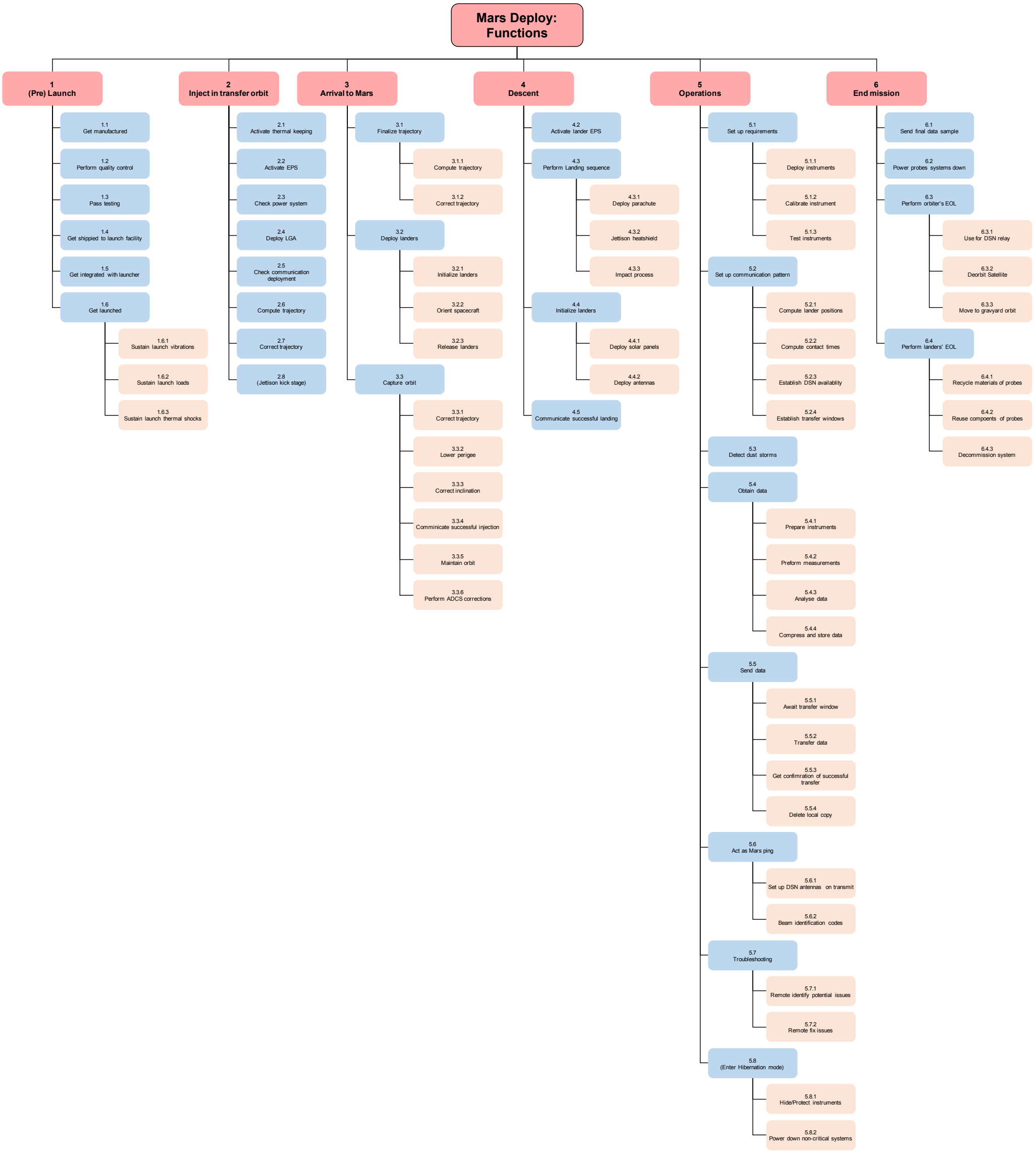

Figure A.3: Functional breakdown structure (FBS)

Propulsion	Control entry capsule trajectory and attitude		Control entry capsule attitude	Control entry capsule trajectory				Communicate propellant levels	
	Structures	Deploy parachute and separate heatshield			Deploy radiator/louvers	Deploy and orient solar arrays	Deploy payload, provide connection to Martian surface	Communicate mechanism status	Deploy and orient antennas
	Decelerate entry capsule	Aerodynamics	Provide passive entry capsule stabilisation		Protect against aerodynamic heating				
Determine RCS burn	Control entry capsule attitude		ADCS	Determine attitude		Determine attitude		Determine attitude	Determine attitude
Define entry trajectory			Determine position and velocity	Guidance & Navigation				Determine position and velocity	Report position to DSN
Provide heating/cooling	Define radiator/louver positions, provide heating/cooling		Provide heating/cooling	Provide heating/cooling	Thermal Control	Provide heating/cooling	Provide heating/cooling	Provide heating/cooling, communicate system temperatures	Provide heating/cooling
Supply nominal & peak power	Provide power, determine required array orientation		Supply nominal & peak power	Supply nominal & peak power	Supply nominal & peak power	EPS	Supply nominal & peak power	Supply nominal & peak power, communicate power levels	Supply nominal & peak power
	Determine required deployment steps						Payload	Generate scientific data	
Provide thruster commands	Provide commands, e.g. deploy solar array, parachute, etc.		Provide attitude commands	Provide positional commands	Provide thermal commands	Regulate power supply	Provide operational commands	C&DH	Transfer scientific and operational data to orbiter via uplink
	Determine required antenna position							Transfer data from orbiter and DSN via downlink	TT&C

Figure A.4: N2 subsystem interfaces diagram for the lander

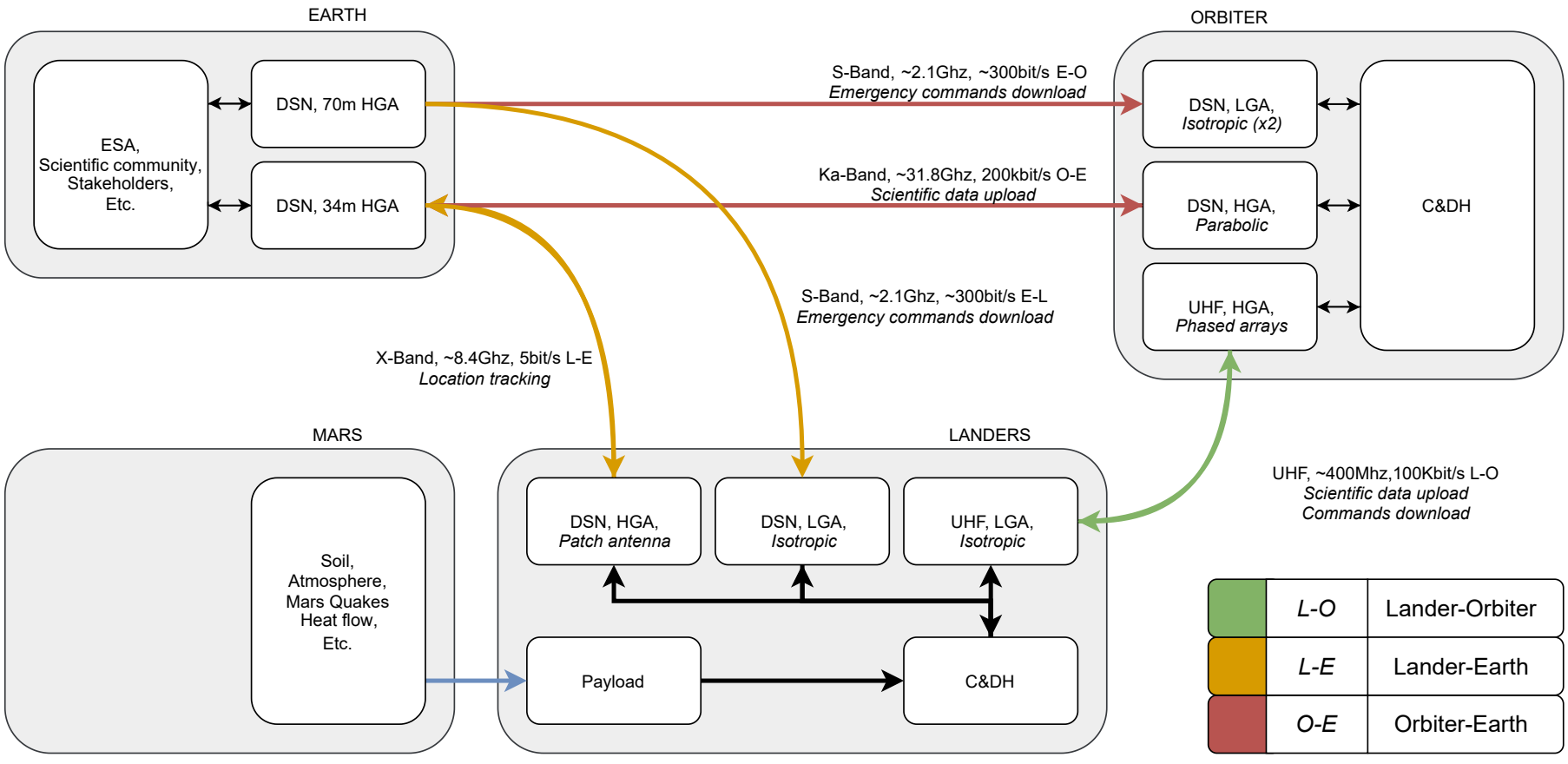

Figure A.5: Communication Diagram, Lander-Orbiter-Earth

B. Manufacturing diagram

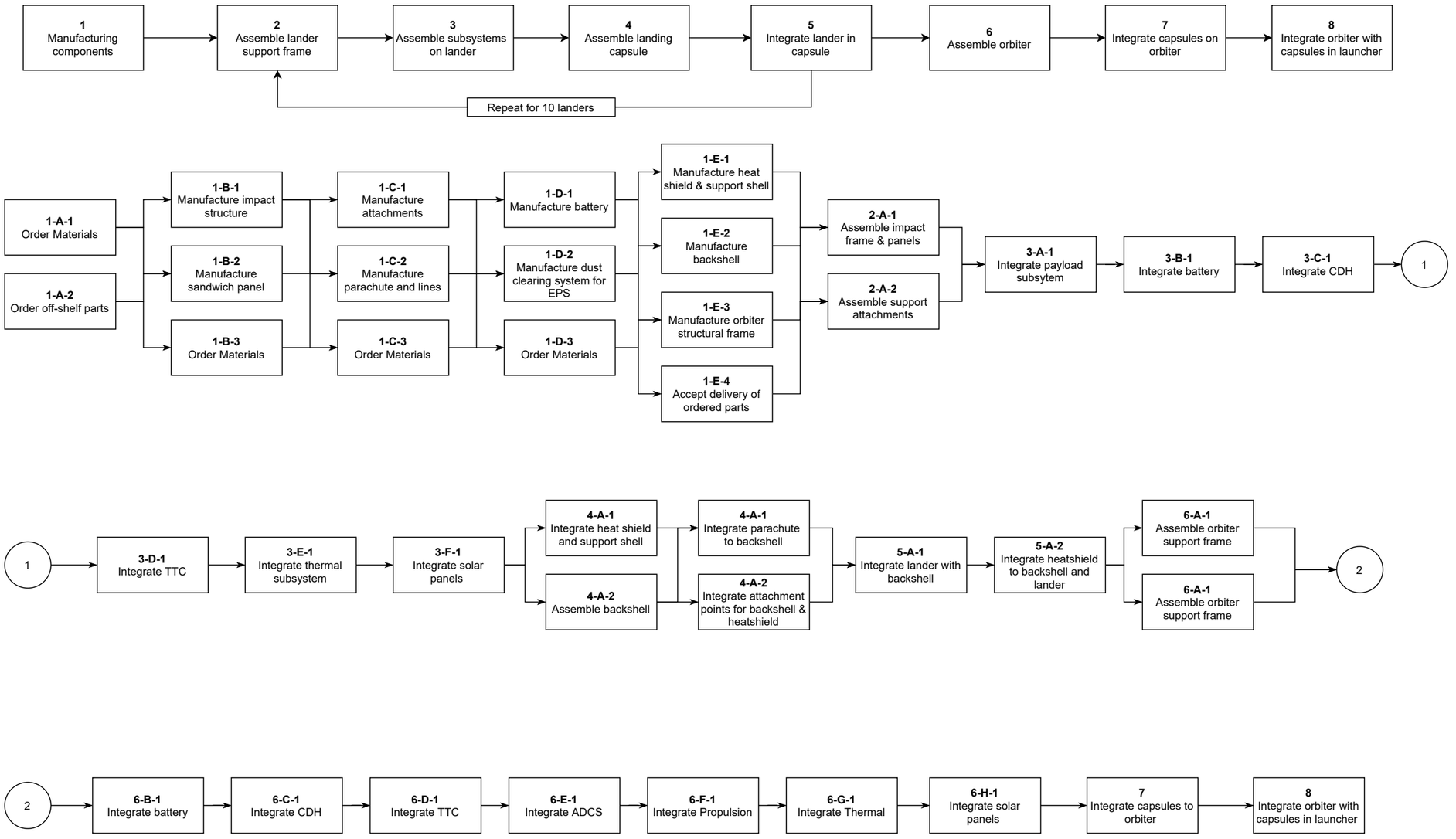

Figure B.1: Manufacturing diagram

C. CAD Drawings

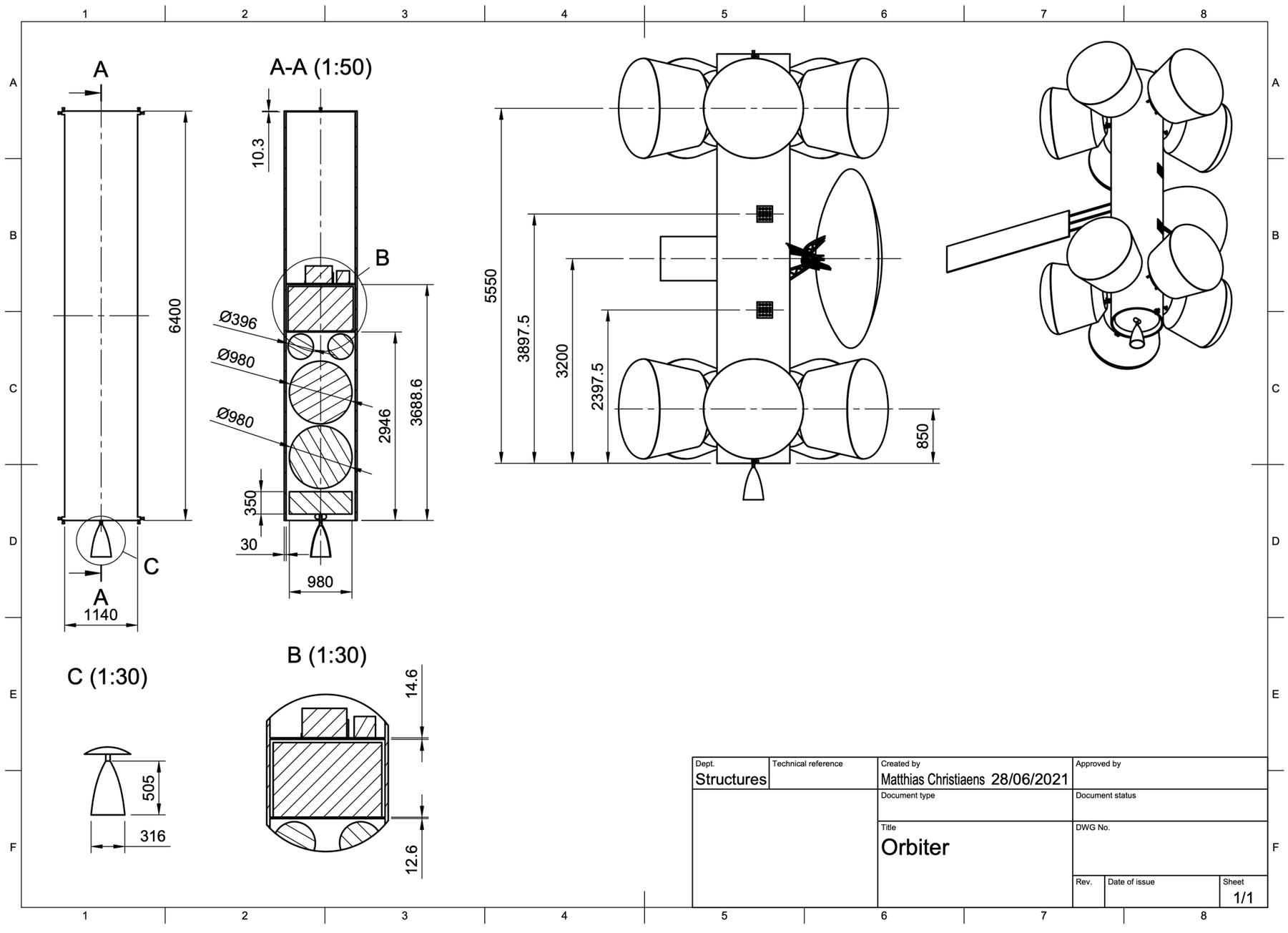

Figure C.1: CAD drawing of the orbiter.

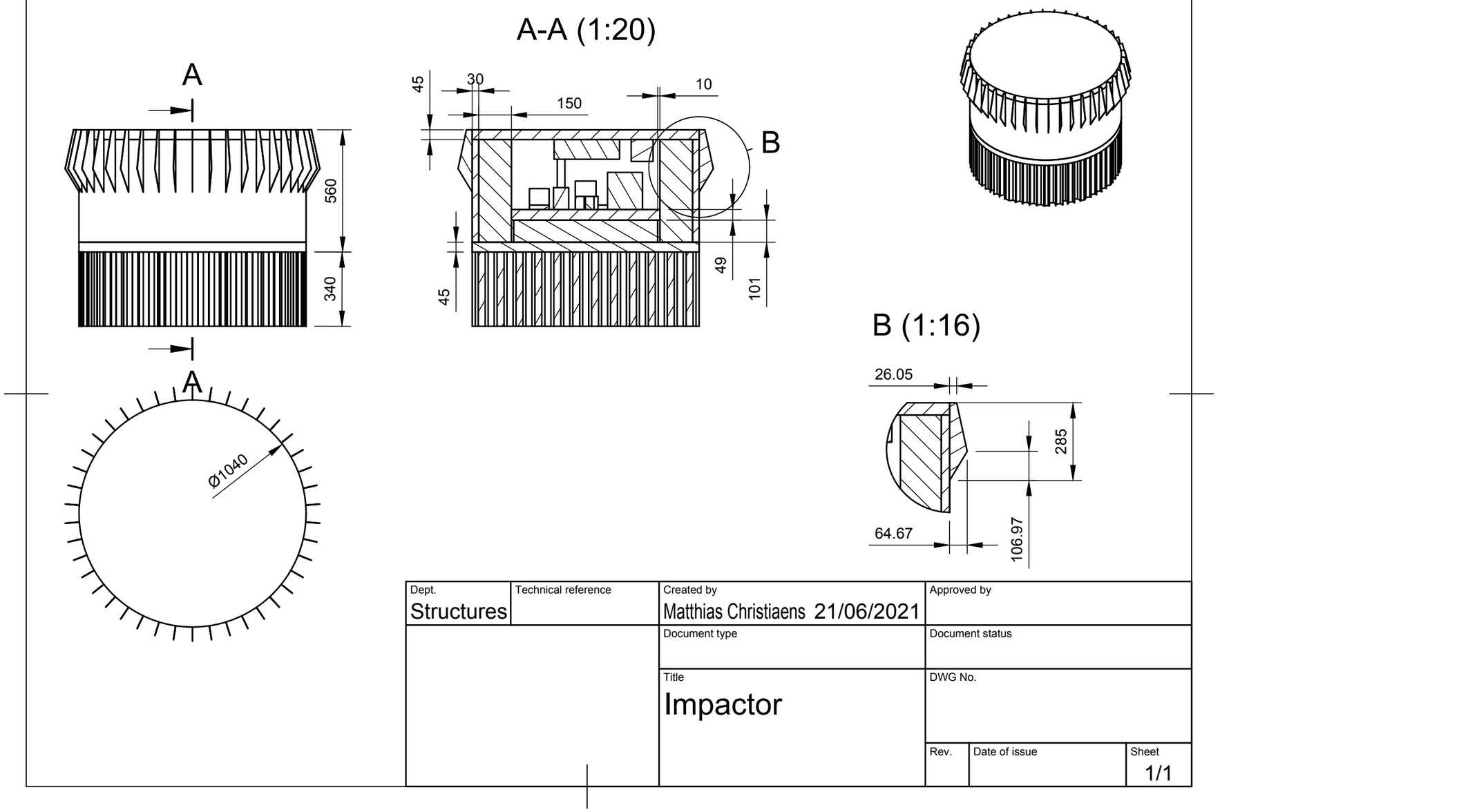

Figure C.2: CAD drawing of the lander.